

Performance Study of an Underlay Cognitive Radio Network in the Presence of Co-channel Interference



Jamal Ahmed Hussein

Newcastle University

Newcastle upon Tyne, UK

A thesis submitted for the degree of

Doctor of Philosophy

April 2017

To my loving parents and family

Seek knowledge from the cradle to the grave.

-Prophet Mohammed (PBUH)

Acknowledgements

First and foremost, I should thank almighty Allah for giving me good health and the strength to do this research. Then, I would like to express my truthful appreciation to my PhD research supervisor Prof. Said Boussakta. His encouragement, guidance and support have been a key factor in successful completion of this thesis. I am really grateful to Dr. Salama Ikki, my second supervisor during the first year of my PhD, for guiding me to the research area of performance study of wireless communication network. He continued supporting me even after he left Newcastle University. In addition, I want to thank Dr. Charalampos Tsimenidis, my second supervisor after the first year of my PhD, for his comments and suggestions for our research papers during my PhD research.

I thankfully recognise the financial support from the Higher Committee for Education Development in Iraq (HCED). I am also grateful to the Ministry of Transportation and Communication, Kurdistan Regional Government-Iraq, for their financial assistance during my PhD study.

My deepest gratitude goes to my loving wife Najwa and my angels Asin, Barin, and Mina for their care, inspiration, and patience. I am at a loss to find appropriate words that express my gratitude for my parents, especially my mother “Faima” her prayers for me have been a guiding light in the darkness. I warmly thank my brothers and sisters for the love and support they have shown me, especially my brother Kamal.

A special thanks to Prof. Jonathon Chambers, Head of the Communications, Sensors, Signal and Information Processing (ComS²IP) Group, for his constructive and useful feedback about some of my research work, in particular for the IEEE TCOM paper. Also, I am thankful to my colleagues in the ComS²IP Group for sharing the research office with me

and providing a suitable research atmosphere. My particular and sincere appreciation goes to Zheng Chu, Yasir, Ali, Bilal, Sinan, Achonu, Zhen Mei for sharing the research office and discussing our research together. Furthermore, my thanks and appreciation go to Helen Woolridge for helping me to proofread my work.

Finally, I should thank all staff in the Department of Electrical and Electronics Engineering at Newcastle University for their continuous generous support. Especially Gill Webber, the Postgraduate Research Coordinator and Deborah Alexander, the Receptionist.

Abstract

Massive innovation in all aspects of the wireless communication network has been witnessed over the last few decades. The demand for data throughput is continuously growing, as such, the current regulations for allocating frequency spectrum are not able to respond to this exponential growth. Cognitive radio (CR), has been proposed as a solution to this problem. One of the possible scenarios of the implementation of CR is underlay cognitive radio. In this thesis the performance of an underlay cognitive radio network (UCRN) in the presence of the co-channel interference (CCI) is assessed.

Firstly, the impact of CCI on the dual-hop cooperative UCRN is investigated over Rayleigh fading channels. In order to do this, the exact outage probability (OP), average error probability (AEP) and the ergodic capacity (EC) are studied. In addition, simple and asymptotic expressions for the OP and AEP are derived. Furthermore, the optimal power allocation is investigated to enhance the network performance. Moreover, the performance of a multi-user scenario is studied by considering the opportunistic SNR-based selection technique.

Secondly, the effect of both primary network interference and CCI on the dual-hop UCRN over Rayleigh fading channels are studied. The equivalent signal-to-interference-plus-noise ratio (SINR) for this network scenario is obtained by considering multi-antenna schemes at all receiver nodes. The different signal combinations at the receiver nodes are investigated and compared, such as selection combining (SC) and maximum ratio combining (MRC) techniques. Then, the equivalent probability density function (PDF) and cumulative distribution function (CDF) of the network's equivalent SINR are derived and discussed. Furthermore, expressions for the exact OP, AEP, and EC are derived and reviewed.

In addition, asymptotic OP expressions are obtained for different case scenarios to gain an insight into the network parameters.

Thirdly, multiple-input multiple-output (MIMO) UCRN is investigated under the influence of primary transmitter interference and CCI over Rayleigh fading channels. The transmit antenna selection and maximum ratio combining (TAS/MRC) techniques are considered for examining the performance of the secondary network. At first the equivalent SINR for the system is derived, then the exact and approximate expressions for the OP are derived and discussed.

Fourthly, considering Nakagami-m fading channels, the performance of the UCRN is thoroughly studied with the consideration of the impact of primary network interference and CCI. The equivalent SINR for the secondary system is derived. Then, the system equivalent PDF and CDF are derived and discussed. Furthermore, the OP and AEP performances are investigated.

Finally, for the cases mentioned above, numerical examples in conjunction with MatLab Monte Carlo simulations are provided to validate the derived results. The results show that CCI is one of the factors that severely reduces the UCRN performance. This can be more observable when the CCI power increases linearly with the transmission power of the secondary transmitter nodes. Furthermore, it was found that in a multi-user scenario the opportunistic SNR-based selection technique consideration can improve the performance of the network. Moreover, adaptive power allocation is found to give better results than equal power allocation. In addition, cooperative communication can be considered to be an effective way to combat the impact of transmission power limitation of the secondary network and interference power constraint. The multi-antenna schemes are another important consideration for enhancing the overall performance. In fact, despite the interference from the CCI and primary user sources, the multi-antennas scheme does not lose its advantage in the UCRN performance improvement.

Contents

List of Figures	xi
List of Tables	xiv
1 Introduction	1
1.1 Performance Analysis	3
1.2 Co-Channel Interference	3
1.3 Literature Review	4
1.4 Motivation of this Work	8
1.5 Contribution of this Work	8
1.6 Publications	9
1.7 Thesis Organisation	10
2 Background Theory	12
2.1 Signal Transmission in Wireless Network	13
2.1.1 Amplify-and-Forward (AF)	14
2.1.2 Decode-and-Forward (DF)	14
2.2 Statistical Analysis of Random Variable	14
2.3 Wireless Fading Channel and its Statistical Modelling	16
2.3.1 Rayleigh Fading Channels	18
2.3.2 Rician Fading Channels	19
2.3.3 Nakagami- m Fading Channels	19
2.4 Mathematical Modelling of Cognitive Radio Networks	20
2.5 Mathematical Representation of the CCI	22
2.6 Common Performance Criteria	23
2.6.1 Outage Probability (OP):	24
2.6.2 Average Error Probability (AEP):	24

2.6.3	Ergodic Capacity (EC):	26
2.7	Chapter Summary:	27
3	Impact of CCI On the Performance of an Underlay Cognitive Network	28
3.1	Introduction	28
3.1.1	Literature Review	29
3.1.2	Contributions	30
3.1.3	Chapter Organization	31
3.2	System Model	31
3.2.1	Network Description	32
3.2.2	Mathematical Representation	33
3.2.3	Multi-Destination User Scenario	35
3.3	Statistical Derivations	35
3.4	Performance Evaluation	37
3.4.1	Exact Outage Probability	37
3.4.2	Average Error Probability	37
3.4.3	Approximate Outage Probability and Average Error Probability	41
3.4.4	Ergodic Capacity	42
3.4.5	Optimum Power Allocation	43
3.5	Numerical Results and Discussions	46
3.6	Conclusion	49
3.7	Appendix	50
3.7.1	First hop Exact CDF Derivation Steps	50
3.7.2	Proof of Theorem 1	52
3.7.3	First hop Average Error Probability Derivation Steps	55
3.7.4	Second hop Opportunistic Ergodic Capacity Derivation Steps	57
4	Performance Analysis of a UCRN with Consideration of Primary Network and CCIs	60
4.1	Introduction	61
4.1.1	Related Work	61
4.1.2	Contribution of this Chapter	62
4.2	System Model	64

4.2.1	Using the SC Technique	66
4.2.2	Using the MRC Technique	67
4.3	Statistical Analysis	67
4.3.1	Exact CDF	67
4.3.2	Asymptotic CDF	72
4.3.3	Per-hop Equivalent PDF	73
4.4	Performance Evaluation	76
4.4.1	Outage Probability	76
4.4.2	Average Error Probability	76
4.4.3	Ergodic Capacity	78
4.5	Numerical Results and Discussions	80
4.6	Conclusion	89
4.7	Appendix	90
4.7.1	Per-hop CDF Derivation	90
4.7.2	Per-hop CDF using SINR-based Selection Combining	92
4.7.3	Per-hop CDF Derivation, Maximum Ratio Combining Technique	93
4.7.4	Error Probability Derivation	94
4.7.5	Ergodic Capacity Derivation	97
5	Performance Study of a MIMO Spectrum Sharing Network in the Presence of CCI	101
5.1	Introduction	102
5.2	System Model	103
5.3	Performance Evaluation	105
5.3.1	Exact Outage Performance	105
5.3.2	Approximate Outage Performance	106
5.3.3	Average Error Probability	109
5.4	Numerical Results and Discussions	110
5.5	Conclusion	113
5.6	Appendix	114
5.6.1	Proof of Proposition 1	114
6	Impact of CCI on a UCRN Over Nakagami-m Fading Channels	120
6.0.1	Related Works	121

6.0.2	Contribution of this Chapter	121
6.1	System Model	122
6.1.1	Network and Channels Description	122
6.1.2	Mathematical Representation	123
6.2	Statistical Derivations and Performance Evaluation	125
6.2.1	The CDF of $\gamma_{\text{eq}}^{\text{tot}}$	125
6.2.2	The PDF of $\gamma_{\text{eq}}^{\text{tot}}$	127
6.2.3	Exact Outage Performance	129
6.2.4	Asymptotic Outage Performance	130
6.2.5	Multi-hop Exact Outage Performance	132
6.2.6	Average Error Probability	132
6.3	Numerical Results and Discussion	133
6.4	Conclusion	139
6.5	Appendix	140
6.5.1	Proof of Corollary 1	140
6.5.2	Proof of Corollary 2	144
7	Conclusion and Further Research	145
7.1	Conclusion	145
7.2	Further Research	147
	References	149

List of Figures

2.1	Typical CRN showing the primary and secondary transceivers; solid lines represent the desired data links, and the dashed lines represent the interference links. T_x and R_x represent the transmitter and receiver nodes, respectively.	21
3.1	The general system model used for analysis.	32
3.2	Outage probability for different numbers of destination users.	45
3.3	Outage probability for different I_{\max} values.	46
3.4	The ergodic capacity for different values of I_{\max} , K and CCI power.	47
3.5	Error probability for different values of I_{\max} and K	48
3.6	Error probability for different values of CCI power.	49
3.7	Performance of optimal power allocation algorithm in comparison to the equal power allocation.	50
4.1	The general system model used for analysis, showing multi-hop underlay CR and primary transceiver networks in the presence of co-channel interference with multi-antennas at all receiver nodes.	64
4.2	Characteristics of the PDF of the per-hop equivalent SINR.	75
4.3	Outage performance through consideration of a different number of hops in the UCRN.	81
4.4	Outage probability for a different number of secondary receiver antennas.	82
4.5	Outage probability for different values of CCI powers.	83
4.6	Outage probability for different values of I_{\max}	84
4.7	Outage probability versus SNR threshold for different values of \bar{I}_{P_R} and signal combining techniques at the secondary receiver nodes.	85

4.8	Average error probability for a different number of CCI signals at the SU receiver nodes.	86
4.9	Average error probability for a different number of antennas at the CR receiver nodes.	87
4.10	Capacity performance for different values of CCI powers and a different number of antennas at the SU receiver nodes.	88
5.1	The general network model used for the analysis showing a MIMO underlay CR network in the presence of primary transceiver and CCI.	104
5.2	Outage performance vs. SNR threshold for different values of interference power constraint I_{\max} and secondary destination antennas N_s .	111
5.3	Outage performance vs. transmission SNR for different PU receiver node positions.	112
5.4	Outage performance for a different number of antennas at the SU transmitter and different number of CCI signals in the scenario where the CCI power linearly increases with the secondary transmission power.	113
5.5	Average error probability for a different number of antennas at the SU transmitter.	114
6.1	The general network model used for analysis showing cooperative underlay CR network in the existence of the primary transceiver and CCI.	122
6.2	Outage probability as a function of SNR threshold for different values of the channel fading severity parameter and the interference power constraint.	134
6.3	Outage probability vs. transmission power constraint for a different number of CCI sources.	135
6.4	Outage probability vs. transmission power constraint for a linear increase of the CCI power and primary transmission power.	136
6.5	Three hops OP as a function of transmission power constraint for different values of channel fading severity parameter and primary network interference power.	137
6.6	Average error probability for the dual-hop CR network for different modulation schemes.	138

6.7 Dual-hop equivalent PDF characteristics for different channel fading severity parameters and CCI powers. 139

List of Tables

1.1	Summary of literature review papers on the performance study of an underlay cognitive radio network	5
2.1	Instantaneous symbol error probability (P_{ser}) and bit error probability (P_{ber}) for coherent detection modulations and their modulation constant values	26
3.1	Comparison between the exact and approximate representations of the exponential integral function	55

Chapter 1

Introduction

The frequency spectrum is the only precious [1] fixed resource that is available to all wireless users for all communications purposes. There are some authorities, such as Office of Communications (Ofcom) in the UK and Federal Communications Commission (FCC) in the United States, that are responsible for publishing regulations and allocating a particular frequency band, i.e., giving a licence, to an intended user. Over time, the allocation of frequency spectrums has been modified based on the requirements of the state of the art technologies. Cognitive radio (CR), as a promising technology has been proposed to utilise the existing frequency spectrum more efficiently. In fact, the idea of CR goes back to 1999, when Joseph Mitola [2] published research on the software defined radio (SDR). This idea has become more compelling and attracted many researchers after 2003 when the FCC issued its report [3] about the status of the frequency spectrum. From that time, CR became an interesting research topic for study and investigation [1,4–6]. Moreover, the FCC has accepted the usage of unoccupied television frequency bands by mobile users [7]. This has motivated many researchers to investigate practically the optimal usage of the radio spectrum. As a proposed network, it is necessary and important to study the performance behaviour of the CR network (CRN) and understand its benefits and capability for the improvement of future wireless communication network.

According to [7], the term CR is defined as a radio system that is aware of the surrounding environment and capable of changing and adapting its transmission parameters based on necessities. In general, in the CR network, the frequency spectrum is not used by the licensed users only. However, the second kind of user, the unlicensed user, can benefit from it. The licensed users, who are also known

as primary users (PUs), have permission to use a particular frequency spectrum at any time without any constraints. The unlicensed users, who are also known as secondary users (SUs), do not have a licence but can share the frequency spectrum with the PU preserving some strict regulations and conditions.

The CRN has been divided into three main categories based on the network topology, the co-existence of the users, and the rules and conditions for assigning different users in the system. These are underlay, overlay and interweave [8]. In the mentioned proposed paradigms, the protection of the quality of service (QoS) of the primary user should have the top priority.

In an underlay CRN paradigm, both PUs and SUs are allowed to use the same frequency spectrum with the condition that the QoS of PUs is maintained. For this purpose an interference power temperature [7], that is known as the interference power constraint (IPC), is imposed on the secondary network transmission nodes. IPC is the maximum acceptable interference that the existence of the secondary network can inflict on the primary network [4]. As a result, SUs should keep the resulting interference to the PUs below the IPC. The quantity of the interference that the SUs produce to the primary network is a crucial matter that the CRN designer should keep in mind. This interference mainly depends on the SUs' transmission power, besides the status of the channel that the SUs transmit on it [7].

In an interweave CR paradigm, the secondary users can use a particular frequency spectrum when it is empty, i.e., not occupied by the primary user. As soon as a primary user requests to use that frequency band, the secondary user should vacate it and search for another empty frequency band. In fact, the CR idea was first originated from this paradigm [7]. The unoccupied frequency band in this paradigm is referred to as a *spectrum hole* or a *white space* [8].

Finally, in an overlay CRN paradigm, the SU requires knowledge of all available channels between all the nodes in the network. This knowledge of the channels allows the SUs to select the appropriate transmission strategy that guarantees the protection of the QoS of the PUs. This paradigm requires sophisticated radio architecture by an advanced network operation [7].

From the above description for different CRN paradigms, it can be observed that the underlay scheme can exploit the frequency spectrum more efficiently than an interweave paradigm. This is due to the fact that both PUs and SUs can simultaneously use the spectrum. Furthermore, in terms of simplicity of implementation,

the underlay paradigm is more feasible than the overlay paradigm. Therefore, in this thesis, the focus is on the performance evaluation of an underlay cognitive radio network (UCRN) paradigm.

1.1 Performance Analysis

For assessing the performance characteristics of any communication network, there are some criteria that can help in understanding the behaviour of the system when it is subjected to particular circumstances. Mathematical analyses and investigations are key to understanding most of the potential benefits of any proposed system before it is implemented in real life. For wireless communication networks, there are some important and common performance measures that can give insights into the system [9, p. 5]. For instance, the outage probability (OP), the average error probability (AEP) and the ergodic capacity (EC). Moreover, these performance criteria can be investigated based on the statistical behaviour of the primary random variable (RV) of interest for the network which is the signal-to-noise ratio (SNR) or in an interference environment system it will be the signal-to-interference-plus-noise ratio (SINR). Furthermore, the average SNR, which is a more suitable performance measure [9, p. 4], is determined by taking the mathematical expectation of the instantaneous SNR over the probability distribution of the fading. Several statistical metrics can be employed to represent the intended RV. For example, probability density function (PDF), cumulative distribution function (CDF) and moment generating function (MGF). In fact, these can provide several insights into the behaviour of the RV. In the next chapter, details about these mentioned statistical metrics are given.

1.2 Co-Channel Interference

Modern communication systems consist of complex and congested network connections. The broadcast nature of wireless communication has the advantage of signal propagation. However, this feature results in the possibility of receiving unwanted signals that will affect the network performance. In addition, the nature of an underlay CRN is based on the co-existence of different users in the same area of operation and the same frequency band. These all lead to a phenomenon which is known as

co-channel interference (CCI). In almost all wireless communication networks, CCI exists over a wide range of the frequency spectrum. It could be from the same frequency bands or other frequency bands that inject energy signals into the desired channel [10]. In fact, the phenomenon of CCI is unavoidable and should be considered to better understand the performance behaviour of the network. Furthermore, in all system models in this thesis, the CCI is mainly considered from the surrounding secondary transmitters that can cause a harmful impact on the performance of the considered CR network.

1.3 Literature Review

The area of cognitive radio performance analysis has been widely researched to examine the potential benefits of this proposed paradigm. In this section, a tabulated summary review of the research papers in the field of a performance study of an underlay CR is presented. More precisely, Table 1.3 is structured so that it will be easy to follow the desired research based on what has been investigated. For instance, in Table 1.3, it is easy to find which paper studied the outage performance of an underlay cognitive radio network considering the primary system transmitter, multi-antenna scheme, and multi-hop network. In fact, this summary is necessary for the purpose of comparison and to ascertain the state of knowledge in this research field. Later on, in chapters 3,4,5, and 6 a more detailed literature review is provided based on the works that are closer to the work in that particular chapter.

Table 1.1: Summary of literature review papers on the performance study of an underlay cognitive radio network

Paper Number	Considering the Following Network Conditions in Calculations								Performance Investigation Metrics ⁴		
	Primary User Transmitter	Secondary Transmission Power Constraint	AWGN	Multi User ¹ Nodes	Multi Hop ²	Multi Antenna	Multi Relay	Fading Channel ³	Outage Probability	Error Probability	Ergodic Capacity
[11]	✓	✓	✓	X	✓	X	X	Ray.	✓	X	X
[12]	✓	✓	✓	X	✓	X	✓	Ray.	✓	X	X
[13]	✓	✓	✓	X	✓	✓	X	Ray.	✓	X	X
[14]	✓	✓	✓	X	X	✓	X	Ray.	✓	X	X
[15]	✓	✓	X	✓	✓	X	X	Ray.	✓	X	X
[16]	✓	✓	X	X	✓	X	✓	Ray.	✓	X	X
[17]	✓	✓	X	X	✓	✓	X	Ray.	✓	X	X
[18]	✓	X	X	X	✓	X	X	Ray.	✓	X	X
[19]	✓	X	✓	X	✓	X	✓	Ray.	✓	X	X
[20]	✓	X	X	X	✓	X	✓	Ray.	✓	X	X
[21]	X	X	✓	X	✓	X	X	Ray.	✓	X	X
[22–24]	X	X	✓	X	✓	X	✓	Ray.	✓	X	X
[25]	X	X	✓	✓	✓	X	X	Ray.	✓	X	X
[26,27]	X	✓	✓	✓	✓	X	✓	Ray.	✓	X	X
[28–30]	X	✓	✓	X	✓	X	✓	Ray.	✓	X	X

[31]	X	✓	✓	✓	✓	✓	✓	X	Ray.	✓	X	X
[32–35]	X	✓	✓	X	✓	✓	✓	X	Ray.	✓	X	X
[36–38]	X	X	✓	X	✓	X	✓	✓	Ray.	✓	✓	✓
[39]	✓	✓	✓	X	X	✓	X	X	Ray.	✓	✓	✓
[40]	✓	X	✓	X	✓	X	✓	✓	Ray.	✓	X	✓
[41]	X	✓	✓	X	X	✓	X	X	Ray.	✓	X	✓
[42–44]	X	X	✓	X	✓	X	X	X	Ray.	✓	✓	✓
[45]	X	✓	✓	X	✓	X	✓	✓	Ray.	X	✓	X
[46]	X	X	✓	X	✓	X	X	X	Ray.	X	✓	X
[47]	X	X	✓	✓	X	X	X	X	Ray.	X	✓	X
[48]	X	✓	✓	X	✓	X	X	X	Ray.	X	✓	X
[49]	X	✓	✓	X	X	✓	X	X	Ray.	X	✓	✓
[50]	X	✓	✓	X	X	✓	X	X	Ray.	X	X	✓
[51]	X	✓	✓	X	X	✓	X	X	Ray.	✓	✓	X
[52]	X	✓	✓	X	✓	X	✓	✓	Ray.	✓	✓	X
[53, 54]	✓	✓	✓	✓	✓	✓	X	X	Nak.	✓	X	X
[55]	✓	✓	X	X	✓	✓	X	X	Nak.	✓	✓	X
[56–61]	X	✓	✓	X	✓	X	X	X	Nak.	✓	X	X
[62]	X	✓	✓	X	✓	X	X	X	Nak.	✓	✓	✓
[63]	X	✓	✓	X	✓	X	✓	✓	Nak.	✓	X	✓
[64]	X	✓	✓	X	✓	X	✓	✓	Nak.	✓	X	X

[65]	X	✓	✓	✓	✓	X	X	Nak.	✓	X	X
[66, 67]	X	X	✓	X	✓	X	X	Nak.	✓	X	X
[68]	X	X	✓	X	✓	X	X	Nak.	✓	✓	X

¹Multi user at the secondary source and destination nodes have been considered.

²Papers dealing with dual-hop have been considered as a multi-hop study.

³For Rayleigh fading channels "Ray." has been used, and for Nakagami- m fading channels "Nak." has been used.

⁴The approximate performance metrics investigation are also considered.

1.4 Motivation of this Work

Cognitive radio aims to better utilise the current frequency spectrum and increasing the spectral efficiency of the network which results in an increase of the user's data throughput. The motivation behind the research in this thesis is to comprehensively investigate the performance behaviour of a more practical scenario of a UCRN. This will lead to a better understanding of the potential advantages of this proposed paradigm. For this purpose, the following network parameters have been considered during performance study: CCI, PU interference, interference power constraint, and SU transmit power constraint. Moreover, the following network conditions have been considered: Multi-hop network, Multi-user, and Multi-antenna. In addition, different statistical channel model have been investigated.

1.5 Contribution of this Work

The aim of this research is to investigate and understand the performance behaviour of a UCRN is subjected to CCI. Different network topology scenarios and parameters are considered and studied. The contribution of this thesis can be summarised as follows:

- An investigation of the performance of an underlay CR network has been carried out when the CCI exists at the secondary receivers. Independent non-identically distributed Rayleigh fading channels between different nodes have been considered in the analysis. For this scenario, the closed-form expressions for the OP, AEP, and EC have been derived. Furthermore, the power optimisation has been investigated to improve the performance behaviour of the intended network. The effect of a multi-user destination has also been considered and analysed.
- The impact of both primary network interference and the CCI have been considered to assess the performance characteristics of a secondary network. Again, the most important performance metrics have been obtained. Furthermore, various network structures have been considered, such as multi-hop network and consideration of multi-antenna schemes. Moreover, at the multi-antenna receiver nodes, different signal combination techniques have been considered and the results have been compared.

- The advantage of the multiple-input multiple-output (MIMO) scheme has been investigated for the UCRN. The effects of primary network interference and CCI are taken into account in the performance study. The exact and approximate expressions for the OP have been obtained. Different antenna selection techniques are considered for the source and destination nodes.
- A more practical fading channel has been considered, which is the Nakagami- m fading channel. For this scenario, the exact and approximate OP performances have been studied. Furthermore, approximate AEP has been investigated.

Finally, the derived expressions in Chapters 3, 4, 5, and 6 have been verified with Monte Carlo simulations, in numerical and simulation results section. It is worth mentioning that the obtained formulas in this thesis are valid for any possible network parameters. Therefore, different case scenarios have been considered to illustrate the performance of UCRN. For example, for the value of the CCI power, fixed value and the aggressive interference case scenario, when the CCI power linearly increases with the transmission power of the UCRN, have been investigated. Furthermore, for the multi-hop UCRN, the channel variances have been calculated based on the two-dimensional topology of the nodes in the network. This is to show the impact of distance between nodes in a multi-hop UCRN and to investigate the advantage of employing multi-hop for performance improvement in the secondary network.

1.6 Publications

The outcome of this thesis has resulted in the following publications [10, 69–74]:

1. J. Hussein, S. Ikki, S. Boussakta, C. Tsimenidis, and J. Chambers, “Performance analysis of a multi-hop UCRN with co-channel interference”, *IEEE Trans. Commun.*, vol. 64, no. 10, pp. 4346-4364, Oct. 2016.
2. J. Hussein, S. Ikki, S. Boussakta, and C. Tsimenidis, “Performance analysis of opportunistic scheduling in dual-hop multi-user underlay cognitive network in the presence of cochannel interference”, *IEEE Trans. Veh. Technol.*, vol. 65, no. 10, pp. 8163-8176, Oct. 2016.

3. J. Hussein, S. Ikki, S. Boussakta, and C. Tsimenidis, "Performance study of opportunistic scheduling in dual-hop multi-user underlay cognitive network", *IET Commun.*, vol. 10, no. 5, pp. 558-566, Mar. 2016
4. J. Hussein, S. Ikki, S. Boussakta, C. Tsimenidis, and Y. Al-Mathehaji, "Study of a multi-relay scheme and co-channel interference within an underlay cognitive radio network", in *Eighth International Conference on Ubiquitous and Future Networks (ICUFN)*, July 2016, pp. 25-29, Vienna, Austria.
5. J. Hussein, S. Ikki, S. Boussakta, and C. Tsimenidis "Exact Outage Performance of the SIMO Cognitive Cooperative Network in the Presence of Co-Channel Interference", in *IEEE Wireless Communications and Networking Conference (WCNC)*, April 2016, pp. 1-6, Doha, Qatar.
6. J. Hussein, S. Ikki, S. Boussakta, and C. Tsimenidis, "Performance study of the dual-hop underlay cognitive network in the presence of co-channel interference", in *IEEE 81st Vehicular Technology Conference, (VTC Spring)*, May 2015, pp. 1-5, Glasgow, UK.
7. J. Hussein, S. Ikki, S. Boussakta, and C. Tsimenidis, "Performance analysis of the opportunistic multi-relay network with co-channel interference", in *Proceedings of the 22nd European Signal Processing Conference (EUSIPCO)*, Sept. 2014, pp. 166-170, Lisbon, Portugal.
8. J. Hussein, S. Ikki, S. Boussakta, and C. Tsimenidis "Impact of Co-Channel Interference on an Underlay Cognitive Radio Network Over Nakagami- m Fading Channels", in *IEEE International Conference on Communications (ICC)*, May 2017, Paris, France, (Accepted).

1.7 Thesis Organisation

The organisation of this thesis is as follows:

- **Chapter Two** presents a basic and essential mathematical background for the performance study in the wireless communication network. For example, channel modelling, statistical representations of a random variable, standard performance metrics, and mathematical modelling of the cognitive radio system.

- **Chapter Three** is devoted to illustrating the impact of CCI on an underlay cognitive radio network. In addition to the derived expressions for system performances, the optimal power allocation is investigated in order to improve the performance behaviour of the underlay cognitive radio network.
- **Chapter Four** The performance characteristics of an underlay cognitive radio network are investigated under both of the primary network interference and the co-channel interference. The advantages of a multi-hop network and using multi-antenna schemes at the receiver nodes are also examined.
- **Chapter Five** MIMO cognitive radio network is considered. The performance of the network is examined considering transmit antenna selection (TAS) technique for the antennas at the source node and maximum ratio combining (MRC) technique at the receiver side.
- **Chapter Six** The Nakagami- m fading channel is considered for all the channels in the primary and secondary network. For this scenario, and under primary network interference and CCI, the performance of the secondary network is investigated.
- **Chapter Seven** gives the overall conclusions of the research in this thesis and discusses the results. Also, it suggests future research extension work that could be carried out.

Chapter 2

Background Theory

A wireless communication network is a system for connecting the intended nodes to enable communication between them through the exchange of messages. It is necessary to consider the fundamental and essential theoretical background of wireless communication networks in order to study and understand their performance behaviour. Therefore, this chapter presents some key knowledge about general wireless communication network performance analysis, specifically for cognitive radio networks.

The system configuration or the node topology plays a crucial role in how the performance of that particular network behaves. Moreover, using diversity techniques for a wireless communication network have a significant advantage of enhancing the system performance. A relay scheme network or cooperative communication system is one of the diversity schemes in which the source node communicates with the destination node through a ‘helping’ node called a relay.

Furthermore, the multi-antenna scheme, another diversity technique, has been a revolution in wireless communication networks in the last decade, providing enormous benefits to the overall system performance. The mathematical modelling of channels for wireless communication networks play a great role in the performance analysis of the whole system. Depending on the node position in the network, the appropriate fading channel can be chosen. The mathematical representation of the channels depends on the type of fading channels considered.

In cognitive radio networks, the system consists of a more complicated structure than the traditional network architecture. Therefore, more robust configurations and analyses are required to ensure sufficient reliability of the proposed systems.

Finally, after gaining knowledge of the considered topology of the network and the detailed information about the physical characteristics of the nodes, and additionally, the recognised channels' statistics and information, some performance metrics can be obtained to predict the behaviour of the network and assess the capability of the proposed system. More details about cooperative communication, channel consideration, and performance metrics will be provided below.

2.1 Signal Transmission in Wireless Network

Generally speaking, the communication between two intended nodes will be either direct communication transmission, or cooperative communication transmission. Direct transmission refers to the communication between the transmitter and receiver nodes directly. On the other hand, in cooperative communication, all available nodes in the network can assist each other in a relay manner to establish the transmission between the intended source and destination nodes. The operation mechanism of this paradigm is based on the broadcast nature of wireless communication signals.

Due to this feature of wireless networks, all the nodes in the network can hear each other in some manner. In fact, when the number of nodes is more than two, cooperation communication is possible [75, p. 30]. There are several advantages of employing this paradigm [76, p. 3]. First, the system can achieve similar benefits as the MIMO system; it results in an enhancement of the communication capacity, speed and overall performance. In addition, cooperative communication reduces the battery consumption, which results in an extension of the network's lifetime. Furthermore, it can extend the coverage area of the transmission [76, p. 3].

However, there are some disadvantages of employing the cooperative communication scheme; for example, it will increase the complexity of the overall system, increase the cost, and require more overhead signalling compared to the use of direct transmission. It is worth mentioning that in the standardisations of the 3GPP LTE-A, cooperative relay communication has been considered, and it is expected to play a vital role in the next generation of mobile communication [77, p. 332].

There are several protocols that can be used at the relay node to process the received signal from the source node and forward it to the destination node. For example, amplify-and-forward (AF), decode-and-forward (DF), and compress-and-forward [76, p. 128]. The transmission in the cooperative network performs within

two orthogonal time slots, i.e., phases. To avoid interference between the transmission signals, Time Division Multiple Access (TDMA) or Frequency Division Multiple Access (FDMA) can be used [76, p. 121]. It is worth noting that both AF and DF are the most two common relay protocol schemes that are used to implement the cooperative communication between the source and destination nodes [78, p. 119].

2.1.1 Amplify-and-Forward (AF)

In AF relay protocol, the relay node receives the signal from the source node, then, amplifies it and forwards it to the destination node. In terms of simplicity, this technique is considered the simplest relay method to implement as it does not require complex signal manipulation at the relay node [77, p. 331].

2.1.2 Decode-and-Forward (DF)

In DF or regenerative relay protocol, the relay node decodes the received signal from the source node, then, encodes and forwards it to the destination node. This relay protocol can achieve close to the optimal performance when the channel between the source and the relay is excellent [75, p. 37]. In terms of complexity, this protocol is more complex than the AF protocol as the received signal requires manipulation before it is forwarded to the destination node.

2.2 Statistical Analysis of Random Variable

Since the wireless communication network is the intended system to deal with its performance behaviour, and includes different entities and variables, it is necessary to have some basic knowledge of the statistical and mathematical representations of these possible random variables in the network. There are two kinds of a random variable (RV); continuous and discrete. In this thesis, the focus is on the continuous RV and hereafter whenever RV is mentioned, it refers to the continuous random variable. The continuous random variable is a variable that can have infinite values at reasonable intervals [79].

Any random variable can be defined statistically by two parameters known as mean and variance of that RV. The mean or the “expected value” represent the average of a random variable. For a RV X , the mathematical representation of

the expected value of X is $\mathbb{E}[X]$ or μ , where $\mathbb{E}[\cdot]$ is the expectation operator. The variance of a random variable is a positive number; it represents how the distribution is spread around the mean value [79]. The mathematical representation of a variance of RV X is $\text{Var}(X) = \sigma^2 = \mathbb{E}[(X - \mathbb{E}[X])^2] = \mathbb{E}[X^2] - (\mathbb{E}[X])^2$.

There are three popular distribution representations of a continuous random variable, which are: PDF, CDF, and MGF. If X represents the intended RV under investigation, then its PDF is represented by $f_X(x)$, and the corresponding CDF and MGF by $F_X(x)$ and $M_X(x)$, respectively. The PDF, CDF, and MGF can be obtained interchangeably from each other. These different representations for the RV are important because they give various options to assess the performance of the intended network based on the suitability of using them.

- Cumulative distribution function (CDF):

The CDF of RV X is defined as the probability that X is less or equal to a particular predefined value. This can be represented by:

$$F_X(x) = \Pr(X \leq x) = \int_{-\infty}^x f_X(t)dt, \quad (2.1)$$

where $\Pr(\cdot)$ is the probability operator.

- Probability density function (PDF):

The PDF is considered the preferred function for representing the distribution of a random variable. For a continuous RV X that has a density of f_X , the following mathematical relation can be written [80, p. 927]:

$$\int_{\alpha}^{\beta} f_X(x)dx = \Pr(\alpha \leq X \leq \beta), \quad (2.2)$$

where α and β are the intervals at which the probability of X exists. Moreover, the PDF of the RV X can be obtained by taking the first derivative of the corresponding CDF:

$$f_X(x) = \frac{d}{dx}F_X(x). \quad (2.3)$$

- Moment generating function (MGF):

The MGF is another representation of the probability distribution of a random

variable. The MGF of RV X can be defined as:

$$M_X(s) = \mathbb{E} [e^{sX}], \quad (2.4)$$

where $\mathbb{E}[\cdot]$ represents the expectation operator. In addition, it can be represented in terms of the PDF as:

$$M_X(s) = \int_{-\infty}^{\infty} e^{sx} f_X(x) dx. \quad (2.5)$$

2.3 Wireless Fading Channel and its Statistical Modelling

The radio signal in a wireless communication is a complex phenomenon that suffers from different effects (multipath and shadowing) due to the fluctuation of amplitude and phase of the signal until arriving at the intended destination [9, p. 17]. The statistical measurements of the wireless fading channels are necessary to understand the behaviour of the system [81, p. 34]. In fact, without a simplified modelling of the wireless system under consideration, the investigation and comparison of different systems becomes impossible [81, p. 35].

Therefore, a statistical, probabilistic modelling approach for the wireless communication channels is essential to provide insights about the intended or proposed wireless system [81, p. 35]. Depending on the conditions and suitability of the network under investigation, different models for the channels can be considered or adopted. In this section, some information about wireless communication channels and relevant statistical models is presented that can be used to represent wireless communication channels.

The wireless channels can be classified into two categories based on the spatial scale variations of the signal between the transmitter and the receiver nodes; large-scale variation and small-scale variation [81, p. 10]. The large-scale variation is due to the path loss that the signal suffers, which is mainly a function of distance, and shadowing, which is due to large objects in the signal propagation path. On the other hand, a small-scale variation is due to the combination of multiple signals from multiple paths between the transmitter and receiver nodes that result in con-

structive and destructive phenomena in the final version of the received signal. This phenomenon is known as ‘multipath fading’. Due to the multipath fading channel, the transmitted signal suffers from variation in the time-domain and power delay spread [82, p. 11]. The multipath fading is divided into ‘slow fading’ and ‘fast fading’, depending on the change in the time domain of the transmitted signal. Furthermore, according to the severity in the power delay spread of the transmitted signal, it is classified as ‘frequency flat fading’ and ‘frequency selective fading’ [82, p. 11].

The wireless channel is said to be slow fading if its *coherence time* is much larger than the symbol period of the transmitted signal. Conversely, the channel is called fast fading [81, p. 34]. The coherence time is the period that the response of the channel stays highly correlated. In fact, slow and fast fading characteristics are mainly dependent on the Doppler shift phenomenon of signal propagation, which is due to the relative motion of the intended transmitter and receiver nodes [82, p. 15].

In real world applications, most of the recent and arising wireless systems are working in a slow fading channel environment. This is to ensure the provision of a relatively high data rate [82, p. 16]. The wireless channel is said to be frequency-flat when the *delay spread* is much smaller than the symbol period of the transmitted signal, or the *coherence bandwidth* is much larger than the signal bandwidth. Inversely, when the delay spread is larger than the symbol period, the channel is called frequency-selective [81, p. 34]. The delay spread is dependent on the power delay profile, which is the distribution of the average signal power on the delay axis, and the coherence bandwidth is the bandwidth to which the frequency response of the channel remains highly correlated [82, p. 12].

The frequency-flat model is used in the design of most of the current wireless technology; for instance, multi-user nodes scheduling, multi-antenna systems, and diversity combining techniques. This is due to the fact that, with the advantages of new technology such as orthogonal frequency-division multiplexing (OFDM), a wideband frequency-selective fading channel is converting to a finite number of parallel frequency-flat fading channels [82, p. 12]. Throughout this thesis, the focus will be on the frequency-flat fading channel model in the performance investigation.

2.3.1 Rayleigh Fading Channels

Rayleigh fading is the simplest and most common statistical model representation of the wireless multipath fading channel. In this model, the envelope of the signal is assumed to be changing randomly due to the scattering phenomenon of the transmitted signal. When a large number of scattered signals arrive at the receiver side, using the Central Limit Theorem [76, p. 17], [82, p. 13], the fading channel coefficients can be modelled as a circularly symmetric complex Gaussian random variable, which has mean zero and variance σ^2 .

It is worth mentioning that the random variable consists of two uncorrelated components, named as ‘in-phase’ and ‘quadrature’ components. They both have zero mean and equal variance of σ^2 . The desired random variable for performance investigation is the envelope of the channel coefficient, which follows the Rayleigh distribution [76, p. 18]. Let X represent the fading channel coefficient, therefore, its PDF can be represented as:

$$f_X(x) = \frac{x}{\sigma^2} e^{-\frac{x^2}{2\sigma^2}}, \quad x \geq 0. \quad (2.6)$$

In performance analysis, channel power gain is an important random variable that is related directly to the fading channel coefficient. The channel power gain is defined as the square of the magnitude of the channel coefficient. For the above scenario the channel power gain will be $|X|^2 = Y$ that follows an exponential distribution [76, p. 18].

$$f_Y(y) = \frac{1}{2\sigma^2} e^{-\frac{y}{2\sigma^2}}, \quad y \geq 0. \quad (2.7)$$

Furthermore, in the case of existence of multiple independent and identical distributed (i.i.d.) channel gains, the sum of them is the Chi-square random variable with $2L$ degrees of freedom, where L represents the available number of i.i.d. channel gains in the resulting sum, i.e., $\sum_{i=1}^L |X_i|^2 = Z$. The resulting PDF is [76, p. 18]:

$$f_Z(z) = \left(\frac{z}{\sigma^2}\right)^L \frac{z}{(L-1)!} e^{-\frac{z}{\sigma^2}}, \quad z \geq 0. \quad (2.8)$$

By observing the above PDF, it can be seen that it follows the gamma distribution. Moreover, in the scenario where channel gains are independent and non-identically

distributed (i.n.d.), it will be more convenient to deal with MGF instead of PDF. Therefore, the resulting MGF expression is expressed as [82, p. 29]:

$$\begin{aligned} M_Z(s) &= \prod_{i=1}^L M_{X_i}(s) \\ &= \prod_{i=1}^L (1 - s\sigma_i^2)^{-1}, \end{aligned} \quad (2.9)$$

where $M_{X_i}(s)$ is the corresponding MGF of $f_{X_i}(x)$.

2.3.2 Rician Fading Channels

The existence of the line of sight (LOS) plays a big role in reshaping the Gaussian random variable. For instance, the envelope of the resulting in-phase and quadrature phase components has a mean which is not zero. Therefore, the PDF of the instantaneous channel amplitude follows the Rician distribution and can be represented as [76, p. 21]:

$$f_X(x) = \frac{x}{\sigma^2} e^{-\frac{x^2+s^2}{2\sigma^2}} I_0\left(\frac{xs}{\sigma^2}\right), \quad x \geq 0, \quad (2.10)$$

where $I_0(\cdot)$ is the zeroth order modified Bessel function of the first kind [83, eq. (10.32.1)]. $2\sigma^2$ and s^2 represent the channel power gains of the non-LOS and LOS components, respectively. Furthermore, the total channel power gain from both non-LOS and LOS components is represented as $\Omega = s^2 + 2\sigma^2$, and the Rician fading parameter is defined by $K = \frac{s^2}{2\sigma^2}$.

By observing the PDF of the Rician distribution, it can be seen that when $s = 0$, the PDF reduces to the Rayleigh scenario, since $I_0(0) = 1$. In the Rician distribution scenario, the channel power gain, i.e., $|X|^2 = Y$, has a non-central χ^2 distribution, where the PDF can be represented by [82, p. 14]:

$$f_Y(y) = \frac{K+1}{\Omega} e^{-(K+\frac{(K+1)y}{\Omega})} I_0\left(2\sqrt{\frac{K(K+1)y}{\Omega}}\right), \quad y \geq 0. \quad (2.11)$$

2.3.3 Nakagami- m Fading Channels

A more generalized fading channel model is the Nakagami- m . Similar to the Rician model, in this statistical model the LOS component is also counted in the PDF of the

channel distribution representation. The PDF of the envelope of the Nakagami- m distribution is represented as [76, p. 21]:

$$f_X(x) = \frac{2m^m x^{2m-1}}{\Gamma(m)\Omega} e^{-\frac{mx^2}{\Omega}}, \quad x \geq 0. \quad (2.12)$$

where m is the Nakagami severity fading parameter, which has a value of $m \geq 0.5$. $\Gamma(\cdot)$ represents the gamma function which is defined as $\Gamma(z) = \int_0^\infty e^{-t} t^{z-1} dt$, in [83, eq. (5.2.1)].

Note that, when $m = 1$ and $s = 0$, the PDF of the Nakagami distribution reduces to the Rayleigh distribution. Furthermore, when the parameter m is less than one, the channel is much more severe than the Rayleigh case. On the other hand, when $m > 1.0$ the channel is considered less severe than the Rayleigh, and when the value of m approaches ∞ , the distribution reduces to the no fading scenario.

A tight relation can be established between Nakagami and Rician distribution through $m = \frac{(K+1)^2}{2K+1}$. The channel power gain for the Nakagami- m fading distribution $|X|^2 = Y$, is written as [82, p. 14]:

$$f_Y(y) = \left(\frac{m}{\Omega}\right)^m \frac{y^{m-1}}{\Gamma(m)} e^{-\frac{my}{\Omega}}, \quad y \geq 0. \quad (2.13)$$

2.4 Mathematical Modelling of Cognitive Radio Networks

The general and straightforward UCRN can be considered as the existence of the primary and secondary transceiver nodes, as shown in Fig 2.1. In UCRN, the QoS of the primary network should be protected and cannot be compromised. To realise the protection to the primary system, the secondary transmitter should adjust its transmission power based on two factors; *a*) the maximum level of interference acceptable at the primary receiver node, and *b*) the channel condition between the secondary transmitter and the primary receiver.

Furthermore, the secondary transmitter has a limit to its capability of power transmission, due to battery size and capacity. The above statement can be translated mathematically, and the allowable transmission power at the secondary transmitter node can be represented as:

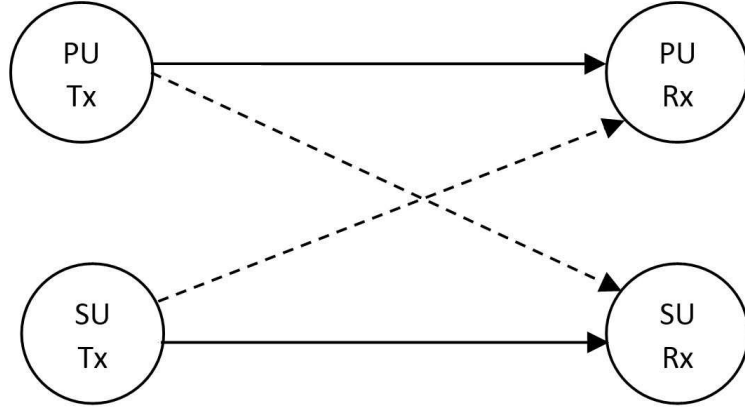


Figure 2.1: Typical CRN showing the primary and secondary transceivers; solid lines represent the desired data links, and the dashed lines represent the interference links. T_x and R_x represent the transmitter and receiver nodes, respectively.

$$E_s = \min \left(\frac{I_{\max}}{|h_{sp}|^2}, P_s \right), \quad (2.14)$$

where E_s is the power that is allowed to be transmitted from the secondary transmitter node. I_{\max} represents the maximum acceptable interference at the primary receiver node, this is known as the *interference power constraint*. $|h_{sp}|^2$ is the channel power gain of the fading channel between the secondary transmitter and the primary receiver nodes. P_s represents the maximum power constraint that the secondary transmitter can use.

The received signal at the secondary receiver node can be expressed as¹:

$$y_r = \sqrt{E_s} h_{sr} x + I_p + n_r, \quad (2.15)$$

where h_{sr} is the fading channel coefficient between the secondary transmitter and the secondary receiver nodes, x is the intended transmitted signal message to the secondary receiver. I_p represents the interference term from the primary network, and n_r is the additive white Gaussian noise (AWGN), which is added to the received signal at the secondary receiver node.

From the above equation, SINR can be obtained, which is an essential and desired random variable that can be used to investigate the network performance. For the

¹The time notation has not been written in the equation for the purpose of simplicity.

scenario above, the SINR for the secondary system¹ is defined as:

$$\begin{aligned}\gamma_{\text{eq}} &= \frac{\text{signal power}}{\text{interference power} + \text{noise power}} \\ &= \frac{\min\left(\frac{I_{\text{max}}}{|h_{sp}|^2}, P_s\right)}{\gamma_{I_p} + N_0} |h_{sr}|^2,\end{aligned}\tag{2.16}$$

where γ_{eq} is the equivalent SINR for the secondary UCRN. In addition, γ_{I_p} is the instantaneous interference power from the primary network. Depending on the distributions considered for the fading channels in the network, the mathematical expressions such as PDF, CDF, and MGF for the SINR can be derived. Finally, one of the obtained expressions can be used, according to mathematical suitability, for investigating the network performance.

2.5 Mathematical Representation of the CCI

In general, CCI signals are from neighbouring clusters. Therefore, the distance from the CCI sources to the affected receiver node is relatively long. As a result, it can be considered that the CCI signals have the same average power at a particularly affected node [10, 84]. Thus, the CCI signals can be considered as independent and identically distributed (i.i.d.), in terms of their average values, at the intended receiver node.

In the case where the Rayleigh fading is considered, the channel power gain of each individual CCI signal is modelled as an exponential distribution. The sum of these i.i.d. random variables is a chi-square, which follows the gamma distribution [76, p. 18], $Z = \sum_{i=1}^L \gamma_{c_i}$, $Z \sim \chi_L^2$, where L is the number of CCI signals at the intended receiver node, $\gamma_{c_i} = \frac{E_c}{N_0} |f_{c_i}|^2$ is the instantaneous interference-to-noise ratio (INR), E_c represents the energy of the CCI signal, N_0 is the power spectral density of the AWGN, and $|f_{c_i}|^2$ is the channel gain for the CCI fading channel f_c .

Therefore, the PDF of Z can be mathematically represented as:

$$f_Z(z) = \frac{z^{L-1}}{\bar{\gamma}_c^L \Gamma(L)} \exp\left(-\frac{z}{\bar{\gamma}_c}\right),\tag{2.17}$$

¹Throughout this thesis, the focus is on the secondary network performance, since the primary network performance is similar to the ordinary systems that have been well investigated in the literature.

where $\bar{\gamma}_c$ is the average INR of each of the CCI signal. Furthermore, for the scenario where Nakagami- m fading channels have been considered, the PDF of random variable Z can be written as:

$$f_Z(z) = \left(\frac{m}{\bar{\gamma}_c}\right)^{mL} \frac{z^{mL-1}}{\Gamma(mL)} \exp\left(-\frac{m}{\bar{\gamma}_c}z\right). \quad (2.18)$$

In the scenario of the independent non-identical Rayleigh fading channels considered for the individual CCI signals, i.e., where the average CCI powers are assumed to be non-identical, the mathematical representation becomes more complicated, especially for generalized L number of CCI signals. However, if the number is known, it is possible to obtain the mathematical expression for the equivalent PDF of the sum of these independent and non-identically distributed exponential RVs. For example, if the number of CCI signals is two, the resulting PDF at the desired receiver node can be represented as:

$$f_Z(z) = \frac{1}{\bar{\gamma}_1 - \bar{\gamma}_2} \left(e^{-\frac{z}{\bar{\gamma}_1}} - e^{-\frac{z}{\bar{\gamma}_2}} \right), \quad (2.19)$$

where $\bar{\gamma}_1$ and $\bar{\gamma}_2$ represent average power gains for the first and second CCI signals, respectively. Moreover, when the number of CCI signals is three, the resulting PDF at the desired receiver node can be represented as:

$$f_Z(z) = \frac{1}{\bar{\gamma}_1 - \bar{\gamma}_2} \left[\frac{\bar{\gamma}_1}{\bar{\gamma}_1 - \bar{\gamma}_3} \left(e^{-\frac{z}{\bar{\gamma}_1}} - e^{-\frac{z}{\bar{\gamma}_3}} \right) + \frac{\bar{\gamma}_2}{\bar{\gamma}_3 - \bar{\gamma}_2} \left(e^{-\frac{z}{\bar{\gamma}_3}} - e^{-\frac{z}{\bar{\gamma}_2}} \right) \right], \quad (2.20)$$

where $\bar{\gamma}_3$ represents the average power gain for the third CCI signal. It can be observed that as the number of non-identical CCI signals increase the resulting equivalent PDF becomes more complicated mathematically. Therefore, for the purpose of mathematical convenience, throughout this thesis, the identical channel power gains for the CCI have been considered.

2.6 Common Performance Criteria

In the sections below, the most important performance metrics for evaluating any wireless communication network are discussed. In addition, mathematical formulas for determining these metrics are provided.

2.6.1 Outage Probability (OP):

The OP is the most common performance criteria for any wireless communication system. It is the probability that the intended RV is less than or equal to a predefined threshold value [9, p. 5]. In the case of considering the SNR¹ as an intended RV, then γ_{th} will represent the threshold value, i.e., SNR-threshold. In addition, this threshold value can be represented in terms of the rate of the transmission R [85, p. 183].

$$\begin{aligned} \text{OP} &= \Pr(\log_2(1 + SNR) \leq R), \\ &= \Pr(SNR \leq \gamma_{\text{th}}). \end{aligned} \quad (2.21)$$

where $\log_2(\cdot)$ represents the logarithm to the base 2, and $\gamma_{\text{th}} = 2^R - 1$.

It can be observed that the outage probability can be directly obtained from the corresponding CDF by substituting variable x with γ_{th} . Furthermore, the OP can be represented in terms of the PDF of the equivalent SNR [82, p. 20]:

$$\text{OP} = \int_0^{\gamma_{\text{th}}} f_{\gamma_{\text{eq}}}(\gamma) d\gamma = F_{\gamma_{\text{eq}}}(\gamma_{\text{th}}). \quad (2.22)$$

2.6.2 Average Error Probability (AEP):

The second important performance metric is the AEP. It is especially vital when the calculation of the number of bit or symbol errors is required to be known for the system under consideration. It depends on two factors; *i*) characteristics of the SNR, and *ii*) the modulation scheme that has been employed for the data transmission.

The AEP over a slow flat fading channels can be found by averaging the error probability in AWGN over the fading distribution [85, p. 184]. Mathematically, this can be represented as [82, p. 21]:

$$\bar{P}_b = \int_0^{\infty} P_b(\gamma) f_{\gamma_{\text{eq}}}(\gamma) d\gamma, \quad (2.23)$$

where \bar{P}_b represents the AEP, and P_b is the error probability in AWGN system, where the considered SNR is γ [82, p. 21]. γ_{eq} represents the equivalent SNR for the intended network. $f_{\gamma_{\text{eq}}}(\gamma)$ is the PDF of the equivalent SNR.

¹Here, SNR is used as a general representation, it can be replaced with SINR according to the required situation.

Note that for several Gray bit-mapped constellations employed in practical systems, P_b is in the form of $a Q(\sqrt{2b\gamma})$ [85, p. 180], where a and b are constants depending on the constellation used [85, Table 6.1, p. 180], and $Q(\cdot)$ is the Gaussian Q -function. For example, $a = 2$ and $b = 0.5$ for the quadrature phase shift keying (QPSK). Hence, the average error probability conditioned on a specific output SNR can be written as:

$$\bar{P}_b = \frac{a}{2} \int_0^{\infty} \operatorname{erfc}(\sqrt{b\gamma}) f_{\gamma_{\text{eq}}}(\gamma) d\gamma, \quad (2.24)$$

where $\operatorname{erfc}(\cdot)$ is the complementary error function defined in [83, eq.(7.2.2)]. The AEP can be studied using either the PDF or the CDF of the equivalent SNR, γ_{eq} .

However, it is not always possible to get a closed-form solution using the above formula. Especially in the scenario where interference is considered in the system. In addition, the AEP can be represented in terms of the CDF as [84]:

$$\bar{P}_b = \frac{a}{2} \sqrt{\frac{b}{\pi}} \int_0^{\infty} \frac{e^{-b\gamma}}{\sqrt{\gamma}} F_{\gamma_{\text{eq}}}(\gamma) d\gamma, \quad (2.25)$$

where $F_{\gamma_{\text{eq}}}(\gamma)$ is the CDF of the equivalent SNR. Furthermore, the AEP can be measured in terms of the MGF of the equivalent SNR. For example, the AEP can be expressed in terms of the MGF as follows [85, p. 189]:

$$\bar{P}_b = \frac{a}{\pi} \int_0^{\frac{\pi}{2}} M_{\gamma_{\text{eq}}}\left(-\frac{b}{\sin^2(\theta)}\right) d\theta, \quad (2.26)$$

where $M_{\gamma_{\text{eq}}}(\cdot)$ is the MGF of the equivalent SNR. Moreover, the exact AEP for different M -ary phase shift keying (MPSK) coherent modulation schemes, can be obtained using [85, p. 189]:

$$\bar{P}_b = \frac{1}{\pi} \int_0^{\frac{(M-1)\pi}{M}} M_{\gamma_{\text{eq}}}\left(-\frac{b}{\sin^2(\theta)}\right) d\theta, \quad (2.27)$$

where $b = \sin^2(\frac{\pi}{M})$. Table 2.1 provides the calculation of modulation constants a and b , for different constellations in a coherent detection system [85, Table 6.1, p. 180], [86, Table 1, p. 7]. In Table 2.1, (BFSP) is the Binary Frequency Shift

Table 2.1: Instantaneous symbol error probability (P_{ser}) and bit error probability (P_{ber}) for coherent detection modulations and their modulation constant values

Modulation	a	b	k	P_{ser}	P_{ber}
BFSK	1	0.5			
BPSK	1	1		$a Q(\sqrt{2 b \gamma_s})$	$\frac{a}{k} Q(\sqrt{2 b k \gamma_b})$
MPSK	2	$\sin^2\left(\frac{\pi}{M}\right)$	$\log_2(M)$	Or	Or
MPAM	$2\frac{(M-1)}{M}$	$\frac{3}{(M^2-1)}$		$\frac{a}{2} \text{erfc}(\sqrt{b \gamma_s})$	$\frac{a}{2k} \text{erfc}(\sqrt{bk \gamma_b})$
MQAM	4	$\frac{3}{2(M-1)}$			

Keying, (BPSK) is the Binary Phase Shift Keying, (MPSK) M-ary Phase Shift Keying, (MPAM) is the M-ary Pulse Amplitude Modulation, and (MQAM) is the M-ary Quadrature Amplitude Modulation. Furthermore, $\gamma_b = \frac{E_b}{N_0} = \frac{\gamma_s}{k}$, and $\gamma_s = \frac{E_s}{N_0}$, where E_b is the energy per bit, and E_s is the energy per symbol. In addition, N_0 is the noise variance.

2.6.3 Ergodic Capacity (EC):

The EC, or Shannon capacity [85, p. 98], is an essential performance criterion for any communication system [49]. It is a measure of the achievable data rate for the considered network, and it gives a basic theoretical understanding of the benefits of the system in terms of the data rate, which is an important measurement for any communication network. The ergodic capacity of flat fading channels can be mathematically obtained by averaging the Shannon capacity for an AWGN channel over the distribution of the equivalent fading SNR [85, p. 101]. It is measured in bits/sec/Hertz.

Therefore, the ergodic capacity can be determined using the PDF of the equivalent SNR [49], [85, p. 101]:

$$\text{EC} = \int_0^{\infty} \ln(1+x) f_{\gamma_{\text{eq}}}(x) dx. \quad (2.28)$$

The above equation can also be represented using the CDF of the equivalent SNR of the network as:

$$\text{EC} = \int_0^{\infty} \frac{\bar{F}_{\gamma_{\text{eq}}}(x)}{1+x} dx, \quad (2.29)$$

where $\bar{F}_{\gamma_{\text{eq}}}(x) = 1 - F_{\gamma_{\text{eq}}}(x)$ is the complementary equivalent CDF.

Besides the above mentioned, other performance metrics can indicate some specific details about the wireless network status. For example, diversity gain, coding gain, and array gain [87, p. 112]. The diversity gain is related to the diversity scheme that is employed in the system to understand to what extent the network has been enhanced. One of the most common and beneficial diversity schemes is the multi-antenna scheme. In fact, it is measured through the slope of the error probability plot versus the transmission SNR.

The coding gain is related to the designed code for the transmitted signal of a specific network; it increases the effectiveness of the network's SNR. The coding gain is measured based on the improvement that the system performance has achieved when specific coding is used for the signal transmission. The array gain is related to the power advantage of the signal combination in the multi-antenna scheme, at the transmitter and/or receiver nodes. Similar to the coding gain, the array gain has the advantage of increasing the effective SNR.

2.7 Chapter Summary:

In this chapter, some basic theoretical background on wireless communication networks was presented which is crucial for understanding the performance study topic in general, and specifically the research that has been done throughout this thesis. First, the cooperative communication network strategy was discussed. Then, the random variable was defined, and its statistical representation was presented. Furthermore, mathematical representations for common wireless channel modelling were provided. In addition, mathematical representations for the general underlay cognitive radio network and CCI signals were provided. Finally, formulas for evaluating some important performance criteria were presented.

Chapter 3

Impact of CCI On the Performance of an Underlay Cognitive Network

3.1 Introduction

The basic principle of a UCRN is the co-existence of both PUs and SUs in the same area. In this scenario, the SUs are allowed to take advantage of the radio spectrum as long as they consider the QoS criteria of the PU. The QoS consideration leads to a limitation of the transmission power at the SU transmitter nodes. Therefore, the SUs transmitter nodes could have the ability to transmit at a higher power, but due to the constraint on their transmission power they might not take advantage of the full power limit. Cooperative communication [88] is a technique that allows a source node to communicate with a destination node through a relay node by taking advantage of the broadcast nature of wireless transmission. It has several advantages; for example, providing diversity links, extending the coverage of transmission, improving the network lifetime, reducing the transmission power, etc. [89, p. 628]. Transmission with relatively less power through cooperative communication could be an important characteristic to combat the transmission power constraint on the SUs transmitter nodes and enhance the overall performance of the CRN [10]. Cooperative communication has different scheme names depending on the protocol that is used at the relay node. The most two common protocols are AF and DF. In an AF, the relay node amplifies the received signal from the source node, then, forwards

it to the destination node. On the other hand, in a DF relay protocol, the relay decodes the received message from the source node, then encodes it and forwards to the destination node. It is worth noting that in terms of simplicity, AF is simpler than DF, as it requires a less complex relay configuration [90]. However, with regard to noise reduction in the propagation, DF relay protocol outperforms the AF relay protocol.

3.1.1 Literature Review

In the last decade, the study of CR has become an interesting research area for numerous researchers [1,5,6,8]. More precisely, in the area of performance analysis, many researchers have started investigating the behaviour of the CRN [51,66]. This is due to the fact that any proposed network paradigm can be better understood through investigation of its performance and the demonstration of its advantages and contributions to future wireless communication networks. In this respect, Duong et al. [66] investigated the OP of the dual-hop single user AF cognitive cooperative network by considering a single primary user and over Nakagami- m fading channels. In [91], a study was carried out on the performance behaviour of the uplink cognitive cellular networks using an opportunistic secondary user selection that causes the lowest interference to the primary user. In addition, the author in [49] investigated the effect of MRC on the single user multi-antenna receiver cognitive radio network. In this work, the asymptotic formulas for the AEP and the system EC have been obtained. In [42], the performance of the multi-hop DF underlay CR network was investigated considering Rayleigh fading channels. In this study, the authors have neglected the transmission power constraint on the secondary transmitter nodes. In [25], the opportunistic selection technique was used to improve the outage performance of the multi-source UCRN.

Huang et al. [53], studied the outage performance of the multi-user dual-hop DF underlay CR over Nakagami- m fading channels in the presence of the primary transmitter. In their calculations, SNR and SINR-based scheduling algorithms have been used to derive the outage performance formula. The authors of [36] investigated the OP of the multi-relay spectrum sharing network. The best relay selection technique was employed, such that it enhances the overall performance of the network. In their analysis, the power limit constraint on the secondary transmitter nodes was

not considered. The outage and error probability of a MIMO underlay cognitive radio network was investigated in [51]. To improve the performance of the secondary network, the MRC technique was used at the secondary receiver nodes. In another study [92], the throughput analysis of the dual-hop DF multi-antenna CR network was investigated.

Moreover, in further study [93], the TAS with MRC technique was used to evaluate the OP of the dual-hop DF MIMO underlay cognitive networks. The impact of the primary transmitter and the imperfect channel state information were considered in their calculation. The OP, AEP and the EC performance were investigated in [62]. A single destination user node was considered and interference on the secondary network was not considered. The authors of [27] investigated the outage performance of the multi-user spectrum sharing network. In their analysis, the selection combining method was used to improve the performance of the secondary network. In [22], the OP, average outage duration, and the average outage rate for the multi-relay underlay CR network were studied by using the best relay selection method. In [94], the outage performance of the dual-hop DF CR was investigated in the presence of a single node at each the source, relay, and destination.

3.1.2 Contributions

In most of the previous studies in the area of UCRN, the outage performance has been extensively studied for different system models. In addition, few works have investigated the error probability and/or capacity performance. However, the impact of the CCI on the UCRN has not been studied. Furthermore, a detailed investigation of the error probability and the capacity performance for the opportunistic multi-user cooperative CR has not been carried out before. Moreover, the adaptive power allocation under the total transmission power constraint and the impact of CCI have not been studied. In fact, the consideration of CCI is indeed necessary because of the aggressive reuse of frequency channels for high spectrum utilization in different wireless systems, and the multi-user dual-hop underlay CR network is no exception. Due to the broadcast nature of wireless signal transmissions, interference always exists over a wide range of frequency bands in almost all practical wireless communication systems. For example, interference may come from other authorized users of the same spectrum, or from other frequency channels injecting energy into

the channel of interest [70].

The contributions of this chapter can be seen as:

- Consideration of the following network conditions in the performance investigation for the secondary network: CCI, secondary transmission power constraint, interference power constraint, and the AWGN.
- Expression derived for the CDF of the per-hop equivalent SINR.
- Derivation of exact and closed-form expressions for both the OP and AEP, and examining their performance behaviour.
- Investigation of the system EC.
- Study of the performance of the secondary network where a multi-user at the destination is considered.
- Examination of the benefit of considering adaptive power allocation instead of equal power allocation.

3.1.3 Chapter Organization

First, the system model is described and mathematically represented. Then, the per-hop equivalent SINR is obtained. In addition, the statistical distributions are derived and discussed. Furthermore, the exact expressions for the OP, AEP and the system EC are obtained. Then, approximate expressions for the OP and the AEP are derived. Moreover, the advantage of optimal power allocation is investigated. Some numerical and simulation examples are also provided to support the derived results and show the cognitive radio performance. Finally, the summary and conclusions regarding this chapter are provided.

3.2 System Model

In the following sections, the network components are described. Then, mathematical representations of the received signals are presented and the formulas for the equivalent SINRs are obtained. In addition, the multi-destination user scenario is discussed and the mathematical equations for this scenario are provided.

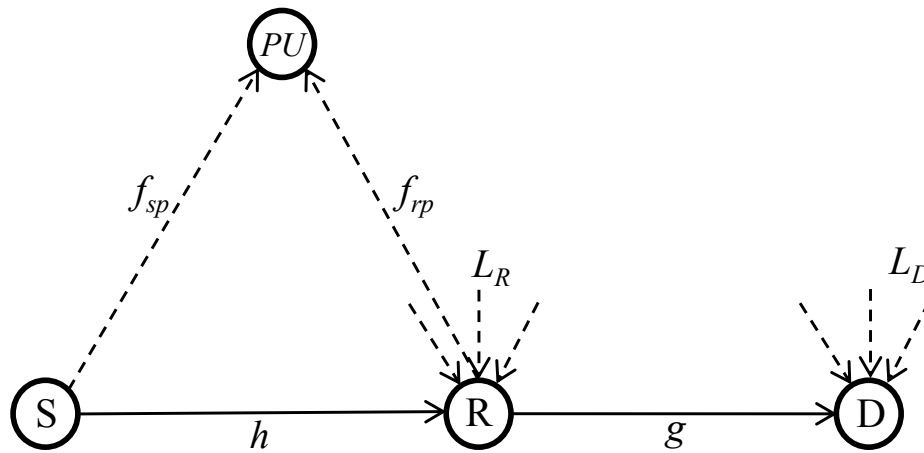


Figure 3.1: The general system model used for analysis.

3.2.1 Network Description

Fig. 3.1 shows the system model under consideration. It is considered that the cognitive network consists of a source node (S), a relay node (R), a destination user (D), and a single primary user node. In addition, all the nodes in the system are equipped with a single antenna and operate in a half-duplex mode. Furthermore, the relay node operates based on the decode-and-forward protocol. In the system model, it is assumed that the impact of the primary transmitter on the secondary network in this specific cell is neglected. One of the possible examples of this system model is when the same network provider controls both primary and secondary nodes, where the level of interference with the secondary users can be controlled within a reasonable range. This can be obtained by managing the nodes according to their position, or it could be possible to interpret the interference as a further addition to the existing noise level at the secondary user receiver [62]. Moreover, the impact of other transmitter nodes in the neighbouring cells cannot be ignored. The interference from outside of the considered cell is regarded as the CCI, which is unavoidable in almost all wireless communication networks. Another possible example of the system model is to represent the impact of the primary transmitter and the other surrounding transmitter nodes as the CCI. This is due to the fact that the CCI could be from any other frequency channels injecting energy into the channel of interest. Furthermore, L_R is the total number of interferers that affect the relay node, and L_D denotes the total number of interferers that affect the destination user node.

In addition, it is assumed that there is no direct link between the secondary

source and destination nodes [53], (i.e., the communication is performed through the relay node only). Moreover, I_{\max} is defined as a threshold interference value, which is the maximum tolerance of interference that the secondary transmitter nodes can produce at the primary receiver node [70,95]. The channels in the dual-hop communication are assumed to be affected by independent non-identical slow Rayleigh fading channels. h and g are the desired channel coefficients between the secondary source-relay and secondary relay-destination nodes, respectively, and f_{sp} and f_{rp} are the interference channel coefficients between secondary source-primary receiver and secondary relay-primary receiver, respectively. Therefore, the corresponding channel power gains can be represented as $|h|^2$, $|g|^2$, $|f_{sp}|^2$, and $|f_{rp}|^2$ that follow the exponential distribution with mean powers of σ_h^2 , σ_g^2 , $\sigma_{f_{sp}}^2$ and $\sigma_{f_{rp}}^2$, respectively. As stated before, the transmission power constraint on the secondary transmitter nodes is also considered. For example, P_s represents the maximum power that the secondary source can achieve. Similarly, P_r is the maximum power that the secondary relay can use.

3.2.2 Mathematical Representation

In a dual-hop decode-and-forward relay protocol, the transmission is performed within two phases (i.e., time slots). In the first phase of transmission, the source node transmits the intended message signal to the relay node using its permitted power. Therefore, the received signal at the relay can be represented as:

$$y_r = \sqrt{E_{us}}hx + \sqrt{E_{IR}} \sum_{j=1}^{L_R} q_j x_j + n_r, \quad (3.1)$$

where $E_{us} = \min\left(\frac{I_{\max}}{|f_{sp}|^2}, P_s\right)$ is the actual transmission power at the source node, i.e., permitted transmission power. x is the transmitted signal with unit energy. E_{IR} is the interference power at the relay node, q_j is the fading channel coefficient between the j^{th} interferer and the relay, x_j is the j^{th} interferer signal, and n_r is the AWGN at the relay node that has a power spectral density (PSD) of N_0 .

In the second phase of transmission, the relay node will decode the received message from the source node. Then, the relay will encode and forward it to the

destination user. The received signal at the destination user has the following form:

$$y_D = \sqrt{E_{ur}}g\hat{x} + \sqrt{E_{ID}}\sum_{i=1}^{L_D} p_i x_i + n_d, \quad (3.2)$$

where $E_{ur} = \min\left(\frac{I_{\max}}{|f_{rp}|^2}, P_r\right)$ is the actual transmission power at the relay node. \hat{x} is the transmitted signal from the relay node. E_{ID} is the interference power at the destination user node, p_i is the fading channel coefficient of the i^{th} interferer, x_i is the i^{th} interferer signal, and n_d represents the AWGN at the destination user that has a PSD of N_0 .

Thus, the instantaneous effective SINR at the input of the relay and destination node can be respectively expressed as:

$$\gamma_h^{\text{eff}} = \frac{\gamma_h}{1 + \sum_{j=1}^{L_R} I_{Rj}}, \quad (3.3)$$

and

$$\gamma_g^{\text{eff}} = \frac{\gamma_g}{1 + \sum_{i=1}^{L_D} I_{Di}}, \quad (3.4)$$

where $\gamma_h = \min\left(\frac{I_{\max}}{|f_{sp}|^2}, P_s\right) |h|^2/N_0$ and $\gamma_g = \min\left(\frac{I_{\max}}{|f_{rp}|^2}, P_r\right) |g|^2/N_0$ are the instantaneous SNR at the relay and destination user nodes, respectively, I_{Rj} , ($j = 1, 2, \dots, L_R$) and I_{Di} , ($i = 1, 2, \dots, L_D$) are the instantaneous INR at the relay and destination nodes, respectively. The instantaneous INRs I_{Rj} and I_{Di} are RVs which follow the exponential distribution with mean values of \bar{I}_R and \bar{I}_D , respectively. Furthermore, it is well-known that the sum of identically exponential RVs can be represented by a gamma distribution.

In the considered system model, it is assumed that the CCI sources are far enough from the relay and destination nodes, so that even though the CCI sources are randomly distributed geographically, the distance from the interferers to the relay and the destination nodes can be assumed to be the same. Therefore, it can be assumed that the received interference signals at the relay and destination nodes are identical in terms of the average energy [96,97]. This example can be observed in a conventional cellular network with a deterministic number of nodes, in which it is reasonable to assume all the nodes will receive interference from an equal number of nodes [84,96]. It is worth mentioning that the derivations in this work are based on

average values rather than instantaneous values. Finally, the dual-hop end-to-end equivalent SINR can be obtained as [98, 99]:

$$\gamma_{\text{eq}}^{\text{e2e}} = \min \left(\gamma_h^{\text{eff}}, \gamma_g^{\text{eff}} \right). \quad (3.5)$$

3.2.3 Multi-Destination User Scenario

Let it be assumed that there are K destination users that are distributed in a homogeneous environment. Therefore, it can be assumed that the channels between the relay node and K destination users are affected by the independent and identically distributed Rayleigh fading channels [96, 100]. In this scenario, the received signal at any of the destination users can be written as:

$$y_{D_k} = \sqrt{E_{ur}} g_k \hat{x} + \sqrt{E_{ID_k}} \sum_{i=1}^{L_D} p_{ki} x_{ki} + n_{d_k}, \quad (3.6)$$

where the subscript k represents any particular user at the destination among K users. Opportunistic scheduling [96, 100–103] is a technique of choosing one node, that has the highest instantaneous SINR value, out of many possible nodes. In this scenario, it can be achieved by selecting the destination user with the highest instantaneous SINR among K destinations, at any particular point in time. Using the above definition, the highest instantaneous SINR of the selected user, i.e., strongest user, denoted as γ_{g^*} can be obtained as [96, 100]:

$$\gamma_{g^*} = \min \left(\frac{I_{\text{max}}}{N_0 |f_{rp}|^2}, \frac{P_r}{N_0} \right) \max_{k=1, \dots, K} \left\{ \frac{|g_k|^2}{1 + \sum_{i=1}^{L_D} I_{D_{ki}}} \right\}. \quad (3.7)$$

Finally, the end-to-end opportunistic SINR denoted as $\gamma_{\text{eq}}^{\text{opp}}$, is determined by [98, 99]:

$$\gamma_{\text{eq}}^{\text{opp}} = \min \left(\gamma_h^{\text{eff}}, \gamma_{g^*} \right). \quad (3.8)$$

3.3 Statistical Derivations

In this section, the per-hop and end-to-end CDFs of the SINR of the secondary network are derived. In a dual-hop DF cooperative communication, the CDF of the

end-to-end SINR named as $F_{\gamma_{\text{eq}}^{2e2}}(\gamma)$ can be expressed as [69]:

$$F_{\gamma_{\text{eq}}^{2e2}}(\gamma) = 1 - \left(1 - F_{\gamma_h^{\text{eff}}}(\gamma)\right) \left(1 - F_{\gamma_g^{\text{eff}}}(\gamma)\right), \quad (3.9)$$

where $F_{\gamma_h^{\text{eff}}}(\gamma)$ and $F_{\gamma_g^{\text{eff}}}(\gamma)$ represent the CDFs of γ_h^{eff} and γ_g^{eff} , respectively. Furthermore, for the scenario of multi-user destination nodes, the CDF of the end-to-end opportunistic SINR, i.e., $F_{\gamma_{\text{eq}}^{\text{opp}}}(\gamma)$, can be obtained by employing $F_{\gamma_{g^*}}(\gamma)$ instead of $F_{\gamma_g^{\text{eff}}}(\gamma)$ in (3.9), where $F_{\gamma_{g^*}}(\gamma)$ is the CDF of the SINR received at the terminal of the selected user. In the sections below, the derivation steps will be provided to obtain the per-hop CDFs.

- Determining $F_{\gamma_h^{\text{eff}}}(\gamma)$:

The first hop CDF is derived as follows:

Corollary 1: The equivalent CDF of the first hop SINR can be written as in (3.10).

$$F_{\gamma_h^{\text{eff}}}(\gamma) = 1 - \left[e^{-\frac{\gamma}{P_s \sigma_h^2} \left(\frac{P_s \sigma_h^2}{P_s \sigma_h^2 + \gamma \bar{I}_R} \right)^{L_R}} \left(1 - e^{-\frac{I_{\text{max}}}{P_s \sigma_{f_{sp}}^2}} \right) + \left(\frac{I_{\text{max}} \sigma_h^2 + \gamma \sigma_{f_{sp}}^2}{\gamma \bar{I}_R \sigma_{f_{sp}}^2} \right)^{L_R} \left(\frac{I_{\text{max}} \sigma_h^2}{I_{\text{max}} \sigma_h^2 + \gamma \sigma_{f_{sp}}^2} \right) e^{\frac{I_{\text{max}} \sigma_h^2 + \gamma \sigma_{f_{sp}}^2}{\gamma \bar{I}_R \sigma_{f_{sp}}^2}} \times \Gamma \left(1 - L_R, \left(\frac{I_{\text{max}} \sigma_h^2 + \gamma \sigma_{f_{sp}}^2}{\gamma \bar{I}_R \sigma_{f_{sp}}^2} \right) \left(\frac{P_s \sigma_h^2 + \gamma \bar{I}_R}{P_s \sigma_h^2} \right) \right) \right]. \quad (3.10)$$

Proof: See Appendix 3.7.1. ■

The second hop CDF $F_{\gamma_g^{\text{eff}}}(\gamma)$ has a similar formula to $F_{\gamma_h^{\text{eff}}}(\gamma)$. It can be expressed by replacing σ_h^2 , $\sigma_{f_{sp}}^2$, L_R and \bar{I}_R in (3.10) with σ_g^2 , $\sigma_{f_{rp}}^2$, L_D and \bar{I}_D , respectively.

- Determining $F_{\gamma_{g^*}}(\gamma)$:

Using quite similar steps, the CDF of γ_{g^*} can be written as in (3.12). Bearing in mind that for this part, different notations corresponding to the second hop entities should be used. Moreover, the CDF of the maximum SINR out of K users should be used, i.e., $\max_{k=1, \dots, K} \left\{ \frac{|g_k|^2}{1 + \sum_{i=1}^{L_D} I_{D_{ki}}} \right\}$, which can be expressed as:

$$F_{\max_{k=1, \dots, K} \left\{ \frac{|g_k|^2}{1 + \sum_{i=1}^{L_D} I_{D_{ki}}} \right\}}(\gamma) = \left[1 - e^{-\frac{\gamma}{\sigma_g^2} \left(\frac{\sigma_g^2}{\sigma_g^2 + \gamma \bar{I}_D} \right)^{L_D}} \right]^K \quad (3.11)$$

$$\begin{aligned}
 F_{\gamma_{g^*}}(\gamma) = & 1 - \sum_{n=1}^K \binom{K}{n} (-1)^{n+1} \left[e^{-\frac{n\gamma}{P_r\sigma_g^2}} \left(\frac{P_r\sigma_g^2}{P_r\sigma_g^2 + \gamma\bar{I}_D} \right)^{nL_D} \left(1 - e^{-\frac{I_{\max}}{P_r\sigma_{f_{rp}}^2}} \right) \right. \\
 & + \left(\frac{I_{\max}\sigma_g^2}{I_{\max}\sigma_g^2 + n\gamma\sigma_{f_{rp}}^2} \right) \left(\frac{I_{\max}\sigma_g^2 + n\gamma\sigma_{f_{rp}}^2}{\gamma\bar{I}_D\sigma_{f_{rp}}^2} \right)^{nL_D} e^{\frac{I_{\max}\sigma_g^2 + n\gamma\sigma_{f_{rp}}^2}{\gamma\bar{I}_D\sigma_{f_{rp}}^2}} \times \\
 & \left. \Gamma\left(1 - nL_D, \left(\frac{I_{\max}\sigma_g^2 + n\gamma\sigma_{f_{rp}}^2}{\gamma\bar{I}_D\sigma_{f_{rp}}^2} \right) \left(\frac{P_r\sigma_g^2 + \gamma\bar{I}_D}{P_r\sigma_g^2} \right) \right) \right]. \quad (3.12)
 \end{aligned}$$

After deriving the per-hop CDFs, i.e., $F_{\gamma_h^{\text{eff}}}(\gamma)$, $F_{\gamma_g^{\text{eff}}}(\gamma)$, and $F_{\gamma_{g^*}}(\gamma)$, the end-to-end equivalent CDF can be obtained by substituting the derived per-hop CDFs into (3.9).

3.4 Performance Evaluation

In the following sections, mathematical expressions for evaluating the performance of the secondary network are derived. First, formulas for the OP and AEP are obtained. Then, approximate equations for assessing the OP and AEP are derived. In addition, an expression for determining the EC of the secondary network is derived. Finally, optimum power allocation is investigated in order to enhance the overall performance of the cognitive radio network.

3.4.1 Exact Outage Probability

The OP is defined as the probability that the equivalent SINR is below a predefined threshold value. From the definition of the CDF in (2.1), the OP can be easily obtained from the previous calculated equivalent CDF by replacing the variable γ with γ_{th} :

$$P_{\text{out}}(\gamma_{\text{th}}) = \Pr(\gamma_{\text{eq}}^{\text{e2e}} \leq \gamma_{\text{th}}) = F_{\gamma_{\text{eq}}^{\text{e2e}}}(\gamma_{\text{th}}). \quad (3.13)$$

From the above formula, it can be observed how important it is for the CDF to be known for evaluating the network performance.

3.4.2 Average Error Probability

The AEP performance can be investigated via different approaches. For example, CDF or PDF can be used to investigate this performance indicator. By observing the derived per-hop CDFs, it can be deduced that using the CDF approach for this

investigation could be more mathematically convenient. Thus, the expression for the AEP can be obtained using the following formula [84]:

$$\bar{P}_b = \frac{a}{2} \sqrt{\frac{b}{\pi}} \int_0^{\infty} \frac{\exp(-bx)}{\sqrt{x}} F_{\gamma_{\text{eq}}}(x) dx, \quad (3.14)$$

where a and b are arbitrary constants depending on the modulation schemes, e.g. QPSK: $a = 2$ and $b = 0.5$ [70]. The AEP for the first and second hop, \bar{P}_b^{sr} , and \bar{P}_b^{rd} can be obtained by substituting the derived corresponding CDFs i.e., $F_{\gamma_h^{\text{eff}}}(z)$, $F_{\gamma_h^{\text{eff}}}(z)$, and/or $F_{\gamma_{g^*}}(z)$ into (3.14). Finally, the end-to-end AEP can be calculated using the following equation [90]:

$$\bar{P}_b^{e2e} = \bar{P}_b^{sr} + \bar{P}_b^{rd} - 2(\bar{P}_b^{sr} \bar{P}_b^{rd}). \quad (3.15)$$

To calculate the per-hop error probability, the following theorem is proposed:

Theorem 1: The aim is to represent the per-hop equivalent CDFs for both first and second hops in a simpler form which are more convenient mathematically, so that further investigation of the system performance can be carried out. First, the following notations are employed for both hops to make the formulas more tractable mathematically.

First hop CDF notations:

$$\Upsilon_1 = \left(1 - e^{-\frac{I_{\max}}{P_s \sigma_{f_{sp}}^2}}\right) \left(\frac{P_s \sigma_h^2}{\bar{I}_R}\right)^{L_R}, \quad (3.16a)$$

$$\Upsilon_2 = \left(\frac{I_{\max} \sigma_h^2}{\sigma_{f_{sp}}^2}\right) \left(\frac{P_s \sigma_h^2}{\bar{I}_R}\right)^{L_R} e^{-\frac{I_{\max}}{P_s \sigma_{f_{sp}}^2}}, \quad (3.16b)$$

$$\alpha = P_s \sigma_h^2, \quad (3.16c)$$

$$\beta = \frac{P_s \sigma_h^2}{\bar{I}_R}. \quad (3.16d)$$

Second hop opportunistic CDF notations:

$$\Upsilon_3 = \left(1 - e^{-\frac{I_{\max}}{P_r \sigma_{f_{rp}}^2}}\right) \left(\frac{P_r \sigma_g^2}{\bar{I}_D}\right)^{nL_D}, \quad (3.17a)$$

$$\Upsilon_4 = \left(\frac{I_{\max} \sigma_g^2}{n \sigma_{f_{rp}}^2}\right) \left(\frac{P_r \sigma_g^2}{\bar{I}_D}\right)^{nL_D} e^{-\frac{I_{\max}}{P_r \sigma_{f_{rp}}^2}}, \quad (3.17b)$$

$$\delta = \frac{P_r \sigma_g^2}{n}, \quad (3.17c)$$

$$\eta = \frac{P_r \sigma_g^2}{\bar{I}_D}. \quad (3.17d)$$

Then, the tight approximate per-hop equivalent CDF of the first and second hops can be written as in (3.18) and (3.19), respectively. It is worth mentioning that these notations have been carefully chosen so that the first and second hop equations look similar in structure. However, the notations for each hop are different; therefore, the same procedure of derivation can be applied to the error probability and EC for one hop to the other with the condition of replacing the notations that have been defined for a particular hop.

Proof: See Appendix 3.7.2. ■

$$F_{\gamma_h^{\text{eff}}}^{\text{app}}(z) \approx 1 - e^{-\frac{z}{\alpha}} \left[\frac{\Upsilon_1}{(\beta + z)^{L_R}} + \frac{\Upsilon_2}{(\beta + z)^{L_R-1} \times (\Lambda_1 + z) \times (\Lambda_2 + z)} \right]. \quad (3.18)$$

$$F_{\gamma_{g^*}}^{\text{app}}(z) \approx 1 - \sum_{n=1}^K \binom{K}{n} (-1)^{n+1} e^{-\frac{z}{\delta}} \left[\frac{\Upsilon_3}{(\eta + z)^{L_D}} + \frac{\Upsilon_4}{(\eta + z)^{L_D-1} \times (\Lambda_3 + z) \times (\Lambda_4 + z)} \right]. \quad (3.19)$$

It is worth noting that the proposed tight approximation does not have a significant impact on the analytical calculations and gives quite accurate results, especially for the case of ($I_{\max} \geq P_s$ and P_r). It is obvious that in the case when $I_{\max} < P_s$ and P_r , i.e., I_{\max} dominant system, the secondary transmitters cannot take full advantage of their transmission power limits, and in this case a performance saturation is expected in the system performance. The accuracy of the proposed tight approximation can be observed later from the Monte Carlo simulations and numerical results. For instance, in Fig. 3.2, the OP has been plotted using the derived tight approximate CDF equations. It can be observed that the proposed tight approximation gives quite accurate results in comparison to the exact results. In addition, the approximation

has been applied only to one term in the CDF formula. Moreover, Table 3.1 has been constructed in Appendix 3.7.2 for the purpose of comparison between the exact and tight approximate values of the exponential integral function terms that have been proposed in the CDF formula.

1. Average error probability for the first hop:

The first hop AEP is derived as follows.

Corollary 2: The first hop AEP can be obtained as in (3.20), where $U(a, b, z)$ is the confluent hypergeometric function defined in [80, eq. (13.2.5)], and $\text{erfc}(\cdot)$ is the complementary error function defined in [83, eq. (7.2.2)]. Moreover, the values of λ_{1_i} , λ_2 , and λ_3 are calculated by using the equations given in (3.21a), (3.21b), and (3.21c) respectively.

$$\begin{aligned} \bar{P}_b^{sr} = & \frac{a}{2} - \frac{a}{2} \sqrt{b} \left[\Upsilon_1 \beta^{\frac{1}{2}-L_R} U \left(\frac{1}{2}, \frac{3}{2} - L_R, \beta \left(b + \frac{1}{\alpha} \right) \right) + \Upsilon_2 \left\{ \sum_{i=1}^{L_R-1} \lambda_{1_i} \beta^{\frac{1}{2}-i} \right. \right. \\ & U \left(\frac{1}{2}, \frac{3}{2} - i, \beta \left(b + \frac{1}{\alpha} \right) \right) + \lambda_2 \sqrt{\frac{\pi}{\Lambda_1}} e^{(b+\frac{1}{\alpha})\Lambda_1} \text{erfc} \left(\sqrt{\left(b + \frac{1}{\alpha} \right) \Lambda_1} \right) \\ & \left. \left. + \lambda_3 \sqrt{\frac{\pi}{\Lambda_2}} e^{(b+\frac{1}{\alpha})\Lambda_2} \text{erfc} \left(\sqrt{\left(b + \frac{1}{\alpha} \right) \Lambda_2} \right) \right\} \right]. \end{aligned} \quad (3.20)$$

$$\lambda_{1_i} = \frac{1}{(L_R - 1 - i)!} \frac{\partial^{L_R-1-i}}{\partial z^{L_R-1-i}} \frac{1}{(\Lambda_1 + z)(\Lambda_2 + z)} \Big|_{z=-\beta}, \quad (3.21a)$$

$$\lambda_2 = (\beta - \Lambda_1)^{1-L_R} (\Lambda_2 - \Lambda_1)^{-1}, \quad (3.21b)$$

$$\lambda_3 = (\beta - \Lambda_2)^{1-L_R} (\Lambda_1 - \Lambda_2)^{-1}. \quad (3.21c)$$

Proof: See Appendix 3.7.3. ■

2. Average error probability for the second hop:

The same procedure as for the first hop can be repeated to derive the AEP of the second hop. The only difference is that the tight approximate CDF for the second hop that was derived in (3.19) should be used. Therefore, the derivation steps have been omitted.

Finally, the end-to-end AEP can be calculated by substituting the calculated

per-hop AEP into (3.15).

3.4.3 Approximate Outage Probability and Average Error Probability

Although the expression for $F_{\gamma_{\text{eq}}^{e2e}}(\gamma)$ allows numerical evaluation of the system outage performance, it may not be computationally intensive and does not offer an insight into the effect of the system parameters. Now, the aim is to express $F_{\gamma_{\text{eq}}^{e2e}}(\gamma)$ and \bar{P}_b in simpler forms. In order to get more accurate results, the exponential integral function is represented in more detailed terms. This can be obtained by using [80, eq. (5.1.14)].

It is widely known that the asymptotic error probability can be derived based on the behaviour of the CDF of the output SINR around the origin [100, 104]. By using Taylor's series and considering $P_s, P_r < I_{\text{max}}$, the end-to-end OP, $P_{\text{out}}(\gamma_{\text{th}})$, can be rewritten as:

$$P_{\text{out}}(\gamma_{\text{th}}) \approx \left(\frac{(1 + L_R \bar{I}_R)}{P_s \sigma_h^2} + \frac{\sigma_{f_{sp}}^2}{I_{\text{max}} \sigma_h^2} e^{-\frac{I_{\text{max}}}{P_s \sigma_h^2}} + \frac{(1 + L_D \bar{I}_D)}{P_r \sigma_g^2} + \frac{\sigma_{f_{rp}}^2}{I_{\text{max}} \sigma_g^2} e^{-\frac{I_{\text{max}}}{P_r \sigma_g^2}} \right) \gamma_{\text{th}}. \quad (3.22)$$

Therefore, the AEP can be written as:

$$\bar{P}_b \approx \frac{a}{4b} \left(\frac{(1 + L_R \bar{I}_R)}{P_s \sigma_h^2} + \frac{\sigma_{f_{sp}}^2}{I_{\text{max}} \sigma_h^2} e^{-\frac{I_{\text{max}}}{P_s \sigma_h^2}} + \frac{(1 + L_D \bar{I}_D)}{P_r \sigma_g^2} + \frac{\sigma_{f_{rp}}^2}{I_{\text{max}} \sigma_g^2} e^{-\frac{I_{\text{max}}}{P_r \sigma_g^2}} \right). \quad (3.23)$$

Moreover, for the scenario of a multi-destination user, the asymptotic opportunistic equivalent CDF can be expressed as:

$$P_{\text{out}}^{\text{opp}}(\gamma_{\text{th}}) \approx \left(\frac{(1 + L_R \bar{I}_R)}{P_s \sigma_h^2} + \frac{\sigma_{f_{sp}}^2}{I_{\text{max}} \sigma_h^2} e^{-\frac{I_{\text{max}}}{P_s \sigma_h^2}} + \sum_{n=1}^K \binom{K}{n} (-1)^{n+1} \left(\frac{n(1 + L_D \bar{I}_D)}{P_r \sigma_g^2} + \frac{n \sigma_{f_{rp}}^2}{I_{\text{max}} \sigma_g^2} e^{-\frac{I_{\text{max}}}{P_r \sigma_g^2}} \right) \right) \gamma_{\text{th}}. \quad (3.24)$$

From (3.24), the diversity gain of the secondary network can be inspected. According to [104], at the high SNR regime, the OP formula can be written as:

$$P_{\text{out}} \approx (O_c \gamma)^{-G_d}, \quad (3.25)$$

where G_d , and O_d are the diversity gain and coding gain, respectively. Now by comparing (3.24) with (3.25) it can be seen that the $G_d = 1$. The result in (3.24) confirms that opportunistic SNR-based selection has no impact on the diversity gain. However, by inspecting (3.24), it can be seen that the effect of opportunistic SNR-based selection is to increase the array gain [100]. Furthermore, the performance for a multi-user destination, i.e., $K > 1$, is dominated by $S - R$ channel. Note that when $I_{\max} \rightarrow \infty$, the same widely known asymptotic expression for ordinary dual-hop DF networks can be obtained which partially validates the derived results.

3.4.4 Ergodic Capacity

Another important performance indicator for the wireless communication network is the EC [49]. It can be defined as the maximum capacity data rate that the system can achieve. To assess the CR network capacity, it is important to know the achievable throughput of the system. The EC can be obtained mathematically by averaging the instantaneous mutual information, from the transmitter node to the receiver node, over the distribution of the equivalent SNR. Furthermore, it can be calculated by using the equivalent CDF of the system [49] and can be represented as:

$$C_{erg} = \int_0^{\infty} \frac{\bar{F}_{\gamma_{eq}}(x)}{1+x} dx, \quad (3.26)$$

where $\bar{F}_{\gamma_{eq}}(x)$ is the complementary CDF. Then, the end-to-end EC can be obtained by using the following formula:

$$C_{erg}^{e2e} = \frac{1}{2} \min(C_{erg}^{sr}, C_{erg}^{rd}), \quad (3.27)$$

where C_{erg}^{sr} and C_{erg}^{rd} are the ergodic capacities of the first and second hop, respectively. Furthermore, $\frac{1}{2}$ comes from the fact that the transmission in a dual-hop cooperative network is performed within two time slots, which means the overall bandwidth should be divided by the number of hops in the network. In the section below, the EC for the second hop, in the scenario of a multi-destination user, is derived.

Corollary 3: The opportunistic second hop EC formula can be expressed as in (3.28).

Proof: See Appendix 3.7.4. ■

$$\begin{aligned}
 C_{erg}^{g*} = & \sum_{n=1}^K \binom{K}{n} (-1)^{n+1} \left\{ \Upsilon_3 \left[\sum_{r_3=1}^{nL_D} \omega_{g1_{r_3}} \eta^{1-r_3} e^{\frac{\eta}{\delta}} E_{r_3} \left(\frac{\eta}{\delta} \right) + \omega_{g2} e^{\frac{1}{\delta}} E_1 \left(\frac{1}{\delta} \right) \right] \right. \\
 & + \Upsilon_4 \left[\sum_{r_4=1}^{nL_D-1} \omega_{g3_{r_4}} \eta^{1-r_4} e^{\frac{\eta}{\delta}} E_{r_4} \left(\frac{\eta}{\delta} \right) + \omega_{g4} e^{\frac{1}{\delta}} E_1 \left(\frac{1}{\delta} \right) + \omega_{g5} e^{\frac{\Lambda_3}{\delta}} E_1 \left(\frac{\Lambda_3}{\delta} \right) \right. \\
 & \left. \left. + \omega_{g6} e^{\frac{\Lambda_4}{\delta}} E_1 \left(\frac{\Lambda_4}{\delta} \right) \right] \right\}. \tag{3.28}
 \end{aligned}$$

In (3.28), $E_1(x)$ is the exponential integral function defined in [83, eq. 6.2.6]. Furthermore, the values of $\omega_{g1_{r_3}}$, ω_{g2} , $\omega_{g3_{r_4}}$, ω_{g4} , ω_{g5} , and ω_{g6} are calculated by using (3.29a), (3.29b), (3.29c), (3.29d), (3.29e), and (3.29f), respectively.

$$\omega_{g1_{r_3}} = \frac{1}{(nL_D - r_3)!} \frac{\partial^{nL_D-r_3}}{\partial z^{nL_D-r_3}} (1+z)^{-1} \Big|_{z=-\eta}, \tag{3.29a}$$

$$\omega_{g2} = (\eta - 1)^{-nL_D}, \tag{3.29b}$$

$$\omega_{g3_{r_4}} = \frac{1}{(nL_D - 1 - r_4)!} \times \frac{\partial^{nL_D-1-r_4}}{\partial z^{nL_D-1-r_4}} \frac{(\Lambda_3 + z)^{-1} (\Lambda_4 + z)^{-1}}{(1+z)} \Big|_{z=-\eta}, \tag{3.29c}$$

$$\omega_{g4} = (\eta - 1)^{1-nL_D} (\Lambda_3 - 1)^{-1} (\Lambda_4 - 1)^{-1}, \tag{3.29d}$$

$$\omega_{g5} = (\eta - \Lambda_3)^{1-nL_D} (1 - \Lambda_3)^{-1} (\Lambda_4 - \Lambda_3)^{-1}, \tag{3.29e}$$

$$\omega_{g6} = (\eta - \Lambda_4)^{1-nL_D} (1 - \Lambda_4)^{-1} (\Lambda_3 - \Lambda_4)^{-1}. \tag{3.29f}$$

For the first hop EC formula, the derived tight approximate first hop complementary CDF is substituted (i.e., $F_{\gamma_h^{\text{app}}}(z)$) from (3.18) into (3.26). Then, an integral formula that has two main parts is obtained. It can be observed that these two parts are quite similar to the two parts in the second hop EC formula that is derived in Appendix 3.7.4, it is only required to replace δ , η , Λ_3 , Λ_4 , Υ_3 , and Υ_4 with α , β , Λ_1 , Λ_2 , Υ_1 , and Υ_2 , respectively.

3.4.5 Optimum Power Allocation

In previous sections it has been shown that only for a single user destination scenario, both source-relay and relay-destination channels have the same impact. Therefore,

a single user scenario for the calculation of the optimum power calculation is the focus of this section. In this section, with the aim of improved system performance, adaptive power allocation subject to a sum power constraint is studied, i.e., $P_s + P_r = P_t$, where P_t is the total given power. The optimization problem can be formulated as:

$$P_s^*, P_r^* = \arg \min_{P_s, P_r} \bar{P}_b,$$

subject to : $P_s + P_r = P_t$, and $P_s, P_r > 0$. (3.30)

By taking the second derivative of \bar{P}_b in (3.23) with respect to P_s , it is easy to see that $\partial^2 \bar{P}_b / \partial P_s^2$ is positive in the interval $P_s \in \{0, P_t\}$. This implies that the objective function is a strictly convex function of P_s in $\{0, P_t\}$. Hence, taking the first derivative of \bar{P}_b in (3.23) with respect to P_s and setting it to zero, the optimal power allocation solution can be found. Specifically, the optimal source power P_s^* is the root of the following equation:

$$\frac{1 + L_D \bar{I}_D - e^{-\frac{I_{\max}}{(P_t - P_s)\sigma_{f_{rp}}^2}}}{\sigma_g^2 (P_t - P_s)^2} = \frac{1 + L_R \bar{I}_R - e^{-\frac{I_{\max}}{P_s \sigma_{f_{sp}}^2}}}{P_s^2 \sigma_h^2}. \quad (3.31)$$

The optimal relay power is given by $P_r^* = P_t - P_s^*$. It is difficult to find a closed-form expression for the optimal source power, P_s^* . However, a numerical solution can be found by using standard iterative root-finding algorithms, such as the Bisection method and Newton's Method, with great efficiency. However, if it is assumed $P_s, P_r \ll I_{\max}$ [49] and after some mathematical manipulations, the closed-form expressions for these optimal power values can be found as:

$$P_s^* \approx \left[\frac{\sqrt{\sigma_g^2 (1 + L_R \bar{I}_R)}}{\sqrt{\sigma_g^2 (1 + L_R \bar{I}_R)} + \sqrt{\sigma_h^2 (1 + L_D \bar{I}_D)}} \right] P_t, \quad (3.32a)$$

and

$$P_r^* \approx \left[\frac{\sqrt{\sigma_h^2 (1 + L_D \bar{I}_D)}}{\sqrt{\sigma_h^2 (1 + L_D \bar{I}_D)} + \sqrt{\sigma_g^2 (1 + L_R \bar{I}_R)}} \right] P_t. \quad (3.32b)$$

In previous optimal power calculations, both optimally calculated powers, P_s^* and P_r^* should satisfy the criteria of the protection of the QoS of the primary receiver. For example, the actual transmission power at the secondary source node should

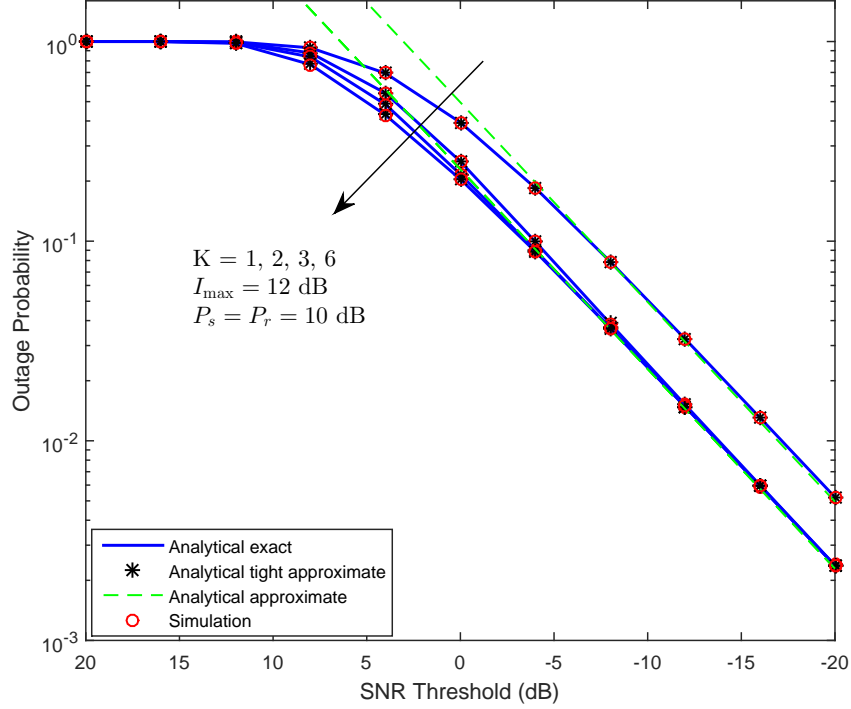


Figure 3.2: Outage probability for different numbers of destination users.

satisfy the following criteria: $E_{us} = \min\left(\frac{I_{\max}}{|f_{sp}|^2}, P_s^*\right)$. Similarly, for the optimal power at the relay node, the actual relay transmission power should satisfy this criteria: $E_{ur} = \min\left(\frac{I_{\max}}{|f_{rp}|^2}, P_r^*\right)$. Therefore, a guarantee of protection of the QoS of the primary user should always be provided.

In the scenario where any of the calculated optimal power values is above the interference power constraint (i.e., I_{\max} dominates the transmission power limits), a performance saturation occurs in the secondary system performance results. This is due to the fact that the secondary transmitters cannot take full advantage of their transmission power limits.

Finally, it is worth mentioning that although numerical calculation is at the source, the complexity of the proposed algorithm is very low, since the computations are needed only once for each system configuration. This is due to the fact that the analysis in this thesis is based on average values rather than the instantaneous values which, in practice, can be obtained through long-term averaging of the received signal power.

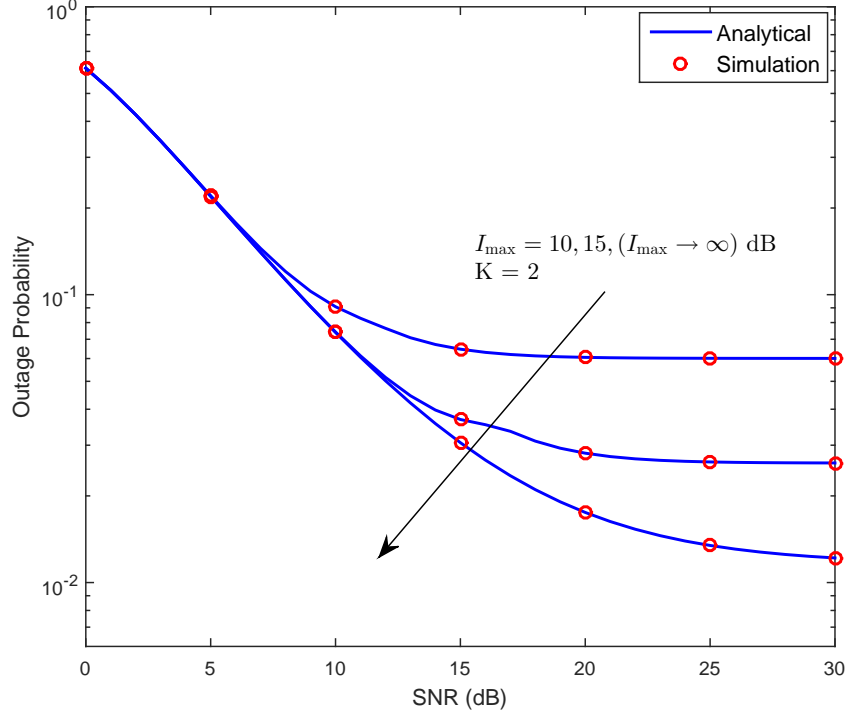


Figure 3.3: Outage probability for different I_{\max} values.

3.5 Numerical Results and Discussions

For the purpose of illustration and to validate the derived mathematical works, some numerical and Monte Carlo simulation examples are presented.

In Fig. 3.2, the OP has been plotted to show the effect of the opportunistic SNR-based selection. The CCI powers are set as $\bar{I}_R = 3$ dB, and $\bar{I}_D = 2$ dB, and $L_R = L_D = 2$. It can be observed that the opportunistic SNR-based selection has less impact on the system performance when $K > 1$ due to the fact that the source-relay link will dominate the performance characteristic.

Fig. 3.3 shows the OP for different values of I_{\max} . The network parameter values for this figure are chosen as: SNR threshold is 1 dB, and the CCI powers \bar{I}_R , and \bar{I}_D are 0.01 of the effective or actual transmission powers at the secondary source and relay node, (i.e., E_{us} and E_{ur}) and $L_R = L_D = 2$. It can be observed that even if there is no interference power constraint, i.e., $I_{\max} \rightarrow \infty$, there is an outage floor. This is because of the linear increase of the CCI power with respect to the effective transmission powers at the source and relay nodes. From this, it can be seen how the CCI power degrades the performance of the system.

Fig. 3.4 shows the EC for different I_{\max} , K , and CCI powers. The network

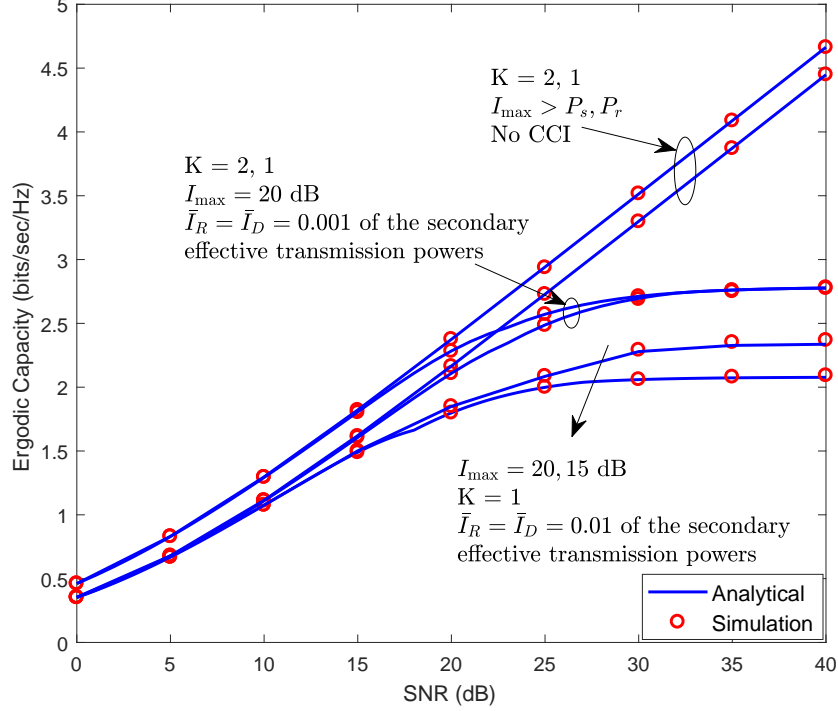


Figure 3.4: The ergodic capacity for different values of I_{\max} , K and CCI power.

parameter values for this figure are chosen as: the CCI exists at the relay and the destination nodes where $L_R = L_D = 2$, and also for the case where there is no CCI and I_{\max} . From the results, it can be deduced that both the CCI and I_{\max} will degrade the system capacity performance. For example, for a single destination user $K = 1$, when both I_{\max} and CCI have impact on the secondary network, i.e., $I_{\max} = 15$ dB and $\bar{I}_R = \bar{I}_D = 0.01 \times E_{us}, E_{ur}$, the capacity saturation occurs at 30 dB and the performance cannot improve better than 2.05 bits/sec/Hz even when the transmission power is further increased. However, when these performance limitations are not present it is possible to reach 3.25 bits/sec/Hz at 30 dB.

Fig. 3.5 shows the error probability versus the total transmission power for different I_{\max} and K . The network parameter values for this figure are chosen as: the CCI powers \bar{I}_R , and \bar{I}_D which have fixed values and also linearly increase with the effective transmission powers by the ratio of 0.01, and $L_R = 3, L_D = 1$. From the figure, it can be seen that higher I_{\max} will lead to better performance. In addition, the error floor in this case is due to both I_{\max} and CCI. Moreover, in a specific region, even for a high value of I_{\max} , an error floor can be observed which is due to the CCI power.

For the purpose of only showing the impact of the CCI power on the error

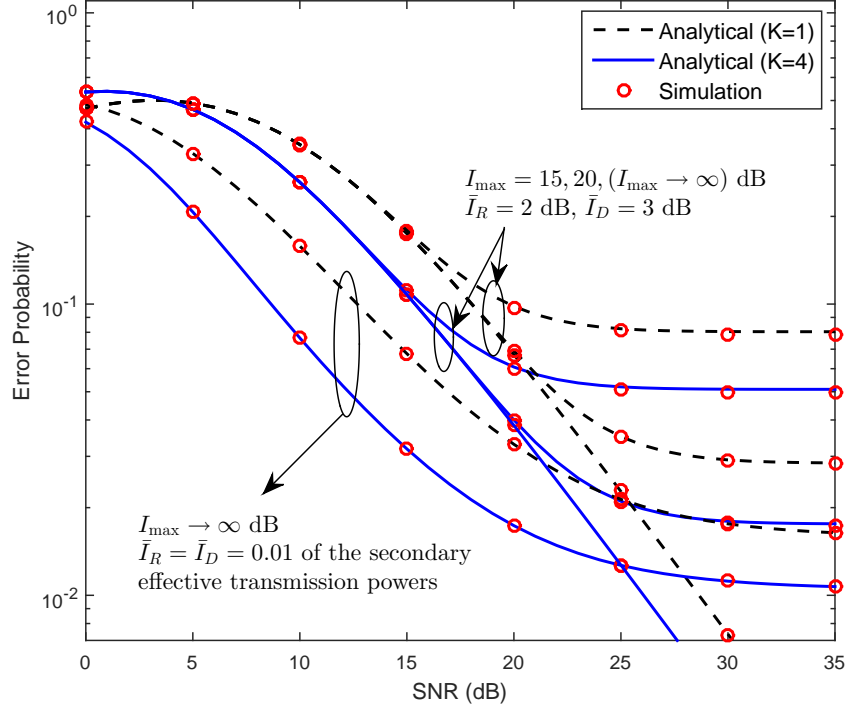


Figure 3.5: Error probability for different values of I_{\max} and K .

probability performance of the CR network, Fig. 3.6 has been plotted, which is the error probability versus the total transmission power for different CCI powers. The network parameter values for this figure are chosen as: $K = 2$, $L_R = 2$, $L_D = 3$ and $I_{\max} > P_s, P_r$. In this case, the error floor is completely due to the impact of CCI power. For example, when the rate of increase of the CCI power with respect to the effective secondary transmission powers is 0.05, the error performance saturates at 0.11, which means that the error probability performance cannot improve further, even if the transmission power increases.

In Fig. 3.7, the error probability performance of the optimal power allocation in comparison with the equal power allocation for the case when $K = 1$ for different CCI powers and I_{\max} has been depicted. With the help of (3.31), and by using the Bisection method, the optimal powers P_s^* and P_r^* have been calculated. It can be observed that the optimal power allocation leads to an improved performance in comparison with the equal power allocation. Moreover, when I_{\max} limits the secondary transmission power and the CCI power is relatively high, the improvement in the error performance due to the optimal power allocation scheme is less significant.

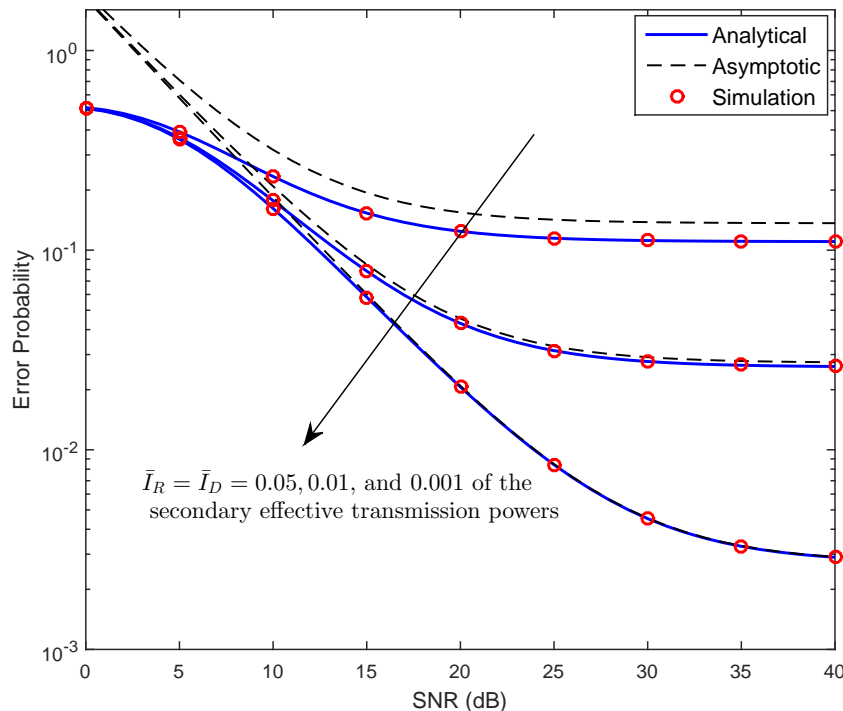


Figure 3.6: Error probability for different values of CCI power.

3.6 Conclusion

In this chapter, a comprehensive study of the performance analysis of the opportunistic dual-hop multi-user DF underlay cognitive cooperative network in the presence of CCI has been presented. An exact closed-form expression for the CDF of the equivalent SINR has been derived, and the exact OP has been investigated. In turn, a tight approximate CDF has been proposed. Based on this, expressions for the AEP and the system EC over Rayleigh fading channels have been derived. In addition, simple approximate expressions for the OP and the AEP have been obtained.

Finally, the system power optimization was investigated in order to minimize the system error probability. Numerical results and Monte Carlo simulations using Matlab have also been presented to validate the correctness of the analytical results. The results showed that applying an opportunistic SNR-based selection technique can improve the CR system performance. On the other hand, CCI and the I_{\max} consideration will cause its degradation.

It is worth mentioning that the proposed approach can be easily extended to the multi-hop cognitive cooperative network. For instance, the OP can be obtained by simply substituting the per-hop results into (8) in [98]. In addition, the error

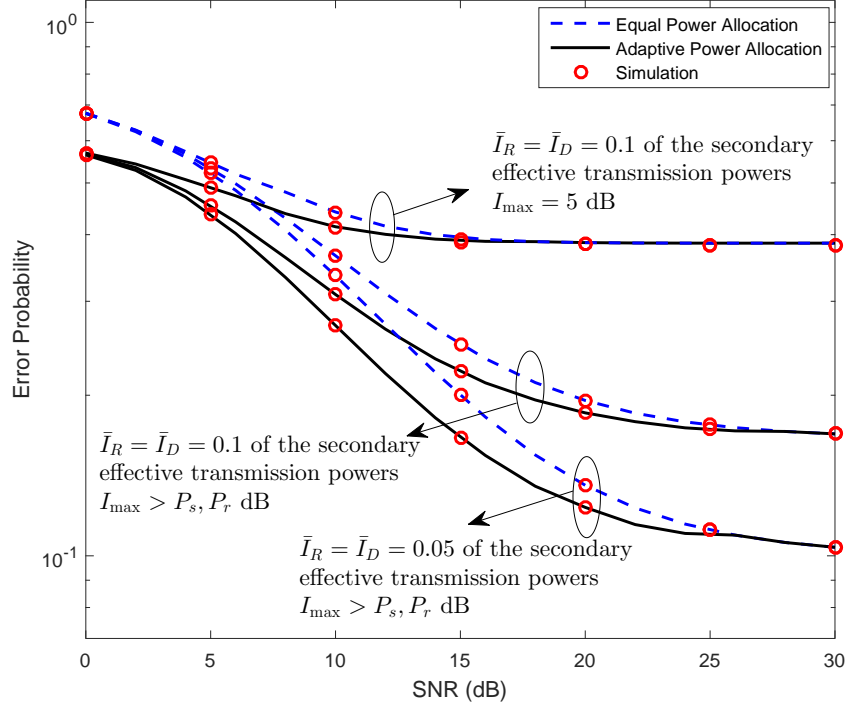


Figure 3.7: Performance of optimal power allocation algorithm in comparison to the equal power allocation.

probability and the EC can be calculated by substituting the per-hop results into (28), (47) in [62], respectively.

3.7 Appendix

3.7.1 First hop Exact CDF Derivation Steps

Recall that the effective SINR for the first hop can be written as $\gamma_h^{\text{eff}} = \frac{\gamma_h}{1 + \sum_{j=1}^{L_R} I_{Rj}}$, hence considering both source node power constraint and the interference power constraint, the above formula can be rewritten as:

$$\gamma_h^{\text{eff}} = \min\left(\frac{I_{\max}}{X}, P_s\right) \left(\frac{Y}{1+Z}\right), \quad (3.33)$$

where X , Y , and Z represent the RVs $|f_{sp}|^2$, $|h|^2$, and $\sum_{j=1}^{L_R} I_{Rj}$, respectively. Since all channels have been assumed as the Rayleigh fading distribution, the PDF of X has an exponential distribution, and is written as $f_X(x) = \frac{1}{\sigma_{fsp}^2} \exp\left(-\frac{x}{\sigma_{fsp}^2}\right)$. In addition, the corresponding CDF can be written as $F_X(x) = 1 - \exp\left(-\frac{x}{\sigma_{fsp}^2}\right)$. First, the equivalent CDF of $\frac{Y}{1+Z}$ is derived. Let W represent the resulting RV of

this combination $W = \frac{Y}{1+Z}$. Therefore, the CDF of W can be written as:

$$F_W(\gamma) = \int_{z=0}^{\infty} F_Y((z+1)\gamma) f_Z(z) dz, \quad (3.34)$$

where $F_Y(\gamma)$ is the CDF of the channel gain between the source and relay node that can be expressed as $F_Y(y) = 1 - \exp\left(-\frac{y}{\sigma_h^2}\right)$. $f_Z(z)$ is the PDF of RV $\sum_{j=1}^{L_R} I_{R_j}$ which can be expressed as $f_Z(z) = \frac{z^{L_R-1}}{\bar{I}_R^{L_R} \Gamma(L_R)} \exp\left(-\frac{z}{\bar{I}_R}\right)$, where \bar{I}_R is the average INR. Bearing in mind that the sum of i.i.d. exponential RVs is a chi-square, which follows the gamma distribution [76, p. 18]. By substituting both formulas of $F_Y(y)$ and $f_Z(z)$ into (3.34) the CDF of RV W can be obtained:

$$F_W(\gamma) = 1 - e^{-\frac{\gamma}{\sigma_h^2}} \left(\frac{\sigma_h^2}{\sigma_h^2 + \gamma \bar{I}_R}\right)^{L_R}. \quad (3.35)$$

Furthermore, the CDF of γ_h^{eff} can be represented by:

$$F_{\gamma_h^{\text{eff}}}(\gamma) = \Pr(\gamma_h^{\text{eff}} \leq \gamma). \quad (3.36)$$

Then, with the help of the total probability theorem, the CDF of $F_{\gamma_h^{\text{eff}}}(\gamma)$ can be expressed by the following formula:

$$F_{\gamma_h^{\text{eff}}}(\gamma) = \Pr\left(\frac{I_{\max}}{X} W \leq \gamma, \frac{I_{\max}}{X} < P_s\right) + \Pr\left(P_s W \leq \gamma, \frac{I_{\max}}{X} > P_s\right). \quad (3.37)$$

The above formula can be represented in terms of the integrals:

$$\begin{aligned} F_{\gamma_h^{\text{eff}}}(\gamma) &= \int_{x=\frac{I_{\max}}{P_s}}^{\infty} \int_{y=0}^{\frac{\gamma x}{I_{\max}}} f_X(x) f_W(y) dx dy + \int_{x=0}^{\frac{I_{\max}}{P_s}} \int_{y=0}^{\frac{\gamma}{P_s}} f_X(x) f_W(y) dx dy \\ &= I_1 + I_2. \end{aligned} \quad (3.38)$$

The second part of the above integrals, (i.e., I_2) can easily be obtained as:

$$I_2 = \left(1 - \left(\frac{\sigma_h^2}{\bar{I}_R}\right)^{L_R} \frac{e^{-\frac{\gamma}{P_s \sigma_h^2}}}{\left(\frac{\sigma_h^2}{\bar{I}_R} + \frac{\gamma}{P_s}\right)^{L_R}}\right) \left(1 - e^{-\frac{I_{\max}}{P_s \sigma_{fs}^2}}\right). \quad (3.39)$$

Moreover, the first part, (i.e., I_1) can be written as:

$$I_1 = \int_{x=\frac{I_{\max}}{P_s}}^{\infty} \frac{1}{\sigma_{f_{sp}}^2} e^{-\frac{x}{\sigma_{f_{sp}}^2}} \times \left(1 - \left(\frac{\sigma_h^2}{\bar{I}_R} \right)^{L_R} \frac{e^{-\frac{\gamma x}{I_{\max} \sigma_h^2}}}{\left(\frac{\sigma_h^2}{\bar{I}_R} + \frac{\gamma x}{I_{\max}} \right)^{L_R}} \right) dx, \quad (3.40)$$

After some rearrangements, the above formula can be written as:

$$I_1 = e^{-\frac{I_{\max}}{P_s \sigma_{f_{sp}}^2}} - \left(\frac{I_{\max} \sigma_h^2}{\gamma \bar{I}_R} \right)^{L_R} \frac{1}{\sigma_{f_{sp}}^2} \int_{x=\frac{I_{\max}}{P_s}}^{\infty} \frac{e^{-x \left(\frac{\gamma}{I_{\max} \sigma_h^2} + \frac{1}{\sigma_{f_{sp}}^2} \right)}}{\left(\frac{I_{\max} \sigma_h^2}{\gamma \bar{I}_R} + x \right)^{L_R}} dx. \quad (3.41)$$

Now, let $t = \frac{I_{\max} \sigma_h^2}{\gamma \bar{I}_R} + x$, therefore, the following expression can be obtained:

$$I_1 = e^{-\frac{I_{\max}}{P_s \sigma_{f_{sp}}^2}} - \left(\frac{I_{\max} \sigma_h^2}{\gamma \bar{I}_R} \right)^{L_R} \frac{1}{\sigma_{f_{sp}}^2} e^{\left(\frac{\gamma \sigma_{f_{sp}}^2 + I_{\max} \sigma_h^2}{I_{\max} \sigma_h^2 \sigma_{f_{sp}}^2} \right) \left(\frac{I_{\max} \sigma_h^2}{\gamma \bar{I}_R} \right)} \times \int_{t=\frac{I_{\max}}{P_s} + \frac{I_{\max} \sigma_h^2}{\gamma \bar{I}_R}}^{\infty} \frac{e^{-t \left(\frac{\gamma \sigma_{f_{sp}}^2 + I_{\max} \sigma_h^2}{I_{\max} \sigma_h^2 \sigma_{f_{sp}}^2} \right)}}{t^{L_R}} dt. \quad (3.42)$$

Next, the variable in the above integral is changed so that $s = t \left(\frac{\gamma \sigma_{f_{sp}}^2 + I_{\max} \sigma_h^2}{I_{\max} \sigma_h^2 \sigma_{f_{sp}}^2} \right)$. After this substitution and by doing some straightforward mathematical manipulation and comparing the obtained formula with [83, eq. (5.2.1)], the desired formula can be obtained as:

$$I_1 = e^{-\frac{I_{\max}}{P_s \sigma_{f_{sp}}^2}} - \left(\frac{I_{\max} \sigma_h^2}{I_{\max} \sigma_h^2 + \gamma \sigma_{f_{sp}}^2} \right) \left(\frac{I_{\max} \sigma_h^2 + \gamma \sigma_{f_{sp}}^2}{\gamma \bar{I}_R \sigma_{f_{sp}}^2} \right)^{L_R} e^{\frac{I_{\max} \sigma_h^2 + \gamma \sigma_{f_{sp}}^2}{\gamma \bar{I}_R \sigma_{f_{sp}}^2}} \times \Gamma \left(1 - L_R, \frac{(\gamma \bar{I}_R + P_s \sigma_h^2) (\gamma \sigma_{f_{sp}}^2 + I_{\max} \sigma_h^2)}{\gamma \sigma_{f_{sp}}^2 P_s \sigma_h^2 \bar{I}_R} \right). \quad (3.43)$$

Finally, an exact equivalent CDF expression for the first hop equivalent SINR (i.e., $F_{\gamma_h^{\text{eff}}}(\gamma)$), can be obtained by combining both parts I_1 , and I_2 , which can be represented as in (3.10).

3.7.2 Proof of Theorem 1

The aim of this theorem is to provide a tight approximate representation of the derived per-hop CDFs, so that further mathematical manipulation can be done on

them. For example, deriving the error probability and EC formulas. Using [80, eq. (5.1.45)] the upper incomplete gamma function can be represented in terms of the exponential integral function as follows:

$$\Gamma(1-n, x) = x^{1-n} E_n(x), \quad (3.44)$$

where $E_n(x)$ is the exponential integral function defined in [83, eq. (8.19.2)]. After this substitution, the CDF of the first hop can be written as in (3.45).

$$F_{\gamma_h^{\text{eff}}}(z) = 1 - \left[e^{-\frac{z}{P_s \sigma_h^2}} \left(\frac{P_s \sigma_h^2}{P_s \sigma_h^2 + z \bar{I}_R} \right)^{L_R} \left(1 - e^{-\frac{I_{\max}}{P_s \sigma_{f_{sp}}^2}} \right) + e^{\frac{I_{\max} \sigma_h^2 + z \sigma_{f_{sp}}^2}{z \bar{I}_R \sigma_{f_{sp}}^2}} \left(\frac{I_{\max} \sigma_h^2}{z \bar{I}_R \sigma_{f_{sp}}^2} \right) E_{L_R} \left(\frac{I_{\max} \sigma_h^2 + z \sigma_{f_{sp}}^2}{z \bar{I}_R \sigma_{f_{sp}}^2} \frac{P_s \sigma_h^2 + z \bar{I}_R}{P_s \sigma_h^2} \right) \left(\frac{P_s \sigma_h^2}{P_s \sigma_h^2 + z \bar{I}_R} \right)^{L_R} \left(\frac{P_s \sigma_h^2 + z \bar{I}_R}{P_s \sigma_h^2} \right) \right]. \quad (3.45)$$

According to [83, eq. (8.19.21)], the exponential integral function can be bounded as:

$$\frac{1}{x+n} < e^x E_n(x) \leq \frac{1}{x+n-1}. \quad (3.46)$$

Furthermore, the following approximation for the exponential integral function is applied:

$$E_n(x) \approx \frac{e^{-x}}{x+n}, \quad (3.47)$$

The next step is to substitute the notations in (3.16a, 3.16b, 3.16c, and 3.16d) into the CDF formula in (3.45), then, apply the proposed approximate formula in (3.47). After doing some mathematical manipulations and rearrangements, the desired and simpler formula is obtained, which is a tight approximate CDF of the first hop equivalent SINR, and is represented in (3.18), where Λ_1 , and Λ_2 are obtained by

using the formulas given in (3.48a, and 3.48b), respectively:

$$\Lambda_1 = \frac{\sigma_h^2}{2} \left[\left(P_s L_R + \frac{I_{\max}}{\sigma_{f_{sp}}^2} + \frac{P_s}{\bar{I}_R} \right) + \sqrt{(P_s L_R)^2 + 2P_s L_R \left(\frac{I_{\max}}{\sigma_{f_{sp}}^2} + \frac{P_s}{\bar{I}_R} \right) + \left(\frac{I_{\max}}{\sigma_{f_{sp}}^2} - \frac{P_s}{\bar{I}_R} \right)^2} \right], \quad (3.48a)$$

$$\Lambda_2 = \frac{\sigma_h^2}{2} \left[\left(P_s L_R + \frac{I_{\max}}{\sigma_{f_{sp}}^2} + \frac{P_s}{\bar{I}_R} \right) - \sqrt{(P_s L_R)^2 + 2P_s L_R \left(\frac{I_{\max}}{\sigma_{f_{sp}}^2} + \frac{P_s}{\bar{I}_R} \right) + \left(\frac{I_{\max}}{\sigma_{f_{sp}}^2} - \frac{P_s}{\bar{I}_R} \right)^2} \right]. \quad (3.48b)$$

The same procedure that has been used for the first hop CDF can be repeated for the opportunistic second hop CDF. Therefore, a tight approximate opportunistic CDF of the second hop opportunistic equivalent SINR can be formulated as in (3.19), where Λ_3 , and Λ_4 are obtained by using the formulas given in (3.49a, and 3.49b), respectively:

$$\Lambda_3 = \frac{\sigma_g^2}{2} \left[\left(P_r L_D + \frac{I_{\max}}{n\sigma_{f_{rp}}^2} + \frac{P_r}{\bar{I}_D} \right) + \sqrt{(P_r L_D)^2 + 2P_r L_D \left(\frac{I_{\max}}{n\sigma_{f_{rp}}^2} + \frac{P_r}{\bar{I}_D} \right) + \left(\frac{I_{\max}}{n\sigma_{f_{rp}}^2} - \frac{P_r}{\bar{I}_D} \right)^2} \right], \quad (3.49a)$$

$$\Lambda_4 = \frac{\sigma_g^2}{2} \left[\left(P_r L_D + \frac{I_{\max}}{n\sigma_{f_{rp}}^2} + \frac{P_r}{\bar{I}_D} \right) - \sqrt{(P_r L_D)^2 + 2P_r L_D \left(\frac{I_{\max}}{n\sigma_{f_{rp}}^2} + \frac{P_r}{\bar{I}_D} \right) + \left(\frac{I_{\max}}{n\sigma_{f_{rp}}^2} - \frac{P_r}{\bar{I}_D} \right)^2} \right]. \quad (3.49b)$$

In the numerical and simulation results section, in Fig. 3.2, the OP was plotted using the derived new expressions for CDF formulas and compared with the exact results. It can be observed that the proposed tight approximation gives quite accurate results, especially for the higher values of I_{\max} .

In addition, to show the accuracy of the proposed tight approximation numerically, Table 3.1 has been constructed, which is a comparison between the exact value of the exponential integral term and its corresponding tight approximated value. It will explain the tightness of the approximation that has been used in the performance analysis. For the exact calculation, the value of $e^z E_{L_R}(z)$ has been calculated, where $z = \left(\frac{I_{\max}\sigma_h^2 + \gamma_{th}\sigma_{f_{sp}}^2}{\gamma_{th}\bar{I}_R\sigma_{f_{sp}}^2} \right) \left(\frac{P_s\sigma_h^2 + \gamma_{th}\bar{I}_R}{P_s\sigma_h^2} \right)$. Furthermore, the following values are assumed for the entities: $\sigma_h^2 = 2.2$, $\sigma_{f_{sp}}^2 = 0.7$, $\bar{I}_R = 3\text{dB}$, $L_R = 2$, and $\gamma_{th} = 2\text{ dB}$. Moreover, for the tight approximate calculation, the value of $\frac{1}{L_R+z}$ has been determined. The

calculations have been made for different values of I_{\max} in dB and P_s .

Table 3.1: Comparison between the exact and approximate representations of the exponential integral function

I_{\max} in dB	$P_s = 10$ dB		$P_s = 15$ dB	
	Exact	Approximate	Exact	Approximate
4	0.194939388	0.184211969	0.207475405	0.194783537
8	0.104513633	0.102612305	0.112473998	0.110134216
12	0.048781832	0.04856972	0.052923924	0.052654999
16	0.020926427	0.020908823	0.02280764	0.022784929
20	0.008603787	0.008602534	0.009397708	0.009396079
24	0.00347106	0.003470977	0.003794922	0.003794814
28	0.001389295	0.001389289	0.001519509	0.001519502
32	0.000554279	0.000554279	0.000606325	0.000606324

3.7.3 First hop Average Error Probability Derivation Steps

For deriving the AEP, a tight proposed approximated CDF in (3.18) was used. After substituting (3.18) into (3.14), a formula can be obtained that has three integral parts. In the sections below, each part will be discussed and/or derived. The first integral part can be easily obtained by comparing the obtained integral formula with [83, eq. (5.2.1)]. Bearing in mind that $n! = \Gamma(n - 1)$ and $\Gamma(1/2) = \sqrt{\pi}$.

$$\bar{P}_b^{sr1} = \frac{a}{2} \sqrt{\frac{b}{\pi}} \int_0^{\infty} \frac{e^{-b x}}{\sqrt{x}} dx = \frac{a}{2}, \quad (3.50)$$

where \bar{P}_b^{sr1} represents the first part of the first hop AEP formula. The second part of the integral has the following form:

$$\bar{P}_b^{sr2} = -\frac{a}{2} \sqrt{\frac{b}{\pi}} \int_0^{\infty} \frac{e^{-b x}}{\sqrt{x}} \Upsilon_1 \frac{e^{-\frac{x}{\alpha}}}{(\beta + z)^{L_R}} dx, \quad (3.51)$$

where \bar{P}_b^{sr2} represents the second part of the first hop AEP formula. The variable in the above integral is exchanged so that $t = \frac{x}{\beta}$, then, after performing some mathematical arrangements, the following expression can be obtained:

$$\bar{P}_b^{sr2} = -\Upsilon_1 \frac{a}{2} \sqrt{\frac{b}{\pi}} \beta^{\frac{1}{2} - L_R} \int_0^{\infty} \frac{e^{-t\beta(b + \frac{1}{\alpha})}}{\sqrt{t}(1+t)^{L_R}} dt, \quad (3.52)$$

using [80, eq. (13.2.5)] the desired formula can be obtained;

$$\bar{P}_b^{sr2} = -\Upsilon_1 \frac{a}{2} \sqrt{b} \beta^{-L_R + \frac{1}{2}} U \left(\frac{1}{2}, \frac{3}{2} - L_R, \beta \left(b + \frac{1}{\alpha} \right) \right). \quad (3.53)$$

The third part of the integral has the following form:

$$\bar{P}_b^{sr3} = -\Upsilon_2 \frac{a}{2} \sqrt{\frac{b}{\pi}} \int_0^\infty \frac{x^{-1/2} (\beta + x)^{1-L_R} e^{-bx} e^{-\frac{x}{\alpha}}}{(\Lambda_1 + x)(\Lambda_2 + x)} dx, \quad (3.54)$$

where \bar{P}_b^{sr3} represents the third part of the first hop AEP formula. For the purpose of mathematical tractability, and to simplify the above integral, the partial fraction decomposition technique has been used to represent the integral formula in a simpler form:

$$\bar{P}_b^{sr3} = -\Upsilon_2 \frac{a}{2} \sqrt{\frac{b}{\pi}} \int_0^\infty \frac{e^{-x(b+\frac{1}{\alpha})}}{\sqrt{x}} \times \left[\sum_{i=1}^{L_R-1} \frac{\lambda_{1_i}}{(\beta+x)^i} + \frac{\lambda_2}{(\Lambda_1+x)} + \frac{\lambda_3}{(\Lambda_2+x)} \right] dx, \quad (3.55)$$

where λ_{1_i} , λ_2 , and λ_3 are coefficient constants, their values are obtained by the formulas given in (3.21a, 3.21b, and 3.21c), respectively. Now, the obtained formula has three parts, which are defined as $\bar{P}_{b_1}^{sr3}$, $\bar{P}_{b_2}^{sr3}$, and $\bar{P}_{b_3}^{sr3}$. By observing the integral formula, it can be deduced that the $\bar{P}_{b_1}^{sr3}$ is quite similar to the formula that was derived in the previous section (i.e., second part of the error probability formula \bar{P}_b^{sr2}). Therefore, it can be written as:

$$\bar{P}_{b_1}^{sr3} = -\Upsilon_2 \frac{a}{2} \sqrt{b} \sum_{i=1}^{L_R-1} \lambda_{1_i} \beta^{\frac{1}{2}-i} U \left(\frac{1}{2}, \frac{3}{2} - i, \beta \left(b + \frac{1}{\alpha} \right) \right). \quad (3.56)$$

Moreover, the integral in $\bar{P}_{b_2}^{sr3}$ can be solved as the following; first, the variable of the integral is changed so that $x = \Lambda_1 t^2$. After doing this exchange operation and performing some mathematical arrangements the following formula can be obtained:

$$\bar{P}_{b_2}^{sr3} = -\frac{2\Upsilon_2 \lambda_2}{\sqrt{\Lambda_1}} \frac{a}{2} \sqrt{\frac{b}{\pi}} \int_0^\infty \frac{e^{-(b+\frac{1}{\alpha})\Lambda_1 t^2}}{(1+t^2)} dt. \quad (3.57)$$

By comparing the above formula with the equation in [83, eq. (7.7.1)] the desired form can be attained:

$$\bar{P}_{b_2}^{sr3} = -\frac{a}{2}\Upsilon_2\lambda_2\sqrt{\frac{b\pi}{\Lambda_1}}e^{(b+\frac{1}{\alpha})\Lambda_1}\operatorname{erfc}\left(\sqrt{\left(b+\frac{1}{\alpha}\right)\Lambda_1}\right). \quad (3.58)$$

The derivation steps of the integral in $\bar{P}_{b_3}^{sr3}$ are similar to previous derivations (i.e., $\bar{P}_{b_2}^{sr3}$). Therefore, it can be written as:

$$\bar{P}_{b_3}^{sr3} = -\frac{a}{2}\Upsilon_2\lambda_3\sqrt{\frac{b\pi}{\Lambda_2}}e^{(b+\frac{1}{\alpha})\Lambda_2}\operatorname{erfc}\left(\sqrt{\left(b+\frac{1}{\alpha}\right)\Lambda_2}\right). \quad (3.59)$$

Finally, the AEP for the first hop can be formulated by combining the three derived parts, and can be written as in (3.20).

3.7.4 Second hop Opportunistic Ergodic Capacity Derivation Steps

After substituting the derived tight approximate opportunistic second hop complementary CDF (i.e., $\bar{F}_{\gamma_{g^*}}^{\text{app}}(z)$) from (3.19) into (3.26), a EC formula can be obtained that has two main parts; which can be named as $C_{erg1}^{g^*}$, and $C_{erg2}^{g^*}$, respectively. In the sections below, each part will be derived and/or discussed. The first part can be represented as:

$$C_{erg1}^{g^*} = \Upsilon_3 \int_0^\infty \frac{e^{-\frac{z}{\delta}}}{(1+z)(\eta+z)^{nL_D}} dz, \quad (3.60)$$

where $C_{erg1}^{g^*}$ represents the first part of the second hop opportunistic EC integral formula. Since it is quite difficult to solve the above integral, it is aimed to represent it in a simpler form so that it can be manipulated and solved. With the help of partial fraction decomposition, the above integral can be represented as the following:

$$C_{erg1}^{g^*} = \Upsilon_3 \int_0^\infty \left[\overbrace{\sum_{r_3=1}^{nL_D} \frac{\omega_{g1_{r_3}} e^{-\frac{z}{\delta}}}{(\eta+z)^{r_3}}}^{C_{erg11}^{g^*}} + \overbrace{\frac{\omega_{g2} e^{-\frac{z}{\delta}}}{(1+z)}}^{C_{erg12}^{g^*}} \right] dz, \quad (3.61)$$

where $\omega_{g1_{r_3}}$, and ω_{g2} are obtained using the formulas given in (3.29a, and 3.29b), respectively. For part $C_{erg11}^{g^*}$ in (3.61), the variable in the integral is exchanged so

that $t = 1 + \frac{z}{\eta}$, therefore after some straightforward mathematical manipulations the following can be attained:

$$C_{erg11}^{g*} = \Upsilon_3 \sum_{r_3=1}^{nL_D} \omega_{g1r_3} \eta^{1-r_3} e^{\frac{\eta}{\delta}} \int_1^{\infty} \frac{e^{-\frac{\eta}{\delta}t}}{t^{r_3}} dt, \quad (3.62)$$

Now, by comparing the above integral formula with [83, eq. (8.19.3)], the desired representation can be achieved:

$$C_{erg11}^{g*} = \Upsilon_3 \sum_{r_3=1}^{nL_D} \omega_{g1r_3} \eta^{1-r_3} e^{\frac{\eta}{\delta}} E_{r_3} \left(\frac{\eta}{\delta} \right). \quad (3.63)$$

For part C_{erg12}^{g*} in (3.61), the variable in the integral is exchanged so that $t = 1 + z$. As a result, the following representation is obtained:

$$C_{erg12}^{g*} = \Upsilon_3 \omega_{g2} e^{\frac{1}{\delta}} \int_1^{\infty} \frac{e^{-\frac{z}{\delta}}}{t} dt, \quad (3.64)$$

With the help of [83, eq. (8.19.3)], a desired formula can be obtained:

$$C_{erg12}^{g*} = \Upsilon_3 \omega_{g2} e^{\frac{1}{\delta}} E_1 \left(\frac{1}{\delta} \right). \quad (3.65)$$

The second part of the second hop opportunistic EC integral formula can be represented as:

$$C_{erg2}^{g*} = \Upsilon_4 \int_0^{\infty} \frac{e^{-\frac{z}{\delta}}}{(\eta + z)^{nL_D-1} (\Lambda_1 + z) (\Lambda_2 + z)} dz, \quad (3.66)$$

where C_{erg2}^{g*} represents the second part of the second hop opportunistic EC integral formula. Similar to the first part of the integral, the partial fraction decomposition technique is employed to represent the above integral in a simpler form so that further mathematical manipulations can be done on it:

$$C_{erg2}^{g*} = \Upsilon_4 \int_0^{\infty} \left[\overbrace{\sum_{r_4=1}^{nL_D-1} \frac{\omega_{g3r_4} e^{-\frac{z}{\delta}}}{(\eta + z)^{r_4}}}^{C_{erg21}^{g*}} + \overbrace{\frac{\omega_{g4} e^{-\frac{z}{\delta}}}{(1 + z)}}^{C_{erg22}^{g*}} + \overbrace{\frac{\omega_{g5} e^{-\frac{z}{\delta}}}{(\Lambda_1 + z)}}^{C_{erg23}^{g*}} + \overbrace{\frac{\omega_{g6} e^{-\frac{z}{\delta}}}{(\Lambda_2 + z)}}^{C_{erg24}^{g*}} \right] dz, \quad (3.67)$$

where $\omega_{g3_{r_4}}$, ω_{g4} , ω_{g5} , and ω_{g6} are obtained using the formulas given in (3.29c, 3.29d, 3.29e, and 3.29f), respectively. It can be observed that similar integral forms as in the first part are obtained. Therefore, just the final equations will be written:

$$C_{erg21}^{g*} = \Upsilon_4 \sum_{r_4=1}^{nL_D-1} \omega_{g3_{r_4}} \eta^{1-r_4} e^{\frac{\eta}{\delta}} E_{r_4} \left(\frac{\eta}{\delta} \right), \quad (3.68)$$

$$C_{erg22}^{g*} = \Upsilon_4 \omega_{g4} e^{\frac{1}{\delta}} E_1 \left(\frac{1}{\delta} \right), \quad (3.69)$$

$$C_{erg23}^{g*} = \Upsilon_4 \omega_{g5} e^{\frac{\Lambda_1}{\delta}} E_1 \left(\frac{\Lambda_1}{\delta} \right), \quad (3.70)$$

$$C_{erg24}^{g*} = \Upsilon_4 \omega_{g6} e^{\frac{\Lambda_2}{\delta}} E_1 \left(\frac{\Lambda_2}{\delta} \right). \quad (3.71)$$

Finally, the opportunistic EC for the second hop can be formulated by combining all derived parts, and it can be written as in (3.28).

Chapter 4

Performance Analysis of a UCRN with Consideration of Primary Network and CCIs

In this chapter, the performance of a multi-hop UCRN is thoroughly assessed. The co-existence of a primary transceiver and CCI are considered along with an uplink single-input multiple-output (SIMO) system utilizing selection combining (SC) and MRC techniques at the receiver nodes. First, the equivalent per-hop SINR for the UCRN is formulated. Second, the exact CDF and the PDF of the per-hop SINR are derived and discussed. Furthermore, to provide more insights about network parameters, approximate expressions exhibiting reduced complexity for the per-hop equivalent CDF are derived.

From the resulting CDF, the exact outage performance of the CR network is thoroughly assessed. In addition, mathematical formulas are derived for the AEP and system EC. Finally, the derived analytical expressions are validated by presenting numerical and simulation results for different network parameters. The results show that several factors contribute to the degradation of the system performance, namely the interference power constraint, the primary transmitter power and the presence of CCI, especially in the case where the CCI increases linearly with the secondary transmission powers.

4.1 Introduction

It is well-known that employing a multi-antenna scheme in a wireless communication network has the advantage of the improvement in the system performance, such as better spectral and power efficiency [93]. In addition, multi-antenna technology has had a major impact on the next generation standards, such as WiMAX and LTE [93, 105]. As a result, it is important to investigate the impact of employing multi-antennas on the UCRN. There are several techniques that can be used to combine the received signal at the receiver of multi-antenna nodes. For example, two common techniques are SC, and MRC. SC is a technique of choosing the best available link, among the possible links between the transmitter and receiver nodes, that has the highest instantaneous SNR [106]. It leads to the retention of the benefits of the multi-antenna scheme and a reduction of the hardware cost [107, 108]. This technique has been widely applied to underlay CR networks [109]. When using an MRC technique, all of the antennas will contribute to the construction of the received signal. This leads to an improvement of the overall system performance [14].

CCI is one of the factors that degrades the performance of a communication network. Due to the spectrum sharing in the CR network and the frequency re-use in wireless signal transmission, this kind of interference could be more predictable. It might come from the adjacent clusters or from other licensed and/or unlicensed users in the same cluster [70]. Therefore, it is important to investigate the impact of such interference on the performance characteristics of an underlay CR network.

4.1.1 Related Work

Outage probability has been widely studied for different underlay CR scenarios [16, 18, 53, 58]. For example, the authors in [58], have thoroughly studied the OP performance of a multi-hop DF spectrum sharing network by considering multiple antennas at the secondary nodes. The direct link between the secondary source and destination was considered. Then, the performance was investigated using both SC and MRC techniques. In the mentioned work, the effect of primary transmitter interference on the secondary network was ignored. In [26], outage performance was studied for dual-hop multi source and multi-relay UCRN. A relay selection method was used in order to improve the performance characteristic; however, no effect of interference was considered for the secondary network. Huang et al. in [53],

investigated the outage performance of a dual-hop DF cognitive radio network with the primary network interference and consideration of Nakagami- m fading channels. Multiple nodes were considered at the secondary destination. Furthermore, SNR and SINR based opportunistic user selection techniques were employed to study the outage performance.

Some works have studied the error probability and/or EC performance investigation for various underlay CR networks [45, 52, 63]. For instance, the bit error rate analysis was carried out for a dual-hop multi relay DF spectrum sharing network in [45]. The relay selection technique was employed to enhance the error probability behaviour for the UCRN. In this analysis, the interference from the primary network was ignored. The authors in [52], have studied the outage and error probability performance in a multiple relay UCRN. In their analysis, the effect of primary network interference was considered on the secondary network. The OP and the EC performances have been investigated in [63] for a dual-hop multiple relay DF UCRN. The relay selection method was used to determine the outage performance, based on the N^{th} best one, and a single relay was considered to investigate the capacity performance. In the mentioned work, the impact of the primary transmitter was not considered. The authors in [44] studied the outage performance, bit error rate and capacity performances for a multi-hop spectrum sharing network. The power constraint on the secondary transmitter nodes was ignored, in addition, primary network interference was ignored. The authors in [70] have investigated the asymptotic outage and error performance in a dual-hop single antenna UCRN. In this work, the effect of primary network and co-channel interferences have been considered, but the effect of AWGN was ignored. Finally, a comprehensive performance for the dual-hop multi-user underlay CR network was investigated in [10], the impact of CCI was considered; yet, the impact of primary network interference on the system performance behaviour of the UCRN was not considered.

4.1.2 Contribution of this Chapter

The majority of the previous works have considered a relatively simplified scenario for the system model; such as, not considering the impact of the primary transmitter, considering a single antenna, considering single and/or dual-hop, and/or only studying outage performance. It is obvious that in the presence of interference, the

system model becomes more complicated, and the mathematical tractability more challenging [70]. In addition, most of the previous work has focused on the outage performance only, and other performance metrics, such as the AEP and the EC, have not been considered.

The key contribution of this chapter is to demonstrate a thorough understanding of the detailed performance behaviour of a pragmatic UCRN. Therefore, the impact of the primary network interference and CCI on the cognitive radio network are examined in the presence of AWGN. In addition, multi-antenna receiver nodes and multi-hop UCRN are studied. More precisely, the OP, AEP and the EC of the UCRN are investigated. In fact, this work is important, especially to a cognitive radio network designer, to better understand the performance characteristics of a UCRN under realistic conditions considered in the network.

Specifically, the DF protocol has been assumed at the relay nodes. First, the exact per-hop equivalent SINR expressions are constructed considering both opportunistic antenna selection and the maximum ratio combining techniques. In particular, two possible scenarios for the selection combining techniques are considered; SNR-based and SINR-based antenna selection. Second, the exact per-hop CDF and the PDF are derived and discussed. Subsequently, the outage performance, AEP and the capacity performance are studied. Finally, several numerical examples are provided to illustrate the system performance characteristics and to support the correctness of the derived results.

From this study, it can be deduced that considering a multi-hop relay network for a UCRN has the advantage of combating the impact of the interference power constraint. It is illustrated that SINR-based antenna selection and MRC consideration provide better performance in comparison to SNR-based antenna selection. However, these approaches require a more complicated hardware configuration and are, hence, practically more challenging. It is also shown that the CCI consideration is severely degrading the performance of the secondary network, especially when its power is considered as linearly increasing with the secondary transmission powers. Furthermore, employment of multi-antennas at the receiver nodes can significantly improve the performance and does not lose its importance even in the presence of interferences and I_{\max} .

The remainder of this chapter is organized as follows. Section 4.2 is devoted to the discussion of the system model. Statistical metrics derivations are presented in

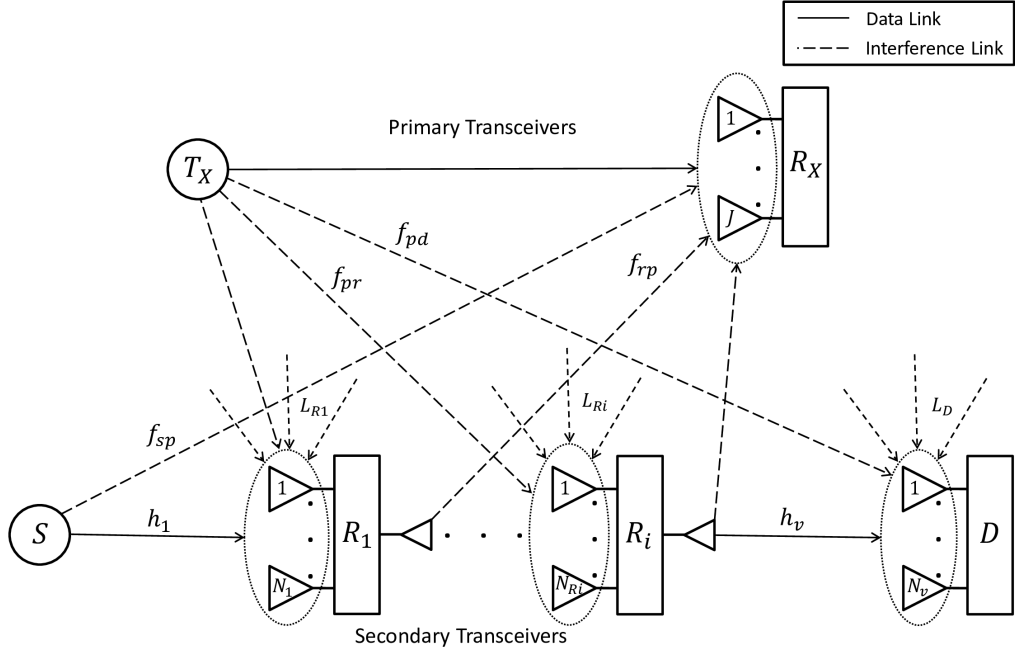


Figure 4.1: The general system model used for analysis, showing multi-hop underlay CR and primary transceiver networks in the presence of co-channel interference with multi-antennas at all receiver nodes.

Section 4.3. Performance analysis metrics are presented and discussed in Section 4.4. Different numerical and Matlab simulations results are presented and discussed in Section 4.5. The summary and conclusions of this chapter are given in Section 4.6. Finally, detailed steps of the analytical derivations are given in Appendices 4.7.1, 4.7.2, 4.7.3, 4.7.4, and 4.7.5.

4.2 System Model

A multi-hop UCRN is considered in which all the nodes in the network have a single transmit antenna and multiple receive antennas. This system model can be seen as an uplink network, where it is reasonable to assume that the mobile transmitter nodes are equipped with single antennas and the receiver nodes, i.e., base stations are equipped with multiple antennas. The network model is shown in Fig. 4.1. Specifically, one source node ($S \equiv R_0$), $(V - 1)$ relay nodes ($R_i, i = 1, 2, \dots, V - 1$) are considered each with N_{Ri} receive antennas, one destination node ($D \equiv R_V$) with N_D antennas ($N_{Dj}, j = 1, \dots, N_D$) and a single primary transceiver with J antennas ($J_j, j = 1, \dots, J$) at the primary receiver node. The nodes in the system operate in half-duplex mode. Relays in the considered system use the decode-and-forward strategy. The fading channels in the multi-hop network are considered

as independent, non-identical, Rayleigh fading channels. In addition, it is assumed that the channels between adjacent transceiver nodes are identical, i.e., the channels between the transmitter and antennas at the receiver side are identical and have the same average channel gains. This is a valid assumption as the distance between the transmitter and either of the corresponding antennas at the receiver node is the same. In the analysis, h is defined as the desired channel and f as an interference channel. Let X_{ij_k} represent a generic fading channel coefficient between the i^{th} transmitter node and the k^{th} antenna at the j^{th} receiver node in the network, where $k = 1, 2, \dots, N_j$, and N_j is the number of antennas at the j^{th} receiver node. For example, the channel coefficient between the source and the k^{th} antenna at the first relay node is $h_{SR_{1k}}$. Also, f_{sp_k} is the interference channel coefficient between the secondary source and the k^{th} antenna at the primary receiver, $f_{pr_{R_{1k}}}$ is the interference channel coefficient between the primary source and the k^{th} antenna at the first relay node. Thus, the channel gains are $|X_{ij_k}|^2$ which all follow exponential distributions with mean powers of $\sigma_{X_{ij}}^2$, which can be calculated using $d_{ij}^{-\alpha}$, where d is the distance between the nodes i and j , and α is the path-loss exponent.

In addition, L_{R_i} and L_D are the finite number of CCI signals that affect the R_i relay nodes and the destination node respectively, which are identical in terms of their average energy at the particular secondary receiver nodes. I_{R_i} and I_D are the instantaneous INRs that affect each of the R_i relay nodes and the destination node, respectively. Due to the broadcast nature of wireless transmission, these CCI signals could be from any source in the neighbouring cells or other frequency channels injecting energy into the channel of interest due to non-linear amplifier operation [10]. The fading energies of the individual CCI signals can be modelled as exponential RVs. Moreover, the sum of the CCI signals at each of the secondary receiver nodes can be modelled by a gamma distributed RV [84]. In addition, \bar{I}_{R_i} and \bar{I}_D are defined as the individual average CCI powers at the R_i relay nodes and the destination node, respectively. It is worth mentioning that analyses and results in this work are calculated depending on the average values of the network parameters and not their instantaneous values.

In the analysis, the transmission power limit of the secondary source nodes are also considered; such that each of the secondary transmitter nodes has a maximum power constraint $P_i, i = 0, 1, 2, \dots, V - 1$, where P_0 represents the transmission power of the source node. The AWGN is assumed as a circular symmetric complex

Gaussian random variable (\mathcal{CN}), at each of the receiver nodes, with zero mean and variance N_0 , i.e., AWGN $\sim \mathcal{CN}(0, N_0)$. In the considered system model, it is assumed that the secondary users have exact knowledge of the channel state information (CSI) between the primary user and the secondary users. In an underlay CR scenario, there should be cooperation between the primary user and the secondary user in terms of providing the CSI and the amount of the interference from the secondary user to the primary user. The CSI at the secondary transmitter can be achieved via the feedback link from the primary receiver or through the channel reciprocity [106]. In a multi-antenna scheme, based on the received signal manipulations at the receiver side, there are different methods to obtain the equivalent SINR. In the following sections, two combining techniques at the secondary receiver nodes are discussed, which are the SC and MRC techniques.

4.2.1 Using the SC Technique

In a SC technique, the best antenna is selected at the relay and destination nodes: This can be achieved by selecting the highest instantaneous SINR out of $N_{R_{ij}}$ and N_{D_j} antennas at both the R_i and D receiver nodes respectively, at any particular point in time. In terms of simplicity of implementation, SC is considered the simplest combining technique at the receiver side, since only one of the diversity links is used in the process [9, p. 404]. Depending on the antenna selection technique employed at the receiver nodes, there are two possible expressions for the per-hop equivalent instantaneous SINR at each of the receivers:

1. **SNR-based antenna selection:** In this case, only the desired channels between the source and N antennas at the destination are used to pick out the antenna which gives the maximum instantaneous SNR. Therefore, the exact instantaneous SINR at the i^{th} hop can be expressed as:

$$\gamma_{\text{eq}}^i = \frac{\min\left(\frac{I_{\max}}{\max_{k=1, \dots, J} (|f_{spk_i}|^2) N_0}, \frac{P_i}{N_0}\right) \max_{n=1, \dots, N_i} (|h_{n_i}|^2)}{\sum_{j=1}^{L_{R_i}} I_{R_{ij}} + I_{P_{R_i}} + 1}, \quad (4.1)$$

where $|f_{spk_i}|^2$ is the channel gain between the secondary transmitter and primary receiver nodes for the i^{th} hop, and $I_{P_{R_i}}$ represent the interference terms from the primary transmitter to the i^{th} hop secondary receiver node. In addition, $I_{R_{ij}}$ represent the CCI terms at the i^{th} hop secondary receiver node.

2. **SINR-based antenna selection:** In this scenario, the interference from the CCI sources and primary network, as well as the noise, are considered in the selection of the best channel. This method is particularly complex practically, since the destination should have complete CSI. However, in the first method, the destination does not need that. Thus, the exact i^{th} hop instantaneous SINR for this scenario can be expressed as:

$$\gamma_{\text{eq}}^i = \min \left(\frac{I_{\text{max}}}{\max_{k=1, \dots, J} (|f_{sp_{k_i}}|^2) N_0}, \frac{P_i}{N_0} \right) \times \max_{n=1, \dots, N_i} \left(\frac{|h_{n_i}|^2}{\sum_{j=1}^{L_{R_i}} I_{R_{n_{ij}}} + I_{P_{R_{n_i}}} + 1} \right). \quad (4.2)$$

4.2.2 Using the MRC Technique

In the MRC technique, all of the antennas at each of the receiver nodes are participating in the resulting SINR. As a result, the exact instantaneous SINR at any i^{th} secondary receiver node can be written as:

$$\gamma_{\text{eq}}^i = \frac{\min \left(\frac{I_{\text{max}}}{\max_{k=1, \dots, J} (|f_{sp_{k_i}}|^2) N_0}, \frac{P_i}{N_0} \right) \sum_{n=1}^{N_i} (|h_{n_i}|^2)}{\sum_{j=1}^{L_{R_i}} I_{R_{ij}} + I_{P_{R_i}} + 1}. \quad (4.3)$$

4.3 Statistical Analysis

In the following sections, the exact and asymptotic per-hop CDFs are derived. Then, the exact per-hop PDF is obtained and discussed.

4.3.1 Exact CDF

In order to analyse the characteristics of a random variable, it is important to obtain and inspect its statistical behaviour. In this section, the CDF of the total SINR is derived, known as $\gamma_{\text{eq}}^{\text{tot}}$, for the UCRN. The CDF of a multi-hop DF cooperative network is obtained by [10]:

$$F_{\gamma_{\text{eq}}^{\text{tot}}}(\gamma) = 1 - \prod_{i=1}^V \left(1 - F_{\gamma_{\text{eq}}^i}(\gamma) \right). \quad (4.4)$$

In (4.4), $F_{\gamma_{\text{eq}}^i}(\gamma)$ represents the CDF of the i^{th} hop. In the sections below, the exact CDF of one hop for the scenario of SNR-based antenna selection will be derived. The

said CDF can be found as follows. Using the formula in (4.1), the CDF expression of the i^{th} hop SINR can be represented as:

$$F_{\gamma_{\text{eq}}^i}(\gamma) = \Pr\left(\min\left(\frac{I_{\text{max}}}{W}, P_s\right) \frac{X}{Y + Z + 1} \leq \gamma\right), \quad (4.5)$$

where W , X , Y , and Z represent RVs $\max_{k=1, \dots, J} (|f_{spk_i}|^2)$, $\max_{n=1, \dots, N_i} (|h_{n_i}|^2)$, $\sum_{j=1}^{L_{R_i}} I_{R_{ij}}$, and $I_{P_{R_i}}$ respectively. Since the decode-and-forward protocol has been assumed at the relay nodes, the CDF derivation steps for any particular hop will be similar to the other hops in the network with the condition of using the corresponding per-hop entities to that particular hop. To avoid confusion and make the calculation simpler and more understandable, simple representations have been used for the PDF and CDF equation entities, (i.e., P_s , σ_h^2 , $\sigma_{f_{sp}}^2$, \bar{I}_R , \bar{I}_{P_R} , N , and L_R have been used instead of P_i , $\sigma_{h_{ij}}^2$, $\sigma_{f_{spij}}^2$, \bar{I}_{R_i} , $\bar{I}_{P_{R_i}}$, N_i , and L_{R_i} respectively), since these are representing the per-hop entities and for each hop the corresponding entities can be replaced. The PDFs of W , X , Y , and Z are expressed respectively as:

$$f_W(w) = \sum_{j=1}^J \binom{J}{j} (-1)^{j+1} \frac{j}{\sigma_{f_{sp}}^2} \exp\left(-\frac{wj}{\sigma_{f_{sp}}^2}\right), \quad (4.6a)$$

$$f_X(x) = \sum_{i=1}^N \binom{N}{i} (-1)^{i+1} \left(\frac{i}{\sigma_h^2}\right) \exp\left(-\frac{xi}{\sigma_h^2}\right), \quad (4.6b)$$

$$f_Y(y) = \frac{y^{L_R-1}}{\bar{I}_R^{L_R} \Gamma(L_R)} \exp\left(-\frac{y}{\bar{I}_R}\right), \quad (4.6c)$$

$$f_Z(z) = \frac{1}{\bar{I}_{P_R}} \exp\left(-\frac{z}{\bar{I}_{P_R}}\right), \quad (4.6d)$$

where $\binom{a}{b}$ are the Binomial coefficients defined in [83, eq. (1.2.1)], and can be represented by this formula: $\frac{a!}{b!(a-b)!}$.

Proposition 1: The exact CDF of the i^{th} equivalent SINR (i.e., $F_{\gamma_{\text{eq}}^i}(\gamma)$) can be written as in (4.7), where Ψ_1 is represented as in (4.8). $E_n(x)$ is the exponential integral function defined in [83, eq. (8.19.2)], and the formula of Ω_n is given in (4.9).

$$F_{\gamma_{\text{eq}}^i}(\gamma) = 1 + \sum_{i=1}^N \binom{N}{i} (-1)^i \left[\left(\frac{P_s \sigma_h^2}{P_s \sigma_h^2 + i\gamma \bar{I}_{P_R}} \right) \left(\frac{P_s \sigma_h^2}{P_s \sigma_h^2 + i\gamma \bar{I}_R} \right)^{L_R} e^{-\frac{i\gamma}{P_s \sigma_h^2}} \left(1 - e^{-\frac{I_{\text{max}}}{P_s \sigma_{f_{sp}}^2}} \right)^J - \sum_{j=1}^J \binom{J}{j} (-1)^j \left(\frac{j I_{\text{max}} \sigma_h^2}{i\gamma \bar{I}_{P_R} \sigma_{f_{sp}}^2} \right) \times \Psi_1 \right], \quad (4.7)$$

$$\Psi_1 = \begin{cases} \left(\frac{P_s \sigma_h^2}{P_s \sigma_h^2 + i\gamma \bar{I}_R} \right)^{L_R} e^{\frac{j I_{\max} \sigma_h^2 + i\gamma \sigma_{f_{sp}}^2}{i\gamma \bar{I}_R \sigma_{f_{sp}}^2}} E_{L_R+1} \left(\left(\frac{j I_{\max} \sigma_h^2 + i\gamma \sigma_{f_{sp}}^2}{\sigma_{f_{sp}}^2 \sigma_h^2} \right) \left(\frac{P_s \sigma_h^2 + i\gamma \bar{I}_R}{i\gamma \bar{I}_R P_s} \right) \right), & \text{if } \bar{I}_{P_R} = \bar{I}_R \\ \left(\frac{\bar{I}_{P_R}}{\bar{I}_{P_R} - \bar{I}_R} \right)^{L_R} e^{\frac{j I_{\max} \sigma_h^2 + i\gamma \sigma_{f_{sp}}^2}{i\gamma \bar{I}_{P_R} \sigma_{f_{sp}}^2}} E_1 \left(\left(\frac{j I_{\max} \sigma_h^2 + i\gamma \sigma_{f_{sp}}^2}{\sigma_{f_{sp}}^2 \sigma_h^2} \right) \left(\frac{P_s \sigma_h^2 + i\gamma \bar{I}_{P_R}}{i\gamma \bar{I}_{P_R} P_s} \right) \right) \\ + \sum_{n=1}^{L_R} \frac{\Omega_n}{\bar{I}_R^{-L_R}} \left(\frac{P_s \sigma_h^2 \bar{I}_R}{P_s \sigma_h^2 + i\gamma \bar{I}_R} \right)^{n-1} e^{\frac{j I_{\max} \sigma_h^2 + i\gamma \sigma_{f_{sp}}^2}{i\gamma \bar{I}_R \sigma_{f_{sp}}^2}} \times \\ E_n \left(\left(\frac{j I_{\max} \sigma_h^2 + i\gamma \sigma_{f_{sp}}^2}{\sigma_{f_{sp}}^2 \sigma_h^2} \right) \left(\frac{P_s \sigma_h^2 + i\gamma \bar{I}_R}{i\gamma \bar{I}_R P_s} \right) \right), & \text{otherwise.} \end{cases} \quad (4.8)$$

$$\Omega_n = \frac{1}{(L_R - n)!} \frac{\partial^{L_R - n}}{\partial w^{L_R - n}} \left(\frac{1}{\bar{I}_{P_R}} + w \right)^{-1} \Big|_{w = -\left(\frac{1}{\bar{I}_R}\right)}. \quad (4.9)$$

Proof: First, the resulting RV from $X/(Y + Z + 1)$ is derived. Then, the exact per-hop unconditional CDF is obtained. Let Q represent the new RV resulting from $Y + Z$. To obtain the sum of two random variables, the following formula can be used [110, eq. (6.47)]:

$$f_Q(q) = \int_0^q f_Y(y) f_Z(q - y) dy. \quad (4.10)$$

After substituting $f_Y(y)$, and $f_Z(q - y)$ into the above formula, and with the help of [83, eq. (8.2.1)], the PDF of RV Q can be written as:

$$f_Q(q) = \frac{e^{-\frac{q}{\bar{I}_{P_R}}}}{\bar{I}_{P_R} \Gamma(L_R)} \left(\frac{\bar{I}_{P_R}}{\bar{I}_{P_R} - \bar{I}_R} \right)^{L_R} \gamma \left(L_R, \frac{\bar{I}_{P_R} - \bar{I}_R}{\bar{I}_{P_R} \bar{I}_R} q \right), \quad (4.11)$$

where $\gamma(., .)$ is the lower incomplete Gamma function. The next step is to obtain the CDF of $\frac{X}{Q+1}$. Let M represent the new RV resulting from $\frac{X}{Q+1}$. To obtain an expression for the CDF of RV M , the following formula can be employed [10]:

$$F_M(\gamma) = \int_0^\infty F_X((q+1)\gamma) f_Q(q) dq. \quad (4.12)$$

After substituting $F_X((q+1)\gamma)$, and $f_Q(q)$ into (4.12), the resulting integral formula can be solved by employing integration by parts, i.e., $\int u dv = uv - \int v du$, as follows:

let $u = \gamma(L_R, \varrho_1 q)$, and $dv = e^{-\varrho_2 q}$; where $\varrho_1 = \left(\frac{\bar{I}_{P_R} - \bar{I}_R}{\bar{I}_{P_R} \bar{I}_R}\right)$ and $\varrho_2 = \left(\frac{i\gamma \bar{I}_{P_R} + \sigma_h^2}{\sigma_h^2 \bar{I}_{P_R}}\right)$. Therefore, the CDF of the RV M can be written as:

$$F_M(\gamma) = 1 - \sum_{i=1}^N \binom{N}{i} (-1)^{i+1} e^{-\frac{i\gamma}{\sigma_h^2}} \times \left(\frac{\sigma_h^2}{\sigma_h^2 + i\gamma \bar{I}_{P_R}}\right) \left(\frac{\sigma_h^2}{\sigma_h^2 + i\gamma \bar{I}_R}\right)^{L_R}. \quad (4.13)$$

Using the total probability theorem, the CDF formula in (4.5) can be expressed as:

$$F_{\gamma_{\text{eq}}^i}(\gamma) = \overbrace{\Pr\left(\frac{I_{\text{max}}}{W} M \leq \gamma, \frac{I_{\text{max}}}{W} < P_s\right)}^{I_1} + \overbrace{\Pr\left(P_s M \leq \gamma, \frac{I_{\text{max}}}{W} \geq P_s\right)}^{I_2}. \quad (4.14)$$

The second part can be directly obtained as follows:

$$I_2 = F_M\left(\frac{\gamma}{P_s}\right) F_W\left(\frac{I_{\text{max}}}{P_s}\right). \quad (4.15)$$

The first part can be represented as:

$$I_1 = \int_{\frac{I_{\text{max}}}{P_s}}^{\infty} F_M\left(\frac{\gamma w}{I_{\text{max}}}\right) f_W(w) dw. \quad (4.16)$$

The detailed steps of the solution for the first part (i.e., I_1) are given in Appendix 4.7.1. Finally, the exact per-hop equivalent CDF can be obtained by combining the derived parts. After some straightforward mathematical arrangements, it can be written as in (4.7) and (4.8). Thus, the exact end-to-end CDF expression of $\gamma_{\text{eq}}^{\text{tot}}$ can be obtained by substituting the per-hop derived expressions $F_{\gamma_{\text{eq}}^i}(\gamma)$ into (4.4). ■

Regarding the per-hop CDF for the case of SINR-based antenna selection, the derivation steps are quite similar to the previous steps, i.e., SNR-based antenna selection. For the sake of saving space, only the final formula expression is provided, which can be written as in (4.44), and (4.45), in Appendix 4.7.2.

From the derived CDF expressions of both SNR-based and SINR-based antenna selection techniques, it can be observed that both formulas are relatively similar in terms of mathematical representations. However, in terms of practical aspects, in the SINR-based antenna selection technique, the receiver is required to process all available branches, which is practically challenging. On the other hand, in the

SNR-based scenario, only the branch with the highest SNR will participate in the data process detection.

Proposition 2: The exact CDF of the i^{th} equivalent SINR (i.e., $F_{\gamma_{\text{eq}}^i}(\gamma)$) for the MRC scenario can be written as:

$$F_{\gamma_{\text{eq}}^i}(\gamma) = 1 - \sum_{n=0}^{N-1} \sum_{i=0}^n \binom{n}{i} \frac{1}{n!} \frac{1}{\bar{I}_{PR}} \left(\frac{\bar{I}_{PR}}{\bar{I}_{PR} - \bar{I}_R} \right)^{L_R} \times \left[I_{\text{mrc}}^2 - I_{\text{mrc}}^1 \right], \quad (4.17)$$

where I_{mrc}^2 and I_{mrc}^1 are given in (4.50) and (4.51) in Appendix 4.7.3.

Proof: The PDF of RV Q , i.e., $f_Q(q)$, can be derived using a similar approach to the previous derivation in Proposition 1, where $Q = Y + Z$. Moreover, in the scenario of the MRC consideration, the following CDF should be used to represent the random variable X [14]:

$$F_X(x) = 1 - \sum_{n=0}^{N-1} \frac{1}{n!} e^{-\frac{x}{\sigma_h^2}} \left(\frac{x}{\sigma_h^2} \right)^n. \quad (4.18)$$

In the next step, $F_X(x)$ and $f_Q(q)$ are substituted into (4.12) to obtain $F_M(\gamma)$. Then, assuming that the number of CCI signals is greater than or equal to 1, the resulting integral can be solved as:

$$F_M(\gamma) = 1 - \sum_{n=0}^{N-1} \sum_{i=0}^n \binom{n}{i} \frac{1}{n!} \frac{1}{\bar{I}_{PR}} \left(\frac{\bar{I}_{PR}}{\bar{I}_{PR} - \bar{I}_R} \right)^{L_R} \left(\frac{\gamma}{\sigma_h^2} \right)^n e^{-\frac{\gamma}{\sigma_h^2}} \times \left[\frac{\Gamma(i+1)}{\left(\frac{1}{\bar{I}_{PR}} + \frac{\gamma}{\sigma_h^2} \right)^{i+1}} - \sum_{m=0}^{L_R-1} (m+1)_i \frac{\left(\frac{\bar{I}_{PR} - \bar{I}_R}{\bar{I}_{PR} \bar{I}_R} \right)^m}{\left(\frac{1}{\bar{I}_R} + \frac{\gamma}{\sigma_h^2} \right)^{m+i+1}} \right], \quad (4.19)$$

where $(m+1)_i = \frac{(m+i)!}{m!}$ represents the Pochhammer symbol defined in [83, eq. (5.2.5)]. In the CDF derivation of the MRC case, the scenario where the average INR of the primary transmitter and the CCI sources are not equal is considered, i.e., $\bar{I}_{PR} \neq \bar{I}_R$. In fact, in the case where $\bar{I}_{PR} = \bar{I}_R$, the system can be assumed to have $L_R + 1$ interferences at the secondary receiver nodes. The CDF formula for the per-hop equivalent SINR in (4.3) can be expressed in a similar way as in (4.14). In addition, I_2 can be obtained similar to (4.15), where $F_M(\gamma/P_s)$ is derived in (4.19). The derivation steps of I_1 are presented in Appendix 4.7.3. Therefore,

the exact per-hop CDF in the MRC case consideration can be obtained by adding both derived parts I_1 and I_2 , and can be expressed as in (4.17). ■

4.3.2 Asymptotic CDF

The CDF derivation in the previous section gives the exact performance behaviour of the secondary network. However, it does not provide insights about the system parameters. Therefore, in this section, the aim is to present simplified expressions for the per-hop equivalent CDF that are less complex in terms of mathematical representation and can give the performance characteristics for a particular network scenario. More specifically, considering the SC technique, two cases are studied as follows:

Case I $I_{\max} \rightarrow \infty$:

By employing the condition of $I_{\max} \rightarrow \infty$ in (4.5) and using the formula in (4.13), the per-hop CDF expression can be obtained directly as:

$$F_{\gamma_{\text{eq}}^i}^i(\gamma) = 1 - \sum_{i=1}^N \binom{N}{i} (-1)^{i+1} e^{-\frac{\gamma}{\varpi_1}} \times \left(\frac{\varpi_2}{\varpi_2 + \gamma} \right) \left(\frac{\varpi_3}{\varpi_3 + \gamma} \right)^{L_R}, \quad (4.20)$$

where $\varpi_1 = \frac{P_s \sigma_h^2}{i}$, $\varpi_2 = \frac{P_s \sigma_h^2}{i I_{P_R}}$, and $\varpi_3 = \frac{P_s \sigma_h^2}{i I_R}$. In this scenario, the output CDF is characterized by the secondary transmission power, primary interference power, and the CCI power. However, the interference power constraint does not have any impact on the system performance. This case can be assumed as a special case of an interweave cognitive radio network [8], when the secondary network is broadcasting only in the absence of the primary user.

Case II $P_s \rightarrow \infty$:

In this case, when $P_s \rightarrow \infty$ in (4.5), it can be observed that the per-hop CDF formula can be obtained by taking the expectation of $F_M(\gamma)$ in (4.13) with respect to the RV W . This can be written mathematically as:

$$F_{\gamma_{\text{eq}}^i}^i(\gamma) = \int_0^{\infty} F_M \left(\frac{\gamma w}{I_{\max}} \right) f_W(w) dw. \quad (4.21)$$

Assuming only the case where $\bar{I}_{P_R} \neq \bar{I}_R$, the above integral can be solved using

similar steps for I_1 in Appendix 4.7.1, Section B. Therefore, the per-hop CDF for case II can be written as:

$$F_{\gamma_{\text{eq}}^i}^{\text{asym-II}}(\gamma) = 1 - \sum_{i=1}^N \sum_{j=1}^J \binom{N}{i} \binom{J}{j} (-1)^{j+i} \left(\frac{j I_{\text{max}}}{\sigma_{f_{sp}}^2} \right) \varpi_5 \varpi_6^{L_R} \left[A e^{\varpi_4 \varpi_5} E_1(\varpi_4 \varpi_5) + \sum_{l=1}^{L_R} \frac{B_l}{\varpi_6^{l-1}} e^{\varpi_4 \varpi_6} E_l(\varpi_4 \varpi_6) \right], \quad (4.22)$$

where $\varpi_4 = \left(\frac{i\gamma}{\sigma_h^2} + \frac{j I_{\text{max}}}{\sigma_{f_{sp}}^2} \right)$, $\varpi_5 = \left(\frac{\sigma_h^2}{i\gamma I_{PR}} \right)$, and $\varpi_6 = \left(\frac{\sigma_h^2}{i\gamma I_R} \right)$. Furthermore, $A = (\varpi_6 - \varpi_5)^{L_R}$, and $B_l = \frac{1}{(L_R-l)!} \frac{\partial^{L_R-l}}{\partial w^{L_R-l}} \left(\varpi_5 + w \right) \Big|_{w=-(\varpi_6)}$. It can be observed that even for the case of unlimited transmission power for the secondary network, the performance behaviour is mainly characterized by the interference power constraint I_{max} . In fact, this I_{max} is the main obstacle against performance improvement in a UCRN. This scenario is called I_{max} dominant power transmission.

4.3.3 Per-hop Equivalent PDF

The PDF is another important statistical metric for the equivalent SINR. Knowing this important metric, the characteristics and behaviour of the RV can be investigated, which in this research case is the equivalent SINR. The PDF can be obtained by taking the first derivative of the derived CDF with respect to γ . Therefore, the exact per-hop equivalent PDF can be written as in (4.23), where Ψ_2 is represented in (4.24).

$$f_{\gamma_{\text{eq}}^i}(x) = \sum_{i=1}^N \binom{N}{i} (-1)^{i+1} \left[\left(\frac{P_s \sigma_h^2}{i \bar{I}_{PR}} \right) \left(\frac{P_s \sigma_h^2}{i \bar{I}_R} \right)^{L_R} \frac{\left(1 - e^{-\frac{I_{\text{max}}}{P_s \sigma_{f_{sp}}^2}} \right)^J}{\left(\frac{P_s \sigma_h^2}{i \bar{I}_{PR}} + x \right) \left(\frac{P_s \sigma_h^2}{i \bar{I}_R} + x \right)^{L_R}} e^{-\frac{x i}{P_s \sigma_h^2}} \left(\frac{L_R}{\left(\frac{P_s \sigma_h^2}{i \bar{I}_R} + x \right)} + \frac{i}{P_s \sigma_h^2} + \frac{1}{\left(\frac{P_s \sigma_h^2}{i \bar{I}_{PR}} + x \right)} \right) + \sum_{j=1}^J \binom{J}{j} (-1)^{j+1} \left(\frac{j I_{\text{max}} \sigma_h^2}{i \bar{I}_{PR} \sigma_{f_{sp}}^2} \right) \times \Psi_2 \right], \quad (4.23)$$

$$\Psi_2 = \begin{cases} \Psi_{21}, & \text{if } \bar{I}_{PR} = \bar{I}_R \\ \Psi_{22}, & \text{otherwise.} \end{cases} \quad (4.24)$$

Furthermore, Ψ_{21} and Ψ_{22} represented by formulas in (4.25) and (4.26), respectively.

$$\begin{aligned} \Psi_{21} = & \left(\frac{P_s \sigma_h^2}{i \bar{I}_R} \right)^{L_R} \frac{e^{\frac{j I_{\max} \sigma_h^2}{x i \bar{I}_R \sigma_{f_{sp}}^2}}}{x \left(\frac{P_s \sigma_h^2}{i \bar{I}_R} + x \right)^{L_R}} \left\{ E_{L_R} \left(\frac{j I_{\max}}{P_s \sigma_{f_{sp}}^2} + \frac{x i \sigma_{f_{sp}}^2 + j I_{\max} \sigma_h^2}{x i \bar{I}_R \sigma_{f_{sp}}^2} + \frac{x i}{P_s \sigma_h^2} \right) \right. \\ & \left. \left(\frac{i}{P_s \sigma_h^2} - \frac{j I_{\max} \sigma_h^2}{x^2 i \bar{I}_R \sigma_{f_{sp}}^2} \right) + \left(\frac{j I_{\max} \sigma_h^2}{x^2 i \bar{I}_R \sigma_{f_{sp}}^2} + \frac{1}{x} + \frac{L_R}{\frac{P_s \sigma_h^2}{i \bar{I}_R} + x} \right) \right. \\ & \left. E_{L_R+1} \left(\frac{j I_{\max}}{P_s \sigma_{f_{sp}}^2} + \frac{x i \sigma_{f_{sp}}^2 + j I_{\max} \sigma_h^2}{x i \bar{I}_R \sigma_{f_{sp}}^2} + \frac{x i}{P_s \sigma_h^2} \right) \right\}, \end{aligned} \quad (4.25)$$

$$\begin{aligned} \Psi_{22} = & \left(\frac{\bar{I}_{P_R}}{\bar{I}_{P_R} - \bar{I}_R} \right)^{L_R} e^{\frac{1}{\bar{I}_{P_R}}} \left\{ \frac{1}{x} E_1 \left(\frac{j I_{\max}}{P_s \sigma_{f_{sp}}^2} + \frac{1}{\bar{I}_{P_R}} + \frac{j I_{\max} \sigma_h^2}{x i \bar{I}_{P_R} \sigma_{f_{sp}}^2} + \frac{x i}{P_s \sigma_h^2} \right) e^{\frac{j I_{\max} \sigma_h^2}{x i \bar{I}_{P_R} \sigma_{f_{sp}}^2}} \right. \\ & \left. \left(\frac{j I_{\max} \sigma_h^2}{x i \bar{I}_{P_R} \sigma_{f_{sp}}^2} + 1 \right) + \frac{\left(\frac{i}{P_s \sigma_h^2} - \frac{j I_{\max} \sigma_h^2}{x^2 i \bar{I}_{P_R} \sigma_{f_{sp}}^2} \right) e^{-\frac{x i}{P_s \sigma_h^2}} e^{-\frac{j I_{\max}}{P_s \sigma_{f_{sp}}^2} - \frac{1}{\bar{I}_{P_R}}}}{\left(\frac{j I_{\max}}{P_s \sigma_{f_{sp}}^2} + \frac{1}{\bar{I}_{P_R}} + \frac{j I_{\max} \sigma_h^2}{x i \bar{I}_{P_R} \sigma_{f_{sp}}^2} + \frac{x i}{P_s \sigma_h^2} \right)} \right\} \\ & + \sum_{n=1}^{L_R} \frac{\Omega_n e^{\frac{1}{\bar{I}_R}}}{\bar{I}_R^{-L_R}} \left(\frac{P_s \sigma_h^2}{i} \right)^{n-1} \frac{e^{\left(\frac{j I_{\max} \sigma_h^2}{x i \bar{I}_R \sigma_{f_{sp}}^2} \right)}}{x \left(\frac{P_s \sigma_h^2}{i \bar{I}_R} + x \right)^n} \left[\left(\frac{P_s \sigma_h^2}{i \bar{I}_R} + x \right) \right. \\ & E_{n-1} \left(\frac{j I_{\max}}{P_s \sigma_{f_{sp}}^2} + \frac{x i \sigma_{f_{sp}}^2 + j I_{\max} \sigma_h^2}{x i \bar{I}_R \sigma_{f_{sp}}^2} + \frac{x i}{P_s \sigma_h^2} \right) \left(\frac{i}{P_s \sigma_h^2} - \frac{j I_{\max} \sigma_h^2}{x^2 i \bar{I}_R \sigma_{f_{sp}}^2} \right) \\ & + \left(\frac{\left(\frac{j I_{\max} \sigma_h^2}{i \bar{I}_R \sigma_{f_{sp}}^2} \right) \left(\frac{P_s \sigma_h^2}{i \bar{I}_R} + x \right) + \frac{P_s \sigma_h^2}{i \bar{I}_R} + x}{x^2} + \frac{P_s \sigma_h^2}{i \bar{I}_R} + x + (n-1) \right) \\ & \left. E_n \left(\frac{j I_{\max}}{P_s \sigma_{f_{sp}}^2} + \frac{x i \sigma_{f_{sp}}^2 + j I_{\max} \sigma_h^2}{x i \bar{I}_R \sigma_{f_{sp}}^2} + \frac{x i}{P_s \sigma_h^2} \right) \right]. \end{aligned} \quad (4.26)$$

To show the distribution of the calculated equivalent PDF in (4.23), Fig. 4.2 has been plotted. The channel variances have been computed based on a two-dimensional network topology scenario, where the secondary source node is located at (0,0), and its corresponding destination at (1,0), and the primary destination node is located at (1,1). The path-loss exponent has a range of values between three to five in a suburban area. In this section, a path-loss exponent of four is assumed. From these plots, the effect of the CCI signal numbers and transmission power limit P_s can clearly be seen. For this analysis, for a fixed value of I_{\max} and different values of the transmission power, it can be observed that decreasing the

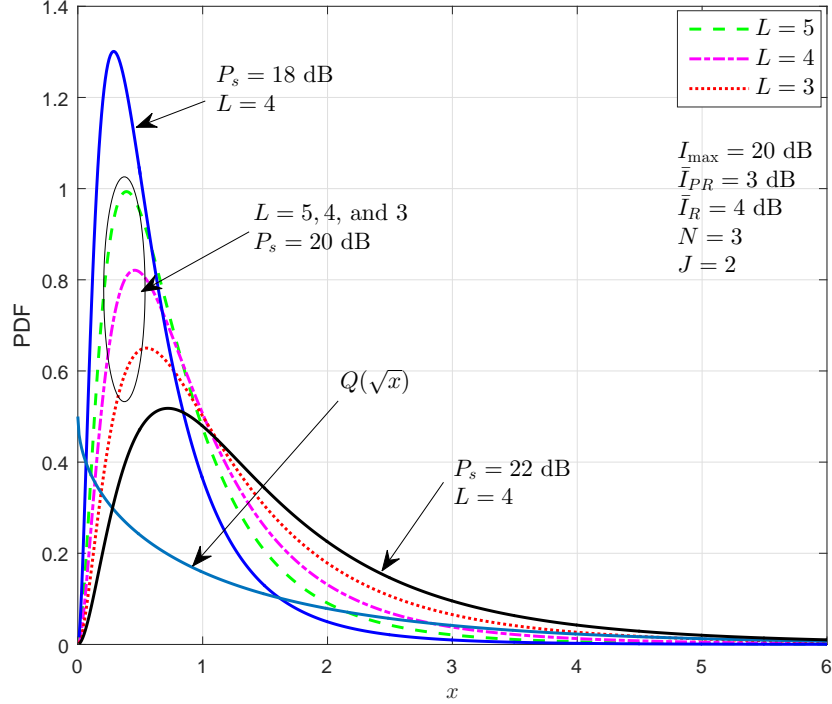


Figure 4.2: Characteristics of the PDF of the per-hop equivalent SINR.

value of P_s deteriorates the PDF behaviour, which will lead to degradation of the network performance.

For further clarification about this claim, the function $Q(\sqrt{x})$ has been plotted in Fig. 4.2. It can be seen that for higher values of x , the behaviour of the PDF gradually becomes insignificant because the Q -function decays to the lowest value, i.e., tends to zero at a higher rate. In this case, the integral is approximately null in most of the integration pattern. However, bearing in mind that $Q(0) = 1/2$, the behaviour of the PDF around the origin is always important. This can be observed in Fig. 4.2, where as P_s increases, the value of the PDF around zero decreases. Moreover, the PDF characteristics have been plotted for the different number of the CCI signals L . It can be seen that for a higher number of CCI signals the PDF curve becomes closer to the origin, i.e., PDF around zero increases, which means the behaviour of the PDF deteriorates which leads to the degradation of the overall system performance.

4.4 Performance Evaluation

In the sections below, to evaluate the secondary network performance behaviour, mathematical expressions for the following performance metrics are derived: OP, AEP and EC.

4.4.1 Outage Probability

The OP performance can be easily investigated from the derived end-to-end CDF. It is referred to in the scenario where the probability of the total calculated SINR of the UCRN is less than or equal to the network predefined SNR threshold γ_{th} . Therefore, the equivalent OP for the UCRN can be calculated using the total equivalent CDF that has been derived in the previous section in (4.4), with the replacement of γ with γ_{th} :

$$P_{\text{out}}(\gamma_{\text{th}}) = \Pr(\gamma_{\text{eq}}^{\text{tot}} \leq \gamma_{\text{th}}) = F_{\gamma_{\text{eq}}^{\text{tot}}}(\gamma_{\text{th}}). \quad (4.27)$$

4.4.2 Average Error Probability

The AEP is one of the important performance criteria for any wireless communication network. The per-hop AEP could be investigated from the PDF or CDF, i.e., $F_{\gamma_{\text{eq}}}^i(\gamma)$ and $f_{\gamma_{\text{eq}}}^i(x)$ [10]. Yet, it can be observed from the PDF obtained in the previous section that the CDF approach could be mathematically more suitable for the calculations, especially in the considered network model. In particular, the CDF is used that has been derived for the scenario of the SNR-based antenna selection. The AEP for each hop can be obtained by using the following formula [111]:

$$\bar{P}_b^i = \frac{a}{2} \sqrt{\frac{b}{\pi}} \int_0^{\infty} \frac{\exp(-b \gamma)}{\sqrt{\gamma}} F_{\gamma_{\text{eq}}}^i(\gamma) d\gamma. \quad (4.28)$$

In (4.28), $F_{\gamma_{\text{eq}}}^i(\gamma)$ represents the per-hop equivalent CDF, a and b are constants that depend on the modulation scheme that is used, for instance, QPSK: $a = 2$ and $b = 0.5$ [70]. Moreover, the end-to-end AEP for a multi-hop decode-and-forward

relay protocol can be determined by [44]:

$$\bar{P}_b^{e2e} = \sum_{i=1}^V \bar{P}_b^i \prod_{j=i+1}^V (1 - 2\bar{P}_b^j). \quad (4.29)$$

Corollary 1: To obtain the exact per-hop AEP, first the exact derived CDF in (4.7) and (4.8) are substituted into (4.28). After solving the equation, the AEP can be written as in (4.30):

$$\bar{P}_b^i = \frac{a}{2} + \sum_{i=1}^N \binom{N}{i} (-1)^i \frac{a}{2} \begin{cases} \bar{P}_b^I, & \text{if } \bar{I}_{P_R} = \bar{I}_R, \\ \bar{P}_b^{II}, & \text{otherwise.} \end{cases} \quad (4.30)$$

where \bar{P}_b^I and \bar{P}_b^{II} have been represented in (4.31) and (4.32), which are the first and second case of the AEP expression, i.e., $\bar{I}_{P_R} = \bar{I}_R$, and $\bar{I}_{P_R} \neq \bar{I}_R$ respectively. $U(a, b, z)$ is the confluent hypergeometric function of the second kind defined in [83, eq. (13.4.4)], and $\text{erfc}(\cdot)$ is the complementary error function defined in [83, eq. (7.2.7)]. In addition, μ_{m_1} , and μ_{m_2} are obtained using the formulas given in (4.33a), and (4.33b) respectively. Moreover, $I_{P_{b1}}$ and $I_{P_{b2}}$ are determined using (4.57), and (4.63) respectively.

$$\begin{aligned} \bar{P}_b^I &= \left(\frac{P_s \sigma_h^2}{i \bar{I}_R} \right)^{L_R+1} \left(1 - e^{-\frac{I_{\max}}{P_s \sigma_{f_{sp}}^2}} \right)^J \sqrt{b} U \left(L_R + 1, L_R + \frac{3}{2}, \frac{1}{\bar{I}_R} \left(\frac{b P_s \sigma_h^2}{i} + 1 \right) \right) \\ &\quad \left(b + \frac{i}{P_s \sigma_h^2} \right)^{L_R + \frac{1}{2}} - \sum_{j=1}^J \binom{J}{j} (-1)^j \left(\frac{j I_{\max} \sigma_h^2}{i \bar{I}_R \sigma_{f_{sp}}^2} \right) \left(\frac{P_s \sigma_h^2}{i \bar{I}_R} \right)^{L_R} \sqrt{\frac{b}{\pi}} I_{P_{b1}}. \end{aligned} \quad (4.31)$$

$$\begin{aligned} \bar{P}_b^{II} &= \left(\frac{P_s \sigma_h^2}{i \bar{I}_{P_R}} \right) \left(\frac{P_s \sigma_h^2}{i \bar{I}_R} \right)^{L_R} \left(1 - e^{-\frac{I_{\max}}{P_s \sigma_{f_{sp}}^2}} \right)^J \left[\sqrt{\frac{b \pi i \bar{I}_{P_R}}{P_s \sigma_h^2}} \mu_3 e^{\frac{1}{\bar{I}_{P_R}} \left(\frac{b P_s \sigma_h^2}{i} + 1 \right)} \right. \\ &\quad \left. \text{erfc} \left(\sqrt{\frac{1}{\bar{I}_{P_R}} \left(\frac{b P_s \sigma_h^2}{i} + 1 \right)} \right) + \sqrt{b} \sum_{m_4=1}^{L_R} \mu_{m_4} \left(b + \frac{i}{P_s \sigma_h^2} \right)^{m_4 - \frac{1}{2}} \times \right. \\ &\quad \left. U \left(m_4, m_4 + \frac{1}{2}, \frac{1}{\bar{I}_R} \left(\frac{b P_s \sigma_h^2}{i} + 1 \right) \right) \right] - \sum_{j=1}^J \binom{J}{j} (-1)^j \left(\frac{j I_{\max} \sigma_h^2}{i \bar{I}_{P_R} \sigma_{f_{sp}}^2} \right) \sqrt{\frac{b}{\pi}} I_{P_{b2}}. \end{aligned} \quad (4.32)$$

$$\mu_{m_1} = \frac{1}{(L_R - m_1)!} \frac{\partial^{L_R - m_1}}{\partial \gamma^{L_R - m_1}} \left(\frac{P_s \sigma_h^2}{i \bar{I}_{P_R}} + \gamma \right)^{-1} \Big|_{\gamma = -\left(\frac{P_s \sigma_h^2}{i \bar{I}_R} \right)}, \quad (4.33a)$$

$$\mu_2 = \left(\frac{P_s \sigma_h^2}{i \bar{I}_R} - \frac{P_s \sigma_h^2}{i \bar{I}_{P_R}} \right)^{-L_R}. \quad (4.33b)$$

Proof: See Appendix 4.7.4. ■

4.4.3 Ergodic Capacity

The EC is another important performance measure for any communication system; its unit is measured in (bits/second/Hz) [10]. It gives an indication of the possible data rate that the considered network can achieve under some predefined circumstances. In fact, this is important specifically for a cognitive radio network to assess its contribution in providing the amount of data throughput to the intended SU. According to Shannon's theorem for the network capacity measurement, the EC can be defined mathematically as the expected value of the instantaneous mutual information between the source and destination. This can be expressed as $C_{erg} \triangleq \mathbb{E}[B \log_2(1 + \gamma_{eq})]$, where $\mathbb{E}[\cdot]$ is the expectation operator, B is the operating bandwidth and γ_{eq} is the total equivalent SNR. Moreover, the EC can be obtained using the CDF formula of the total equivalent SINR [10]:

$$C_{erg}^i = \int_0^{\infty} \frac{1}{1 + \gamma} \left(1 - F_{\gamma_{eq}^i}(\gamma) \right) d\gamma, \quad (4.34)$$

where $F_{\gamma_{eq}^i}(\gamma)$ represents the CDF of the i^{th} hop of the secondary network. Furthermore, the EC for a multi-hop decode-and-forward relay protocol can be calculated as:

$$C_{erg}^{e2e} = \frac{1}{V} \min_{i=1, \dots, V} (C_{erg}^i), \quad (4.35)$$

where C_{erg}^i represents the i^{th} hop EC of the CR network. In addition, $\frac{1}{V}$ comes from the fact that the transmission in a V multi-hop network is performed within V time slots, which means the overall bandwidth should be divided by the number of hops in the network.

Corollary 2:

Here, the derivation of the per-hop EC is provided. Then, the total system capacity for the UCRN is calculated by substituting the obtained per-hop EC from (4.34) into (4.35). First, the per-hop complementary CDF formula from (4.17) is substituted

into (4.34). After the evaluation of the integral, the closed-form expression of the per-hop EC can be obtained as:

$$C_{erg}^i = \sum_{i=1}^N \binom{N}{i} (-1)^{i+1} \times \begin{cases} C_{erg}^I, & \text{if } \bar{I}_{P_R} = \bar{I}_R, \\ C_{erg}^{II}, & \text{otherwise.} \end{cases} \quad (4.36)$$

where C_{erg}^I and C_{erg}^{II} are represented in (4.37) and (4.38) respectively. Furthermore, the entities λ_1 , λ_{r_2} , λ_{r_3} , λ_4 , and λ_5 are obtained using the formulas given in (4.39a), (4.39b), (4.39c), (4.39d), and (4.39e) respectively. Moreover, $I_{C_{erg1}}$ and $I_{C_{erg2}}$ are determined using (4.69), and (4.75) respectively.

$$C_{erg}^I = \left(\frac{P_s \sigma_h^2}{i \bar{I}_R} \right)^{L_R+1} \left(1 - e^{-\frac{I_{\max}}{P_s \sigma_{f_{sp}}^2}} \right)^J \left(\lambda_1 e^{\frac{i}{P_s \sigma_h^2}} E_1 \left(\frac{i}{P_s \sigma_h^2} \right) + \sum_{r_2=1}^{L_R+1} \lambda_{r_2} \left(\frac{P_s \sigma_h^2}{i \bar{I}_R} \right)^{1-r_2} \times e^{\frac{1}{\bar{I}_R}} E_{r_2} \left(\frac{1}{\bar{I}_R} \right) \right) - \sum_{j=1}^J \binom{J}{j} (-1)^j \frac{j I_{\max} \sigma_h^2}{i \bar{I}_R \sigma_{f_{sp}}^2} \left(\frac{P_s \sigma_h^2}{i \bar{I}_R} \right)^{L_R} I_{C_{erg1}}. \quad (4.37)$$

$$C_{erg}^{II} = \left(\frac{P_s \sigma_h^2}{i \bar{I}_{P_R}} \right) \left(\frac{P_s \sigma_h^2}{i \bar{I}_R} \right)^{L_R} \left(1 - e^{-\frac{I_{\max}}{P_s \sigma_{f_{sp}}^2}} \right)^J \left(\sum_{r_3=1}^{L_R} \lambda_{r_3} \left(\frac{P_s \sigma_h^2}{i \bar{I}_R} \right)^{1-r_3} e^{\frac{1}{\bar{I}_R}} E_{r_3} \left(\frac{1}{\bar{I}_R} \right) + \lambda_4 e^{\frac{1}{\bar{I}_{P_R}}} E_1 \left(\frac{1}{\bar{I}_{P_R}} \right) + \lambda_5 e^{\frac{i}{P_s \sigma_h^2}} E_1 \left(\frac{i}{P_s \sigma_h^2} \right) \right) - \sum_{j=1}^J \binom{J}{j} (-1)^j \left(\frac{j I_{\max} \sigma_h^2}{i \bar{I}_{P_R} \sigma_{f_{sp}}^2} \right) I_{C_{erg2}}. \quad (4.38)$$

$$\lambda_1 = \left(\frac{P_s \sigma_h^2}{i \bar{I}_R} - 1 \right)^{-(L_R+1)} \quad (4.39a)$$

$$\lambda_{r_2} = \frac{1}{(L_R + 1 - r_2)!} \frac{\partial^{L_R+1-r_2}}{\partial \gamma^{L_R+1-r_2}} \left(1 + \gamma \right)^{-1} \Big|_{\gamma = -\frac{P_s \sigma_h^2}{i \bar{I}_R}} \quad (4.39b)$$

$$\lambda_{r_3} = \frac{1}{(L_R - r_3)!} \frac{\partial^{L_R-r_3}}{\partial \gamma^{L_R-r_3}} \left(1 + \gamma \right)^{-1} \left(\frac{P_s \sigma_h^2}{i \bar{I}_{P_R}} + \gamma \right)^{-1} \Big|_{\gamma = -\frac{P_s \sigma_h^2}{i \bar{I}_R}} \quad (4.39c)$$

$$\lambda_4 = \left(\frac{P_s \sigma_h^2}{i \bar{I}_R} - \frac{P_s \sigma_h^2}{i \bar{I}_{P_R}} \right)^{-L_R} \left(1 - \frac{P_s \sigma_h^2}{i \bar{I}_{P_R}} \right)^{-1} \quad (4.39d)$$

$$\lambda_5 = \left(\frac{P_s \sigma_h^2}{i \bar{I}_R} - 1 \right)^{-L_R} \left(\frac{P_s \sigma_h^2}{i \bar{I}_{P_R}} - 1 \right)^{-1} \quad (4.39e)$$

Proof: See Appendix 4.7.5. ■

It is worth mentioning that in the previously derived formulas for the AEP and EC, the terms in the final equations that include $I_{P_{b1}}$, $I_{P_{b2}}$, $I_{C_{erg1}}$ and $I_{C_{erg2}}$ mainly

affect the system performance in the case of $\frac{I_{\max}}{W} < P_t$, where W is the channel gain between the primary transmitter and the secondary receiver, and P_t is the maximum transmission power constraint of the primary transmitter node. Moreover, in the above scenario, the CR network performance does not depend on the secondary transmission power, and therefore a performance saturation phenomenon is expected. However, the secondary network can be considered as a self-controlled system performance only when $\frac{I_{\max}}{W} \geq P_t$.

4.5 Numerical Results and Discussions

To verify the theoretical derived expressions, extend numerical and simulation results are presented in this section. In particular, a three-hop underlay CR network is considered in the calculation. The following network parameters are considered in this section unless otherwise stated. The channel variances have been calculated based on the two-dimensional network topology, where the secondary source is located at the origin $(0, 0)$, the destination node is located at $(1, 0)$, and the primary receiver node is located at $(1, 1)$. In addition, the first and second relay nodes are located at $(0.25, 0)$ and $(0.6, 0)$ respectively. The path-loss exponent is assumed to be 4. The SNR threshold is assumed to be 1 dB. Furthermore, these notations are used: \bar{I}_{P_1} , \bar{I}_{P_2} , and \bar{I}_{P_3} represent the average interference powers from the primary source to the secondary receiver nodes, where the subscripts 1, 2, and 3 refer to the first relay node, the second relay and destination nodes. \bar{I}_{R_1} , \bar{I}_{R_2} , and \bar{I}_{R_3} represent the average CCI powers at the corresponding receiver nodes in the three hops secondary network respectively. J is the number of antennas at the primary receiver. N_1 , N_2 , and N_3 are the number of receiver antennas at the relay and destination nodes respectively. L_1 , L_2 , and L_3 are the number of CCI signals at the relay and destination nodes respectively.

First, the impact of considering multi-hop cooperative communication on the performance of the secondary network is illustrated. Fig. 4.3 shows the OP versus the transmission SNR. In this figure, the OP performance for one, two, and three hops is compared. To make this comparison fair, only in Fig. 4.3, the same network parameters are assumed for all possible hops. For example, for the two hops network scenario, it is assumed that the relay node is located at $(1/2, 0)$, and for the three hops network scenario, the first and second relay nodes are located at $(1/3, 0)$, and

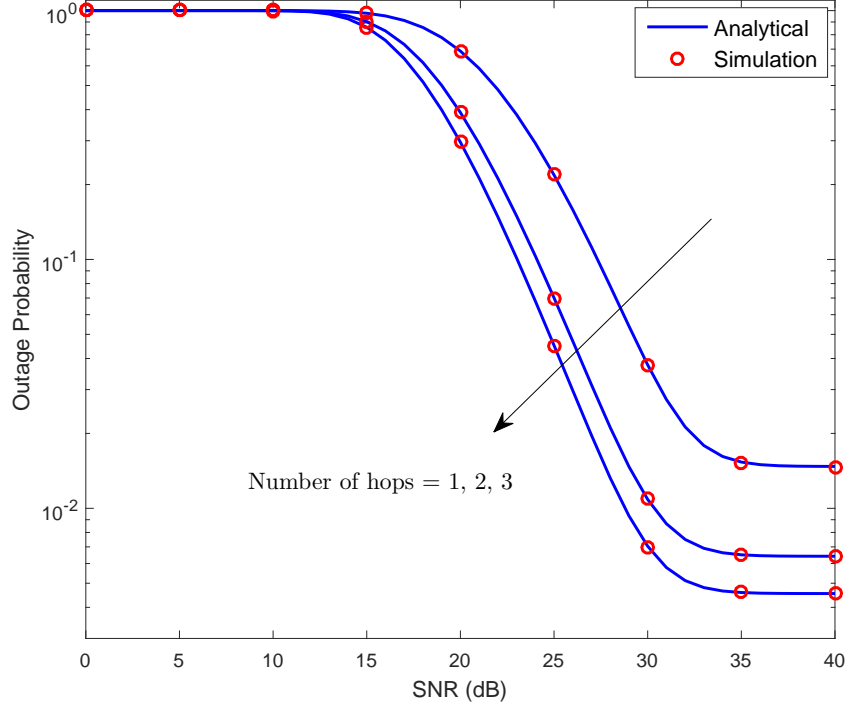


Figure 4.3: Outage performance through consideration of a different number of hops in the UCRN.

(2/3, 0) respectively. The parameter values for this case are as follows: $\bar{I}_P = 4$ dB, $\bar{I}_R = 2$ dB, $I_{\max} = 20$ dB, $J = 3$, $N = 2$, and $L = 4$. From these results, it can be seen that, for example, if the required outage performance target is 10^{-2} , then it is possible to achieve this target with two hops using the same transmission power budget. However, it is not possible to achieve this target with a direct transmission, i.e., single hop. This will prove the effectiveness of a multi-hop cooperative transmission in improving the performance of the UCRN by combating the effect of the interference power constraint. Moreover, it can be seen that the significance of the performance improvement reduces when the number of hops increases, which is due to the fact that a DF relay protocol has been employed which means the end-to-end performance is affected by the unsuccessful decoding at any of the relay nodes.

Fig. 4.4 demonstrates the outage performance versus SNR threshold for different numbers of secondary receiver antennas. The parameter values for this case are as follows: the transmission power at each of the secondary transmitters is 20 dB. In addition, \bar{I}_{R_1} , \bar{I}_{R_2} , and \bar{I}_{R_3} are 2, 3, and 5 dB respectively, \bar{I}_{P_1} , \bar{I}_{P_2} , and \bar{I}_{P_3} are 6, 4, and 5 dB respectively. Furthermore, $I_{\max} = 20$ dB, $J = 2$, and L_1 , L_2 , and L_3 are 4, 4, and 3 respectively. As expected, when the number of antennas at the SU

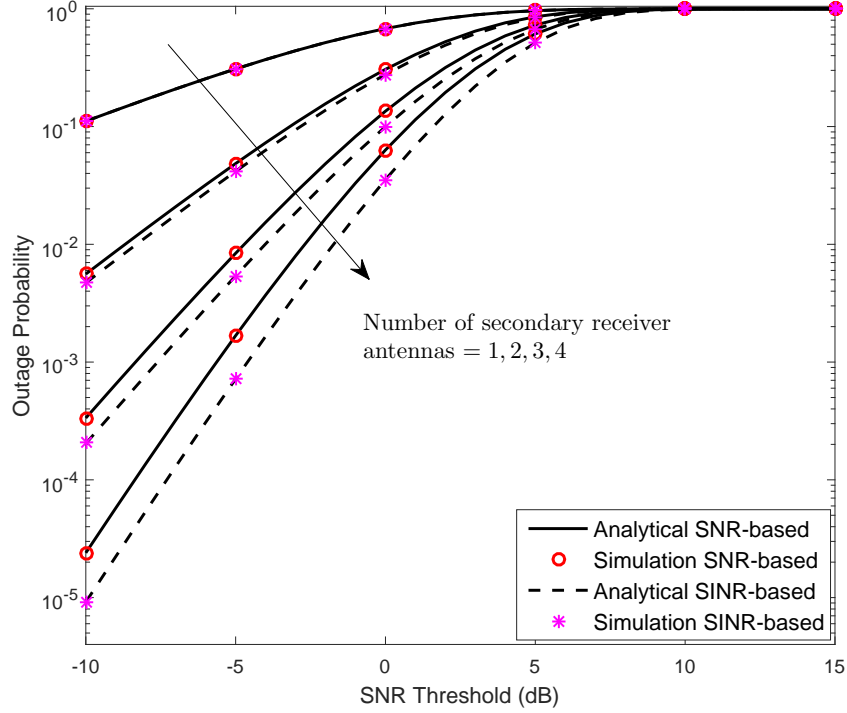


Figure 4.4: Outage probability for a different number of secondary receiver antennas.

receivers is increased, the system performance is apparently enhanced. Moreover, for the purpose of comparison, the outage performance for the scenario of SINR-based antenna selection using the formula in (4.44) have been also plotted. An improvement in the outage performance can be observed when SINR-based antenna selection is considered. However, this consideration requires more complicated system design. Furthermore, for the case of a single antenna at the secondary receiver nodes, both scenarios give the same result which partially proves the correctness and accuracy of the analysis in this work.

To illustrate the impact of the CCI on the CR network, Fig. 4.5 has been plotted, which is the OP performance for different CCI powers at the secondary receiver nodes. The parameter values for this case are as follows: \bar{I}_{P_1} , \bar{I}_{P_2} , and \bar{I}_{P_3} are 3, 3, and 5 dB respectively. Furthermore, $I_{\max} = 15$ dB, $J = 3$, and N_1 , N_2 , and N_3 are 2, 3, and 4 respectively, and L_1 , L_2 , and L_3 are 2, 4, and 3 respectively. From these results, it can be clearly seen how the CCI power affects the performance of the secondary network, for example, when the power of the CCI signals is 6 dB, the outage performance cannot improve more than 2.59×10^{-2} , whereas when it is 2 dB, the outage performance saturates at 5.3×10^{-3} . In addition, the approximate outage performance has been plotted using derived approximate CDF expressions.

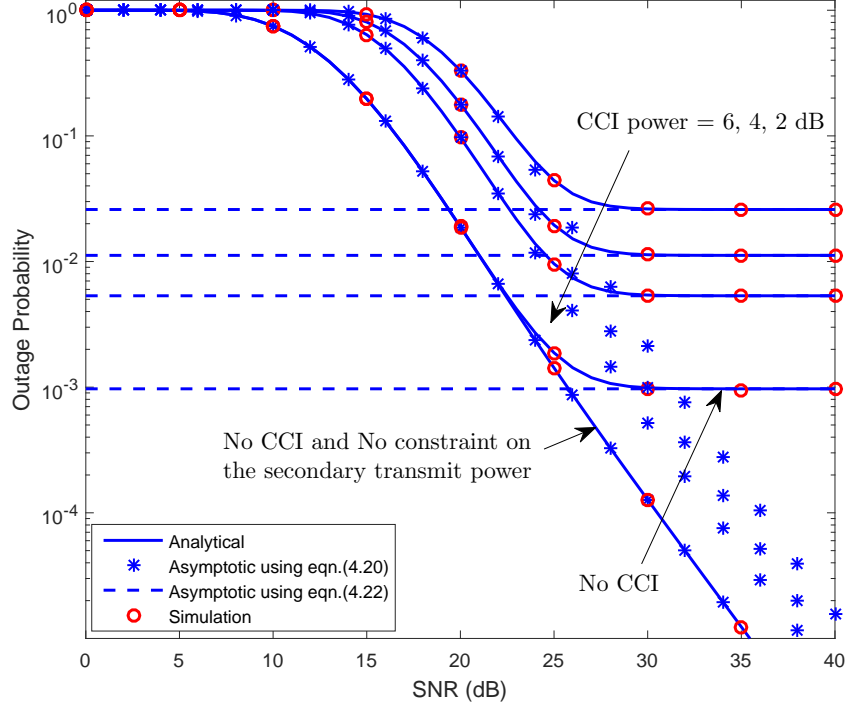


Figure 4.5: Outage probability for different values of CCI powers.

It can be observed that these asymptotic expressions give relatively accurate results depending on the approximation consideration. For example, in an I_{\max} dominant system, the derived expression in (4.22) gives better results, and for a high I_{\max} system, the derived expression in (4.20) gives more accurate results. Moreover, to compare these results with the previous work in this field, the OP has been plotted for the cases *a*) absence of CCI, as in [58], and *b*) absence of CCI and no constraint on the secondary transmission power, as in [18].

Fig. 4.6 shows the outage performance for different values of I_{\max} . The considered parameters are similar to the previous case, except \bar{I}_{R_1} , \bar{I}_{R_2} , and \bar{I}_{R_3} are 4, 3, and 5 dB respectively. As expected, in the scenario where I_{\max} is less than the transmission power of the secondary network (i.e., the I_{\max} dominant region), there is an outage floor, which implies that the system performance could not improve even when the transmission power is increased. Furthermore, to better show the impact of I_{\max} and a linear increase of the CCI on the performance of the UCRN, the outage performance has been plotted for the case where $I_{\max} \gg P_s$, (i.e., no transmission power restriction on the UCRN transmitter nodes due to the primary receiver), and a proportional increase of the CCI power, by 1%, is considered with regards to the secondary transmission powers. It can be observed that even with no interference

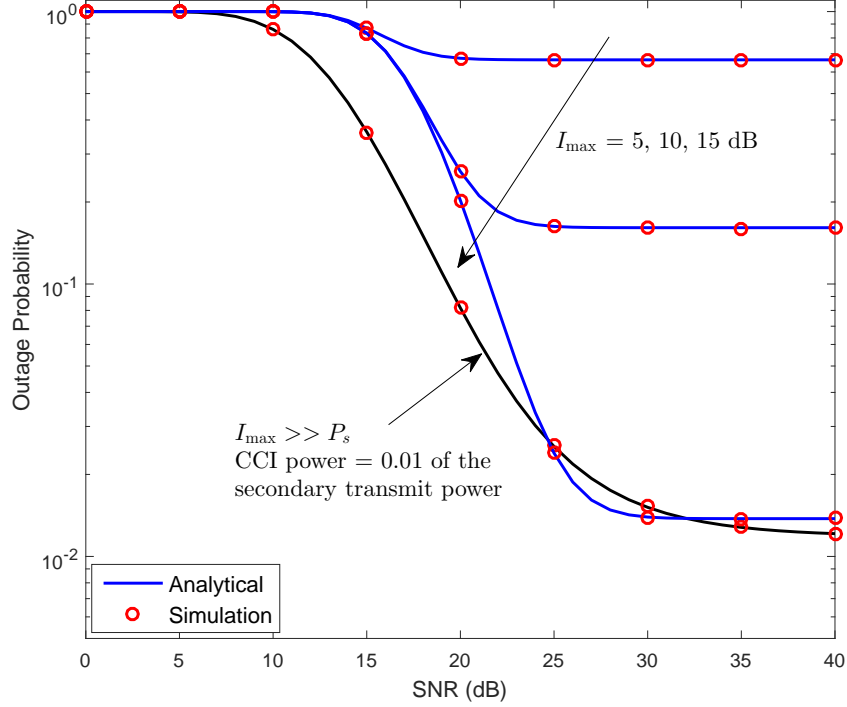


Figure 4.6: Outage probability for different values of I_{\max} .

power constraint present, there is an outage floor. This is caused by the proportional consideration of the CCI power. From this, the severe impact of the CCI power can be deduced when it increases in proportion to the SU transmission power. Moreover, the plot of the result for the case when $I_{\max} = 15$ dB, with a fixed value of CCI, outperforms the result for the linear increase of CCI consideration in a particular region. This is due to two factors: *a*) the strength of the CCI power, and *b*) the fact that the outage floor did not occur at that region for the scenario of the linear increase of the CCI power. However, the situation is reversed when the outage floor occurs.

To illustrate the effect of primary transmitter interference on the performance behaviour of the UCRN, Fig. 4.7 has been plotted, which shows the outage performance versus SNR threshold for different \bar{I}_{P_R} and different signal combination techniques, at the secondary receiver nodes. The parameter values for this case are as follows: the secondary transmitters power and I_{\max} are assumed to be 10 dB. \bar{I}_{R_1} , \bar{I}_{R_2} , and \bar{I}_{R_3} are 4, 3, and 5 dB respectively. In addition, $J = 3$, the number of antennas at each of the secondary receiver nodes is 3, and $L_1 = L_2 = L_3 = 2$. Similar to the case of different CCI considerations in Fig. 4.5, when the considered interference power from the primary network increases, the performance of the CR

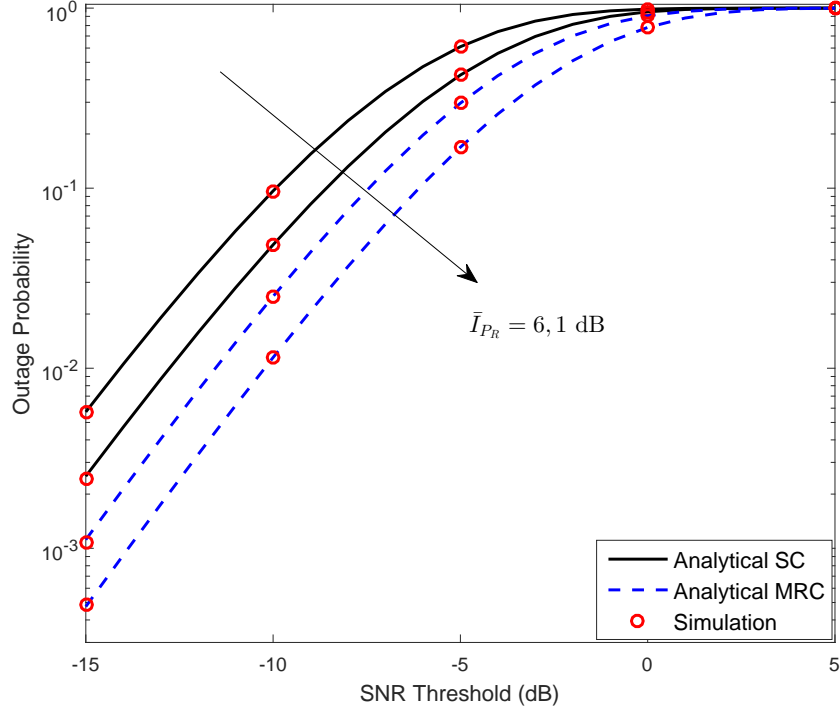


Figure 4.7: Outage probability versus SNR threshold for different values of \bar{I}_{P_R} and signal combining techniques at the secondary receiver nodes.

network degrades. Furthermore, the MRC consideration has a significant improvement in comparison to the SC technique. However, both techniques give similar diversity gain advantage. Furthermore, in terms of simplicity, the SC technique is less complex than the MRC technique [9, p. 404]. In the previous figures and results, it was illustrated that these three factors, (i.e., I_{\max} , CCI, and primary transmitter interference), could severely degrade the performance of the UCRN depending on their consideration in the system model. More precisely, I_{\max} mainly limits the secondary transmission power range, and CCI signals and primary transmitter interferences deteriorate the performance of the secondary network according to their energy values. Besides, when I_{\max} limits the secondary transmission power, and CCI and primary transmitter interferences impact on the network performance at the same time, the probability of outage saturation occurs much faster as can be seen in Fig. 4.6.

Fig. 4.8 shows the AEP performance for a different number of CCI signals at the SU relays and destination nodes. The parameter values for this case are as follows: $I_{\max} = 20$ dB, $\bar{I}_{R_1} = 2$ dB, $\bar{I}_{R_2} = 4$ dB, $\bar{I}_{R_3} = 3$ dB, and $\bar{I}_{P_1} = 4$ dB, $\bar{I}_{P_2} = 6$ dB, $\bar{I}_{P_3} = 5$ dB. The number of antennas at each receiver node in the system is 2.

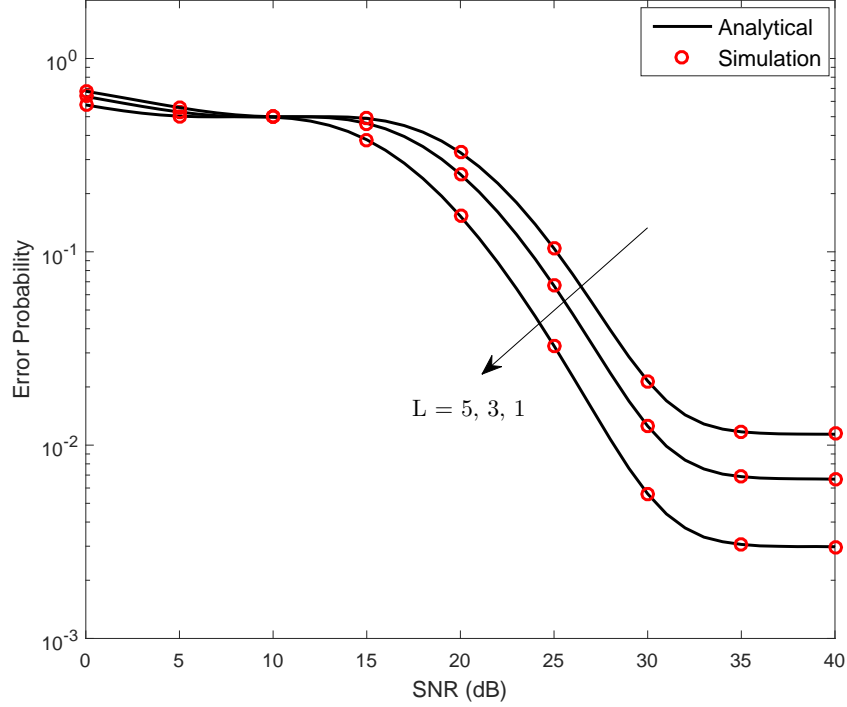


Figure 4.8: Average error probability for a different number of CCI signals at the SU receiver nodes.

From these results, it can be seen that considering a higher number of CCI links can apparently degrade the system performance. For example, when the number of CCI signals is 5, the performance saturation occurs at 1.14×10^{-2} , while it happens at 3.0×10^{-3} when $L = 1$.

To demonstrate the impact of the number of antennas at each of the secondary receiver nodes on the AEP performance, Fig. 4.9 has been plotted. The parameter values for this case are as follows: the CCI power is considered as increasing linearly with respect to the secondary transmission powers by 1%, (i.e., $0.01 \times P_t$, where P_t is the transmission power at each of the secondary transmitter nodes). The other parameters are assumed as follows: $I_{\max} = 15$ dB, $\bar{I}_{P_1} = \bar{I}_{P_2} = 3$ dB, $\bar{I}_{P_3} = 5$ dB. $J = 3$, L_1, L_2, L_3 are 2, 1, and 3 respectively. In the above results, a performance degradation can be observed, which is mainly due to consideration of a linear increase of the CCI power and I_{\max} . In this case, the system performance starts degrading after I_{\max} limits the secondary transmission power. In fact, this is the worst-case scenario of a secondary network performance. However, as expected, employing more antennas at the secondary receiver will enhance the error probability performance. It is worth noting that, despite the impact of interference

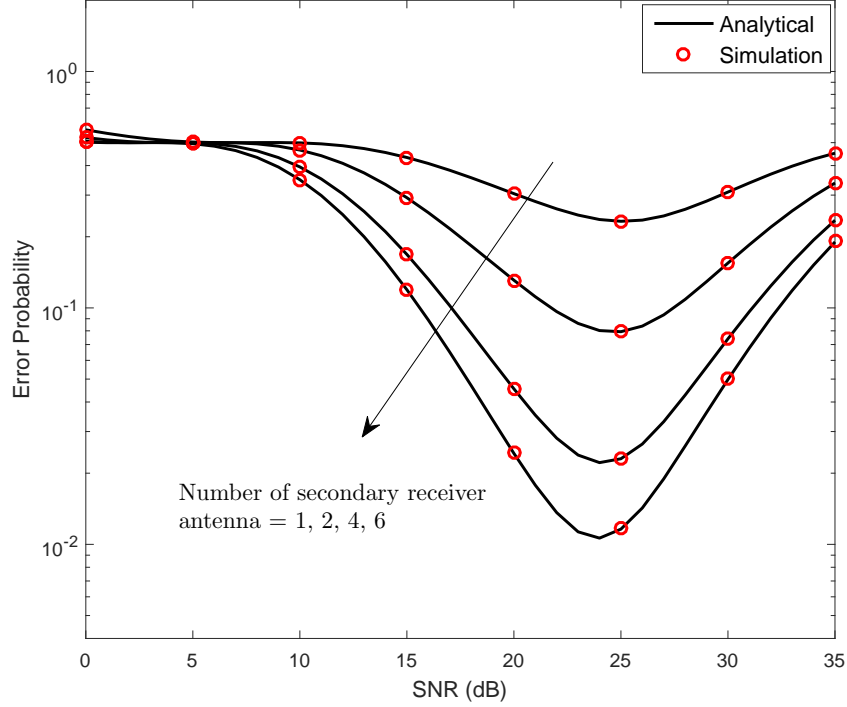


Figure 4.9: Average error probability for a different number of antennas at the CR receiver nodes.

and I_{\max} , the multi-antenna scheme does not lose its importance in enhancing the error probability performance of the UCRN. The impact of performance saturation due to the proportional increase of the interferences can be reduced by employing a multi-hop network. For example, when the interference power is studied as a proportional increase with regards to the secondary transmission powers, it is more likely that the performance saturation will occur according to the considered ratio of the interference power with the secondary transmission powers. In a multi-hop network, the source nodes can broadcast their signals at a lower power to achieve a specific performance in comparison with a direct transmission. Therefore, when the transmission power at the source nodes is reduced, the considered interference power is reduced too. Thus, improved performance will be expected.

In Fig. 4.10, the throughput performance has been illustrated for a different number of antennas at the secondary receiver nodes and different CCI powers. The values of the CCI powers are assumed to be increasing linearly as regards the transmission powers in the secondary nodes. The parameter values for this case are as follows: $\bar{I}_{P_1} = 6$ dB, $\bar{I}_{P_2} = 4$ dB, $\bar{I}_{P_3} = 2$ dB. $J = 2$, $L_1 = 4$, $L_2 = 3$, and $L_3 = 2$. From these results, it can be observed that the capacity saturation has occurred at

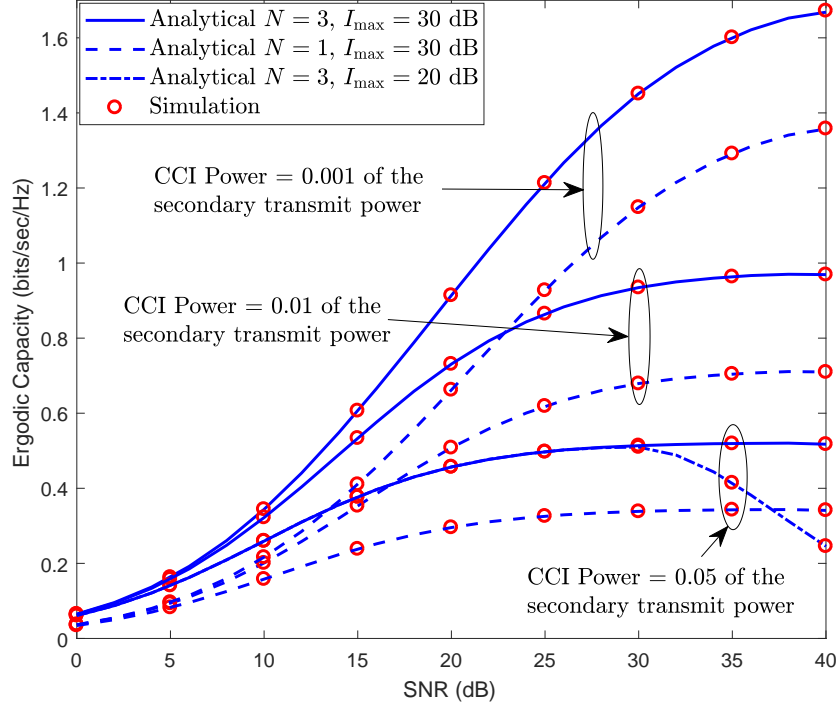


Figure 4.10: Capacity performance for different values of CCI powers and a different number of antennas at the SU receiver nodes.

0.342 bits/sec/Hz, when the relatively higher CCI is considered, (i.e., 0.05) with a single antenna at the secondary receiver nodes. In addition, when three antennas are employed, the capacity saturation occurs at 0.512 bits/sec/Hz. The capacity saturation in these scenarios is mainly due to the CCI power. Moreover, the case where $I_{\max} = 20$ dB and CCI power is 5% of the secondary transmission powers has been plotted. In this case, the capacity degradation is observed instead of the capacity saturation. Moreover, it can be seen that a higher number of receiver antennas, in conjunction with the SC, can enhance the capacity performance of the CR network. Furthermore, it can be deduced that in an underlay CR paradigm, despite the impact of I_{\max} , other factors might limit the advantage of employing a multi-antenna scheme on the network performance, such as the presence of CCI signals and the primary network interference. It has also been illustrated that according to their power strength consideration, they could severely degrade the CR network's performance.

Finally, from the previous results and analysis, the following observations can be summarized:

- SINR-based antenna selection gives better performance in comparison to SNR-

based antenna selection. However, this approach requires more complicated configuration and is practically more challenging.

- It has been shown that the MRC technique outperforms the SC technique, however, the later one is simpler to be realized in practice.
- Communication through a multi-hop relay network has the advantage of combating the impact of interference power constraint on the secondary network. In addition, it has the advantage of extending the coverage of the network.
- Performance saturation, (i.e., floor), in the system performance of the secondary network, can occur due to three factors: interference from primary network, CCI power and I_{\max} .
- The performance saturation phenomenon could be more noticeable when the interference power increases linearly with the secondary transmission powers. It might cause performance reduction instead of a floor when both I_{\max} and CCI have an impact on the CR network.
- An improvement in the system performance can be observed when multi-antenna receivers are considered, and the best antenna selection technique is applied.
- Using multi-antenna receivers might not be an optimal solution for enhancing the system performance in power limited communication networks with the presence of interference. For example, the advantage of multi-antenna receivers, through increasing the diversity gain, can clearly be seen when there is no performance saturation. On the other hand, when performance saturation occurs, the diversity gain reduces to zero.

4.6 Conclusion

In this chapter, a detailed performance investigation of an uplink multi-hop multi-antenna regenerative UCRN has been presented. A more practical case scenario was assumed through the consideration of CCI in addition to the primary transmitter interference on the secondary network. Different signal combining techniques were investigated and discussed at the secondary receiver nodes. OP, AEP and the

EC were thoroughly studied. It was shown that employing a relaying cooperative network has the advantage of enhancing the system performance by reducing the impact of the interference power constraint.

Furthermore, the system performance including the impact of CCI, primary transmitter interference and interference power constraint was enhanced by a multi-antenna scheme. However, it may not provide the optimum advantage due to the constraint on the transmission power and the presence of interferences, especially when performance saturation occurs. The impact of performance saturation can be reduced by employing a multi-hop relay network. Moreover, the severity of interference leads to performance reduction rather than performance floor, especially when its power is considered to be linearly increasing with the secondary transmission power and at a relatively high ratio. Finally, different numerical and simulation examples have been presented to illustrate the performance behaviour and to support the correctness of the derived results. The analysis in this chapter is significant for better understanding the characteristics and behaviour of a more practical scenario of an underlay CR network.

4.7 Appendix

4.7.1 Per-hop CDF Derivation

After substituting the formulas of $F_M\left(\frac{\gamma W}{I_{\max}}\right)$ and $f_W(w)$ into (4.16), the following formula can be obtained:

$$I_1 = \int_{\frac{I_{\max}}{P_s}}^{\infty} \left[1 - \sum_{i=1}^N \binom{N}{i} (-1)^{i+1} \frac{e^{-\frac{i\gamma w}{I_{\max}\sigma_h^2}} \sigma_h^2}{\left(\sigma_h^2 + \frac{wi\gamma\bar{I}_{P_R}}{I_{\max}}\right)} \left(\frac{\sigma_h^2}{\sigma_h^2 + \frac{wi\gamma\bar{I}_R}{I_{\max}}}\right)^{L_R} \right] \times \sum_{j=1}^J \binom{J}{j} (-1)^{j+1} \frac{j e^{-\frac{wj}{\sigma_{f_{sp}}^2}}}{\sigma_{f_{sp}}^2} dw. \quad (4.40)$$

Depending on the values of \bar{I}_R and \bar{I}_{P_R} , there are two possible cases for the solution of the above integral. In the sections below, each case will be derived in detail.

- Case I, $\bar{I}_{P_R} = \bar{I}_R$:

For this case, the variable in the integral is changed so that $w = t \left(\frac{I_{\max}\sigma_{f_{sp}}^2 \sigma_h^2}{jI_{\max}\sigma_h^2 + i\gamma\sigma_{f_{sp}}^2} \right) - \frac{I_{\max}\sigma_h^2}{i\gamma\bar{I}_R}$. Then, after some mathematical manipulation and with the help of [83,

eq. (8.19.2)], a desired representation for the above formula can be obtained.

$$\begin{aligned}
 I_1^I = & \sum_{j=1}^J \binom{J}{j} (-1)^{j+1} e^{\frac{-jI_{\max}}{P_s \sigma_{f_{sp}}^2}} - \sum_{j=1}^J \sum_{i=1}^N \binom{J}{j} \binom{N}{i} (-1)^{j+i} \left(\frac{P_s \sigma_h^2}{P_s \sigma_h^2 + i\gamma \bar{I}_R} \right)^{L_R} \\
 & \left(\frac{jI_{\max} \sigma_h^2}{i\gamma \bar{I}_R \sigma_{f_{sp}}^2} \right) e^{\left(\frac{jI_{\max} \sigma_h^2 + i\gamma \sigma_{f_{sp}}^2}{i\gamma \bar{I}_R \sigma_{f_{sp}}^2} \right)} E_{L_R+1} \left(\frac{\left(jI_{\max} \sigma_h^2 + i\gamma \sigma_{f_{sp}}^2 \right) (P_s \sigma_h^2 + i\gamma \bar{I}_R)}{\sigma_{f_{sp}}^2 \sigma_h^2 i\gamma \bar{I}_R P_s} \right),
 \end{aligned} \tag{4.41}$$

where I_1^I represents the integral of I_1 for the case when $\bar{I}_{P_R} = \bar{I}_R$, and $E_n(x)$ is the exponential integral function.

- Case II, $\bar{I}_{P_R} \neq \bar{I}_R$:

For the case when $\bar{I}_{P_R} \neq \bar{I}_R$, the partial fraction decomposition method was used to solve the integral in (4.40) as follows:

$$\begin{aligned}
 I_1^{II} = & \sum_{j=1}^J \binom{J}{j} (-1)^{j+1} e^{\frac{-I_{\max} j}{P_s \sigma_{f_{sp}}^2}} - \sum_{j=1}^J \sum_{i=1}^N \binom{J}{j} \binom{N}{i} (-1)^{j+i} \left(\frac{jI_{\max} \sigma_h^2}{i\sigma_{f_{sp}}^2 \gamma \bar{I}_{P_R}} \right) \\
 & \left(\frac{I_{\max} \sigma_h^2}{i\gamma \bar{I}_R} \right)^{L_R} \left[\overbrace{\int_{\frac{I_{\max}}{P_s}}^{\infty} \frac{e^{-w \left(\frac{jI_{\max} \sigma_h^2 + i\gamma \sigma_{f_{sp}}^2}{I_{\max} \sigma_{f_{sp}}^2 \sigma_h^2} \right)}}{\left(\frac{I_{\max} \sigma_h^2}{i\gamma \bar{I}_{P_R}} + w \right)} dw}^{I_{21}} + \sum_{n=1}^{L_R} \left(\frac{i\gamma}{I_{\max} \sigma_h^2} \right)^{L_R+1-n} \Omega_n \right. \\
 & \left. \overbrace{\int_{\frac{I_{\max}}{P_s}}^{\infty} \frac{e^{-w \left(\frac{jI_{\max} \sigma_h^2 + i\gamma \sigma_{f_{sp}}^2}{I_{\max} \sigma_{f_{sp}}^2 \sigma_h^2} \right)}}{\left(\frac{I_{\max} \sigma_h^2}{i\gamma \bar{I}_R} + w \right)^n} dw}^{I_{22}} \right],
 \end{aligned} \tag{4.42}$$

where $\zeta = \left(\frac{I_{\max} \sigma_h^2}{i\gamma \bar{I}_R} - \frac{I_{\max} \sigma_h^2}{i\gamma \bar{I}_{P_R}} \right)^{-L_R}$, and Ω_n is obtained by the formula given in (4.9). It can be observed that the above integrals, i.e., I_{21} and I_{22} , are quite similar to the previous derived integral in the first case, i.e., I_1^I in (4.41),

therefore the final formula can be written as in (4.43):

$$\begin{aligned}
 I_1^{II} = & \sum_{j=1}^J \binom{J}{j} (-1)^{j+1} e^{-\frac{I_{\max} j}{P_s \sigma_{f_{sp}}^2}} - \sum_{j=1}^J \sum_{i=1}^N \binom{J}{j} \binom{N}{i} (-1)^{j+i} \frac{j}{\sigma_{f_{sp}}^2} \left(\frac{I_{\max} \sigma_h^2}{i \gamma} \right)^{L_R+1} \\
 & \left(\frac{1}{\bar{I}_{P_R}} \right) \left(\frac{1}{\bar{I}_R} \right)^{L_R} \left[\zeta E_1 \left(\left(\frac{j I_{\max} \sigma_h^2 + i \gamma \sigma_{f_{sp}}^2}{\sigma_{f_{sp}}^2 \sigma_h^2} \right) \left(\frac{P_s \sigma_h^2 + i \gamma \bar{I}_{P_R}}{i \gamma \bar{I}_{P_R} P_s} \right) \right) \right. \\
 & e^{\left(\frac{j I_{\max} \sigma_h^2 + i \gamma \sigma_{f_{sp}}^2}{i \gamma \bar{I}_{P_R} \sigma_{f_{sp}}^2} \right)} + \sum_{n=1}^{L_R} \Omega_n e^{\frac{j I_{\max} \sigma_h^2 + i \gamma \sigma_{f_{sp}}^2}{i \gamma \bar{I}_R \sigma_{f_{sp}}^2}} \left(\frac{i \gamma \bar{I}_R P_s}{P_s I_{\max} \sigma_h^2 + i \gamma \bar{I}_R I_{\max}} \right)^{n-1} \times \\
 & \left. E_n \left(\left(\frac{j I_{\max} \sigma_h^2 + i \gamma \sigma_{f_{sp}}^2}{\sigma_{f_{sp}}^2 \sigma_h^2} \right) \left(\frac{P_s \sigma_h^2 + i \gamma \bar{I}_R}{i \gamma \bar{I}_R P_s} \right) \right) \right]. \quad (4.43)
 \end{aligned}$$

4.7.2 Per-hop CDF using SINR-based Selection Combining

In this section, the per-hop CDF is represented in the case where SINR-based antenna selection is considered. The CDF can be expressed as in (4.44), and (4.45). In addition, Ω_m , and Ω_n are obtained by using (4.46), and (4.47) respectively.

$$\begin{aligned}
 F_{\gamma_{\text{eq}}}^i(\gamma) = & 1 + \sum_{i=1}^N \binom{N}{i} (-1)^i \left[e^{-\frac{i \gamma}{P_s \sigma_h^2}} \left(\frac{P_s \sigma_h^2}{P_s \sigma_h^2 + \gamma \bar{I}_{P_R}} \right)^i \left(\frac{P_s \sigma_h^2}{P_s \sigma_h^2 + \gamma \bar{I}_R} \right)^{i L_R} \times \right. \\
 & \left. \left(1 - e^{-\frac{I_{\max}}{P_s \sigma_{f_{sp}}^2}} \right)^J - \sum_{j=1}^J \binom{J}{j} (-1)^j \frac{j I_{\max}}{\sigma_{f_{sp}}^2} \left(\frac{1}{\bar{I}_{P_R}} \right)^i \left(\frac{1}{\bar{I}_R} \right)^{i L_R} \times \Psi_3 \right]. \quad (4.44)
 \end{aligned}$$

$$\Psi_3 = \begin{cases} e^{\frac{j I_{\max} \sigma_h^2 + i \gamma \sigma_{f_{sp}}^2}{\gamma \bar{I}_R \sigma_{f_{sp}}^2}} \left(\frac{P_s \sigma_h^2 + \gamma \bar{I}_R}{\gamma \bar{I}_R P_s} \right) \left(\frac{\bar{I}_R P_s \sigma_h^2}{P_s \sigma_h^2 + \gamma \bar{I}_R} \right)^{i L_R + i} \times \\ E_{i L_R + i} \left(\left(\frac{j I_{\max} \sigma_h^2 + i \gamma \sigma_{f_{sp}}^2}{\sigma_{f_{sp}}^2 \sigma_h^2} \right) \left(\frac{P_s \sigma_h^2 + \gamma \bar{I}_R}{\gamma \bar{I}_R P_s} \right) \right), & \text{if } \bar{I}_{P_R} = \bar{I}_R \\ \sum_{m=1}^i \Omega_m e^{\frac{j I_{\max} \sigma_h^2 + i \gamma \sigma_{f_{sp}}^2}{\gamma \bar{I}_{P_R} \sigma_{f_{sp}}^2}} \left(\frac{P_s \sigma_h^2 + \gamma \bar{I}_{P_R}}{\gamma \bar{I}_{P_R} P_s} \right) \left(\frac{\bar{I}_{P_R} P_s \sigma_h^2}{P_s \sigma_h^2 + \gamma \bar{I}_{P_R}} \right)^m \times \\ E_m \left(\left(\frac{j I_{\max} \sigma_h^2 + i \gamma \sigma_{f_{sp}}^2}{\sigma_{f_{sp}}^2 \sigma_h^2} \right) \left(\frac{P_s \sigma_h^2 + \gamma \bar{I}_{P_R}}{\gamma \bar{I}_{P_R} P_s} \right) \right) \\ + \sum_{n=1}^{i L_R} \Omega_n e^{\frac{j I_{\max} \sigma_h^2 + i \gamma \sigma_{f_{sp}}^2}{\gamma \bar{I}_R \sigma_{f_{sp}}^2}} \left(\frac{P_s \sigma_h^2 + \gamma \bar{I}_R}{\gamma \bar{I}_R P_s} \right) \left(\frac{\bar{I}_R P_s \sigma_h^2}{P_s \sigma_h^2 + \gamma \bar{I}_R} \right)^n \times \\ E_n \left(\left(\frac{j I_{\max} \sigma_h^2 + i \gamma \sigma_{f_{sp}}^2}{\sigma_{f_{sp}}^2 \sigma_h^2} \right) \left(\frac{P_s \sigma_h^2 + \gamma \bar{I}_R}{\gamma \bar{I}_R P_s} \right) \right), & \text{otherwise.} \end{cases} \quad (4.45)$$

$$\Omega_m = \frac{1}{(i-m)!} \frac{\partial^{i-m}}{\partial w^{i-m}} \left(\frac{1}{\bar{I}_R} + w \right)^{-i L_R} \Big|_{w = -\left(\frac{1}{\bar{I}_{P_R}} \right)}. \quad (4.46)$$

$$\Omega_n = \frac{1}{(iL_R - n)!} \frac{\partial^{iL_R - n}}{\partial w^{iL_R - n}} \left(\frac{1}{\bar{I}_{P_R}} + w \right)^{-i} \Big|_{w = -\left(\frac{1}{\bar{I}_R}\right)}. \quad (4.47)$$

Finally, it is worth mentioning that the SINR-based antenna selection technique outperforms the SNR-based antenna selection technique in terms of the performance enhancement, especially for the relatively large number of antennas at the receiver nodes. This can be seen in Fig. 4.4 in the numerical results section. However, the practical aspects of the SINR-based scheme are more complex to implement. Accordingly, for a specific network with particular requirements, an appropriate antenna selection technique can be chosen according to the desired performance and complexity of the network.

4.7.3 Per-hop CDF Derivation, Maximum Ratio Combining Technique

After substituting $F_M\left(\frac{\gamma w}{I_{\max}}\right)$ from (4.19) and $f_W(w)$ from (4.6a) into the first part integral i.e., $I_1 = \int_{\frac{I_{\max}}{P_s}}^{\infty} F_M\left(\frac{\gamma w}{I_{\max}}\right) f_W(w) dw$, and doing some mathematical arrangements, the first part of the formula can be obtained:

$$\begin{aligned} I_1 = & \sum_{j=1}^J \binom{J}{j} (-1)^{j+1} e^{-\frac{jI_{\max}}{P_s \sigma_{f_{sp}}^2}} - \sum_{n=0}^{N-1} \sum_{i=0}^n \sum_{j=1}^J \binom{n}{i} \binom{J}{j} \frac{(-1)^{j+1}}{n!} \left(\frac{\bar{I}_{P_R}}{\bar{I}_{P_R} - \bar{I}_R} \right)^{L_R} \\ & \frac{\left(\frac{j}{\sigma_{f_{sp}}^2 I_{P_R}} \right)}{(\sigma_h^2)^n} \left[\Gamma(i+1) \left(\frac{\gamma}{I_{\max}} \right)^{n-i-1} (\sigma_h^2)^{i+1} \times \overbrace{\int_{\frac{I_{\max}}{P_s}}^{\infty} \frac{(w)^n e^{-w \left(\frac{j}{\sigma_{f_{sp}}^2} + \frac{\gamma}{I_{\max} \sigma_h^2} \right)}}{\left(\frac{I_{\max} \sigma_h^2}{\gamma I_{P_R}} + w \right)^{i+1}} dw}^{I_1^a} \right. \\ & \left. - \sum_{m=0}^{L_R-1} \frac{(m+i)! (\sigma_h^2)^n}{m!} \left(\frac{\bar{I}_{P_R} - \bar{I}_R}{\bar{I}_{P_R} \bar{I}_R} \right)^m \left(\frac{\gamma}{I_{\max} \sigma_h^2} \right)^{n-m-i-1} \times \right. \\ & \left. \overbrace{\int_{\frac{I_{\max}}{P_s}}^{\infty} \frac{(w)^n e^{-w \left(\frac{j}{\sigma_{f_{sp}}^2} + \frac{\gamma}{I_{\max} \sigma_h^2} \right)}}{\left(\frac{I_{\max} \sigma_h^2}{\gamma I_R} + w \right)^{m+i+1}} dw}^{I_1^b} \right]. \end{aligned} \quad (4.48)$$

For the purpose of simplicity and mathematical tractability, these entities are used to define the following terms; $\hat{\beta}_1 = \frac{\gamma}{I_{\max} \sigma_h^2}$, $\hat{\beta}_2 = \frac{I_{\max} \sigma_h^2}{\gamma I_{P_R}}$, $\hat{\beta}_3 = \frac{I_{\max} \sigma_h^2}{\gamma I_R}$, and $\hat{\beta}_4 = \frac{j}{\sigma_{f_{sp}}^2}$. Then, the variable in the I_1^b integral formula is exchanged, so that $w = \frac{x}{\hat{\beta}_1 + \hat{\beta}_4} - \hat{\beta}_2$. Subsequently, the Binomial expansion is used to further simplify the integral

formula and, after some mathematical manipulation, the following expression can be obtained:

$$I_1^a = \sum_{n_1=0}^n \binom{n}{n_1} (-\hat{\beta}_2)^{n-n_1} (\hat{\beta}_1 + \hat{\beta}_4)^{i-n_1} e^{\hat{\beta}_2(\hat{\beta}_1+\hat{\beta}_4)} \int_{\left(\frac{I_{\max}}{P_s} + \hat{\beta}_2\right)(\hat{\beta}_1+\hat{\beta}_4)}^{\infty} \frac{e^{-x}}{x^{i+1-n_1}} dx. \quad (4.49)$$

Finally, with the help of [83, eq. (8.19.2)], the desired representation for the above formula can be achieved. Similar steps can be repeated to solve the integral formula I_1^b . Therefore, by combining the above derived expressions, an exact formula for the per-hop CDF can be obtained in the scenario where the MRC technique is considered at the secondary receiver nodes, and the formula can be written as in (4.17). The formulas of I_{mrc}^2 and I_{mrc}^1 are represented as in (4.50) and (4.51):

$$I_{mrc}^2 = \left(\frac{\gamma}{P_s \sigma_h^2}\right)^n e^{\frac{-\gamma}{P_s \sigma_h^2}} \left(1 - e^{-\frac{I_{\max}}{P_s \sigma_{fsp}^2}}\right)^J \left[\frac{\Gamma(i+1)}{\left(\frac{1}{\bar{I}_{P_R}} + \frac{\gamma}{P_s \sigma_h^2}\right)^{i+1}} - \sum_{m=0}^{L_R-1} \frac{1}{m!} \left(\frac{\bar{I}_{P_R} - \bar{I}_R}{\bar{I}_{P_R} \bar{I}_R}\right)^m \frac{\Gamma(m+i+1)}{\left(\frac{1}{\bar{I}_R} + \frac{\gamma}{P_s \sigma_h^2}\right)^{m+i+1}} \right]. \quad (4.50)$$

$$I_{mrc}^1 = \sum_{j=1}^J \binom{J}{j} (-1)^{j+1} \left(\frac{j}{\sigma_{fsp}^2}\right) (\sigma_h^2)^{i+1-n} \left[\sum_{n_1=0}^n \binom{n}{n_1} (-\hat{\beta}_2)^{n-n_1} \Gamma(i+1) \left(\frac{\gamma}{I_{\max}}\right)^{n-i-1} (\hat{\beta}_1 + \hat{\beta}_4)^{i-n_1} e^{\hat{\beta}_2(\hat{\beta}_1+\hat{\beta}_4)} E_{i+1-n_1} \left(\left(\frac{I_{\max}}{P_s} + \hat{\beta}_2\right) (\hat{\beta}_1 + \hat{\beta}_4) \right) - \sum_{m=0}^{L_R-1} \sum_{n_2=0}^n \binom{n}{n_2} (-\hat{\beta}_3)^{n-n_2} \frac{\Gamma(m+i+1)}{\Gamma(m+1)} (\sigma_h^2)^m \left(\frac{\bar{I}_{P_R} - \bar{I}_R}{\bar{I}_{P_R} \bar{I}_R}\right)^m \left(\frac{\gamma}{I_{\max}}\right)^{n-m-i-1} (\hat{\beta}_1 + \hat{\beta}_4)^{m+i-n_2} e^{\hat{\beta}_3(\hat{\beta}_1+\hat{\beta}_4)} E_{m+i+1-n_2} \left(\left(\frac{I_{\max}}{P_s} + \hat{\beta}_3\right) (\hat{\beta}_1 + \hat{\beta}_4) \right) \right] \quad (4.51)$$

4.7.4 Error Probability Derivation

To obtain a closed-form expression for the AEP, the derived CDF in (4.7) is used. First, (4.7) is substituted into (4.28), as a result, the average per-hop error probability integral expression is obtained for two cases, (i.e., $\bar{I}_{P_R} = \bar{I}_R$, and $\bar{I}_{P_R} \neq \bar{I}_R$). In the derivations below, the following notation is used to make the derivation more tractable and easier to follow. First, let $\alpha_1 = \frac{P_s \sigma_h^2}{i}$, $\alpha_2 = \frac{P_s \sigma_h^2}{i \bar{I}_{P_R}}$, $\alpha_3 = \frac{P_s \sigma_h^2}{i \bar{I}_R}$,

$\alpha_4 = \frac{jI_{\max}\sigma_h^2}{i\bar{I}_R\sigma_{fsp}^2}$, $\alpha_5 = \frac{jI_{\max}\sigma_h^2}{i\bar{I}_{P_R}\sigma_{fsp}^2}$, $\alpha_6 = \frac{jI_{\max}}{P_s\sigma_{fsp}^2} + \frac{1}{\bar{I}_R}$, and $\alpha_7 = \frac{jI_{\max}}{P_s\sigma_{fsp}^2} + \frac{1}{\bar{I}_{P_R}}$. Then, let

$$\Upsilon_1 = \alpha_2 \alpha_3^{L_R} \left(1 - e^{-\frac{I_{\max}}{P_s\sigma_{fsp}^2}} \right)^J, \quad (4.52a)$$

$$\Upsilon_2 = \frac{e^{\left(\frac{\alpha_4}{\gamma} + \frac{1}{\bar{I}_R}\right)}}{\gamma (\alpha_3 + \gamma)^{L_R}} E_{L_R+1} \left(\frac{\alpha_4}{\gamma} + \frac{\gamma}{\alpha_1} + \alpha_6 \right), \quad (4.52b)$$

$$\begin{aligned} \Upsilon_3 = & \left(\frac{\bar{I}_{P_R}}{\bar{I}_{P_R} - \bar{I}_R} \right)^{L_R} \frac{e^{\frac{\alpha_5}{\gamma} + \frac{1}{\bar{I}_{P_R}}}}{\gamma} E_1 \left(\frac{\alpha_5}{\gamma} + \frac{\gamma}{\alpha_1} + \alpha_7 \right) \\ & + \sum_{n=1}^{L_R} \Omega_n \frac{\alpha_1^{n-1}}{\bar{I}_R^{L_R}} \frac{e^{\frac{\alpha_4}{\gamma} + \frac{1}{\bar{I}_R}}}{\gamma (\alpha_3 + \gamma)^{n-1}} E_n \left(\frac{\alpha_4}{\gamma} + \frac{\gamma}{\alpha_1} + \alpha_6 \right). \end{aligned} \quad (4.52c)$$

- First Case (i.e., $\bar{I}_{P_R} = \bar{I}_R$):

For this case, the integral formula contains three main parts. In this section, the detailed steps and explanation of each part are presented. The integral in the first part is obtained with the help of [83, eq. (5.2.1)]. In this derivation, some basic functions manipulation should be taken into account, such as; $n! = \Gamma(n + 1)$ and $\Gamma(1/2) = \sqrt{\pi}$. The second part can be written as follows:

$$\bar{P}_{b_I}^2 = \Upsilon_1 \frac{a}{2} \sqrt{\frac{b}{\pi}} \int_0^\infty \frac{e^{-b\gamma}}{\sqrt{\gamma}} \frac{e^{-\frac{\gamma}{\alpha_1}}}{(\alpha_3 + \gamma)^{L_R+1}} d\gamma, \quad (4.53)$$

For the second part i.e., $\bar{P}_{b_I}^2$ first the variable in the integral is exchanged as $\gamma = t\alpha_3$. Then, by using [83, eq. (13.4.4)] the desired formula can be obtained:

$$\bar{P}_{b_I}^2 = \Upsilon_1 \frac{a}{2} \sqrt{b} \left(b + \frac{1}{\alpha_1} \right)^{L_R + \frac{1}{2}} U \left(L_R + 1, L_R + \frac{3}{2}, \left(b + \frac{1}{\alpha_1} \right) \alpha_3 \right). \quad (4.54)$$

In (4.54), $U(\alpha, \beta, z)$ represents the confluent hypergeometric function. The third part can be written as:

$$\bar{P}_{b_I}^3 = \frac{a}{2} \sum_{j=1}^J \binom{J}{j} (-1)^j \alpha_4 \alpha_3^{L_R} \sqrt{\frac{b}{\pi}} \times \int_0^\infty \frac{e^{-\gamma b}}{\sqrt{\gamma}} \Upsilon_2 d\gamma, \quad (4.55)$$

where $\bar{P}_{b_I}^3$ is the third part of the first case AEP equation. To the best of the author's knowledge, it would be quite difficult, if not impossible to solve the above integral. In addition, it should be noted that there is more than one term that includes the exponential integral function in the CDF formula.

Therefore, it is not an efficient method to approximate these terms. However, these terms can be determined numerically by utilizing different software tools, for example, Matlab, Maple and Mathematica. Thus, this part of the above formula is determined numerically and it is written as:

$$\bar{P}_{b_I}^3 = \frac{a}{2} \sum_{j=1}^J \binom{J}{j} (-1)^j \alpha_4 \alpha_3^{L_R} \sqrt{\frac{b}{\pi}} I_{P_{b_1}}. \quad (4.56)$$

Therefore, the value of $I_{P_{b_1}}$ is determined numerically using the following integral formula:

$$I_{P_{b_1}} = \int_0^{\infty} \frac{e^{-\gamma b}}{\sqrt{\gamma}} \Upsilon_2 d\gamma, \quad (4.57)$$

where Υ_2 is defined in (4.52b).

- Second Case (i.e., $\bar{I}_{P_R} \neq \bar{I}_R$):

For the second case, a formula is obtained that has three integral parts. The first part is similar to the first part of the previous case. The part two, second case of the AEP formula, can be expressed as:

$$\bar{P}_{b_{II}}^2 = \Upsilon_1 \frac{a}{2} \sqrt{\frac{b}{\pi}} \int_0^{\infty} \frac{e^{-\gamma(b+\frac{1}{\alpha_1})} \gamma^{-\frac{1}{2}}}{(\alpha_2 + \gamma) \times (\alpha_3 + \gamma)^{L_R}} d\gamma, \quad (4.58)$$

As previously mentioned and demonstrated, using the partial fraction can make some expressions simpler. Consequently, this technique is employed to make the integral expression in (4.58) easier to manipulate as follows:

$$\bar{P}_{b_{II}}^2 = \Upsilon_1 \frac{a}{2} \sqrt{\frac{b}{\pi}} \int_0^{\infty} e^{-\gamma(b+\frac{1}{\alpha_1})} \times \gamma^{-\frac{1}{2}} \left[\sum_{m_1=1}^{L_R} \frac{\mu_{m_1}}{(\alpha_3 + \gamma)^{m_1}} + \frac{\mu_2}{(\alpha_2 + \gamma)} \right] d\gamma, \quad (4.59)$$

where μ_{m_1} , and μ_2 are calculated using the expressions provided in (4.33a, and 4.33b) respectively. Therefore, each sub part for the second part is rewritten as $\bar{P}_{b_{II}}^{21}$, and $\bar{P}_{b_{II}}^{22}$ respectively. Next, the variable for $\bar{P}_{b_{II}}^{21}$ is exchanged so that $\gamma = t^2 \alpha_2$. Then, by comparing the obtained formula with [83, eq. (7.7.1)], and after performing some mathematical manipulations and arrangements the

desired formula can be obtained as:

$$\bar{P}_{b_{II}}^{21} = \Upsilon_1 \frac{a}{2} \sqrt{\frac{b\pi}{\alpha_2}} \mu_2 e^{\alpha_2 \left(b + \frac{1}{\alpha_1}\right)} \operatorname{erfc} \left(\sqrt{\alpha_2 \left(b + \frac{1}{\alpha_1}\right)} \right). \quad (4.60)$$

In (4.60), $\operatorname{erfc}(x)$ represents the complementary error function. The solution of the integral formula for $\bar{P}_{b_{II}}^{22}$ is quite similar to the second part of the first case, i.e., $\bar{P}_{b_I}^2$. Therefore, it can be solved as:

$$\bar{P}_{b_{II}}^{22} = \Upsilon_1 \times \frac{a}{2} \sqrt{b} \sum_{m_1=1}^{L_R} \mu_{m_1} \left(b + \frac{1}{\alpha_1}\right)^{m_1 - \frac{1}{2}} \operatorname{U} \left(m_1, m_1 + \frac{1}{2}, \left(b + \frac{1}{\alpha_1}\right) \alpha_3 \right). \quad (4.61)$$

Similar to the third part of the first case, the third part of the second case is evaluated numerically:

$$\bar{P}_{b_{II}}^3 = \frac{a}{2} \sum_{j=1}^J \binom{J}{j} (-1)^j \alpha_5 \sqrt{\frac{b}{\pi}} I_{P_{b_2}}. \quad (4.62)$$

The value of $I_{P_{b_2}}$ in (4.62) is determined using the following integral formula:

$$I_{P_{b_2}} = \int_0^{\infty} \frac{e^{-\gamma b}}{\sqrt{\gamma}} \Upsilon_3 d\gamma, \quad (4.63)$$

where Υ_3 is defined in (4.52c). Finally, a closed-form expression for the AEP can be obtained through summing all derived parts and substituting the notations that have been used for the derivations, it is represented in the formula in (4.30).

4.7.5 Ergodic Capacity Derivation

To derive a closed-form EC formula for the multi-hop UCRN, the formula of the per-hop equivalent CDF is used. This can be obtained by substituting (4.7) into (4.34). This will resulting in an integral formula for the two different cases: *case I* (i.e., $\bar{I}_{PR} = \bar{I}_R$) and *case II* (i.e., $\bar{I}_{PR} \neq \bar{I}_R$). In this section, the detailed steps of the derivation for both cases are presented. In addition, the same notations that have been defined in Appendix 4.7.4 are used.

- First Case (i.e., $\bar{I}_{P_R} = \bar{I}_R$):

For the first case, the formula has two integral parts. The first part is represented by $C_{erg_1}^1$, and the second part by $C_{erg_1}^2$. The first integral part has the following integral form:

$$C_{erg_1}^1 = \Upsilon_1 \int_0^{\infty} \frac{1}{(1+\gamma)} \frac{e^{-\frac{\gamma}{\alpha_1}}}{(\alpha_3 + \gamma)^{L_R+1}} d\gamma, \quad (4.64)$$

where Υ_1 is defined in (4.52a). With the help of a partial fraction, the above integral expression can be written in a simpler form. More specifically, it can be represented by two terms as:

$$C_{erg_1}^1 = \Upsilon_1 \int_0^{\infty} e^{-\frac{\gamma}{\alpha_1}} \left[\frac{\lambda_1}{(1+\gamma)} + \sum_{r_2=1}^{L_R+1} \frac{\lambda_{r_2}}{(\alpha_3 + \gamma)^{r_2}} \right] d\gamma. \quad (4.65)$$

In (4.65), λ_1 , and λ_{r_2} are determined using formulas provided in (4.39a), and (4.39b) respectively. *In the above formula, it is assumed that $P_s \sigma_h^2 \neq i\bar{I}_R$, i.e., $\alpha_3 \neq 1$. In fact, in the case of $\alpha_3 = 1$, there will be an extra possible case, which is similar to the existing forms.* Then, after some straightforward mathematical manipulation and with the help of [83, eq. (8.19.2)], a desired representation can be obtained for the integral formula in (4.64).

$$C_{erg_1}^1 = \Upsilon_1 \left[\lambda_1 e^{\frac{1}{\alpha_1}} E_1 \left(\frac{1}{\alpha_1} \right) + \sum_{r_2=1}^{L_R+1} \lambda_{r_2} (\alpha_3)^{1-r_2} e^{\frac{\alpha_3}{\alpha_1}} E_{r_2} \left(\frac{\alpha_3}{\alpha_1} \right) \right]. \quad (4.66)$$

Part $C_{erg_1}^2$ of the EC integral formula has the following form:

$$C_{erg_1}^2 = \sum_{j=1}^J \binom{J}{j} (-1)^j \alpha_4 \alpha_3^{L_R} \int_0^{\infty} \frac{\Upsilon_2}{1+\gamma} d\gamma, \quad (4.67)$$

where Υ_2 is defined in (4.52b). The integral in this part is kept and solve it numerically. Therefore, it can be obtained as:

$$C_{erg_1}^2 = \sum_{j=1}^J \binom{J}{j} (-1)^j \alpha_4 \alpha_3^{L_R} I_{C_{erg_1}}, \quad (4.68)$$

where

$$I_{C_{erg1}} = \int_0^{\infty} \frac{\Upsilon_2}{1+\gamma} d\gamma. \quad (4.69)$$

- Second Case (i.e., $\bar{I}_{P_R} \neq \bar{I}_R$):

In this case, the integral formula has two parts. Part one is denoted by C_{ergII}^1 , and part two by C_{ergII}^2 . In this section, the derivation steps for each part are presented.

$$C_{ergII}^1 = \Upsilon_1 \int_0^{\infty} \frac{e^{-\frac{\gamma}{\alpha_1}}}{(1+\gamma)(\alpha_2+\gamma)(\alpha_3+\gamma)^{L_R}} d\gamma. \quad (4.70)$$

The above integral formula is mathematically difficult to manipulate, by employing the partial fraction decomposition technique, the integral can be represented in a simpler form as:

$$C_{ergII}^1 = \Upsilon_1 \int_0^{\infty} e^{-\frac{\gamma}{\alpha_1}} \left[\sum_{r_3=1}^{L_R} \frac{\lambda_{r_3}}{(\alpha_3+\gamma)^{r_3}} + \frac{\lambda_4}{(\alpha_2+\gamma)} + \frac{\lambda_5}{(1+\gamma)} \right] d\gamma. \quad (4.71)$$

In (4.71) λ_{r_3} , λ_4 and λ_5 are determined using formulas provided in (4.39c), (4.39d) and (4.39e) respectively. *In the above formula, it is assumed that $P_s \sigma_h^2 \neq i\bar{I}_{P_R}$ and/or $P_s \sigma_h^2 \neq i\bar{I}_R$. If the following scenarios are considered, there will be two extra possible cases, which are similar to the existing forms.* It can be observed that the integrals in (4.71) have similar forms to the integrals in the first case, i.e., C_{erg1}^1 . Therefore, the final formula can be written as:

$$C_{ergII}^1 = \Upsilon_1 \left[\sum_{r_3=1}^{L_R} \lambda_{r_3} (\alpha_3)^{1-r_3} e^{\frac{\alpha_3}{\alpha_1}} E_{r_3} \left(\frac{\alpha_3}{\alpha_1} \right) + \lambda_4 e^{\frac{\alpha_2}{\alpha_1}} E_1 \left(\frac{\alpha_2}{\alpha_1} \right) + \lambda_5 e^{\frac{1}{\alpha_1}} E_1 \left(\frac{1}{\alpha_1} \right) \right]. \quad (4.72)$$

Part two in the second case of the EC integral formula can be written as:

$$C_{ergII}^2 = \sum_{j=1}^J \binom{J}{j} (-1)^j \alpha_4 \alpha_3^{L_R} \int_0^{\infty} \frac{\Upsilon_2}{1+\gamma} d\gamma, \quad (4.73)$$

where Υ_3 is defined in (4.52c). Similar to the second part of the first case, C_{ergII}^2 is numerically evaluated as:

$$C_{ergII}^2 = \sum_{j=1}^J \binom{J}{j} (-1)^j \alpha_5 I_{C_{erg2}}, \quad (4.74)$$

where

$$I_{C_{erg2}} = \int_0^{\infty} \frac{\Upsilon_3}{1+\gamma} d\gamma. \quad (4.75)$$

Finally, a closed-form EC expression for one hop of the secondary network can be obtained by summing all parts and substituting the notations that have been used for the derivations, and it can be written as in (4.36).

Chapter 5

Performance Study of a MIMO Spectrum Sharing Network in the Presence of CCI

In this chapter, the outage and error probability performances of a MIMO underlay CRN are investigated under the presence of the primary transceiver and CCI. In addition, the impact of the interference power constraint and the secondary network transmitter power constraint are considered. The TAS/MRC techniques are considered in the performance investigation. First, the equivalent SINR is constructed. Then, the exact outage performance is thoroughly examined. Furthermore, different case studies are considered to investigate the approximate outage performance. Moreover, an expression for the asymptotic AEP is derived.

From this investigation, it is found that the MIMO system in conjunction with TAS/MRC can significantly enhance the performance of the CR network by combating the impact of transmission power limitation in the secondary network. Moreover, the MIMO scheme does not lose its advantage despite the presence of interference from the primary transmitter and CCI sources. However, the interference power decreases the performance of the secondary network especially when it increases linearly with the secondary transmission power, in which performance floor or, even worse, “performance degradation” are expected. Finally, to validate and discuss the results, numerical examples are presented with Monte Carlo simulations.

5.1 Introduction

To enhance the performance of the secondary network and combat the impact of the interference power constraint, some approaches can be used; such as, employing multi-antenna, or considering relay communication [10, 39]. Moreover, the multi-antenna scheme outperforms other techniques in terms of reducing a large number of required overhead signals and improving the secondary network throughput [39]. It is well-known that the multi-antenna scheme has the advantage of performance improvement of any wireless communication system. However, it increases the cost and complexity of the system. To reduce these drawbacks, an antenna selection technique can be used which has the advantage of reducing the cost and complexity of the system configuration. More importantly, it keeps the same benefits as the multi-antenna usage regarding the diversity gain advantages [39]. Transmit antenna selection is a technique of selecting the antenna at the transmitter node that results in the highest SNR. Among the signal combining techniques at a receiver node, MRC is considered as the most efficient one in terms of the performance enhancement [14]. As a result, combining these two techniques, i.e., TAS/MRC, in a MIMO wireless system can apparently enhance the overall performance.

Studying the advantage of a MIMO system for cognitive radio has attracted several researchers [13, 17, 31, 32, 41, 50, 51]. For example, Huang et al. [14] investigated the underlay CR performance under the assumption that the secondary transmitter has a single antenna. Furthermore, the authors in [39] have considered a single antenna at both the primary transmitter and receiver nodes and multiple antennas at the secondary transceiver to study the performance of the secondary network. Recently, the authors in [31] have examined the advantages of the multi-antenna scheme for the secondary network under the absence of the primary transmitter. More recently, Yeoh et al. in [17], considered multi-antennas at both primary and secondary transceivers and investigated the secondary network's performance using the TAS/MRC technique. In these papers, the influence of the CCI has not been considered in the performance investigation. The authors in [70, 72, 74], have considered the impact of CCI on the performance of an underlay CR network; however, multi-antenna schemes at all the nodes have not been considered.

The significant contribution of the research in this chapter is to investigate a more practical and state-of-the art network consideration. More precisely, compre-

hensive OP and AEP performances of a MIMO underlay CR network in conjunction with the TAS/MRC technique are investigated under the following network conditions: *i*) the presence of interference from the primary network and the CCI sources, *ii*) consideration of the secondary transmitter power constraint, *iii*) consideration of the interference power constraint, *iv*) taking into account AWGN, and *v*) the multi-antennas at all nodes in the network, i.e., primary and secondary transceiver nodes. In fact, the performance investigation of a UCRN considering the above network constraints and conditions has not been studied yet.

The remainder of this chapter is structured as follows. In Section 5.2 the considered system model is discussed. Section 5.3 gives an analytical investigation of the outage performance and error probability performance of the MIMO underlay cognitive network. In Section 5.4, some numerical examples with Monte Carlo simulations are presented to illustrate the network behaviour and validate the derived expressions. Section 5.5 gives a summary and conclusions of this chapter. Finally, the detailed derivation steps of the analytical results are given in Appendix 5.6.1.

5.2 System Model

Fig. 5.1 shows the system model under consideration. The network consists of primary and secondary transceiver nodes in which all the nodes are equipped with multiple antennas. M_p and N_p are the number of antennas at the PU transmitter and receiver, respectively. M_s , and N_s are the number of antennas at the SU transmitter and receiver, respectively. L is the number of CCI signals that affect the SU destination node. In fact, there are L_p CCI signals that affect the PU destination node. However, in this work, the focus is only on the secondary network performance analysis.

It is assumed that the fading channels in the network are subject to a block of i.i.d. Rayleigh fading channels. This is a valid assumption as channels between the antennas of the two adjacent nodes in the network have the same distance and therefore they can be assumed to be identical. Therefore, the generic channel power gain between any two nodes in the network can be represented as $|g_{xy}|^2$, where g represents the fading channel coefficient, and x and y are the two adjacent nodes between g . Furthermore, the channel gain $|g_{xy}|^2$ follows the exponential distribution with a mean power of $\sigma_{g_{xy}}^2$, which can be defined as $\sigma_{g_{xy}}^2 \triangleq d_{xy}^{-\alpha}$, where d_{xy} is the

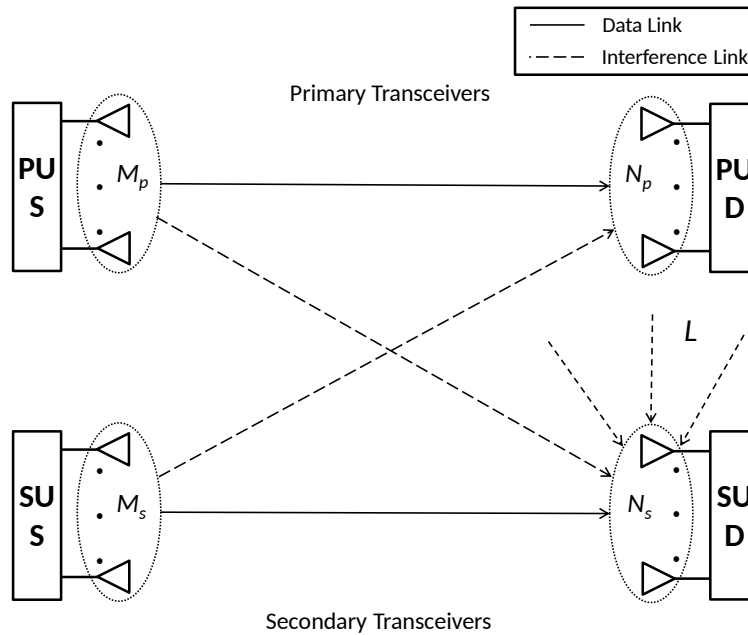


Figure 5.1: The general network model used for the analysis showing a MIMO underlay CR network in the presence of primary transceiver and CCI.

distance between nodes x and y , and α is the path-loss exponent. For example, $|g_{sd}|^2$ is the channel power gain between the SU transmitter and receiver nodes, respectively, and the corresponding channel variance is $\sigma_{g_{sd}}^2$. In addition, $|g_{sp}|^2$ is the channel power gain between the SU transmitter and PU receiver nodes, respectively. The average channel power gain of the individual CCI signals has an exponential distribution; therefore, the sum of L independent average channel power gains of the CCI signals has a gamma distribution [84].

Moreover, it is assumed that perfect knowledge of the CSI is available [41]. In this work, the average value of the channel power gain has been used in the mathematical analysis, which is the square of the amplitude, rather than instantaneous values. The CSI at the secondary transmitter node can be obtained through different approaches [65]. For example, it can be obtained through feedback from the primary receiver or with the help of the band manager [41]. For the mentioned network, the received signal at the secondary user destination node can be written as:

$$\mathbf{y}_d = \sqrt{E_s} \mathbf{g}_{sd} \lambda_x + I_c + I_p + n_d, \quad (5.1)$$

where E_s is the permitted transmission power at the secondary transmitter node, \mathbf{g}_{sd} represents the $(M_s \times N_s)$ fading channel matrix between the secondary transmitter and receiver nodes, and λ_x represents the intended message to be transmitted from

the secondary transmitter node to the secondary destination node, which has a unit energy. I_c and I_p are RVs representing the interference terms at the secondary receiver node from the CCI sources and the primary transmitter, respectively. In addition, n_d is the noise term at the secondary destination node, which is assumed to be AWGN. From the above formula, the resulting SINR at the SU destination node after employing the TAS/MRC technique is represented as:

$$\gamma_{\text{eq}} = \frac{E_s \|g_{sd_n}^*\|^2}{\sum_{l=1}^L \gamma_{c_l} + \sum_{i=1}^{M_p} \gamma_{p_i} + N_0}, \quad (5.2)$$

where γ_c and γ_p are the instantaneous interference power terms from the CCI sources and the primary transmitter, respectively. In addition, N_0 represents the power spectral density (PSD) of the AWGN term. Also, $\|\cdot\|^2$ is the Frobenius norm:

$$\|g_{sd_n}^*\|^2 = \max_{n \in \{1, \dots, M_S\}} \left\{ \|g_{sd_{n_1}}, \dots, g_{sd_{n_{N_D}}}\|^2 \right\}. \quad (5.3)$$

Furthermore, to protect the primary network, the transmission power at the secondary transmitter, E_s , should have the following power constraint:

$$E_s = \min \left(I_{\max} \left(\max_{j \in \{1, \dots, N_p\}} \{|g_{sp_j}|^2\} \right)^{-1}, P_s \right). \quad (5.4)$$

5.3 Performance Evaluation

In the sections below, first, mathematical expressions for the exact and asymptotic outage performance of the MIMO UCRN are derived. Second, the AEP performance is investigated.

5.3.1 Exact Outage Performance

Proposition 1: The exact outage performance of the underlay MIMO CR network in the presence of primary network and CCIs, and with consideration of the TAS/MRC technique, can be written as in (5.5), where Ψ is represented in (5.6), ζ_2^a and ζ_2^b are represented by formulas in (5.7) and (5.8), respectively. Furthermore, $\alpha_1 = \frac{I_{\max}}{P_s}$, $\alpha_2 = \left(\frac{n_1 \gamma}{I_{\max} \sigma_{g_{sd}}^2} + \frac{j}{\sigma_{g_{sp}}^2} \right)$, $\alpha_3 = \frac{I_{\max} \sigma_{g_{sd}}^2}{\gamma n_1 \bar{\gamma}_p}$, $\alpha_4 = M_p + n_2 - n_3$, $\alpha_5 = \frac{I_{\max} \sigma_{g_{sd}}^2}{\gamma n_1 \bar{\gamma}_c}$, and $\alpha_6 = M_p + n_2 + m - n_3$.

$$\begin{aligned}
 P_{\text{out}}(\gamma_{\text{th}}) = & 1 - \Psi \left\{ e^{-\frac{n_1 \gamma_{\text{th}}}{P_s \sigma_{g_{sd}}^2}} \left(\frac{\gamma_{\text{th}}}{P_s \sigma_{g_{sd}}^2} \right)^{\sum_k} \left(1 - e^{-\frac{I_{\text{max}}}{P_s \sigma_{g_{sp}}^2}} \right)^{N_p} \left[\Gamma(M_p + n_2 - n_3) \right. \right. \\
 & \left. \left(\frac{\bar{\gamma}_p \sigma_{g_{sd}}^2}{\sigma_{g_{sd}}^2 + \frac{\gamma_{\text{th}} n_1 \bar{\gamma}_p}{P_s}} \right)^{M_p + n_2 - n_3} - \sum_{m=0}^{L+n_3-1} \frac{1}{m!} \left(\frac{\bar{\gamma}_p - \bar{\gamma}_c}{\bar{\gamma}_c \bar{\gamma}_p} \right)^m \Gamma(M_p + n_2 + m - n_3) \right. \\
 & \left. \left(\frac{\bar{\gamma}_c \sigma_{g_{sd}}^2}{\sigma_{g_{sd}}^2 + \frac{\gamma_{\text{th}} n_1 \bar{\gamma}_c}{P_s}} \right)^{M_p + n_2 + m - n_3} \right] + \sum_{j=1}^{N_p} \binom{N_p}{j} (-1)^{j+1} \frac{j}{\sigma_{g_{sp}}^2} \left(\frac{\gamma_{\text{th}}}{I_{\text{max}} \sigma_{g_{sd}}^2} \right)^{\sum_k} \\
 & \left[\Gamma(M_p + n_2 - n_3) \left(\frac{I_{\text{max}} \sigma_{g_{sd}}^2}{\gamma_{\text{th}} n_1} \right)^{M_p + n_2 - n_3} \varsigma_2^a - \sum_{m=0}^{L+n_3-1} \frac{1}{m!} \left(\frac{\bar{\gamma}_p - \bar{\gamma}_c}{\bar{\gamma}_c \bar{\gamma}_p} \right)^m \right. \\
 & \left. \Gamma(M_p + n_2 + m - n_3) \left(\frac{I_{\text{max}} \sigma_{g_{sd}}^2}{\gamma_{\text{th}} n_1} \right)^{M_p + n_2 + m - n_3} \varsigma_2^b \right] \left. \right\}. \quad (5.5)
 \end{aligned}$$

$$\begin{aligned}
 \Psi = & \sum_{n_1=1}^{M_s} \sum_{k_1, k_{n_1}}^{N_s-1} \sum_{n_2=0}^{\sum_k} \sum_{n_3=0}^{M_p-1} \binom{M_s}{n_1} \binom{\sum_k}{n_2} \binom{M_p-1}{n_3} (-1)^{n_1+n_3+1} \frac{\Gamma(L+n_3)}{k_1! \dots k_{n_1}!} \times \\
 & \frac{\left(\frac{\bar{\gamma}_c \bar{\gamma}_p}{\bar{\gamma}_p - \bar{\gamma}_c} \right)^{L+n_3}}{\bar{\gamma}_c^L \bar{\gamma}_p^{M_p} \Gamma(L) \Gamma(M_p)}. \quad (5.6)
 \end{aligned}$$

$$\varsigma_2^a = \sum_{r_1=0}^{\sum_k} \binom{\sum_k}{r_1} (-1)^{\sum_k - r_1} (\alpha_3)^{\sum_k - r_1} (\alpha_2)^{\alpha_4 - r_1 - 1} e^{\alpha_2 \alpha_3} \Gamma(1 + r_1 - \alpha_4, \alpha_2 (\alpha_1 + \alpha_3)). \quad (5.7)$$

$$\varsigma_2^b = \sum_{r_2=0}^{\sum_k} \binom{\sum_k}{r_2} (-1)^{\sum_k - r_2} (\alpha_5)^{\sum_k - r_2} (\alpha_2)^{\alpha_6 - r_2 - 1} e^{\alpha_2 \alpha_5} \Gamma(1 + r_2 - \alpha_6, \alpha_2 (\alpha_1 + \alpha_5)). \quad (5.8)$$

Proof: See Appendix 5.6.1. ■

5.3.2 Approximate Outage Performance

Despite the fact that in the previous section the exact outage performance can be examined, its representation is too difficult to infer insights about the network parameters. In this section, approximate and simpler expressions for the outage

performance are derived for two scenarios as follows:

- No interference power constraint, i.e., $I_{\max} \rightarrow \infty$:

By substituting this condition in (5.20) and (5.35), the resulting CDF formula will reduce to the CDF of RV M that has been derived and represented in (5.34), i.e., $F_M(\frac{\gamma}{P_s})$. Then, the approximate OP in this case will be:

$$P_{\text{out}}(\gamma_{\text{th}}) \approx 1 - \Psi \left(\frac{\gamma_{\text{th}}}{P_s \sigma_{g_{sd}}^2} \right)^{\sum_k} e^{-\frac{n_1 \gamma_{\text{th}}}{P_s \sigma_{g_{sd}}^2}} \left[\Gamma(M_p + n_2 - n_3) \left(\frac{\bar{\gamma}_p \sigma_{g_{sd}}^2}{\sigma_{g_{sd}}^2 + \frac{\gamma_{\text{th}} n_1 \bar{\gamma}_p}{P_s}} \right)^{M_p + n_2 - n_3} - \sum_{m=0}^{L+n_3-1} \frac{1}{m!} \left(\frac{\bar{\gamma}_p - \bar{\gamma}_c}{\bar{\gamma}_c \bar{\gamma}_p} \right)^m \Gamma(M_p + n_2 + m - n_3) \left(\frac{\bar{\gamma}_c \sigma_{g_{sd}}^2}{\sigma_{g_{sd}}^2 + \frac{\gamma_{\text{th}} n_1 \bar{\gamma}_c}{P_s}} \right)^{M_p + n_2 + m - n_3} \right]. \quad (5.9)$$

In this scenario, the secondary transmitter can take advantage of using the full range of its transmission power. However, this does not mean that the performance of the secondary network can enhance linearly with the increase of transmission power of the secondary transmitter node. There are other performance improvement obstacles due to the PU transmitter and CCIs, in which it is still possible for performance saturation to occur as a worst case scenario. The obtained expression for the OP in this scenario is simpler than the exact derived expression, yet, it is still difficult to obtain an explicit formula to deal with the diversity gain due to the sum terms in the expression. However, through the observation of the approximate outage formula it can be seen that the diversity gain is proportional to \sum_k . In fact, the value of \sum_k is related to the number of antennas at the SU transmitter and receiver nodes, i.e., M_s , and N_s . Therefore, the generalized expression including the diversity gain can be inferred and written as $P_{\text{out}}(\gamma_{\text{th}}) \propto \frac{1}{(P_s \sigma_{g_{sd}}^2)^{\sum_k}}$, where $P_s \sigma_{g_{sd}}^2$ represents the secondary transmitter SNR. The advantage of diversity gain can be further understood later in the numerical section, more specifically in Fig. 5.3.

- No power constraint on the secondary transmitter, i.e., $P_s \rightarrow \infty$:

In this scenario, the conditional equivalent CDF can be represented as:

$$F_{\gamma_{\text{eq}}}(\gamma)|_W = \Pr\left(M \leq \frac{\gamma w}{I_{\max}}\right). \quad (5.10)$$

Therefore, the unconditional CDF can be obtained by taking the expectation of $F_M\left(\frac{\gamma w}{I_{\max}}\right)$ over the PDF of RV W . Mathematically, this can be written as:

$$\varsigma_3 = \int_0^{\infty} F_M\left(\frac{\gamma w}{I_{\max}}\right) f_W(w) dw. \quad (5.11)$$

The steps of derivation for the above formula are quite similar to the steps for solving ς_2 in (5.39). As a result, and for the sake of saving space, only the final expression for this scenario is provided and can be written as in (5.12).

$$\begin{aligned} P_{\text{out}}(\gamma_{\text{th}}) \approx & 1 - \Psi \sum_{j=1}^{N_p} \binom{N_p}{j} (-1)^{j+1} \left(\frac{j}{\sigma_{g_{sp}}^2}\right) \left(\frac{\gamma_{\text{th}}}{I_{\max} \sigma_{g_{sd}}^2}\right)^{\sum_k} \Gamma(L + n_3) \\ & \left[\Gamma(M_p + n_2 - n_3) \left(\frac{I_{\max} \sigma_{g_{sd}}^2}{\gamma_{\text{th}} n_1}\right)^{M_p + n_2 - n_3} \varsigma_3^a - \sum_{m=0}^{L + n_3 - 1} \frac{1}{m!} \left(\frac{\bar{\gamma}_p - \bar{\gamma}_c}{\bar{\gamma}_c \bar{\gamma}_p}\right)^m \right. \\ & \left. \Gamma(M_p + n_2 + m - n_3) \left(\frac{I_{\max} \sigma_{g_{sd}}^2}{\gamma_{\text{th}} n_1}\right)^{M_p + n_2 + m - n_3} \varsigma_3^b \right]. \end{aligned} \quad (5.12)$$

Moreover, in this scenario, ς_3^a and ς_3^b are obtained by using the following formulas:

$$\varsigma_3^a = \sum_{r_1=0}^{\sum_k} \binom{\sum_k}{r_1} (-1)^{\sum_k - r_1} (\alpha_3)^{\sum_k - r_1} (\alpha_2)^{\alpha_4 - r_1 - 1} e^{\alpha_2 \alpha_3} \Gamma(1 + r_1 - \alpha_4, \alpha_2 \alpha_3), \quad (5.13)$$

and

$$\varsigma_3^b = \sum_{r_2=0}^{\sum_k} \binom{\sum_k}{r_2} (-1)^{\sum_k - r_2} (\alpha_5)^{\sum_k - r_2} (\alpha_2)^{\alpha_6 - r_2 - 1} e^{\alpha_2 \alpha_5} \Gamma(1 + r_2 - \alpha_6, \alpha_2 \alpha_5). \quad (5.14)$$

From the derived formula in (5.12), it can be seen that the dominant power is I_{\max} instead of P_s , which is the key guarantee of the protection of the primary network. In fact, when the network is working based on this scenario, it has the advantage of promising that the secondary network is working on the optimal possible performance. This can be seen in Fig. 5.3 in the numerical results section.

5.3.3 Average Error Probability

In this section, the AEP performance for the secondary network is investigated. First, it is important to find a proper method to derive and represent a closed-form expression for the AEP. Using the CDF for investigating the AEP is an efficient way, since its representation is relatively simpler than PDF. However, by observing the derived CDF for the considered system in this research, it is quite difficult to obtain a closed-form expression for the AEP. Fortunately, an approximate formula can be derived from the asymptotic derived CDF in (5.9) [72]. The AEP can be obtained by using the formula in (4.28).

For the purpose of representing the formulas in a simpler way, the following notations are used: $\delta_0 = \sum_k$, $\delta_1 = \frac{P_s \sigma_{g_{sd}}^2}{n_1}$, $\delta_2 = \frac{P_s \sigma_{g_{sd}}^2}{n_1 \bar{\gamma}_p}$, $\delta_3 = \frac{P_s \sigma_{g_{sd}}^2}{n_1 \bar{\gamma}_c}$, $\delta_4 = M_p + n_2 - n_3$, $\delta_5 = M_p + n_2 + m - n_3$, and $\delta_6 = \frac{1}{\delta_1} + b$. Then, after employing these notations and substituting (5.9) into (4.28), the following expression is obtained:

$$\begin{aligned} \bar{P}_b \approx & \frac{a}{2} - \frac{a}{2} \sqrt{\frac{b}{\pi}} \Psi \frac{1}{(P_s \sigma_{g_{sd}}^2)^{\sum_k}} \left[\Gamma(M_p + n_2 - n_3) (\delta_1)^{\delta_4} \overbrace{\int_0^\infty \frac{e^{-\delta_6}}{\sqrt{\gamma}} \frac{(\gamma)^{\delta_0}}{(\delta_2 + \gamma)^{\delta_4}} d\gamma}^{\Omega_1} \right. \\ & \left. - \sum_{m=0}^{L+n_3-1} \frac{1}{m!} \left(\frac{\bar{\gamma}_p - \bar{\gamma}_c}{\bar{\gamma}_c \bar{\gamma}_p} \right)^m \Gamma(M_p + n_2 + m - n_3) (\delta_1)^{\delta_5} \overbrace{\int_0^\infty \frac{e^{-\delta_6}}{\sqrt{\gamma}} \frac{(\gamma)^{\delta_0}}{(\delta_3 + \gamma)^{\delta_5}} d\gamma}^{\Omega_2} \right], \end{aligned} \quad (5.15)$$

where Ψ is represented by the formula in (5.6). To solve the integral in part Ω_1 , first, the variable in the integral is changed such that $t = \frac{\gamma}{\delta_2}$. After this, the integral formula in Ω_1 part can be written as:

$$\Omega_1 = (\delta_2)^{\delta_0 + \frac{1}{2} - \delta_4} \int_0^\infty e^{-\delta_2 \delta_6 t} (t)^{\delta_0 - \frac{1}{2}} (1+t)^{-\delta_4} dt. \quad (5.16)$$

Now, using [80, eq. (13.2.5)] the desired formula can be obtained:

$$\Omega_1 = (\delta_2)^{\delta_0 + \frac{1}{2} - \delta_4} \Gamma\left(\delta_0 + \frac{1}{2}\right) U\left(\delta_0 + \frac{1}{2}, \delta_0 + \frac{1}{2}, \delta_0 + \frac{3}{2} - \delta_4, \delta_2 \delta_6\right), \quad (5.17)$$

where $U(a, b, z)$ is the confluent hypergeometric function of the second kind defined in [83, eq. (13.4.4)]. Using similar steps, the integral in part Ω_2 can be solved and

written as:

$$\Omega_2 = (\delta_3)^{\delta_0 + \frac{1}{2} - \delta_5} \Gamma\left(\delta_0 + \frac{1}{2}\right) U\left(\delta_0 + \frac{1}{2}, \delta_0 + \frac{3}{2} - \delta_5, \delta_3 \delta_6\right). \quad (5.18)$$

Finally, the approximate AEP can be expressed as in (5.19).

$$\begin{aligned} \bar{P}_b \approx & \frac{a}{2} - \frac{a}{2} \sqrt{\frac{b}{\pi}} \Psi \frac{1}{(P_s \sigma_{gsd}^2)^{\sum k}} \left[\Gamma(M_p + n_2 - n_3) (\delta_1)^{\delta_4} \Omega_1 \right. \\ & \left. - \sum_{m=0}^{L+n_3-1} \frac{1}{m!} \left(\frac{\bar{\gamma}_p - \bar{\gamma}_c}{\bar{\gamma}_c \bar{\gamma}_p} \right)^m \Gamma(M_p + n_2 + m - n_3) (\delta_1)^{\delta_5} \Omega_2 \right], \end{aligned} \quad (5.19)$$

where Ω_1 and Ω_2 are calculated by using the formulas in (5.17) and (5.18), respectively.

5.4 Numerical Results and Discussions

In this section, some numerical and simulation examples are presented to validate the derived expressions and to discuss the MIMO underlay CR network under some practical circumstances. In the calculation of channel variances, a two-dimensional network topology is considered. More precisely, the SU source node is considered at $(0, 0)$. In addition, the channel variance between two nodes at a distance d is calculated as $1/1 + d^\alpha$, where α represents the path-loss exponent and is assumed to be four in all results in this section. Furthermore, the PSD of the noise is assumed to be one.

In Fig. 5.2, the OP performance is plotted versus SNR threshold for different values of I_{\max} and different number of antennas at the secondary destination node. The locations of the PU receiver and SU destination nodes are considered to be at $(1, 1)$ and $(1, 0)$, respectively. Furthermore, the following network parameters are considered; $P_s = 15$ dB, $\bar{\gamma}_c = 3$ dB, $\bar{\gamma}_p = 4$ dB, $M_s = 2$, $N_s = 3$, $M_p = 2$, $N_p = 2$, $L = 2$. The results in Fig. 5.2 show that higher interference power constraint leads to better performance. Moreover, increasing the number of antennas at the secondary receiver node results in an observable improvement in the performance despite the consideration of interference power constraint and interferences from the CCI sources and primary transmitter.

Fig. 5.3 shows the OP versus the transmission SNR for different locations of the

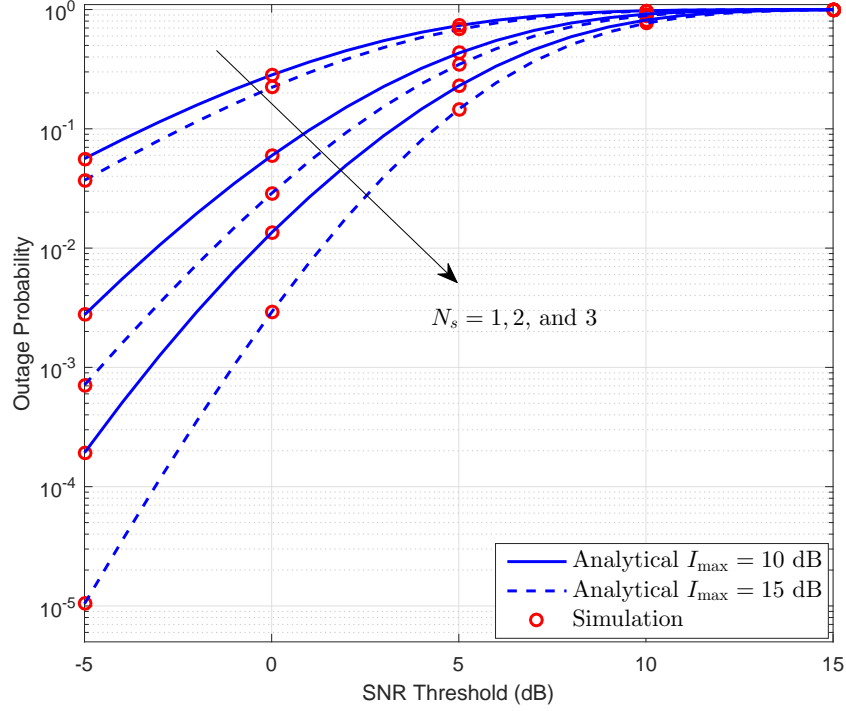


Figure 5.2: Outage performance vs. SNR threshold for different values of interference power constraint I_{\max} and secondary destination antennas N_s .

primary receiver node. The SU destination node is considered to be at $(1, 0)$. In addition, the following network parameters are considered; $I_{\max} = 20$, dB, $\bar{\gamma}_c = 5$ dB, $\bar{\gamma}_p = 7$ dB, $M_s = 2$, $N_s = 3$, $M_p = 2$, $N_p = 3$, $L = 3$. From the results in Fig. 5.3, it can be observed that as the PU receiver node gets closer to the SU transmitter node, the performance degrades, and vice versa. Furthermore, when the value of $I_{\max} \rightarrow \infty$, the position of the primary user receiver does not have any influence on the system performance. This situation can be considered when the primary network is in the silent mode. Furthermore, it can be treated as an interweave scenario [8], when the secondary network can use a specific spectrum when it is vacated by the primary user. Moreover, the advantage of diversity gain can be clearly seen when $I_{\max} \rightarrow \infty$. For the scenario when $P_s \rightarrow \infty$, the flat performance can be seen, which gives the maximum boundary that the performance can achieve.

To investigate the impact of the linear increase of the CCI power, Fig. 5.4 has been plotted. In this figure, the OP has been depicted for a different number of antennas at the SU transmitter and a different number of CCI signals that affect the SU destination node. The CCI power is considered to increase in proportion with SU transmitter power by a rate of 5%, i.e., $\bar{\gamma}_c = 5 \times 10^{-2} \times P_s$. The positions

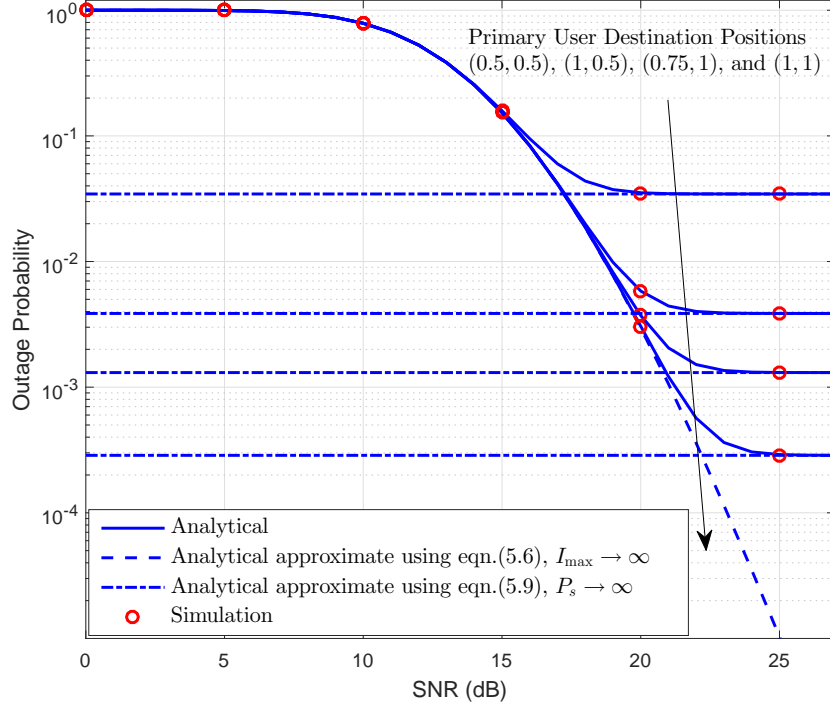


Figure 5.3: Outage performance vs. transmission SNR for different PU receiver node positions.

of the PU receiver and SU destination nodes are considered to be at (0.8, 1) and (0.9, 0), respectively. Furthermore, the following network parameters are considered; $I_{\max} = 20$, dB, $\bar{\gamma}_p = 3$ dB, $N_s = 4$, $M_p = 2$, $N_p = 4$. Fig. 5.4 demonstrates that despite the worst scenario of the interference power, the multi-antenna scheme with the TAS/MRC technique can improve the system performance. In addition, the number of CCI signals plays a negative role in the performance characteristics. It should be observed that the performance starts degrading instead of saturating, after the 20 dB transmission SNR. This degradation is due to the linear increase of the CCI power with respect to the secondary transmission power. This scenario can be considered as a worst case for the secondary network performance.

Fig. 5.5 shows the AEP performance versus the transmission SNR for a different number of antennas at the secondary user source node. In this figure, the value of the interference power constraint has been chosen to be higher than the secondary transmission power to illustrate the performance of the secondary network in the absence of transmission power limitation, due to the interference power constraint. Additionally, the positions of the PU receiver and SU destination nodes are considered to be at (1, 1) and (1, 0), respectively. In addition, the following network

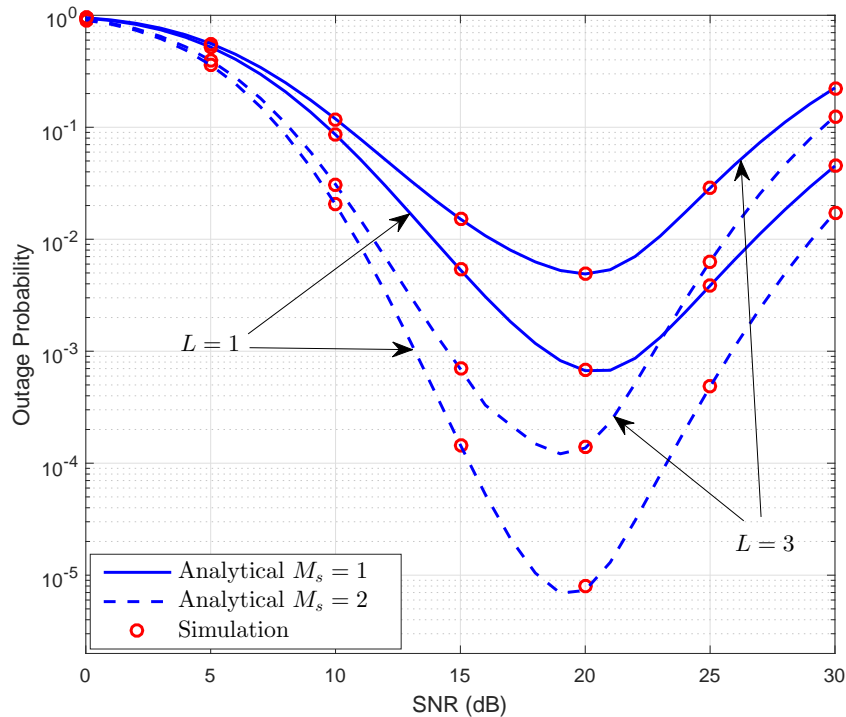


Figure 5.4: Outage performance for a different number of antennas at the SU transmitter and different number of CCI signals in the scenario where the CCI power linearly increases with the secondary transmission power.

parameters are considered for the calculations: $\bar{\gamma}_p = 7$ dB, $\bar{\gamma}_c = 5$ dB, $N_s = 3$, $M_p = 2$, $N_p = 3$, $L = 3$. It is obvious that when the number of antennas at the secondary source node increases, the network performance improves accordingly. This implies that the diversity advantage is possible for a UCRN under the circumstances where the secondary transmitter takes advantage of its transmission power.

5.5 Conclusion

In this chapter, the performance of a MIMO UCRN has been thoroughly investigated when both primary transmitter and CCIs have impacted on the secondary network. Considering the TAS/MRC technique first, the equivalent SINR formula for the secondary network has been obtained. Then, the exact and approximate OP expressions have been derived. Furthermore, an approximate expression for the AEP has been obtained. From the derived expressions, the system performance has been assessed through numerical and simulation examples.

The results showed that considering the MIMO system with the TAS/MRC technique can effectively enhance the performance of the secondary network. It is

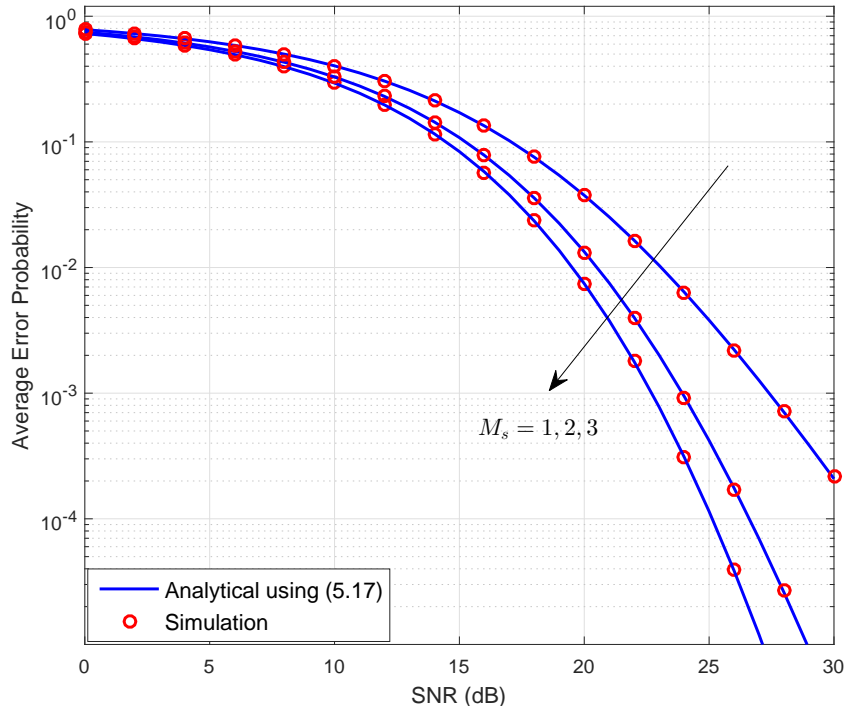


Figure 5.5: Average error probability for a different number of antennas at the SU transmitter.

also found that the power constraint and interferences on the secondary network can severely affect the system performance which could lead to performance floor or, in the worst case, to performance degradation. This research is important in terms of considering a more practical and complete network scenario for an underlay CRN and to understand its behaviour under these practical circumstances.

5.6 Appendix

5.6.1 Proof of Proposition 1

Outage probability is defined as the probability that the equivalent SINR falls below a predefined SNR threshold value γ_{th} . In fact, the OP performance can be investigated directly from the CDF of the equivalent SINR. The definition of CDF of the RV γ_{eq} is $F_{\gamma_{eq}}(\gamma) = \Pr(\gamma_{eq} \leq \gamma)$. Then, by replacing γ with γ_{th} the OP can be obtained. Therefore, the CDF will be derived first, then, the OP can be investigated.

Based on (5.2), the CDF of the end-to-end equivalent SINR, i.e., γ_{eq} , can be

mathematically expressed as:

$$F_{\gamma_{\text{eq}}}(\gamma) = \Pr\left(\min\left(\frac{I_{\text{max}}}{W}, P_s\right) \frac{X}{Y + Z + 1} \leq \gamma\right), \quad (5.20)$$

where $W \triangleq \max_{j \in \{1, \dots, N_p\}} \{|g_{sp_j}|^2\}$, $X \triangleq \|g_{sd_n}^*\|^2$, $Y \triangleq \sum_{l=1}^L \frac{\gamma_{c_l}}{N_0}$, and $Z \triangleq \sum_{i=1}^{M_p} \frac{\gamma_{p_i}}{N_0}$. In the sections below, the detailed steps of deriving $F_{\gamma_{\text{eq}}}(\gamma)$ are given. It is more convenient to start the derivation by finding the resulting RV from the combination of several RVs. First, let M be a new RV such that $M = X/(Y + Z + 1)$. Then, the resulting RV from $Y + Z$ in the denominator can be obtained. Let Q be the new RV from $Y + Z$. The PDF of the sum of these two RVs can be derived by using the following formula [10]:

$$f_Q(q) = \int_0^q f_Y(y) f_Z(q - y) dy. \quad (5.21)$$

The PDFs of RVs Y , and Z can be represented as:

$$f_Y(y) = \frac{y^{L-1}}{\bar{\gamma}_c^L \Gamma(L)} e^{-\frac{y}{\bar{\gamma}_c}}, \quad (5.22)$$

$$f_Z(z) = \frac{z^{M_p-1}}{\bar{\gamma}_p^{M_p} \Gamma(M_p)} e^{-\frac{z}{\bar{\gamma}_p}}, \quad (5.23)$$

where $\bar{\gamma}_c$, and $\bar{\gamma}_p$ are the average INR from the CCI signals and the M_p antennas at the primary transmitter, respectively. So that, $\bar{\gamma}_c \triangleq \frac{P_{CCI}}{N_0} \sigma_{g_{cd}}^2$, and $\bar{\gamma}_p \triangleq \frac{P_{PU}}{N_0} \sigma_{g_{pd}}^2$, where P_{CCI} and P_{PU} are the power of CCI signals and the interference power from the primary user transmitter, respectively, at the secondary destination node. Moreover, $\sigma_{g_{cd}}^2$, and $\sigma_{g_{pd}}^2$ represent the variance values of the channels for CCI sources and primary transmitter to the secondary destination node, respectively. After substituting the mentioned PDFs into (5.21), the following integral formula can be obtained:

$$f_Q(q) = \frac{e^{-\frac{q}{\bar{\gamma}_p}}}{\bar{\gamma}_c^L \bar{\gamma}_p^{M_p} \Gamma(L) \Gamma(M_p)} \int_0^q y^{L-1} (q - y)^{M_p-1} e^{-y\left(\frac{1}{\bar{\gamma}_c} - \frac{1}{\bar{\gamma}_p}\right)} dy. \quad (5.24)$$

Using the Binomial expansion, the term $(q - y)^{M_p-1}$ can be expanded. Then, the

above equation can be rewritten as:

$$f_Q(q) = \frac{e^{-\frac{q}{\bar{\gamma}_p}}}{\bar{\gamma}_c^L \bar{\gamma}_p^{M_p} \Gamma(L) \Gamma(M_p)} \sum_{n_3=0}^{M_p-1} \binom{M_p-1}{n_3} (-1)^{n_3} q^{M_p-1-n_3} \overbrace{\int_0^q y^{L+n_3-1} e^{-y\left(\frac{1}{\bar{\gamma}_c} - \frac{1}{\bar{\gamma}_p}\right)} dy}^{\eta}. \quad (5.25)$$

In (5.25), the variable in the integral is exchanged as $t = y \left(\frac{\bar{\gamma}_p - \bar{\gamma}_c}{\bar{\gamma}_c \bar{\gamma}_p} \right)$, therefore, η can be written as:

$$\eta = \left(\frac{\bar{\gamma}_c \bar{\gamma}_p}{\bar{\gamma}_p - \bar{\gamma}_c} \right)^{L+n_3} \int_0^{q\left(\frac{\bar{\gamma}_p - \bar{\gamma}_c}{\bar{\gamma}_c \bar{\gamma}_p}\right)} t^{L+n_3-1} e^{-t} dt. \quad (5.26)$$

Then, by comparing the above integral with the formula in [83, eq. (8.2.1)] the desired expression can be obtained and written as:

$$\eta = \left(\frac{\bar{\gamma}_c \bar{\gamma}_p}{\bar{\gamma}_p - \bar{\gamma}_c} \right)^{L+n_3} \gamma \left(L + n_3, \left(\frac{\bar{\gamma}_p - \bar{\gamma}_c}{\bar{\gamma}_c \bar{\gamma}_p} \right) q \right). \quad (5.27)$$

Finally, after substituting its derived parts, the PDF of RV Q can be expressed as in (5.28):

$$f_Q(q) = \frac{q^{M_p-1-n_3} e^{-\frac{q}{\bar{\gamma}_p}}}{\bar{\gamma}_c^L \bar{\gamma}_p^{M_p} \Gamma(L) \Gamma(M_p)} \sum_{n_3=0}^{M_p-1} \binom{M_p-1}{n_3} (-1)^{n_3} \left(\frac{\bar{\gamma}_c \bar{\gamma}_p}{\bar{\gamma}_p - \bar{\gamma}_c} \right)^{L+n_3} \times \gamma \left(L + n_3, \left(\frac{\bar{\gamma}_p - \bar{\gamma}_c}{\bar{\gamma}_c \bar{\gamma}_p} \right) q \right), \quad (5.28)$$

where $\gamma(\cdot, \cdot)$ is the lower incomplete Gamma function defined in [83, eq. (8.2.1)].

The next step is to obtain the CDF of M , where $M = \frac{X}{Q+1}$. This division of two RVs can be obtained by averaging the CDF of RV X over the PDF of the RV $Q + 1$. Mathematically, the above statement can be written as [10]:

$$F_M(\gamma) = \int_0^\infty F_X((q+1)\gamma) f_Q(q) dq. \quad (5.29)$$

The CDF expression of RV X under the consideration of TAS/MRC technique can

be represented as [17, eq. (25)]:

$$F_X(x) = 1 - \sum_{n_1=1}^{M_s} \binom{M_s}{n_1} (-1)^{n_1+1} e^{-\frac{n_1 x}{\sigma_{g_{sd}}^2}} \left(\sum_{k=0}^{N_s-1} \frac{\left(\frac{x}{\sigma_{g_{sd}}^2}\right)^k}{k!} \right)^{n_1}. \quad (5.30)$$

Furthermore, using the multinomial expansion, the power of the sum term in the above formula can be written as:

$$\left(\sum_{k=0}^{N_s-1} \frac{\left(\frac{x}{\sigma_{g_{sd}}^2}\right)^k}{k!} \right)^{n_1} = \sum_{k_1, k_{n_1}}^{N_s-1} \frac{1}{k_1! \cdots k_{n_1}!} \left(\frac{x}{\sigma_{g_{sd}}^2}\right)^{\sum k}, \quad (5.31)$$

where

$$\sum_{k_1, k_{n_1}}^{N_s-1} = \sum_{k_1=0}^{N_s-1} \cdots \sum_{k_{n_1}=0}^{N_s-1}, \quad (5.32)$$

and

$$\sum_k = k_1 + k_2 + \cdots + k_{n_1}. \quad (5.33)$$

Then, after substituting the CDF of X , $F_X((q+1)\gamma)$ and the PDF of Q , $f_Q(q)$ into (5.29), and with the help of [112, eq. (8.352.6)] for representing the lower incomplete Gamma function in terms of a finite number of sums, and [83, eq. (5.2.1)], the CDF of RV M can be obtained and written as in (5.34), where Ψ is represented by the formula in (5.6).

$$\begin{aligned} F_M(\gamma) = & 1 - \Psi \left(\frac{\bar{\gamma}_c \bar{\gamma}_p}{\bar{\gamma}_p - \bar{\gamma}_c} \right)^{L+n_3} \Gamma(L+n_3) \left[\left(\frac{\bar{\gamma}_p \sigma_{g_{sd}}^2}{\sigma_{g_{sd}}^2 + \gamma n_1 \bar{\gamma}_p} \right)^{M_p+n_2-n_3} \right. \\ & \Gamma(M_p+n_2-n_3) - \sum_{m=0}^{L+n_3-1} \frac{1}{m!} \left(\frac{\bar{\gamma}_p - \bar{\gamma}_c}{\bar{\gamma}_c \bar{\gamma}_p} \right)^m \Gamma(M_p+n_2+m-n_3) \times \\ & \left. \left(\frac{\bar{\gamma}_c \sigma_{g_{sd}}^2}{\sigma_{g_{sd}}^2 + \gamma n_1 \bar{\gamma}_c} \right)^{M_p+n_2+m-n_3} \right]. \end{aligned} \quad (5.34)$$

In this analysis, it is assumed that the average INR values of the primary network and the CCI sources at the secondary destination node are not equal, i.e., $\bar{\gamma}_p \neq \bar{\gamma}_c$. It is obvious that in the scenario where $\bar{\gamma}_p = \bar{\gamma}_c$, the mathematical representation can be assumed as an existence of $M_p + L$ interferences at the secondary destination

node. Based on the formula in (5.20), the CDF expression can be written in terms of the probability as follows:

$$F_{\gamma_{\text{eq}}}(\gamma) = \begin{cases} \Pr(P_s M \leq \gamma), & \text{when } \frac{I_{\text{max}}}{W} \geq P_s \triangleq \varsigma_1 \\ \Pr\left(\frac{I_{\text{max}}}{W} M \leq \gamma\right), & \text{when } \frac{I_{\text{max}}}{W} < P_s \triangleq \varsigma_2. \end{cases} \quad (5.35)$$

The first part in the above formula can be directly obtained as:

$$\varsigma_1 = F_M\left(\frac{\gamma}{P_s}\right) F_W\left(\frac{I_{\text{max}}}{P_s}\right), \quad (5.36)$$

where $F_M(\cdot)$ is the CDF of RV M that has been obtained in (5.34), with replacing γ by $\frac{\gamma}{P_s}$. In addition, the CDF of RV W can be written as:

$$F_W(w) = 1 - \sum_{j=1}^{N_p} \binom{N_p}{j} (-1)^{j+1} \exp\left(-\frac{wj}{\sigma_{g_{sp}}^2}\right), \quad (5.37)$$

where the variable w should be substituted with $\frac{I_{\text{max}}}{P_s}$. The second part in (5.35) can be expressed as:

$$\varsigma_2 = \int_{\frac{I_{\text{max}}}{P_s}}^{\infty} F_M\left(\frac{\gamma w}{I_{\text{max}}}\right) f_W(w) dw. \quad (5.38)$$

After substituting the entities and doing some mathematical arrangements, the formula for ς_2 can be rewritten as in (5.39):

$$\begin{aligned} \varsigma_2 = & \sum_{j=1}^{N_p} \binom{N_p}{j} (-1)^{j+1} e^{-\frac{jI_{\text{max}}}{P_s \sigma_{g_{sp}}^2}} - \Psi \sum_{j=1}^{N_p} \binom{N_p}{j} (-1)^{j+1} \left(\frac{j}{\sigma_{g_{sp}}^2}\right) \left(\frac{\gamma}{I_{\text{max}} \sigma_{g_{sd}}^2}\right)^{\sum_k} \\ & \left[\Gamma(M_p + n_2 - n_3) \left(\frac{I_{\text{max}} \sigma_{g_{sd}}^2}{\gamma n_1}\right)^{M_p + n_2 - n_3} \times \int_{\frac{I_{\text{max}}}{P_s}}^{\infty} \frac{(w)^{\sum_k} e^{-w\left(\frac{n_1 \gamma}{I_{\text{max}} \sigma_{g_{sd}}^2} + \frac{j}{\sigma_{g_{sp}}^2}\right)}}{\left(\frac{I_{\text{max}} \sigma_{g_{sd}}^2}{\gamma n_1 \bar{\gamma}_p} + w\right)^{M_p + n_2 - n_3}} dw \right. \\ & - \sum_{m=0}^{L+n_3-1} \frac{1}{m!} \left(\frac{\bar{\gamma}_p - \bar{\gamma}_c}{\bar{\gamma}_c \bar{\gamma}_p}\right)^m \Gamma(M_p + n_2 + m - n_3) \times \left(\frac{I_{\text{max}} \sigma_{g_{sd}}^2}{\gamma n_1}\right)^{M_p + n_2 + m - n_3} \\ & \left. \int_{\frac{I_{\text{max}}}{P_s}}^{\infty} \frac{(w)^{\sum_k} e^{-w\left(\frac{n_1 \gamma}{I_{\text{max}} \sigma_{g_{sd}}^2} + \frac{j}{\sigma_{g_{sp}}^2}\right)}}{\left(\frac{I_{\text{max}} \sigma_{g_{sd}}^2}{\gamma n_1 \bar{\gamma}_c} + w\right)^{M_p + n_2 + m - n_3}} dw \right]. \quad (5.39) \end{aligned}$$

By observing (5.39), it can be seen that the two integral formulas are identical

in terms of the structure. Therefore, one integral will be solved in the upcoming section, and the second integral can be solved using similar steps. First, to make the expressions inside the integral more tractable mathematically, some notations are employed. Let $\alpha_1 = \frac{I_{\max}}{P_s}$, $\alpha_2 = \left(\frac{n_1 \gamma}{I_{\max} \sigma_{g_{sd}}^2} + \frac{j}{\sigma_{g_{sp}}^2} \right)$, $\alpha_3 = \frac{I_{\max} \sigma_{g_{sd}}^2}{\gamma n_1 \bar{\gamma}_p}$, $\alpha_4 = M_p + n_2 - n_3$, $\alpha_5 = \frac{I_{\max} \sigma_{g_{sd}}^2}{\gamma n_1 \bar{\gamma}_c}$, and $\alpha_6 = M_p + n_2 + m - n_3$. Furthermore, let ζ_2^a and ζ_2^b represent the first and second integral parts in (5.39). Then, the formula for ζ_2^a can be written as:

$$\zeta_2^a = \int_{\alpha_1}^{\infty} \frac{(w)^{\sum_k} e^{-w\alpha_2}}{(\alpha_3 + w)^{\alpha_4}} dw. \quad (5.40)$$

The integral formula in (5.40) to its current form is quite hard to solve if not impossible, since there is no standard function that can represent its structure. Therefore, one should find methods to re-represent the integral equation so that it can be solved by comparing it to one of the available standard mathematical functions. First, the variable in the integral is replaced as follows: $t = \alpha_3 + w$, therefore, the formula of ζ_2^a can be written as:

$$\zeta_2^a = e^{\alpha_2 \alpha_3} \int_{\alpha_1 + \alpha_3}^{\infty} \frac{(t - \alpha_3)^{\sum_k} e^{-t\alpha_2}}{t^{\alpha_4}} dt. \quad (5.41)$$

Thanks to the Binomial theorem, the above integral representation can be made simpler and more tractable mathematically. Therefore, using the Binomial expansion, the above integral formula can be rewritten as:

$$\zeta_2^a = e^{\alpha_2 \alpha_3} \sum_{r_1=0}^{\sum_k} \binom{\sum_k}{r_1} (-1)^{\sum_k - r_1} (\alpha_3)^{\sum_k - r_1} \int_{\alpha_1 + \alpha_3}^{\infty} \frac{e^{-t\alpha_2}}{t^{\alpha_4 - r_1}} dt. \quad (5.42)$$

In the next step the variable in the integral is exchanged such that $x = t \alpha_2$, then, by comparing the resulting integral with [112, eq. (8.350.2)], the desired expression can be obtained and written as in (5.7). Similar steps can be repeated to derive the second part integral, which can be represented as in (5.8).

Finally, the formula of $F_{\gamma_{\text{eq}}}(\gamma)$ can be obtained by adding both derived parts in ζ_1 and ζ_2 . From this, the OP can be easily obtained by replacing the variable γ in the equivalent CDF formula with γ_{th} , which can be written as in (5.5).

Chapter 6

Impact of CCI on a UCRN Over Nakagami- m Fading Channels

In this chapter, the impact of CCI on the performance of an underlay CR network over Nakagami- m fading channels is presented and analysed. More precisely, a DF relay protocol for a dual-hop cognitive cooperative network is considered. In this study, the impact of both the primary transmitter interference and CCI on the secondary system performance are considered. First, an exact expression for the equivalent SINR of the secondary system is obtained. Then, the corresponding exact and asymptotic CDFs are derived. From this, the exact outage performance for the secondary network is investigated. Furthermore, the equivalent PDF is obtained and discussed. In addition, an approximate expression for the AEP performance is derived.

From the results, it can be inferred that the presence of the CCI and primary network interference severely degrades the system performance. Moreover, a higher value of the shape parameter of the desired fading channel gives better performance and diversity gain. Finally, the analytically derived results have been supported by providing numerical and Monte Carlo simulations results.

Furthermore, Nakagami- m fading channels are more practical to consider in the performance investigation of a wireless communication system, as they can better represent the physical channel characteristics than Rayleigh and Rician fading channels [57]. For instance, Nakagami- m fading channels define the envelope of the received signal after maximal ratio combining diversity. In addition, Rayleigh fading channels can be considered to be a special case within the Nakagami model. More-

over, Rician and Nakagami distributions demonstrate almost the same behaviour close to their mean values [113].

6.0.1 Related Works

Investigations into outage performance for an underlay CR paradigm has been widely studied [57, 58, 65]. For example, the outage performance of the cooperative DF underlay cognitive network was studied in [57] over Nakagami- m fading channels. The authors in [65] and [66] extended the previous work in [57] by considering multi-primary receivers and multi-secondary destinations. In [63], the outage performance of an underlay DF CR network was investigated using the relay selection technique and over Nakagami- m fading channels. In recent work [114], the authors made a comprehensive performance study of a DF cognitive network using the antenna SC technique and by considering proportional and fixed interference power constraint. In the works mentioned above, the impacts of the primary transmission power and CCI on the cognitive radio network were not considered.

Some recent studies have examined the impact of primary transmission interference on the secondary network's performance [15, 55]. For instance, in [15], the asymptotic outage performance of the cooperative AF CR network was studied over Rayleigh fading channels. Finally, the authors in [10, 72] have investigated the impact of CCI on an underlay CR network considering Rayleigh fading channels. In addition, detailed performance analyses were investigated in [10].

6.0.2 Contribution of this Chapter

A good background understanding in the area of the performance study of an underlay CR network has been garnered from the works mentioned above. However, most of them have neglected the interference from the primary transmitter and/or considered only Rayleigh fading channels. In fact, the impact of CCI has to be considered in practical cognitive relaying techniques. To the best of the author's knowledge, the effects of such CCI on a UCRN over Nakagami- m fading channels has not yet been studied.

In this chapter, the performance of a UCRN scenario over Nakagami- m fading channels is studied when the CCI signals and the primary network interferences are present. Specifically, the exact equivalent per-hop and end-to-end SINR of the

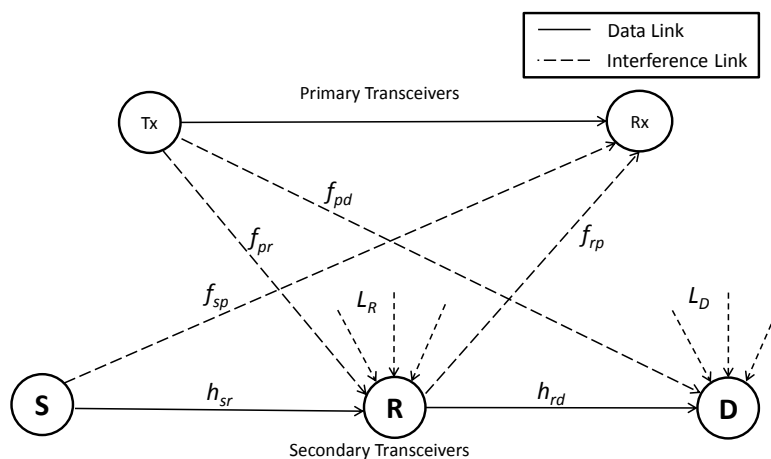


Figure 6.1: The general network model used for analysis showing cooperative underlay CR network in the existence of the primary transceiver and CCI.

secondary network over Nakagami- m fading channels is addressed. Then, the exact CDF of the system SINR is obtained. Based on these results, the outage and AEP performances of the secondary network are thoroughly investigated.

The remainder of this chapter is structured as follows. In Section 6.1 the system model is described and represented mathematically. Section 6.2 is devoted to the derivation of the statistical and performance metrics. In Section 6.3, numerical results are presented to validate the derivations and analysis. Section 6.4 summarizes the main findings of the research in this chapter. Finally, the steps of the theoretical derivations are given in Appendices 6.5.1, and 6.5.2.

6.1 System Model

In the following sections, first, the network parameters and channels are described. Then, mathematical representations of the received signals are presented, and the formula for the equivalent SINR of the network is obtained.

6.1.1 Network and Channels Description

The system model under consideration is shown in Fig. 6.1. S , R , and D are the secondary source, relay and destination nodes, respectively. The existence of a primary transceiver is considered in the network, where T_x is the transmitter node and R_x is the receiver node. Each node in the system has a single antenna and is working in half-duplex mode. Due to the presence of obstacles between the

secondary source and destination, it is assumed that there is no direct link between them [53]. In addition, the relay node employs the DF protocol. Moreover, it is assumed that all the channels between the nodes are subject to independent and non-identically distributed Nakagami- m fading channels. The channels have a scale parameter of $\sigma_{X_{ij}}^2$ and a shape parameter of $m_{X_{ij}}$, where X represents the generic channel coefficient; i and j represent the source and destination node for the channel X , respectively.

Furthermore, it is assumed that the CCI links are identical, in terms of their average INR, at the secondary user relay and destination nodes, respectively [10, 84]. This is a valid assumption especially when L_R and L_D interference sources are from other neighbouring clusters. For instance, the distance from L_R sources to the relay node is relatively large enough that the interference signals can be assumed to have similar average power gain [10]. h_{sr} , and h_{rd} represent the first and second hop data channel fading coefficients of the secondary network, respectively. f_{sp} , and f_{rp} represent the interference channel fading coefficients of the secondary source and relay to the primary receiver, respectively. f_{pr} , f_{pd} represent the interference channel fading coefficients of the T_x to the secondary relay and destination, respectively. f_{ir_j} ($j = 1, 2, \dots, L_R$), and f_{id_i} ($i = 1, 2, \dots, L_D$) represent the CCI fading coefficients of the j^{th} interference channel at the secondary relay and i^{th} interference channel at the secondary destination, respectively. In fact, the CCI signals affect the primary receiver as well. However, this research focuses on the performance of the secondary network. It is obvious that the performance of the primary network is similar to the extensively studied performance in the literature [115]. In addition, the corresponding channel power gains for the mentioned Nakagami- m channel coefficients are $|h_{sr}|^2$, $|h_{rd}|^2$, $|f_{sp}|^2$, $|f_{rp}|^2$, $|f_{pr}|^2$, $|f_{pd}|^2$, $|f_{ir_j}|^2$, and $|f_{id_i}|^2$ respectively, which follow the gamma distribution with the scale parameters of $\sigma_{h_{sr}}^2$, $\sigma_{h_{rd}}^2$, $\sigma_{f_{sp}}^2$, $\sigma_{f_{rp}}^2$, $\sigma_{f_{pr}}^2$, $\sigma_{f_{pd}}^2$, $\sigma_{f_{ir}}^2$ and $\sigma_{f_{id}}^2$, respectively, and the corresponding channel fading severity parameters are $m_{h_{sr}}$, $m_{h_{rd}}$, $m_{f_{sp}}$, $m_{f_{rp}}$, m_{pr} , m_{pd} , m_{ir} , and m_{id} , respectively.

6.1.2 Mathematical Representation

The transmission in the secondary network is performed in two phases. In the first phase, the source node transmits its message signal to the relay node. The relay node receives the transmitted message from S plus noise, which is represented as

AWGN, plus the interference from T_x , and the CCI from L_R interference sources.

In the second phase, the relay node decodes the received signal then encodes it and broadcasts the message to the destination node. Similar to the first phase, the received signal at the destination node will be a combination of the desired message, noise and interferences from the primary transmitter and the CCI signals. Thus, the received signal at both relay and destination nodes can respectively be represented as:

$$y_r = \sqrt{E_S}h_{sr}x + \sqrt{E_{IR}} \sum_{j=1}^{L_R} f_{ir_j}x_{r_j} + \sqrt{E_{PR}}f_{pr}x_{pr} + n_r, \quad (6.1)$$

and

$$y_d = \sqrt{E_R}h_{rd}\hat{x} + \sqrt{E_{ID}} \sum_{i=1}^{L_D} f_{id_i}x_{d_i} + \sqrt{E_{PD}}f_{pd}x_{pd} + n_d, \quad (6.2)$$

where E_S , and E_R are the secondary source and relay permitted transmission energy signals, respectively. E_{IR} , and E_{ID} are the CCI energies at the secondary relay and destination nodes, respectively. E_{PR} , and E_{PD} are the interference energy signals of the primary transmitter at the secondary relay and destination nodes, respectively.

Furthermore, x represents the desired signal to be transmitted from the secondary source and \hat{x} is the desired signal to be transmitted from the secondary relay. x_{r_j} and x_{d_i} are the j^{th} and i^{th} co-channel interferer's signals that are affecting the secondary relay and destination nodes, respectively, x_{pr} , and x_{pd} are the primary interferer's signals that are affecting the secondary relay and destination nodes, respectively. All signals are assumed to have unit energy. Finally, n_r and n_d represent the AWGN terms at the secondary relay and destination nodes, respectively.

In an underlay CR network, the secondary transmitters should adjust their transmission power so that the quality of service of the primary network is maintained. Therefore, the transmission powers at S and R are $E_S \leq \min\left(\frac{I_{\max}}{|f_{sp}|^2}, P_s\right)$ and $E_R \leq \min\left(\frac{I_{\max}}{|f_{rp}|^2}, P_r\right)$, respectively, where P_s and P_r are maximum transmission power limits at S and R , respectively. Moreover, I_{\max} is the interference power constraint, which is the maximum level of interference that the secondary network can produce at the primary receiver node. Therefore, the received equivalent SINR

in the first time-slot at the relay is represented as:

$$\begin{aligned}\gamma_{SR}^{\text{eq}} &= \frac{\text{signal power}}{\text{CCI power} + \text{primary interference} + \text{noise power}} \\ &= \frac{\gamma_{SR}}{\gamma_{IR} + \gamma_{PR} + 1},\end{aligned}\quad (6.3)$$

where $\gamma_{SR} = \frac{E_S}{N_0} |h_{sr}|^2 = \min\left(\frac{I_{\max}}{|f_{sp}|^2}, P_s\right) \frac{|h_{sr}|^2}{N_0}$, $\gamma_{IR} = \sum_{j=1}^{L_R} \left(\frac{E_{IR}}{N_0} |f_{ir_j}|^2 \triangleq I_{R_j}\right)$ and $\gamma_{PR} = \frac{E_{PR}}{N_0} |f_{pr}|^2 \triangleq I_{PR}$. In addition, $\gamma_{RD} = \min\left(\frac{I_{\max}}{|f_{rp}|^2}, P_r\right) \frac{|h_{rd}|^2}{N_0}$, $\gamma_{PD} = \frac{E_{PD}}{N_0} |f_{pd}|^2 \triangleq I_{PD}$, and $\gamma_{ID} = \sum_{i=1}^{L_D} \left(\frac{E_{ID}}{N_0} |f_{id_i}|^2 \triangleq I_{D_i}\right)$. Moreover, \bar{I}_R , \bar{I}_D , \bar{I}_{PR} , and \bar{I}_{PD} represent the average INR values corresponding to I_R , I_D , I_{PR} , and I_{PD} , respectively.

6.2 Statistical Derivations and Performance Evaluation

In the following sections, first the per-hop and total equivalent CDF and PDF are derived. Then, exact and asymptotic expressions for the outage performance are derived. In addition, multi-hop outage performance is examined. Finally, the system AEP is investigated.

6.2.1 The CDF of $\gamma_{\text{eq}}^{\text{tot}}$

For a dual-hop DF cognitive secondary network, the end-to-end equivalent SINR known as $\gamma_{\text{eq}}^{\text{tot}}$ can be represented as [115]:

$$\gamma_{\text{eq}}^{\text{tot}} = \min(\gamma_{SR}^{\text{eq}}, \gamma_{RD}^{\text{eq}}), \quad (6.4)$$

where γ_{SR}^{eq} , and γ_{RD}^{eq} are the equivalent SINR for the first and second hop, respectively. Moreover, the total equivalent CDF can be obtained by using the following formula [69]:

$$F_{\gamma_{\text{eq}}^{\text{tot}}}(\gamma) = 1 - \left(1 - F_{\gamma_{SR}^{\text{eq}}}(\gamma)\right) \left(1 - F_{\gamma_{RD}^{\text{eq}}}(\gamma)\right), \quad (6.5)$$

where $F_{\gamma_{SR}^{\text{eq}}}(\gamma)$ and $F_{\gamma_{RD}^{\text{eq}}}(\gamma)$ are the CDFs of the first and second hop equivalent SINR, i.e., γ_{SR}^{eq} and γ_{RD}^{eq} , respectively. The CDFs of γ_{SR}^{eq} and γ_{RD}^{eq} can be found as follows: from the equivalent SINR formula in (6.3), the CDF of γ_{SR}^{eq} can be written

as:

$$\begin{aligned} F_{\gamma_{SR}^{\text{eq}}}(\gamma) &= \Pr(\gamma_{SR}^{\text{eq}} \leq \gamma) \\ &= \Pr\left(\min\left(\frac{I_{\max}}{Y}, P_s\right) \frac{X}{(I+P+1)} \leq \gamma\right), \end{aligned} \quad (6.6)$$

where X , Y , I , P represent the RVs $\frac{|h_{sr}|^2}{N_0}$, $|f_{rp}|^2$, $\frac{E_{IR}}{N_0} \sum_{j=1}^{L_R} |f_{ir_j}|^2$, and $\frac{E_{PR}}{N_0} |f_{pr}|^2$, respectively, with $\Pr(\cdot)$ denoting probability operator. The PDFs of X , Y , I , P are represented as the following:

$$f_X(x) = \left(\frac{m_{h_{sr}}}{\sigma_{h_{sr}}^2}\right)^{m_{h_{sr}}} \frac{x^{m_{h_{sr}}-1}}{\Gamma(m_{h_{sr}})} \exp\left(-\frac{m_{h_{sr}}}{\sigma_{h_{sr}}^2}x\right), \quad (6.7)$$

$$f_Y(y) = \left(\frac{m_{f_{sp}}}{\sigma_{f_{sp}}^2}\right)^{m_{f_{sp}}} \frac{y^{m_{f_{sp}}-1}}{\Gamma(m_{f_{sp}})} \exp\left(-\frac{m_{f_{sp}}}{\sigma_{f_{sp}}^2}y\right), \quad (6.8)$$

$$f_I(\gamma_{IR}) = \left(\frac{m_{ir}}{\bar{I}_R}\right)^{m_{ir}L_R} \frac{\gamma_{IR}^{m_{ir}L_R-1}}{\Gamma(m_{ir}L_R)} \exp\left(-\frac{m_{ir}}{\bar{I}_R}\gamma_{IR}\right), \quad (6.9)$$

$$f_P(\gamma_{PR}) = \left(\frac{m_{pr}}{\bar{I}_{PR}}\right)^{m_{pr}} \frac{\gamma_{PR}^{m_{pr}-1}}{\Gamma(m_{pr})} \exp\left(-\frac{m_{pr}}{\bar{I}_{PR}}\gamma_{PR}\right), \quad (6.10)$$

where $m_{h_{sr}}$, $m_{f_{sp}}$, m_{ir} , and m_{pr} are the Nakagami- m channel fading severity parameters for the channels between the nodes of the SU source to the SU relay, the SU source to R_x , CCI signals to the SU relay, and T_x to the SU relay, respectively.

Corollary 1: The equivalent CDF of the source to relay SINR can be expressed as in (6.11), where Υ is defined in (6.12). In addition, $\Gamma(\cdot, \cdot)$ is the upper incomplete gamma function defined in [112, eq. (8.350.2)]. Furthermore, for the purpose of representing the equations in a simpler form, the following entities have been defined as follows: $\beta_1 = \frac{P_s \sigma_{h_{sr}}^2}{m_{h_{sr}}}$, $\beta_2 = \frac{m_{ir}}{\bar{I}_R}$, $\beta_3 = \frac{m_{pr}}{\bar{I}_{PR}}$, $\beta_4 = \frac{\bar{I}_{PR} m_{ir} - \bar{I}_R m_{pr}}{\bar{I}_{PR} \bar{I}_R}$, $\beta_5 = \frac{m_{f_{sp}} I_{\max}}{P_s \sigma_{f_{sp}}^2}$, $\beta_6 = \frac{m_{f_{sp}} \sigma_{h_{sr}}^2 I_{\max}}{m_{h_{sr}} \sigma_{f_{sp}}^2}$, $\beta_7 = \frac{m_{pr} m_{f_{sp}} \sigma_{h_{sr}}^2 I_{\max}}{m_{h_{sr}} \sigma_{f_{sp}}^2 \bar{I}_{PR}}$, and $\beta_8 = \frac{m_{ir} m_{f_{sp}} \sigma_{h_{sr}}^2 I_{\max}}{m_{h_{sr}} \sigma_{f_{sp}}^2 \bar{I}_R}$.

$$\begin{aligned}
 F_{\gamma_{SR}^{\text{eq}}}(\gamma) = & 1 - \Upsilon \left\{ e^{-\frac{\gamma}{\beta_1}} \left(\frac{\gamma}{\beta_1} \right)^i \left(1 - \frac{\Gamma(m_{fsp}, \beta_5)}{\Gamma(m_{fsp})} \right) \left[\left(\frac{\gamma}{\beta_1} + \beta_3 \right)^{l-j-m_{pr}} \right. \right. \\
 & \left. \left. \Gamma(j + m_{pr} - l) - \sum_{k=0}^{m_{ir}L_R+l-1} \frac{(\beta_4)^k}{k!} \left(\frac{\gamma}{\beta_1} + \beta_2 \right)^{l-j-k-m_{pr}} \Gamma(j + k + m_{pr} - l) \right] \right. \\
 & \left. + \frac{\left(\frac{\beta_6}{\gamma} \right)^{m_{fsp}}}{\Gamma(m_{fsp})} \left[\Gamma(j + m_{pr} - l) I_{1a} - \sum_{k=0}^{m_{ir}L_R+l-1} \frac{(\beta_4)^k}{k!} \Gamma(j + k + m_{pr} - l) I_{1b} \right] \right\}. \quad (6.11)
 \end{aligned}$$

$$\begin{aligned}
 \Upsilon = & \sum_{i=0}^{m_{hsr}-1} \sum_{j=0}^i \sum_{l=0}^{m_{pr}-1} \binom{m_{pr}-1}{l} \binom{i}{j} \frac{(-1)^l}{i!} \left(\frac{m_{ir}}{\bar{I}_R} \right)^{m_{ir}L_R} \left(\frac{m_{pr}}{\bar{I}_{PR}} \right)^{m_{pr}} \times \\
 & \frac{\Gamma(m_{ir}L_R + l)}{\Gamma(m_{ir}L_R) \Gamma(m_{pr})} \left(\frac{\bar{I}_{PR} \bar{I}_R}{\bar{I}_{PR} m_{ir} - \bar{I}_R m_{pr}} \right)^{m_{ir}L_R+l}. \quad (6.12)
 \end{aligned}$$

Proof: See Appendix 6.5.1. ■

To obtain the second hop CDF, similar derivation steps can be repeated by replacing the following parameters ($P_s, m_{hsr}, m_{fsp}, m_{ir}, m_{pr}, \sigma_{hsr}^2, \sigma_{fsp}^2, \bar{I}_R, \bar{I}_{PR}, \gamma_{SR}^{\text{eq}}, \gamma_{SR}, \gamma_{IR}, \gamma_{PR}$) with the following parameters ($P_r, m_{hrd}, m_{frp}, m_{id}, m_{pd}, \sigma_{hrd}^2, \sigma_{frp}^2, \bar{I}_D, \bar{I}_{PD}, \gamma_{RD}^{\text{eq}}, \gamma_{RD}, \gamma_{ID}, \gamma_{PD}$), respectively. Finally, the dual-hop cognitive network equivalent CDF can be obtained by substituting the derived per-hop CDFs into (6.5).

6.2.2 The PDF of $\gamma_{\text{eq}}^{\text{tot}}$

Another efficient performance indicator of the RVs is the PDF of the total equivalent SINR of the system. By knowing this, the behaviour of the RV over the specified range can be investigated. The PDF can be obtained by taking the first derivative of the CDF; therefore, the total equivalent PDF of the secondary network can be obtained using the following formula:

$$f_{\gamma_{\text{eq}}^{\text{tot}}}(x) = f_{\gamma_{SR}^{\text{eq}}}(x) \left(1 - F_{\gamma_{RD}^{\text{eq}}}(x) \right) + f_{\gamma_{RD}^{\text{eq}}}(x) \left(1 - F_{\gamma_{SR}^{\text{eq}}}(x) \right), \quad (6.13)$$

where $f_{\gamma_{SR}^{\text{eq}}}(x)$ and $f_{\gamma_{RD}^{\text{eq}}}(x)$ are the PDFs of γ_{SR}^{eq} and γ_{RD}^{eq} , respectively. In the previous sections the CDFs for both hops were already derived. The PDFs of γ_{SR}^{eq} and γ_{RD}^{eq} are found as follows:

- Determining $f_{\gamma_{SR}^{\text{eq}}}(x)$:

In this section, the exact equivalent PDF of the first hop SINR is derived.

$f_{\gamma_{SR}^{\text{eq}}}(x)$ can be obtained by taking the first derivative of the equivalent CDF,

i.e., $F_{\gamma_{SR}^{\text{eq}}}(\gamma)$:

$$f_{\gamma_{SR}^{\text{eq}}}(x) = \frac{d}{d\gamma} F_{\gamma_{SR}^{\text{eq}}}(\gamma). \quad (6.14)$$

Bearing in mind that the derivative of upper incomplete gamma function can be implemented using the chain rule as follows:

$$\frac{d}{dx} \Gamma(s, g(x)) = -(g(x))^{s-1} e^{-g(x)} \times \frac{d}{dx} g(x). \quad (6.15)$$

After performing the derivative of each term and some mathematical arrangements, the first hop equivalent PDF can be obtained and written as in (6.16).

Υ_2 , Υ_3 , Υ_4 , and Υ_5 are represented by formulas in (6.17a - 6.17d), respectively.

Furthermore, ψ_2 , ψ_3 , ψ_4 , and ψ_5 represent the terms that are involved with derivatives, and are represented by the formulas (6.18 - 6.21), respectively.

$$f_{\gamma_{SR}^{\text{eq}}}(x) = \Upsilon \left\{ (\beta_1)^{m_{pr}+j-l-i} \left(1 - \frac{\Gamma(m_{fsp}, \beta_5)}{\Gamma(m_{fsp})} \right) \left[\Upsilon_3 \psi_3 - \Upsilon_2 \psi_2 \right] - \frac{(\beta_6)^{m_{fsp}}}{\Gamma(m_{fsp})} \left[\Upsilon_4 \psi_4 - \Upsilon_5 \psi_5 \right] \right\}. \quad (6.16)$$

$$\Upsilon_2 = \Gamma(j + m_{pr} - l), \quad (6.17a)$$

$$\Upsilon_3 = \sum_{k=0}^{m_{ir}L_R+l-1} \frac{(\beta_1\beta_4)^k}{k!} \Gamma(j + k + m_{pr} - l), \quad (6.17b)$$

$$\Upsilon_4 = \Gamma(j + m_{pr} - l) \sum_{r_1=0}^{m_{fsp}+i-1} \binom{m_{fsp}+i-1}{r_1} (-\beta_3)^{m_{fsp}+i-1-r_1} e^{\beta_3}, \quad (6.17c)$$

$$\Upsilon_5 = \sum_{k=0}^{m_{ir}L_R+l-1} \sum_{r_2=0}^{m_{fsp}+i-1} \binom{m_{fsp}+i-1}{r_2} \frac{(\beta_4)^k}{k!} \Gamma(j + k + m_{pr} - l) (-\beta_2)^{m_{fsp}+i-1-r_2} e^{\beta_2}, \quad (6.17d)$$

$$\psi_2 = e^{-\frac{x}{\beta_1}} x^i (\beta_1 \beta_3 + x)^{l-j-m_{pr}} \left(\frac{(l-j-m_{pr})}{(\beta_1 \beta_3 + x)} - \frac{1}{\beta_1} + \frac{i}{x} \right), \quad (6.18)$$

$$\psi_3 = e^{-\frac{x}{\beta_1}} x^i (\beta_1 \beta_2 + x)^{l-j-k-m_{pr}} \left(\frac{(l-j-k-m_{pr})}{(\beta_1 \beta_2 + x)} - \frac{1}{\beta_1} + \frac{i}{x} \right), \quad (6.19)$$

$$\begin{aligned} \psi_4 = & -\frac{(x)^{r_1+l-j-m_{pr}-m_{fsp}}}{(\beta_6+x)^{r_1+l-j-m_{pr}+1}} \left\{ e^{-\frac{x}{\beta_1}-\beta_3-\beta_5} \left(\frac{x}{\beta_1} + \frac{\beta_7}{x} + \beta_3 + \beta_5 \right)^{r_1+l-j-m_{pr}} \right. \\ & \left(\frac{x}{\beta_1} - \frac{\beta_7}{x} \right) + \Gamma \left(r_1+l-j-m_{pr}+1, \beta_3 + \beta_5 + \frac{x}{\beta_1} + \frac{\beta_7}{x} \right) e^{\frac{\beta_7}{x}} \times \\ & \left. \left[m_{fsp} + \frac{\beta_7}{x} - (r_1+l-j-m_{pr}+1) \left(\frac{\beta_6}{\beta_6+x} \right) \right] \right\}, \quad (6.20) \end{aligned}$$

$$\begin{aligned} \psi_5 = & -\frac{(x)^{r_2+l-j-k-m_{pr}-m_{fsp}}}{(\beta_6+x)^{r_2+l-j-k-m_{pr}+1}} \left\{ e^{-\frac{x}{\beta_1}-\beta_2-\beta_5} \left(\frac{x}{\beta_1} + \frac{\beta_8}{x} + \beta_2 + \beta_5 \right)^{r_2+l-j-k-m_{pr}} \right. \\ & \left(\frac{x}{\beta_1} - \frac{\beta_8}{x} \right) + \Gamma \left(r_2+l-j-k-m_{pr}+1, \beta_2 + \beta_5 + \frac{x}{\beta_1} + \frac{\beta_8}{x} \right) e^{\frac{\beta_8}{x}} \times \\ & \left. \left[m_{fsp} + \frac{\beta_8}{x} - (r_2+l-j-k-m_{pr}+1) \left(\frac{\beta_6}{\beta_6+x} \right) \right] \right\}. \quad (6.21) \end{aligned}$$

- Determining $f_{\gamma_{RD}^{\text{eq}}}(x)$:

Similar steps can be repeated to obtain the PDF of the second hop. Finally, the total equivalent PDF is obtained by substituting the derived per-hop PDFs and CDFs into (6.13).

6.2.3 Exact Outage Performance

From the derived total equivalent CDF of the secondary network's SINR, the exact OP of a cognitive network can be investigated by replacing the variable γ with γ_{th} (i.e., SNR threshold).

$$P_{\text{out}}(\gamma_{\text{th}}) = \Pr(\gamma_{\text{eq}}^{\text{tot}} \leq \gamma_{\text{th}}) = F_{\gamma_{\text{eq}}^{\text{tot}}}(\gamma_{\text{th}}). \quad (6.22)$$

The value of γ_{th} for the dual-hop network has the following representation: $\gamma_{\text{th}} = 2^{2R} - 1$, where R is the target data rate and 2 comes from the fact that the transmission is performed within two time-slots.

6.2.4 Asymptotic Outage Performance

In this section, two scenarios for the asymptotic CDF are presented, from which the asymptotic outage performance can be investigated.

- No interference power constraint, i.e., $I_{\max} \rightarrow \infty$:

By substituting this condition in (6.6), the resulting CDF formula will reduce to the CDF of RV G that has been derived and represented in (6.44), in Appendix 6.5.1, with the condition of replacing the RV γ by $\frac{\gamma}{P_s}$, i.e., $F_G\left(\frac{\gamma}{P_s}\right)$. Then, the approximate first hop CDF in this case will be:

$$F_{\gamma_{SR}^{\text{eq}}}(\gamma) \approx 1 - \Upsilon\left(\frac{\gamma}{\beta_1}\right)^i e^{-\frac{\gamma}{\beta_1}} \left[\left(\frac{\gamma}{\beta_1} + \beta_3\right)^{l-j-m_{pr}} \Gamma(j+m_{pr}-l) - \sum_{k=0}^{m_{ir}L_R+l-1} \frac{(\beta_4)^k}{k!} \left(\frac{\gamma}{\beta_1} + \beta_2\right)^{l-j-k-m_{pr}} \Gamma(j+k+m_{pr}-l) \right]. \quad (6.23)$$

This scenario can be considered when the primary network is not active. In fact, this can also be considered as a special case of interweave cognitive radio [8], in which the secondary user can use a specific frequency spectrum when this particular spectrum is vacant. In this scenario, the secondary transmission power is the dominant power, however, due to the existence of interference on the secondary network, it is still possible for the performance saturation to occur. Finally, by performing similar steps, the second hop asymptotic CDF can be obtained; then, the asymptotic outage performance can be studied using (6.5) and (6.22).

- No power constraint on the secondary transmitter, i.e., $P_s \rightarrow \infty$:

In this scenario, the first hop conditional equivalent CDF can be represented as:

$$F_{\gamma_{SR}^{\text{eq}}}(\gamma)|_y = \Pr\left(G \leq \frac{\gamma y}{I_{\max}}\right). \quad (6.24)$$

Therefore, the unconditional CDF can be obtained by taking the expectation of $F_G(\frac{\gamma y}{I_{\max}})$ over the PDF of RV Y .

$$F_{\gamma_{SR}^{\text{eq}}}(\gamma) = \int_0^{\infty} F_G\left(\frac{\gamma y}{I_{\max}}\right) f_Y(y) dy. \quad (6.25)$$

The steps for solving the above integral are quite similar to the steps for solving I_1 in (6.45), in Appendix 6.5.1. Therefore, for the sake of saving space they have been omitted. Finally, the asymptotic first hop CDF for this scenario can be written as in (6.26), where I_{1b}^{app} and I_{1a}^{app} are obtained by using the formulas in (6.27) and (6.28), respectively.

$$F_{\gamma_{SR}^{\text{eq}}}(\gamma) \approx 1 - \Upsilon\left(\frac{\beta_6}{\gamma}\right)^{m_{fsp}} \frac{1}{\Gamma(m_{fsp})} \left[\Gamma(j + m_{pr} - l) I_{1a}^{\text{app}} - \sum_{k=0}^{a_3-1} \frac{(\beta_4)^k}{k!} \Gamma(j + k + m_{pr} - l) I_{1b}^{\text{app}} \right], \quad (6.26)$$

$$I_{1a}^{\text{app}} = \sum_{r_1=0}^{m_{fsp}+i-1} \binom{m_{fsp}+i-1}{r_1} \frac{(-1)^{m_{fsp}+i-1-r_1}}{(\beta_3)^{r_1+1-m_{fsp}-i}} \left(\frac{\gamma}{\gamma+\beta_6}\right)^{r_1-j-m_{pr}+1+l} e^{\beta_3(1+\frac{\beta_6}{\gamma})} \Gamma\left(l+r_1-j-m_{pr}+1, \beta_3\left(1+\frac{\beta_6}{\gamma}\right)\right), \quad (6.27)$$

$$I_{1b}^{\text{app}} = \sum_{r_2=0}^{m_{fsp}+i-1} \binom{m_{fsp}+i-1}{r_2} \frac{(-1)^{m_{fsp}+i-1-r_2}}{(\beta_2)^{r_2+1-m_{fsp}-i}} \left(\frac{\gamma}{\gamma+\beta_6}\right)^{r_2-j-k-m_{pr}+1+l} e^{\beta_2(1+\frac{\beta_6}{\gamma})} \Gamma\left(l+r_2-j-k-m_{pr}+1, \beta_2\left(1+\frac{\beta_6}{\gamma}\right)\right). \quad (6.28)$$

In this scenario, I_{\max} is the dominant power limit for the secondary transmitter nodes. Furthermore, in terms of performance criteria, it can be considered to be the maximum performance limit that the secondary network can achieve. More explanation about the asymptotic results can be found in Fig. 6.3 in the numerical results section.

6.2.5 Multi-hop Exact Outage Performance

In the case of the multi-hop DF cooperative communication, the end-to-end equivalent SINR $\gamma_{\text{eq}}^{\text{e2e}}$ is calculated based on the weakest per-hop SINR. Mathematically, this can be represented as:

$$\gamma_{\text{eq}}^{\text{e2e}} = \min_{i=1, \dots, N} (\gamma_{\text{eq}}^i), \quad (6.29)$$

where γ_{eq}^i is the i^{th} hop equivalent SINR, and N is the number of hops in the multi-hop cognitive cooperative network. Therefore, the exact end-to-end multi-hop outage performance can be obtained by [98]:

$$P_{\text{out}}^{\text{e2e}}(\gamma_{\text{th}}) = 1 - \prod_{i=1}^N \left(1 - F_{\gamma_{\text{eq}}^i}(\gamma_{\text{th}})\right), \quad (6.30)$$

where $F_{\gamma_{\text{eq}}^i}(\gamma_{\text{th}})$ is the i^{th} hop equivalent CDF. From the previous derivations, it can be noted that the exact multi-hop outage performance can be easily obtained by substituting the per-hop CDF derived in (6.11) into (6.30).

6.2.6 Average Error Probability

The AEP over slow flat fading channels can be found using different approaches, such as the PDF or CDF of the equivalent SINR of the system. Furthermore, by observing the derived per-hop CDF and PDF in the previous sections, it can be deduced that using CDF is mathematically more convenient. Therefore, the per-hop AEP can be obtained by using [72]:

$$\bar{P}_b^i = \frac{a}{2} \sqrt{\frac{b}{\pi}} \int_0^{\infty} \frac{e^{-b\gamma}}{\sqrt{\gamma}} F_{\gamma_{\text{eq}}^i}(\gamma) d\gamma, \quad (6.31)$$

where \bar{P}_b^i is the average symbol error probability for the i^{th} hop. In addition, a and b are modulation constants depending on the constellation used. Finally, the end-to-end AEP can be evaluated by:

$$\bar{P}_b^{\text{e2e}} = \sum_{i=1}^N \bar{P}_b^i \prod_{j=i+1}^N (1 - 2\bar{P}_b^j), \quad (6.32)$$

For the case of a dual-hop DF network, the above formula reduces to [90]:

$$\bar{P}_b^{e2e} = \bar{P}_b^{SR} + \bar{P}_b^{RD} - 2(\bar{P}_b^{SR} \bar{P}_b^{RD}) \quad (6.33)$$

where \bar{P}_b^{SR} and \bar{P}_b^{RD} are the AEPs for the first and second hop, respectively, which are obtained by using (6.31). Unfortunately, it is very difficult if not impossible to get the exact expression from the above equation. However, an approximate expression can be obtained using the approximate derived CDF expression in (6.23).

Corollary 2: The first hop approximate AEP can be represented as in (6.34).

$$\begin{aligned} \bar{P}_b^{SR} \approx & \frac{a}{2} - \frac{a}{2} \sqrt{\frac{b}{\pi}} \Upsilon(\beta_1)^{m_{pr}+j-l-i} \left[\Gamma(j + m_{pr} - l) \Omega_1 \right. \\ & \left. - \sum_{k=0}^{m_{ir}L_R+l-1} \frac{(\beta_1\beta_4)^k}{k!} \Gamma(j + k + m_{pr} - l) \Omega_2 \right], \end{aligned} \quad (6.34)$$

where Ω_1 and Ω_2 are calculated using formulas represented in (6.35) and (6.36), respectively.

$$\Omega_1 = (\beta_1\beta_3)^{l-j-m_{pr}+i+\frac{1}{2}} \Gamma\left(i + \frac{1}{2}\right) U\left(i + \frac{1}{2}, l - j - m_{pr} + i + \frac{3}{2}, \beta_1\beta_3 \left(b + \frac{1}{\beta_1}\right)\right), \quad (6.35)$$

$$\begin{aligned} \Omega_2 = & (\beta_1\beta_2)^{l-j-k-m_{pr}+i+\frac{1}{2}} \Gamma\left(i + \frac{1}{2}\right) \times \\ & U\left(i + \frac{1}{2}, l - j - k - m_{pr} + i + \frac{3}{2}, \beta_1\beta_2 \left(b + \frac{1}{\beta_1}\right)\right). \end{aligned} \quad (6.36)$$

Proof: See Appendix 6.5.2. ■

6.3 Numerical Results and Discussion

This section presents numerical and Monte Carlo simulation results for the purpose of validation of the derived analytical results and to highlight the characteristics of the system performance under the consideration of interference from the primary transmitter and the CCI.

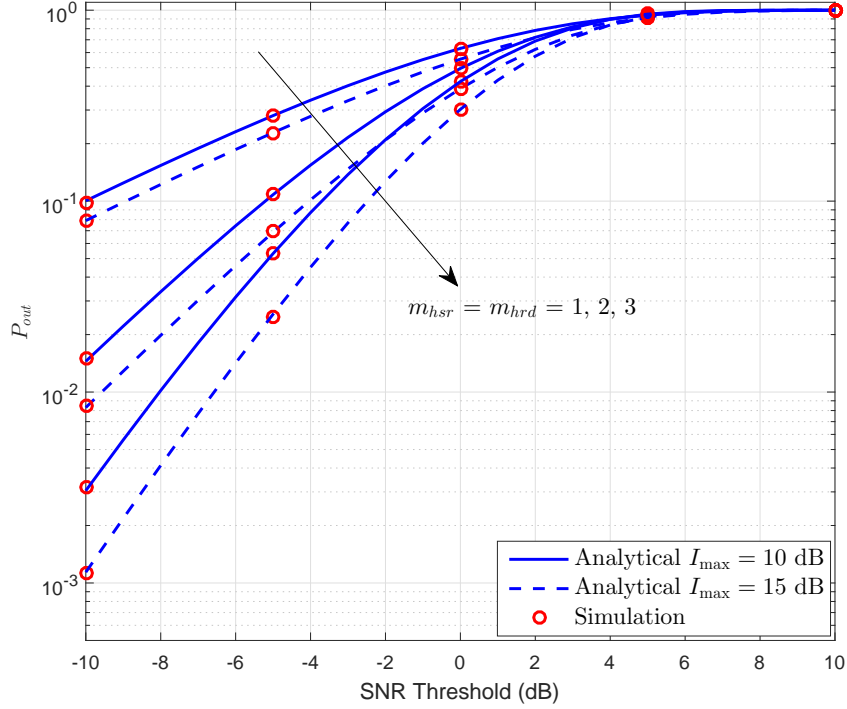


Figure 6.2: Outage probability as a function of SNR threshold for different values of the channel fading severity parameter and the interference power constraint.

Fig. 6.2 shows the impact of the desired channel fading parameter values and the value of interference power constraint on the outage performance. For this figure, the following network parameter values are used: the CCI powers are $\bar{I}_R = 2$ dB, $\bar{I}_D = 3$ dB, the primary interference powers are $\bar{I}_{PR} = 3$ dB, $\bar{I}_{PD} = 4$ dB, and $L_R = 2, L_D = 4, P_s = P_r = 15$ dB. In addition, the interference channel fading severity parameters have the following values; $m_{fsp} = m_{frp} = m_{pr} = m_{pd} = m_{ir} = m_{id} = 2$. Furthermore, in all figures, the following channel variance values are assumed: $\sigma_{h_{sr}}^2 = 0.9, \sigma_{h_{rd}}^2 = 0.6, \sigma_{f_{sp}}^2 = 0.4, \sigma_{f_{rp}}^2 = 0.3$.

As expected, a higher value of the fading channel severity parameter, i.e., the shape parameter, and consideration of the desired channel will result in better performance. This shows that having more channel paths provides more diversity; as a result, the diversity gain of the network increases leading to an enhancement of the system performance. It can also be observed that for the case of the Rayleigh fading channel (i.e., $m_{hsr} = m_{hrd} = 1$), the system has the worst performance when compared to other less severe fading parameter values. Furthermore, as the value of the interference power constraint increases the performance improves accordingly. The simulation and analytical results match, which validates the derived formulas.

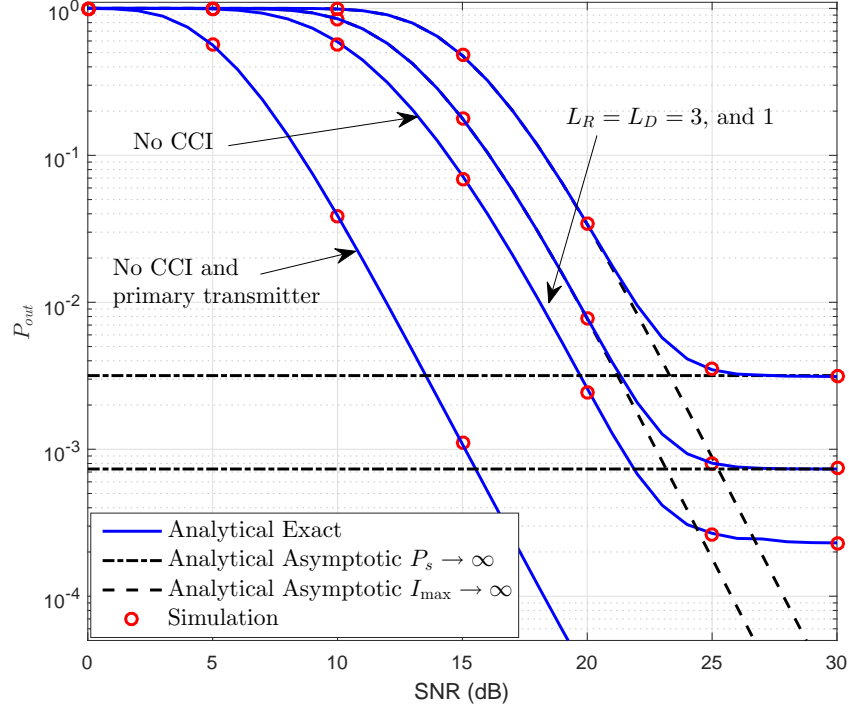


Figure 6.3: Outage probability vs. transmission power constraint for a different number of CCI sources.

Fig. 6.3 shows the outage performance versus transmission power for the different number of CCI sources. For this illustration, the following network parameter values are used: $\bar{I}_R = 2$ dB, $\bar{I}_D = 3$ dB, the primary interference powers are $\bar{I}_{PR} = 3$ dB, $\bar{I}_{PD} = 4$ dB, $I_{\max} = 20$ dB, and $\gamma_{\text{th}} = 2$ dB. In addition, the channel fading severity parameters are as follows: $m_{hsr} = 3$, $m_{hrd} = 4$, $m_{fsp} = 2$, $m_{frp} = 3$, $m_{pr} = 3$, $m_{pd} = 2$, $m_{ir} = 2$, $m_{id} = 3$. In this figure, the outage performance is also plotted for the special cases where no CCI exists (as in [54]) and no CCI and primary transmitter exist (as in [66]). It can be observed how the number of CCI signals and the existence of both CCI and primary transmitter interference affect the secondary system performance. Furthermore, asymptotic results are presented to better illustrate the performance boundaries of a UCRN. For instance, in the scenario where $P_s \rightarrow \infty$, i.e., no transmission power constraint on the secondary transmitter nodes, I_{\max} is the dominant parameter to limit the outage performance achievement. In addition, where $I_{\max} \rightarrow \infty$, the secondary user transmission nodes can take full advantage of their transmission power limits.

In Fig. 6.4 the impact of the linear increase of interference powers on the outage performance of the CR network is investigated. For this figure, the following network

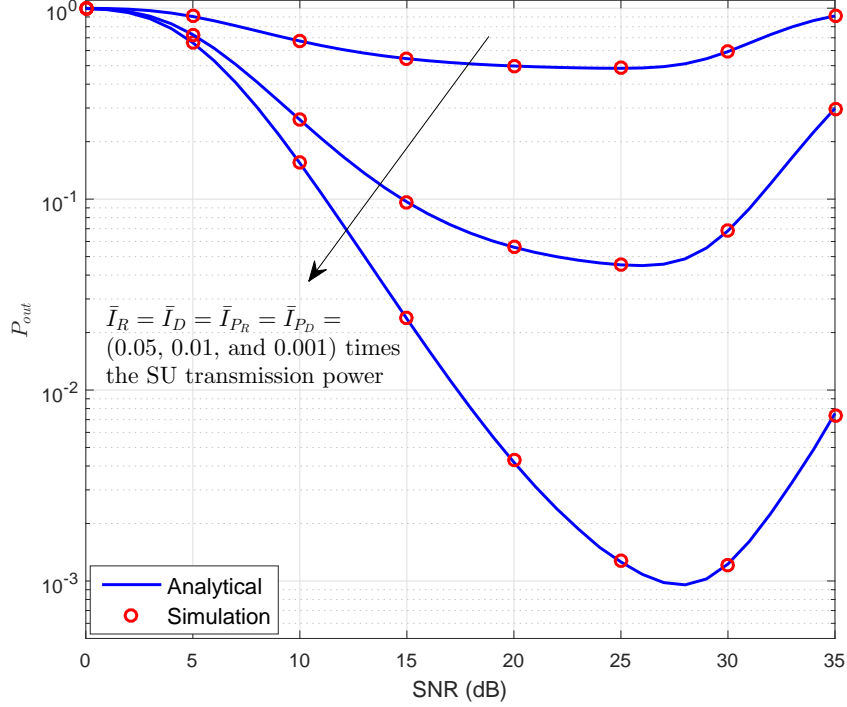


Figure 6.4: Outage probability vs. transmission power constraint for a linear increase of the CCI power and primary transmission power.

parameter values are used: $m_{hsr} = 2, m_{hrd} = 2, m_{fsp} = 2, m_{frp} = 3, m_{pr} = 3, m_{pd} = 2, m_{ir} = 2, m_{id} = 3, L_R = 3, L_D = 4, I_{\max} = 25$ dB, and $\gamma_{\text{th}} = 2$ dB. The results in Fig. 6.4 show how the ratio of the interference powers with respect to the secondary network's power limit range can degrade the outage performance behaviour. In addition, an outage degradation phenomenon, instead of outage floor, can be noticed for the relatively higher secondary transmission power. It is worth mentioning that in the worst scenario of the interference on the secondary network, the performance degrades as the secondary transmission power increases, consequently, the diversity gain will lose its advantage. For example, in the case where the considered CCI power increases linearly by the ratio of 1%, the outage performance stops improving and starts degrading at around 4.4×10^{-2} , which means the secondary network performance cannot further increase even if the transmission power increased.

In Fig. 6.5, the outage performance of the three hops DF cooperative CR network is investigated using the formula in (6.30). In addition, the effect of different values of the desired channel fading parameter and the primary interference power value are shown on the outage performance. In this figure, the subscripts 1, 2, 3 represent the parameters that belong to that hop index (i.e., first, second, and third hop,

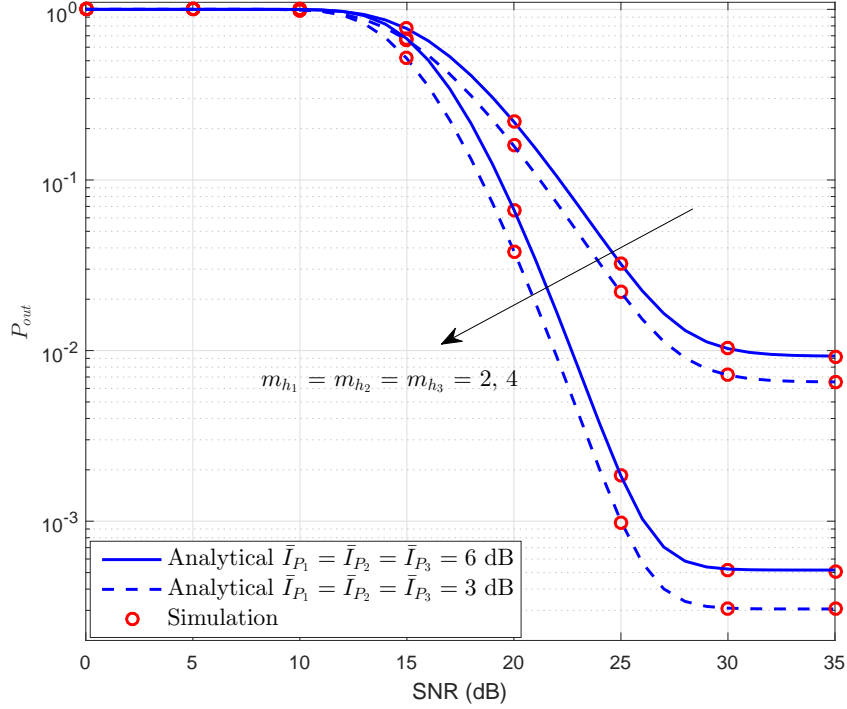


Figure 6.5: Three hops OP as a function of transmission power constraint for different values of channel fading severity parameter and primary network interference power.

respectively). For this figure, the following network parameter values are used: $m_{f_1} = 2, m_{f_2} = 1, m_{f_3} = 2, m_{p_1} = 1, m_{p_2} = 2, m_{p_3} = 2, m_{i_1} = 2, m_{i_2} = 2, m_{i_3} = 1, \sigma_{h_3}^2 = 0.8, \sigma_{f_{sp_3}}^2 = 0.5$. In addition, $\gamma_{th} = 2$ dB, $I_{max} = 25$ dB, $\bar{I}_{R_1} = 2$ dB, $\bar{I}_{R_2} = 1$ dB, $\bar{I}_{R_3} = 5$ dB. Similar to the case in Fig. 6.2, when the fading severity parameters have higher values, better performance will be expected. On the other hand, a higher interference power from the primary network results in relatively lower performance; these can be clearly observed in the results. Moreover, since a DF protocol has been employed at the relay nodes, the outage performance depends on the weakest hop SINR in the secondary network, this means that for a larger number of hops in the network, better performance is not expected. It is worth mentioning that the analytical results match the simulation results which sustain the correctness of the derived formulas.

Fig. 6.6 illustrates the average symbol error probability performance for the dual-hop secondary network for different modulation schemes. For this figure, the following network parameter values are used: $m_{h_{sr}} = 4, m_{h_{rd}} = 5, m_{f_{sp}} = 3, m_{f_{rp}} = 3, m_{p_r} = 2, m_{p_d} = 2, m_{i_r} = 3, m_{i_d} = 3, L_R = 2, L_D = 3, I_{max} = 25$ dB, $\bar{I}_R = 2$ dB, $\bar{I}_D = 3$ dB, $\bar{I}_{PR} = 5$ dB, and $\bar{I}_{PD} = 4$ dB. Furthermore, formulas in (6.34), (6.35)

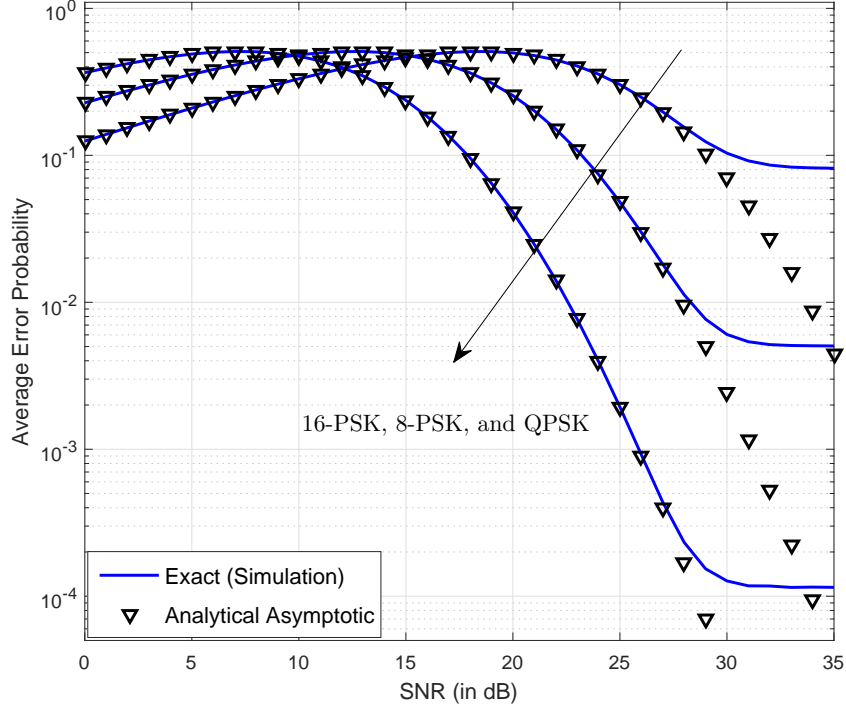


Figure 6.6: Average error probability for the dual-hop CR network for different modulation schemes.

and (6.36) have been used to calculate and plot the approximate analytical AEP. From this it can be deduced that, in the scenario of QPSK, the error performance saturates at 1.14×10^{-4} , while for 8-PSK, it saturates at around 5.0×10^{-3} . The main reason behind these saturation phenomena is the interference power constraint that limits the transmission power at the secondary transmitter nodes. Furthermore, it can be observed the derived approximate error probability formula gives more accurate results in the secondary transmitter's power dominant region.

Finally, Fig. 6.7 shows the PDF versus RV x for different CCI powers and desired fading channel parameter values. This figure is for the purpose of investigation of the characteristics of the secondary network's equivalent PDF and to better understand its behaviour. For this figure, the following network parameter values are used: $m_{fsp} = 2, m_{frp} = 3, m_{pr} = 3, m_{pd} = 2, m_{ir} = 2, m_{id} = 3, P_s = P_r = 12$ dB, $I_{\max} = 15$ dB, $\bar{I}_{PR} = \bar{I}_{PD} = 1$ dB, $L_R = L_D = 2$. The figure has been plotted by using (6.13). From this result, it can be observed that the value of the channel fading parameter and the number of CCI signals largely affect the characteristic of the PDF. For example, a lower value of the desired fading channel parameter m_h deteriorates the PDF behaviour characteristic that results in degrading the performance of the

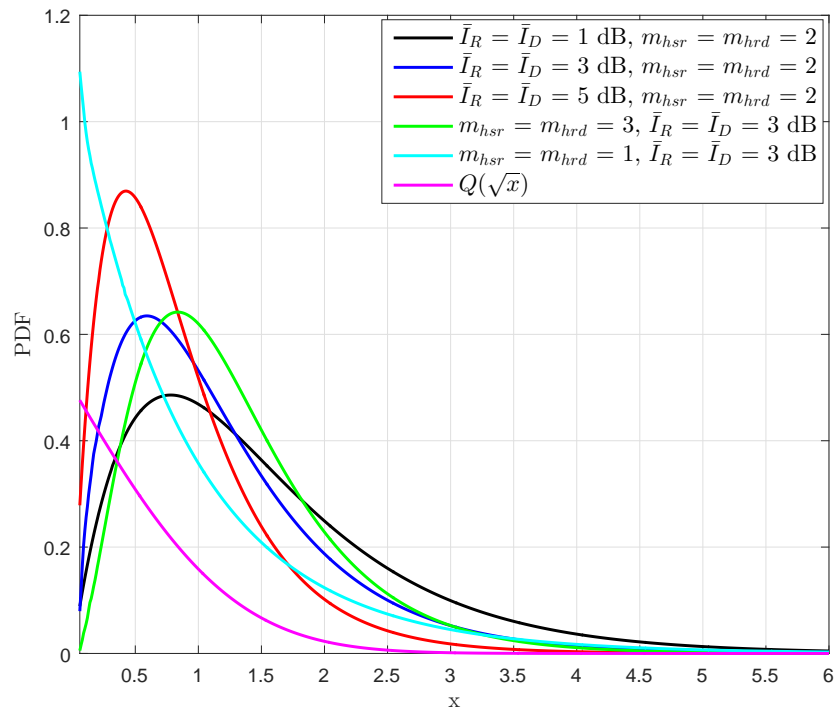


Figure 6.7: Dual-hop equivalent PDF characteristics for different channel fading severity parameters and CCI powers.

system.

In addition, for the Rayleigh fading channel scenario consideration for the desired channels between the secondary transmitter and receiver nodes, i.e., $m_h = 1$, the PDF behaviour has its worst scenario, since most of the area under the curve tends to zero. Furthermore, for the purpose of comparison, the function $Q(\sqrt{x})$ has also been plotted. In all plots, it can be seen that the characteristics of the PDF around the origin are always important. For example, when the value of m_h increases, the PDF around zero also decreases, which means better diversity for the network. Similarly, when the interference signal power is increased from 1 dB to 5 dB, the behaviour of the PDF tends to be closer to the origin, the red line plot in Fig. 6.7, which means degrading the characteristic of the equivalent SINR which results in poorer performance for the secondary network.

6.4 Conclusion

In this chapter, outage and error performance for an underlay cooperative cognitive network over Nakagami- m fading channels were extensively studied. In the analysis,

the presence of interference from the primary transmitter and CCI sources were considered. First, exact expressions for the CDF and PDF of the equivalent SINR were derived. Then, the exact and asymptotic OP for the dual-hop DF cognitive network were investigated. Moreover, the asymptotic AEP was examined.

Numerical examples with Monte Carlo simulations have also been given to support the correctness of the theoretical derivations. Results show that the presence of the primary network and CCI interferences apparently degrade the performance of the secondary network. Specifically, in the case of a linear increase of the interference power, this degradation is more noticeable, such that the system performance is expected to get worse when the transmission power increases. The analysis in this chapter is necessary to better understand the performance behaviour of the underlay CR network when both primary transmitter interference and the CCI are considered over Nakagami- m fading channels.

6.5 Appendix

6.5.1 Proof of Corollary 1

Using the formula in (6.6), the first hop CDF can be expanded and written as:

$$\begin{aligned} F_{\gamma_{SR}^{\text{eq}}}(\gamma) &= \Pr\left(G \leq \frac{\gamma Y}{I_{\max}}, Y > \frac{I_{\max}}{P_s}\right) + \Pr\left(G \leq \frac{\gamma}{P_s}, Y \leq \frac{I_{\max}}{P_s}\right), \\ &= I_1 + I_2, \end{aligned} \quad (6.37)$$

where $G = \frac{X}{(I+P+1)}$. By observing the above CDF formula, it is easy to find that the second part can be represented as:

$$I_2 = F_G\left(\frac{\gamma}{P_s}\right) F_Y\left(\frac{I_{\max}}{P_s}\right). \quad (6.38)$$

In the sections below, the derivation steps of the first part, i.e., I_1 is presented. The derivation is started by finding the PDF of the sum of the two RVs (i.e., $Z = I + P$). This can be found by using the following formula:

$$f_Z(z) = \int_0^z f_I(\gamma_{IR}) f_P(z - \gamma_{IR}) d\gamma_{IR}. \quad (6.39)$$

With the advantage of the Binomial theorem, (6.39) can be rewritten as:

$$f_Z(z) = \sum_{l=0}^{m_{pr}-1} \binom{m_{pr}-1}{l} \frac{(-1)^l \left(\frac{m_{ir}}{\bar{I}_R}\right)^{m_{ir}L_R}}{\Gamma(m_{pr})} \left(\frac{m_{pr}}{\bar{I}_{PR}}\right)^{m_{pr}} \frac{z^{m_{pr}-1-l} e^{-\frac{m_{pr}}{\bar{I}_{PR}}z}}{\Gamma(m_{ir}L_R)} \int_0^z \gamma_{IR}^{m_{ir}L_R+l-1} e^{-\gamma_{IR}\left(\frac{m_{ir}}{\bar{I}_R} - \frac{m_{pr}}{\bar{I}_{PR}}\right)} d\gamma_{IR}. \quad (6.40)$$

The integral in (6.40) can be solved with the help of [112, eq. (8.350.1)] and written as in (6.41):

$$f_Z(z) = \sum_{l=0}^{m_{pr}-1} \binom{m_{pr}-1}{l} (-1)^l \left(\frac{m_{ir}}{\bar{I}_R}\right)^{m_{ir}L_R} \left(\frac{m_{pr}}{\bar{I}_{PR}}\right)^{m_{pr}} \frac{z^{m_{pr}-1-l} e^{-\frac{m_{pr}}{\bar{I}_{PR}}z}}{\Gamma(m_{ir}L_R)\Gamma(m_{pr})} \times \left(\frac{\bar{I}_{PR}\bar{I}_R}{\bar{I}_{PR}m_{ir} - \bar{I}_Rm_{pr}}\right)^{m_{ir}L_R+l} \gamma\left(m_{ir}L_R+l, \left(\frac{\bar{I}_{PR}m_{ir} - \bar{I}_Rm_{pr}}{\bar{I}_{PR}\bar{I}_R}\right)z\right). \quad (6.41)$$

In the next step, the CDF of $G = \frac{X}{Z+1}$ is obtained, which is the CDF of the division of two RVs. This can be obtained by using the following formula:

$$F_G(g) = \int_0^{\infty} F_X(g(z+1)) f_Z(z) dz. \quad (6.42)$$

The CDF of RV X can be obtained directly from (6.7), and written as follows:

$$F_X(x) = 1 - Q\left(m_{hsr}, \frac{m_{hsr}}{\sigma_{hsr}^2 \bar{\gamma}} x\right), \quad (6.43)$$

where $Q(\cdot, \cdot)$ is the regularized incomplete gamma function [112, eq. (8.350.2)]. Assuming integer values for the fading parameters and by using [112, eq.(8.352.7)], the upper incomplete gamma function in the CDF formula of the $F_X(x)$ can be represented by a sum of a finite series. Then, substituting both CDF and PDF of X and Z into (6.42), respectively, the integral can be solved and written as:

$$F_G(g) = 1 - \Upsilon e^{-\left(\frac{m_{hsr}}{\sigma_{hsr}^2} g\right)} \left(\frac{m_{hsr}}{\sigma_{hsr}^2} g\right)^i \left[\Gamma(j + m_{pr} - l) \left(\frac{m_{hsr}}{\sigma_{hsr}^2} g + \frac{m_{pr}}{\bar{I}_{PR}}\right)^{l-j-m_{pr}} - \sum_{k=0}^{m_{ir}L_R+l-1} \frac{\left(\frac{\bar{I}_{PR}m_{ir} - \bar{I}_Rm_{pr}}{\bar{I}_{PR}\bar{I}_R}\right)^k}{k!} \left(\frac{m_{hsr}}{\sigma_{hsr}^2} g + \frac{m_{ir}}{\bar{I}_R}\right)^{l-j-k-m_{pr}} \Gamma(j + k + m_{pr} - l) \right], \quad (6.44)$$

where Υ is represented by the formula in (6.12). Finally, I_1 in the first hop equivalent CDF can be obtained by taking the expectation of the $F_G(g)$ with respect to $f_Y(y)$. After substituting the entities and doing some mathematical arrangements, I_1 can be expressed as:

$$I_1 = \frac{1}{\Gamma(m_{fsp})} \Gamma\left(m_{fsp}, \frac{m_{fsp} I_{\max}}{\sigma_{fsp}^2 P_s}\right) - \Upsilon\left(\frac{m_{fsp}}{\sigma_{fsp}^2}\right) \frac{1}{\Gamma(m_{fsp})} \left(\frac{m_{hsr}\gamma}{I_{\max}\sigma_{hsr}^2}\right)^i \left[\Gamma(j + m_{pr} - l) I_{1a} - \sum_{k=0}^{m_{ir}L_R + l - 1} \frac{\left(\frac{\bar{I}_{PR} m_{ir} - \bar{I}_R m_{pr}}{\bar{I}_{PR} \bar{I}_R}\right)^k}{k!} \Gamma(j + k + m_{pr} - l) I_{1b} \right], \quad (6.45)$$

where I_{1a} and I_{1b} have the following expressions, respectively.

$$I_{1a} = \int_{\frac{I_{\max}}{P_s}}^{\infty} e^{-y\left(\frac{m_{hsr}\gamma}{I_{\max}\sigma_{hsr}^2} + \frac{m_{fsp}}{\sigma_{fsp}^2}\right)} \left(\frac{m_{hsr}\gamma}{I_{\max}\sigma_{hsr}^2} y + \frac{m_{pr}}{\bar{I}_{PR}}\right)^{-j-m_{pr}+l} y^{m_{fsp}+i-1} dy, \quad (6.46)$$

$$I_{1b} = \int_{\frac{I_{\max}}{P_s}}^{\infty} e^{-y\left(\frac{m_{hsr}\gamma}{I_{\max}\sigma_{hsr}^2} + \frac{m_{fsp}}{\sigma_{fsp}^2}\right)} \left(\frac{m_{hsr}\gamma}{I_{\max}\sigma_{hsr}^2} y + \frac{m_{ir}}{\bar{I}_R}\right)^{-j-k-m_{pr}+l} y^{m_{fsp}+i-1} dy. \quad (6.47)$$

For part I_{1a} , the integral in its current form is quite difficult to solve. Therefore, it is necessary to change its representation so that it will be easy to compare it with the available standard mathematical functions. First, the following notations are used to make the integral formulas simpler; $\eta_1 = \frac{m_{pr}}{\bar{I}_{PR}}$, $\eta_2 = \frac{m_{hsr}\gamma}{I_{\max}\sigma_{hsr}^2}$, and $\eta_3 = \eta_2 + \frac{m_{fsp}}{\sigma_{fsp}^2}$. Then, let $t = \eta_2 y + \eta_1$, therefore, I_{1a} can be represented as:

$$I_{1a} = \left(\frac{1}{\eta_2}\right)^{m_{fsp}+i} e^{\eta_1\left(\frac{\eta_3}{\eta_2}\right)} \int_{\eta_2 \frac{I_{\max}}{P_s} + \eta_1}^{\infty} e^{-t\left(\frac{\eta_3}{\eta_2}\right)} (t)^{-j-m_{pr}+l} (t - \eta_1)^{m_{fsp}+i-1} dt. \quad (6.48)$$

Using binomial expansion, the above formula can be written as:

$$I_{1a} = \left(\frac{1}{\eta_2}\right)^{m_{fsp}+i} \sum_{r_1=0}^{m_{fsp}+i-1} \binom{m_{fsp}+i-1}{r_1} (-\eta_1)^{m_{fsp}+i-1-r_1} e^{\eta_1\left(\frac{\eta_3}{\eta_2}\right)} \int_{\eta_2 \frac{I_{\max}}{P_s} + \eta_1}^{\infty} e^{-t\left(\frac{\eta_3}{\eta_2}\right)} (t)^{-j-m_{pr}+l+r_1} dt. \quad (6.49)$$

The next step is to change the variable of the above integral so that $x = t \left(\frac{\eta_3}{\eta_2} \right)$. After this change of variable, the integral can be written as:

$$I_{1a} = \left(\frac{1}{\eta_2} \right)^{m_{fsp}+i} \sum_{r_1=0}^{m_{fsp}+i-1} \binom{m_{fsp}+i-1}{r_1} \frac{1}{(-\eta_1)^{r_1+1-m_{fsp}-i}} e^{\eta_1 \left(\frac{\eta_3}{\eta_2} \right)} \left(\frac{\eta_2}{\eta_3} \right)^{-j-(m_{pr}-1-l)-1+r_1} \binom{\eta_2}{\eta_3} \int_{\left(\eta_2 \frac{I_{\max}}{P_s} + \eta_1 \right) \left(\frac{\eta_3}{\eta_2} \right)}^{\infty} e^{-x} (x)^{l+r_1-j-m_{pr}} dx. \quad (6.50)$$

Now, by comparing the above integral representation with [112, eq.(8.350.2)], it is easy to represent I_{1a} in terms of the standard available function, which the upper incomplete gamma function.

$$I_{1a} = \left(\frac{1}{\eta_2} \right)^{m_{fsp}+i} \sum_{r_1=0}^{m_{fsp}+i-1} \binom{m_{fsp}+i-1}{r_1} \frac{1}{(-\eta_1)^{r_1+1-m_{fsp}-i}} e^{\eta_1 \left(\frac{\eta_3}{\eta_2} \right)} \left(\frac{\eta_2}{\eta_3} \right)^{r_1-j-(m_{pr}-1-l)} \Gamma \left(l+r_1-j-m_{pr}+1, \left(\eta_2 \frac{I_{\max}}{P_s} + \eta_1 \right) \left(\frac{\eta_3}{\eta_2} \right) \right). \quad (6.51)$$

Similar steps can be repeated to solve part I_{1b} . Finally, both I_{1a} and I_{1b} can be written in a more convenient and compact form as in (6.52) and (6.53), respectively.

$$I_{1a} = \sum_{r_1=0}^{m_{fsp}+i-1} \binom{m_{fsp}+i-1}{r_1} \frac{e^{\frac{\beta_7}{\gamma} + \beta_3}}{(-\beta_3)^{r_1+1-m_{fsp}-i}} \left(\frac{\gamma}{\gamma + \beta_6} \right)^{r_1-j-m_{pr}+1+l} \times \Gamma \left(l+r_1-j-m_{pr}+1, \frac{\gamma}{\beta_1} + \frac{\beta_7}{\gamma} + \beta_5 + \beta_3 \right), \quad (6.52)$$

$$I_{1b} = \sum_{r_2=0}^{m_{fsp}+i-1} \binom{m_{fsp}+i-1}{r_2} \frac{e^{\frac{\beta_8}{\gamma} + \beta_2}}{(-\beta_2)^{r_2+1-m_{fsp}-i}} \left(\frac{\gamma}{\gamma + \beta_6} \right)^{r_2-j-k-m_{pr}+1+l} \times \Gamma \left(l+r_2-j-k-m_{pr}+1, \frac{\gamma}{\beta_1} + \frac{\beta_8}{\gamma} + \beta_5 + \beta_2 \right), \quad (6.53)$$

where $\beta_1 = \frac{P_s \sigma_{h_{sr}}^2}{m_{h_{sr}}}$, $\beta_2 = \frac{m_{ir}}{I_R}$, $\beta_3 = \frac{m_{pr}}{I_{PR}}$, $\beta_5 = \frac{m_{fsp} I_{\max}}{P_s \sigma_{fsp}^2}$, $\beta_7 = \frac{m_{pr} m_{fsp} \sigma_{h_{sr}}^2 I_{\max}}{m_{h_{sr}} \sigma_{fsp}^2 I_{PR}}$, and $\beta_8 = \frac{m_{ir} m_{fsp} \sigma_{h_{sr}}^2 I_{\max}}{m_{h_{sr}} \sigma_{fsp}^2 I_R}$. Then, I_1 can be obtained by substituting (6.52) and (6.53) in (6.45). Finally, the exact equivalent CDF of the first hop can be obtained by adding both derived parts, i.e., I_1 and I_2 , and it can be represented as in (6.11).

6.5.2 Proof of Corollary 2

After substituting the approximate CDF formula derived in (6.23) into (6.31), three integral terms appear. The first part can be directly evaluated as:

$$\bar{P}_b^{SR_1} = \frac{a}{2} \sqrt{\frac{b}{\pi}} \int_0^{\infty} \frac{e^{-b\gamma}}{\sqrt{\gamma}} d\gamma = \frac{a}{2}. \quad (6.54)$$

The second and third integral parts are represented as follows:

$$\bar{P}_b^{SR_2} \triangleq \Omega_1 = \int_0^{\infty} \frac{e^{-b\gamma}}{\sqrt{\gamma}} (\gamma)^i e^{-\frac{\gamma}{\beta_1}} (\gamma + \beta_1\beta_3)^{l-j-m_{pr}} d\gamma, \quad (6.55)$$

$$\bar{P}_b^{SR_3} \triangleq \Omega_2 = \int_0^{\infty} \frac{e^{-b\gamma}}{\sqrt{\gamma}} (\gamma)^i e^{-\frac{\gamma}{\beta_1}} (\gamma + \beta_1\beta_2)^{l-j-k-m_{pr}} d\gamma. \quad (6.56)$$

It can be observed that the second and third part, i.e., $\bar{P}_b^{SR_2}$ and $\bar{P}_b^{SR_3}$, are identical in terms of the integral evaluation structure. Therefore, only the second part integral, i.e., Ω_1 , is derived in the sections below. For part Ω_1 , first, the variable of the integral is exchanged so that $t = \frac{\gamma}{\beta_1\beta_3}$. The resulting integral has the following expression:

$$\Omega_1 = (\beta_1\beta_3)^{l-j-m_{pr}+i+\frac{1}{2}} \int_0^{\infty} e^{-t\beta_1\beta_3(b+\frac{1}{\beta_1})} (t)^{i-\frac{1}{2}} (t+1)^{l-j-m_{pr}} dt. \quad (6.57)$$

Now, by comparing the above formula with [80, eq. (13.2.5)], it is easy to come up with the formula in (6.35).

Chapter 7

Conclusion and Further Research

Cognitive radio is regarded as a promising technology for future wireless communication networks. Its potential benefits can be discovered through studying its performance subjected to a more practical network scenario. In this thesis, a thorough performance investigation has been carried out for an underlay cognitive radio network. More practical case scenarios were considered for finding and analysing the performance metrics of the secondary network. In the following sections a brief summary of this research is outlined, then some interesting research topics closely related to this thesis are presented as possible future research directions.

7.1 Conclusion

In chapter three, the impact of co-channel interference was investigated on the dual-hop UCRN. Mathematical expressions for the following performance metrics were derived: outage probability, average error probability, and ergodic capacity. Furthermore, multi-destination users at the secondary network, in conjunction with the opportunistic SNR-based selection technique, are investigated. The results indicated that, besides the interference power constraint, the CCI consideration could apparently degrade the secondary network performance, especially when its power is considered as linearly increasing with the actual secondary transmission power. For improving the performance of the secondary system, an optimal power allocation technique has been adapted.

In chapter four, the impact of CCI, primary network interference, and the interference power constraint on a UCRN was exhaustively studied. Furthermore, the advantage of employing multi-antenna scheme at the receiver nodes and using

multi-hop cooperative communication was investigated. The results showed that the SINR-based antenna selection approach provides better performance than the SNR-based antenna selection when the received signals are manipulated at the secondary receiver nodes. Although, the SINR-based approach needs a more sophisticated hardware configuration and is practically harder to implement. In addition, it was illustrated that the MRC technique provides better performance than the SC technique. However, in practice, the SC technique is simpler to implement. Interestingly, it was shown that employing a multi-hop cooperative scheme is an efficient method for combating the impact of the interference power constraint. Moreover, it was illustrated that the performance saturation is possible due to the CCI, primary transmitter power and the interference power constraint. A performance degradation occurred when the interference power is considered to increase linearly with the secondary transmission power; this is the worst case scenario for the performance of the secondary network. Finally, it was proved that the advantage of a multi-antenna scheme does not lose its importance even in the worst case scenario of the existence of the interference power.

In chapter five, the MIMO network was considered for a UCRN, and its performance was investigated. Specifically, the transmit antenna selection technique was taken into account at the transmitter node, and the maximal ratio combining technique at the receiver node. It was found that considering the MIMO scheme for a UCRN can enhance the overall performance of the secondary network through combating limitations of its transmission power and providing diversity advantage for the system. Additionally, the MIMO scheme does not lose its benefit despite the existence of interference from the primary transmitter and co-channel interference signals. Although, the interference power decreases the performance, especially when the considered interference power increases linearly with the secondary transmission power, in which a performance floor or, even worse, “performance degradation” are expected.

In chapter six, Nakagami- m fading channels were considered for all channels in the primary and secondary network and the performance of the secondary network has been thoroughly studied. It was found that the existence of the primary transmitter and CCI signals reduce the performance of the secondary network. Precisely, in the scenario where a linear increase of the interference power is considered with respect to the secondary transmission power constraint limit, this degradation is more

noticeable, such that the system performance is expected to get worse when the transmission power increases. It was illustrated that a higher value consideration of the fading severity parameter of the desired channel results in better diversity which leads to better performance. Finally, considering more practical fading channels, such as Nakagami- m , in conjunction with CCI and primary network transceiver, makes the system more practical and clarifies the benefits of using UCRN.

7.2 Further Research

The area of performance analysis of cognitive radio is a wide field for research. In this section, some possible future topics are proposed:

1. The available information about the states of the fading channel plays a crucial role in determining the performance behaviour of the wireless communication network. Therefore, consideration of imperfect channel state information in the performance analysis for the underlay cognitive radio network in the presence of co-channel interference is a significant research extension to work on in this thesis. It is understandable that this will increase the mathematical complexity of the analysis. However, it would provide better views of and understanding about the cognitive radio network performance behaviour.
2. Continuous growth of the demand for the data throughput in wireless communication networks led to the establishment of many paradigms. The Full Duplex (FD) communication scheme is one of the promising techniques for better utilising the current frequency spectrum. In the FD scheme, the nodes in the network are allowed to transmit and receive signals simultaneously on the same frequency spectrum. Increasing the achievable spectral efficiency for the wireless communication network is the main advantage of employing the FD scheme. The FD scheme, alongside the cognitive radio network, is among the most promising developments in 5G wireless communications. Therefore, merging the benefits of both CRN and FD could result in better performance of the considered network. The research that has been carried out in this thesis can be extended to consider an FD network that will be a novel and interesting further research.
3. Future wireless communication networks will tend to move toward the usage

of energy sources that are more environmentally friendly and cost-effective. Recently, energy harvesting has become a fascinating research topic which has aroused considerable interest among researchers. This is due to the potential advantages of energy harvesting for the next generation of wireless communication networks. Simultaneous wireless information and power transfer (SWIPT) is one of the energy harvesting schemes in which the energy of the radio frequency can be harvested and used to provide additional support to the power budget in the network. It would be an interesting and novel research topic to extend the work in this thesis to consider SWIPT for a MIMO cognitive radio network in the presence of co-channel interference. In addition, secrecy analysis in conjunction with SWIPT could become an attractive future research area.

References

- [1] S. Haykin, “Cognitive radio: brain-empowered wireless communications,” *IEEE J. Select. Areas Commun.*, vol. 23, no. 2, pp. 201–220, Feb. 2005.
- [2] J. Mitola and G. Q. Maguire Jr, “Cognitive radio: making software radios more personal,” *IEEE Personal Commun.*, vol. 6, no. 4, pp. 13–18, 1999.
- [3] Federal Communications Commission, “Spectrum Policy Task Force,” Tech. Rep., 02-135, Nov. 2002.
- [4] Y.-C. Liang, Y. Zeng, E. Peh, and A. T. Hoang, “Sensing-throughput tradeoff for cognitive radio networks,” *IEEE Trans. Wireless Commun.*, vol. 7, no. 4, pp. 1326–1337, Apr. 2008.
- [5] T. Yucek and H. Arslan, “A survey of spectrum sensing algorithms for cognitive radio applications,” *IEEE Commun. Surveys Tutorials*, vol. 11, no. 1, pp. 116–130, Jan. 2009.
- [6] S. Srinivasa and S. Jafar, “Cognitive radios for dynamic spectrum access - the throughput potential of cognitive radio: A theoretical perspective,” *IEEE Commun. Mag.*, vol. 45, no. 5, pp. 73–79, May 2007.
- [7] E. Biglieri, A. J. Goldsmith, L. J. Greenstein, N. B. Mandayam, and H. V. Poor, *Principles of Cognitive Radio*. Cambridge University Press, 2012.
- [8] A. Goldsmith, S. A. Jafar, I. Maric, and S. Srinivasa, “Breaking spectrum gridlock with cognitive radios: An information theoretic perspective,” *Proc. IEEE*, vol. 97, no. 5, pp. 894–914, 2009.
- [9] M. K. Simon and M.-S. Alouini, *Digital communication over fading channels*, 2nd ed. New Jersey: John Wiley & Sons, 2005.

-
- [10] J. A. Hussein, S. S. Ikki, S. Boussakta, and C. C. Tsimenidis, "Performance analysis of opportunistic scheduling in dual-hop multiuser underlay cognitive network in the presence of cochannel interference," *IEEE Trans. Veh. Technol.*, vol. 65, no. 10, pp. 8163–8176, Oct. 2016.
- [11] W. Xu, J. Zhang, P. Zhang, and C. Tellambura, "Outage probability of decode-and-forward cognitive relay in presence of primary user's interference," *IEEE Commun. Lett.*, vol. 16, no. 8, pp. 1252–1255, Aug. 2012.
- [12] M. Seyfi, S. Muhaidat, and J. Liang, "Relay selection in cognitive radio networks with interference constraints," *IET Commun.*, vol. 7, no. 10, pp. 922–930, July 2013.
- [13] P. S. Bithas and A. A. Rontogiannis, "Outage probability analysis of multihop cognitive networks under multiple primary users interference," in *21th Proceedings European Wireless Conference*, May 2015, pp. 1–5.
- [14] Y. Huang, J. Wang, Q. Wu, C. Zhong, and C. Li, "Outage performance of spectrum sharing systems with MRC diversity under multiple primary user's interference," *IEEE Commun. Lett.*, vol. 18, no. 4, pp. 576–579, Apr. 2014.
- [15] T. Q. Duong, P. L. Yeoh, V. N. Q. Bao, M. ElKashlan, and N. Yang, "Cognitive relay networks with multiple primary transceivers under spectrum-sharing," *IEEE Signal Process. Lett.*, vol. 19, no. 11, pp. 741–744, Nov. 2012.
- [16] Q. Wu, Z. Zhang, and J. Wang, "Outage analysis of cognitive relay networks with relay selection under imperfect CSI environment," *IEEE Commun. Lett.*, vol. 17, no. 7, pp. 1297–1300, July 2013.
- [17] P. L. Yeoh, M. ElKashlan, K. J. Kim, T. Q. Duong, and G. K. Karagiannidis, "Transmit antenna selection in cognitive MIMO relaying with multiple primary transceivers," *IEEE Trans. Veh. Technol.*, vol. 65, no. 1, pp. 483–489, Jan. 2016.
- [18] T. Q. Duong, V. N. Q. Bao, H. Tran, G. C. Alexandropoulos, and H.-J. Zepernick, "Effect of primary network on performance of spectrum sharing AF relaying," *Electron. Lett.*, vol. 48, no. 1, pp. 25–27, Jan. 2012.

-
- [19] H. Huang, Z. Li, J. Si, and R. Gao, "Outage analysis of underlay cognitive multiple relays networks with a direct link," *IEEE Commun. Lett.*, vol. 17, no. 8, pp. 1600–1603, Aug. 2013.
- [20] J. M. Moualeu, W. Hamouda, and F. Takawira, "AF relaying in underlay spectrum-sharing systems with outdated CSI," in *IEEE International Conference on Communications (ICC)*, May 2016, pp. 1–6.
- [21] T. Q. Duong, V. N. Q. Bao, and H.-J. Zepernick, "Exact outage probability of cognitive af relaying with underlay spectrum sharing," *Elec. Lett.*, vol. 47, no. 17, pp. 1001–1002, Aug. 2011.
- [22] X. Jia, L. Yang, and H. Zhu, "Cognitive opportunistic relaying systems with mobile nodes: average outage rates and outage durations," *IET Commun.*, vol. 8, no. 6, pp. 789–799, Apr. 2014.
- [23] Y. Guo, G. Kang, N. Zhang, W. Zhou, and P. Zhang, "Outage performance of relay-assisted cognitive-radio system under spectrum-sharing constraints," *Electron. Lett.*, vol. 46, no. 2, pp. 182–184, Jan. 2010.
- [24] J. M. Moualeu, W. Hamouda, and F. Takawira, "Performance of AF relay selection with outdated channel estimates in spectrum-sharing systems," *IEEE Commun. Lett.*, vol. 20, no. 9, pp. 1844–1847, Sept. 2016.
- [25] L. Fan, X. Lei, T. Q. Duong, R. Q. Hu, and M. ElKashlan, "Multiuser cognitive relay networks: Joint impact of direct and relay communications," *IEEE Trans. Wireless Commun.*, vol. 13, no. 9, pp. 5043–5055, Sept. 2014.
- [26] H. Huang, N. Beaulieu, Z. Li, and J. Si, "On the performance of underlay cognitive multisource multirelay cooperative networks," *IEEE Commun. Lett.*, vol. 19, no. 4, pp. 605–608, Apr. 2015.
- [27] F. Guimaraes, D. da Costa, T. Tsiftsis, C. Cavalcante, and G. Karagiannidis, "Multiuser and multirelay cognitive radio networks under spectrum-sharing constraints," *IEEE Trans. Veh. Technol.*, vol. 63, no. 1, pp. 433–439, Jan. 2014.

-
- [28] K. Ho-Van, "Exact outage analysis of modified partial relay selection in cooperative cognitive networks under channel estimation errors," *IET Commun.*, vol. 10, no. 2, pp. 219–226, 2016.
- [29] H. K. Boddapati, S. Prakriya, and M. R. Bhatnagar, "Outage analysis of cluster-based multi-hop cognitive radio networks," in *IEEE 83rd Vehicular Technology Conference (VTC Spring)*, May 2016, pp. 1–5.
- [30] X. Zhang, Z. Yan, Y. Gao, and W. Wang, "On the study of outage performance for cognitive relay networks (CRN) with the Nth best-relay selection in Rayleigh-fading channels," *IEEE Wireless Commun. Lett.*, vol. 2, no. 1, pp. 110–113, Feb. 2013.
- [31] A. Abd El-Malek, F. Al-Qahtani, S. Zummo, and H. Alnuweiri, "MIMO multiuser cognitive relay network in spectrum sharing environment with antenna correlation over Rayleigh fading channels," in *IEEE Wireless Communications and Networking Conference (WCNC)*, Mar. 2015, pp. 504–509.
- [32] A. H. A. El-Malek, F. Al-Qahtani, S. A. Zummo, and H. Alnuweiri, "TAS/MRC in cognitive relay networks over rayleigh fading channels with correlated antennas," in *IEEE International Conference on Communications (ICC)*, June 2014, pp. 1520–1524.
- [33] A. H. A. El-Malek, F. S. Al-Qahtani, T. Q. Duong, S. A. Zummo, and H. Alnuweiri, "MIMO cognitive relay networks with correlated antennas over rayleigh fading channels," *IEEE Trans. Veh. Technol.*, vol. 65, no. 7, pp. 5349–5363, July 2016.
- [34] T. Zhang, Y. Cai, Y. Huang, T. Q. Duong, and W. Yang, "Secure transmission in cognitive MIMO relaying networks with outdated channel state information," *IEEE Access*, to be published.
- [35] T. Zhang, Y. Huang, Y. Cai, C. Zhong, W. Yang, and G. Karagiannidis, "Secure multi-antenna cognitive wiretap networks," *IEEE Trans. Veh. Technol.*, to be published.
- [36] V. N. Q. Bao, T. Q. Duong, D. Benevides da Costa, G. Alexandropoulos, and A. Nallanathan, "Cognitive amplify-and-forward relaying with best relay

- selection in non-identical Rayleigh fading,” *IEEE Commun. Lett.*, vol. 17, no. 3, pp. 475–478, Mar. 2013.
- [37] H. Chamkhia and M. Hasna, “Performance analysis of relay selection schemes in underlay cognitive networks with imperfect channel state information,” in *International Conference on ICT Convergence (ICTC)*, Oct. 2013, pp. 556–560.
- [38] B. Zhong, Y. Li, J. Wang, Z. Zhang, and K. Long, “Partial relay selection with fixed-gain relays and outdated CSI in underlay cognitive networks,” in *IEEE Wireless Communications and Networking Conference (WCNC)*, Apr. 2013, pp. 3670–3675.
- [39] F. A. Khan, K. Tourki, M. S. Alouini, and K. A. Qaraqe, “Performance analysis of a power limited spectrum sharing system with TAS/MRC,” *IEEE Trans. Signal Process.*, vol. 62, no. 4, pp. 954–967, Feb. 2014.
- [40] J. Si, Z. Li, H. Huang, J. Chen, and R. Gao, “Capacity analysis of cognitive relay networks with the PU’s interference,” *IEEE Commun. Lett.*, vol. 16, no. 12, pp. 2020–2023, Dec. 2012.
- [41] A. H. Y. Kong, “Ergodic and outage capacity of interference temperature-limited cognitive radio multi-input multi-output channel,” *IET Commun.*, vol. 5, no. 5, pp. 652–659, Mar. 2011.
- [42] T.-T. Tran, V. N. Q. Bao, V. D. Thanh, and T.-D. Nguyen, “Performance analysis of spectrum sharing-based multi-hop decode-and-forward relay networks under interference constraints,” in *Fourth International Conference on Communications and Electronics (ICCE)*, Aug. 2012, pp. 200–205.
- [43] V. N. Q. Bao, T. T. Thanh, T. D. Nguyen, and T. D. Vu, “Spectrum sharing-based multi-hop decode-and-forward relay networks under interference constraints: Performance analysis and relay position optimization,” *Journal of Communications and Networks*, vol. 15, no. 3, pp. 266–275, June 2013.
- [44] V. N. Q. Bao, T. Q. Duong, and C. Tellambura, “On the performance of cognitive underlay multihop networks with imperfect channel state information,” *IEEE Trans. Commun.*, vol. 61, no. 12, pp. 4864–4873, Dec. 2013.

-
- [45] K. Ho-Van, P. C. Sofotasios, G. C. Alexandropoulos, and S. Freear, "Bit error rate of underlay decode-and-forward cognitive networks with best relay selection," *Journal of Commun. and Net.*, vol. 17, no. 2, pp. 162–171, Apr. 2015.
- [46] K. Ho-Van, P. Sofotasios, S. V. Que, T. D. Anh, T. P. Quang, and L. P. Hong, "Analytic performance evaluation of underlay relay cognitive networks with channel estimation errors," in *International Conference on Advanced Technologies for Communications (ATC)*, Oct. 2013, pp. 631–636.
- [47] L. Li, P. Derwin, and M. Pesavento, "Symbol error rate analysis in multiuser underlay cognitive radio systems," in *IEEE 22nd International Symposium on Personal Indoor and Mobile Radio Communications (PIMRC)*, Sept. 2011, pp. 681–684.
- [48] K. Ho-Van and P. Sofotasios, "Exact bit-error-rate analysis of underlay decode-andforward multi-hop cognitive networks with estimation errors," *IET Commun.*, vol. 7, no. 18, pp. 2122–2132, Dec. 2013.
- [49] D. Li, "Performance analysis of MRC diversity for cognitive radio systems," *IEEE Trans. Veh. Technol.*, vol. 61, no. 2, pp. 849–853, Feb. 2012.
- [50] V. Blagojevic and P. Ivanis, "Ergodic capacity for TAS/MRC spectrum sharing cognitive radio," *IEEE Commun. Lett.*, vol. 16, no. 3, pp. 321–323, Mar. 2012.
- [51] F. Khan, K. Tourki, M.-S. Alouini, and K. Qaraqe, "Outage and SER performance of spectrum sharing system with TAS/MRC," in *IEEE Int. Conf. Commun. Workshops (ICC)*, June 2013, pp. 381–385.
- [52] A. Afana, V. Asghari, A. Ghayeb, and S. Affes, "On the performance of cooperative relaying spectrum-sharing systems with collaborative distributed beamforming," *IEEE Trans. Commun.*, vol. 62, no. 3, pp. 857–871, Mar. 2014.
- [53] Y. Huang, F. Al-Qahtani, Q. Wu, C. Zhong, J. Wang, and H. Alnuweiri, "Outage analysis of spectrum sharing relay systems with multiple secondary destinations under primary user's interference," *IEEE Trans. Veh. Technol.*, vol. 63, no. 7, pp. 3456–3464, Sept. 2014.

-
- [54] Y. Huang, F. Al-Qahtani, C. Zhong, and Q. Wu, "Outage analysis of spectrum sharing relay systems with multi-secondary destinations in the presence of primary user's interference," in *International Conference on Wireless Communications Signal Processing (WCSP)*, Oct. 2013, pp. 1–6.
- [55] P. L. Yeoh, M. ElKashlan, K. J. Kim, T. Q. Duong, and G. K. Karagiannis, "Cognitive MIMO relaying with multiple primary transceivers," in *IEEE Global Communications Conference (GLOBECOM)*, Dec. 2013, pp. 1956–1961.
- [56] K. Ho-Van, "Exact outage analysis of underlay cooperative cognitive networks over Nakagami-m fading channels," *IET Commun.*, vol. 7, no. 12, pp. 1254–1262, Aug. 2013.
- [57] C. Zhong, T. Ratnarajah, and K.-K. Wong, "Outage analysis of decode-and-forward cognitive dual-hop systems with the interference constraint in Nakagami-m fading channels," *IEEE Trans. Veh. Technol.*, vol. 60, no. 6, pp. 2875–2879, July 2011.
- [58] P. L. Yeoh, M. ElKashlan, T. Q. Duong, N. Yang, and D. B. da Costa, "Transmit antenna selection for interference management in cognitive relay networks," *IEEE Trans. Veh. Technol.*, vol. 63, no. 7, pp. 3250–3262, Sept. 2014.
- [59] P. L. Yeoh, M. ElKashlan, T. Q. Duong, N. Yang, and C. Leung, "Cognitive MIMO relaying in Nakagami-m fading," in *IEEE 77th Vehicular Technology Conference (VTC Spring)*, June 2013, pp. 1–5.
- [60] P. L. Yeoh, M. ElKashlan, T. Q. Duong, N. Yang, and D. Benevides da Costa, "Transmit antenna selection in cognitive relay networks with Nakagami-m fading," in *IEEE International Conference on Communications (ICC)*, June 2013, pp. 2775–2779.
- [61] H. Zhang, X. Wang, T. Gulliver, W. Shi, and H. Zhang, "Outage performance of MIMO cognitive relay networks with antenna selection," in *IEEE Pacific Rim Conference on Communications, Computers and Signal Processing (PACRIM)*, Aug. 2013, pp. 10–14.

-
- [62] A. Hyadi, M. Benjillali, M.-S. Alouini, and D. da Costa, "Performance analysis of underlay cognitive multihop regenerative relaying systems with multiple primary receivers," *IEEE Trans. Wireless Commun.*, vol. 12, no. 12, pp. 6418–6429, Dec. 2013.
- [63] X. Zhang, Y. Zhang, Z. Yan, J. Xing, and W. Wang, "Performance analysis of cognitive relay networks over Nakagami-m fading channels," *IEEE Jour. Sel. Areas Commun.*, vol. 33, no. 5, pp. 865–877, May 2015.
- [64] T. Q. Duong, K. J. Kim, H.-J. Zepernick, and C. Tellambura, "Opportunistic relaying for cognitive network with multiple primary users over Nakagami-m fading," in *IEEE International Conference on Communications (ICC)*, June 2013, pp. 5668–5673.
- [65] D. Benevides da Costa, M. ElKashlan, P. L. Yeoh, N. Yang, and M. Yacoub, "Dual-hop cooperative spectrum sharing systems with multi-primary users and multi-secondary destinations over Nakagami-m fading," in *IEEE 23rd International Symposium on Personal Indoor and Mobile Radio Communications (PIMRC)*, Sept. 2012, pp. 1577–1581.
- [66] T. Q. Duong, D. Benevides da Costa, M. ElKashlan, and V. N. Q. Bao, "Cognitive amplify-and-forward relay networks over Nakagami-m fading," *IEEE Trans. Veh. Technol.*, vol. 61, no. 5, pp. 2368–2374, June 2012.
- [67] M. M. Shurman, M. F. Al-Mistarihi, and M. M. Alhulayil, "Performance analysis of amplify-and-forward cognitive relay networks with interference power constraints over Nakagami-m fading channels," *IET Commun.*, vol. 10, no. 5, pp. 594–605, 2016.
- [68] H. Phan, H. Zepernick, and H. Tran, "Impact of interference power constraint on multi-hop cognitive amplify-and-forward relay networks over Nakagami-m fading," *IET Commun.*, vol. 7, no. 9, pp. 860–866, June 2013.
- [69] J. Hussein, S. Ikki, S. Boussakta, and C. Tsimenidis, "Performance analysis of the opportunistic multi-relay network with co-channel interference," in *Proceedings of the 22nd European Signal Processing Conference (EUSIPCO)*, Sept. 2014, pp. 166–170.

- [70] —, “Performance study of the dual-hop underlay cognitive network in the presence of co-channel interference,” in *IEEE 81st Vehicular Technology Conference, (VTC Spring)*, May 2015, pp. 1–5.
- [71] —, “Performance study of opportunistic scheduling in dual-hop multi-user underlay cognitive network,” *IET Commun.*, vol. 10, no. 5, pp. 558–566, Mar. 2016.
- [72] J. A. Hussein, S. S. Ikki, S. Boussakta, C. C. Tsimenidis, and J. Chambers, “Performance analysis of a multi-hop UCRN with co-channel interference,” *IEEE Trans. Commun.*, vol. 64, no. 10, pp. 4346–4364, Oct. 2016.
- [73] J. Hussein, S. Ikki, S. Boussakta, C. Tsimenidis, and Y. Al-Mathehaji, “Study of a multi-relay scheme and co-channel interference within an underlay cognitive radio network,” in *Eighth International Conference on Ubiquitous and Future Networks (ICUFN)*, July 2016, pp. 25–29.
- [74] J. Hussein, S. Ikki, S. Boussakta, and C. Tsimenidis, “Exact outage performance of the SIMO cognitive cooperative network in the presence of co-channel interference,” in *IEEE Wireless Communications and Networking Conference (WCNC)*, Apr. 2016, pp. 1–6.
- [75] F. H. Fitzek and M. D. Katz, *Cooperation in wireless networks: principles and applications*. Springer, 2006.
- [76] K. R. Liu, *Cooperative communications and networking*. Cambridge university press, 2009.
- [77] E. Dahlman, S. Parkvall, and J. Skold, *4G: LTE/LTE-advanced for mobile broadband*. Amsterdam: Academic press, 2011.
- [78] Y. Zhang, H.-H. Chen, and M. Guizani, *Cooperative wireless communications*. CRC press, 2009.
- [79] J. Easton and J. H. McColl, “Statistics glossary v1.1,” 2016, [Accessed 26-Aug.-2016]. [Online]. Available: <http://www.stats.gla.ac.uk/steps/glossary/>
- [80] M. Abramowitz and I. A. Stegun, *Handbook of mathematical functions: with formulas, graphs, and mathematical tables*. Courier Dover Publications, 1972.

-
- [81] D. Tse and P. Viswanath, *Fundamentals of wireless communication*. Cambridge university press, 2005.
- [82] H.-C. Yang and M.-S. Alouini, *Order statistics in wireless communications: diversity, adaptation, and scheduling in MIMO and OFDM systems*. Cambridge University Press, 2011.
- [83] F. W. J. Olver, D. W. Lozier, R. F. Boisvert, and C. W. Clark, editors., *NIST Handbook of Mathematical Functions*. New York, NY: Cambridge University Press, 2010.
- [84] S. Ikki, P. Ubaidulla, and S. Aissa, “Performance study and optimization of cooperative diversity networks with co-channel interference,” *IEEE Trans. Wireless Commun.*, vol. 13, no. 1, pp. 14–23, Jan. 2014.
- [85] A. Goldsmith, *Wireless communications*. Cambridge university press, 2005.
- [86] R. C. Robertson and N. E. Beltz, *Digital communications over fading channels*. Monterey, California. Naval Postgraduate School, 2004.
- [87] A. Paulraj, R. Nabar, and D. Gore, *Introduction to space-time wireless communications*. Cambridge university press, 2003.
- [88] J. N. Laneman, D. N. Tse, and G. W. Wornell, “Cooperative diversity in wireless networks: Efficient protocols and outage behavior,” *IEEE Trans. Inf. Theory*, vol. 50, no. 12, pp. 3062–3080, 2004.
- [89] J. D. Gibson, *Mobile communications handbook*, 3rd ed. New York: CRC press, 2013.
- [90] M. Hasna and M.-S. Alouini, “End-to-end performance of transmission systems with relays over Rayleigh-fading channels,” *IEEE Trans. Wireless Commun.*, vol. 2, no. 6, pp. 1126–1131, Nov. 2003.
- [91] D. Li, “Performance analysis of uplink cognitive cellular networks with opportunistic scheduling,” *IEEE Commun. Lett.*, vol. 14, no. 9, pp. 827–829, Sept. 2010.
- [92] S. Mishra and A. Trivedi, “Exploiting opportunistic decode-and-forward cooperation for cognitive radio relay channels in multi-antenna cognitive radio

- networks,” in *2013 International Conference on Advances in Computing, Communications and Informatics.*, Aug. 2013, pp. 155–158.
- [93] Y. Huang, F. Al-Qahtani, C. Zhong, Q. Wu, J. Wang, and H. Alnuweiri, “Cognitive MIMO relaying networks with primary user’s interference and outdated channel state information,” *IEEE Trans. Commun.*, vol. 62, no. 12, pp. 4241–4254, Dec. 2014.
- [94] D. Li, “Cognitive relay networks: Opportunistic or uncoded decode-and-forward relaying?” *IEEE Trans. Veh. Technol.*, vol. 63, no. 3, pp. 1486–1491, Mar. 2014.
- [95] X. Kang, Y.-C. Liang, and A. Nallanathan, “Optimal power allocation for fading channels in cognitive radio networks: Delay-limited capacity and outage capacity,” in *IEEE Vehicular Technology Conference (VTC Spring)*, May 2008, pp. 1544–1548.
- [96] K. Hemachandra and N. Beaulieu, “Outage analysis of opportunistic scheduling in dual-hop multiuser relay networks in the presence of interference,” *IEEE Trans. Commun.*, vol. 61, no. 5, pp. 1786–1796, May 2013.
- [97] H. Yu, I.-H. Lee, and G. Stuber, “Outage probability of decode-and-forward cooperative relaying systems with co-channel interference,” *IEEE Trans. Wireless Commun.*, vol. 11, no. 1, pp. 266–274, Jan. 2012.
- [98] M. Hasna and M.-S. Alouini, “Outage probability of multihop transmission over Nakagami fading channels,” *IEEE Commun. Lett.*, vol. 7, no. 5, pp. 216–218, May 2003.
- [99] S. Ikki and S. Aissa, “Performance analysis of dual-hop relaying systems in the presence of co-channel interference,” in *IEEE Global Telecommunications Conference (GLOBECOM)*, Dec. 2010, pp. 1–5.
- [100] N. Yang, M. ElKashlan, and J. Yuan, “Impact of opportunistic scheduling on cooperative dual-hop relay networks,” *IEEE Trans. Commun.*, vol. 59, no. 3, pp. 689–694, Mar. 2011.

-
- [101] J. Kim, J. Lee, K. Son, S. Song, and S. Chong, "Two-hop opportunistic scheduling in cooperative cellular networks," *IEEE Trans. Veh. Technol.*, vol. 61, no. 9, pp. 4194–4199, 2012.
- [102] S. Ikki and M. Ahmed, "Performance analysis of cooperative diversity with incremental-best-relay technique over Rayleigh fading channels," *IEEE Trans. Commun.*, vol. 59, no. 8, pp. 2152–2161, Aug. 2011.
- [103] Y. Huang, F. Al-Qahtani, C. Zhong, Q. Wu, J. Wang, and H. Alnuweiri, "Performance analysis of multiuser multiple antenna relaying networks with co-channel interference and feedback delay," *IEEE Trans. Commun.*, vol. 62, no. 1, pp. 59–73, Jan. 2014.
- [104] Z. Wang and G. Giannakis, "A simple and general parameterization quantifying performance in fading channels," *IEEE Trans. Commun.*, vol. 51, no. 8, pp. 1389–1398, Aug. 2003.
- [105] Q. Li, G. Li, W. Lee, M. il Lee, D. Mazzaresse, B. Clerckx, and Z. Li, "MIMO techniques in WiMAX and LTE: a feature overview," *IEEE Commun. Mag.*, vol. 48, no. 5, pp. 86–92, May 2010.
- [106] M. Hanif, H.-C. Yang, and M.-S. Alouini, "Receive antenna selection for underlay cognitive radio with instantaneous interference constraint," *IEEE Signal Process. Lett.*, vol. 22, no. 6, pp. 738–742, June 2015.
- [107] Y. Zhang, C. Ji, W. Malik, D. O'brien, and D. Edwards, "Receive antenna selection for MIMO systems over correlated fading channels," *IEEE Trans. Wireless Commun.*, vol. 8, no. 9, pp. 4393–4399, Sept. 2009.
- [108] A. Molisch, M. Win, Y. seok Choi, and J. Winters, "Capacity of MIMO systems with antenna selection," *IEEE Trans. Wireless Commun.*, vol. 4, no. 4, pp. 1759–1772, July 2005.
- [109] Y. Deng, M. El-kashlan, N. Yang, P. Yeoh, and R. Mallik, "Impact of primary network on secondary network with generalized selection combining," *IEEE Trans. Veh. Tech.*, vol. 64, no. 7, pp. 3280–3285, July 2015.
- [110] B. A. Ogunnaike, *Random phenomena: fundamentals of probability and statistics for engineers*. New York: CRC Press, 2010.

-
- [111] S. Ikki and S. Aissa, "Effects of co-channel interference on the error probability performance of multi-hop relaying networks," in *IEEE Global Telecommunications Conference (GLOBECOM)*, Dec. 2011, pp. 1–5.
- [112] I. S. Gradshteyn and I. M. Ryzhik, *Tables of Integrals, Series, and Products*, 7th ed. Amsterdam: Academic Press, 2007.
- [113] J.-P. Linnartz, "Wireless communication," 2016, [Accessed 12-Oct.-2016]. [Online]. Available: <http://www.wirelesscommunication.nl/reference/contents.htm>
- [114] Y. Deng, L. Wang, M. El Kashlan, K. J. Kim, and T. Q. Duong, "Generalized selection combining for cognitive relay networks over Nakagami-m fading," *IEEE Trans. Signal Process.*, vol. 63, no. 8, pp. 1993–2006, Apr. 2015.
- [115] S. Ikki and S. Aissa, "Performance evaluation and optimization of dual-hop communication over Nakagami-m fading channels in the presence of co-channel interferences," *IEEE Commun. Lett.*, vol. 16, no. 8, pp. 1149–1152, Aug. 2012.